

SAINT-PETERSBURG STATE UNIVERSITY

Printed as manuscript

**RYBAKOV**

**ALEKSANDR**

**Orthodontic treatment optimization based on neural networks, finite  
element analysis and oral mucosa digital maps**

3.1.7. Dentistry

DISSERTATION

for the degree of  
candidate of medical sciences

Translation from Russian

Research advisor:

Sokolovich Natalia Alexandrovna

Doctor of Medical Science

Saint-Petersburg – 2024

## TABLE OF CONTENTS

<b>INTRODUCTION</b> .....	4
<b>Chapter 1: LITERATURE REVIEW</b> .....	15
1.1 Methods for assessing mucosal biotype.....	15
1.2 Clear Aligner Therapy. Finite element analysis .....	20
1.3 Mucosa biotype significance in orthodontic treatment.....	30
1.4 Application of AI in segmentation of 3D models from CBCT data.....	34
1.4.1 Deep learning .....	42
1.4.2 Segmentation of medical images .....	42
1.4.3 Training neural networks .....	46
1.4.4 Evaluation indicators.....	48
1.4.5 Modern methods of segmentation of medical images .....	49
<b>Chapter 2. MATERIALS AND METHODS</b> .....	57
2.1 Protocol for obtaining three-dimensional models of dental arches .....	59
2.2 Creating 3D models for finite element analysis.....	61
2.3 Building a correlational model for the digital oral mucosa map .....	62
2.4 Neural network training .....	63
2.5 Laboratory phase.....	64
2.6 Clinical and diagnostic appointment.....	66
2.6.1 Photo protocol and diagnosis .....	66
2.6.2 Evaluation of oral soft tissue inflammation .....	75
<b>Chapter 3. RESULTS</b> .....	78
3.1 Protocol for obtaining three-dimensional dentition models .....	78
3.1.1 Protocol for obtaining three-dimensional dentition models .....	82
3.2 CT data segmentation.....	83
3.2.1 Manual segmentation of CT data.....	84

3.2.2	Creating a digital model of the mucosa biotype .....	95
3.2.3	CT data segmentation methodology choice .....	100
3.2.4	CT data segmentation.....	105
3.3	AI Segmentation.....	107
3.3.1	Normalization of CT data .....	107
3.3.2	Annotation of CT layers data .....	109
3.3.3	Increasing the amount of AI training data .....	110
3.3.4	Semantic segmentation of images using U-net.....	111
3.3.5	AI based CT segmentation .....	114
3.4	Creating a correlation model of the mucosa digital map .....	116
3.4.1	Oral mucosa digital map correlation modelling .....	122
3.5	Creating 3D models for FEA .....	123
3.5.1	Reverse modelling.....	132
3.5.2	Preclinical modelling of tooth movement.....	138
3.5.3	Three-dimensional models creation for FEA.....	143
3.6	Clinical and laboratory methods .....	147
3.6.1	Treatment protocol with aligners .....	159
	<b>SUMMARY</b> .....	163
	<b>CONCLUSIONS</b> .....	172
	<b>CLINICAL GUIDELINES</b> .....	174
	<b>LIST OF ABBREVIATIONS</b> .....	176
	<b>BIBLIOGRAPHY</b> .....	177

## INTRODUCTION

Digital technologies have become essential components of our daily lives, creating a level of global interconnectivity that is unmatched in history. Innovation, especially in the digital realm, is occurring on an unprecedented scale.

In the future, dentistry will be revolutionized by a wide range of new technologies, including virtual reality, artificial intelligence (AI) and CRISPR. The pursuit of advancements in dentistry is a constant endeavour, and it is crucial to embrace these new technologies and stay informed about their associated risks and advantages in the dental field. It is becoming evident that emerging innovative technologies have the potential to offer alternative treatments to patients, while also improving workflow efficiency, increasing productivity, and enhancing the quality of oral care. Dentistry, like other healthcare sectors, has undergone significant transformation recently due to the implementation of computer-based advanced technologies, new preventative measures against diseases, and improved diagnostic techniques [264].

Malocclusion anomalies have a very high prevalence, which indicates the need of an effective orthodontic treatment that does not have relapses [5, 32].

At the moment, the ideas and development of new modern methods in effective bite correction and their successful application is a very important and demanded task [225, 261, 273].

There are various techniques for bite correction. Obviously, the most technologically advanced ones, i.e. those using digital technology, which allows them to be completely predictable, are currently in the forefront. Currently, the most advanced technique is treatment with aligners [104, 170, 192].

However, special attention should be paid to the possibility of periodontal diseases when using orthopaedic and orthodontic designs due to the presence of unphysiological pressure on the gums, poor oral hygiene and aligners non-optimal trimming edges [4, 44].

With the use of modern digital technologies and their combinations, [85, 180, 304] it is possible to perform detailed analysis and predict the risks of complications. Such as gingival recession due to excessive forces applied to the tooth to be moved, or incorrect planning and selection of the aligner topology, as well as excessive pressure on the gingiva with a thin biotype. Hence, in order to avoid complications in the form of gingival recession, an accurate and simple method of determining the biotype of the oral mucosa is essential [232].

In the literature described above, no optimal methods for determining oral mucosal biotype have been found. Invasive methods in orthodontic treatment are not a rational solution. At the same time, the existing methods of biotype determination are too time-consuming and may give incorrect information under certain conditions. This may occur in cases where gingival recession already exists, or a retained tooth position is present, or surgical interventions have been performed [218].

Hence, the search for new methods of comprehensive treatment of orthodontic patients on aligners requires the development of a new efficient automated treatment protocol [284].

Modern techniques provide an opportunity to implement the best and most individualised approaches to the treatment of orthodontic patients and can serve as a basis for new methods of effective planning of compliant and non-compliant patients with the most predictable result of orthodontic treatment [53, 59, 67, 87, 104, 189, 243, 246, 269, 281]. With the use of modern digital technologies and their combinations, [85, 180, 304] it is possible to perform detailed analyses and predict the risks of complications. Such as gingival recession due to excessive forces applied to the tooth to be moved, or incorrect planning and selection of the aligner topology, as well as excessive pressure on the gingiva with a thin biotype. In order to avoid complications such as gingival recession, an accurate and simple method of determining the biotype of the oral mucosa is essential [232]. Traditional biotype evaluations accurately assess the mucosa, but miss information

about its full thickness. When digital protocols and sufficient data are available, objectification is achieved, thus obtaining a more accurate diagnosis and better prediction of patient treatment [143].

The protocols which are currently used with aligners are insufficiently studied and do not take into account the influence of oral mucosal biotype on the final outcome.

A literature review revealed no comprehensive information on using digital methods to determine oral mucosa biotype or on how mucosa biotype relates to aligner trimming type.

An important point that affects the effectiveness of orthodontic treatment is the use of different approaches to trimming aligners [175]. However, the manufacturers of aligners offer only one type of trimming without taking into account the individual characteristics of the patient's mucosa. It can be concluded that the development and application of a digital method of diagnosis and treatment planning is also an urgent task.

Thus, the research is concerned with one of the most relevant issues of orthodontics - the development of modern digital methods of orthodontic treatment. The aim is to individualize orthodontic treatment, which improves the quality of care provided, reduces the time, and increases patient compliance and motivation. This determines dissertation research's relevance.

**Aim of the study:** to increase the effectiveness of complex treatment of orthodontic patients with aligners.

**Research objectives:**

1. Obtain 3D models and analyse the results of orthodontic patients' oral scans.
2. Process a stack of received CT data of orthodontic patients using four different methods and choose the most suitable one for use with additional input data used in the research.

3. Compare methods for determining the biotype by digital and traditional methods in the absence of inflammatory processes in the mucosa, create an algorithm for obtaining an oral mucosa digital map.
4. Analyse and justify the features of the use of aligners with two different types of trimming.
5. Analyse and justify the specifics of using aligners with two different types of trimming and with modified topology of the aesthetic component in the area of missing teeth.
6. Create virtual models of aligners. Train the U-Net neural network model based on the results of annotated CT samples. Develop and determine the efficacy of an orthodontic treatment protocol on aligners based on the defined oral mucosa biotype.

### **Scientific novelty**

For the first time, correlations have been established between the biotype of the oral mucosa and the types of aligners used.

For the first time, the finite element analysis method was applied to calculate the efficiency of distribution of loads and deformations in the design of aligners.

For the first time, the individualization of aligner trimming was substantiated for various oral mucosa biotypes.

An algorithm for obtaining an oral mucosa digital map was created.

### **Practical significance**

Of great practical importance for orthodontists is new knowledge in determining the oral mucosa biotype in a digital non-invasive way, as well as obtaining new knowledge on the optimal manufacture of orthodontic aligners.

Volumetric visualization of the obtained oral cavity data empowers orthodontists to individualize the shape of manufactured aligners, potentially reducing treatment duration for patients and the risk of gum recession.

This study made it possible to create treatment protocols using additional digital examination techniques.

### **Author's personal contribution**

The author personally analysed literature on the topic of the dissertation, all the results presented in the work are the author's contribution to the process of individualization of orthodontic treatment on aligners. The author carried out the accumulation of clinical data of patients, compiled and applied new algorithms for the effective treatment of orthodontic patients. The author trained neural networks. The trained models were used for processing CBCT data. The author carried out and interpreted data to obtain mucosa digital visualization. The author developed mathematical models of physical virtual aligners. The author interpreted data from virtual



finite element analysis. The author also compiled algorithms for optimizing the topology of the aligners. Modelling, printing and manufacturing of modified aligners were carried out. The clinical approbation of the improved aligners has been carried out successfully.

### **Publications**

On the subject of the thesis 13 scientific papers have been published: in the journals indexed by SCOPUS - 1, VAK and RSCI - 2, in collections - 3, in the materials of the scientific-practical conference - 9.

### **The structure and scope of the dissertation**

The dissertation is presented in 3 chapters, presented on 217 pages, illustrated with 152 figures. The list of references includes 328 sources, of which 25 are national and 303 are foreign.

### **Dissertation results approbation and implementation in practice**

The research results have been implemented in the work of the Dentistry Department of the Federal State Budgetary Educational Institution “The Saint-Petersburg State University” and “Trydent” Ltd. dental clinic.

### **Main scientific results**

#### **Publications**

1. Deep negative volume segmentation [51] pages 1-11 – *A method of using artificial intelligence in orthodontic practice using manually obtained input data for training a neural network is described. Methods of obtaining input data - segmented cranial bone structures and temporomandibular joint volume by manual method is presented. Author's contribution 30%.*

2. Temporomandibular joint position assessment technique [20] pages 90-98 – *Systematic work on segmentation of cranial bone structures and application of the*

*obtained three-dimensional models in orthodontic practice. The methods of combining three-dimensional models of segmented bone structures with intraoral scanner scanned tooth arches to obtain the exact position of the mandible and condyles in central occlusion are described. Author's contribution 100%.*

3. Indirect braces bonding using the new Russian orthodontic adhesive [6] page 52 – *Validation and retrieval of a correlation model of oral mucosa using “Colour-test №1”*. Author's contribution 20%.

**List of conferences, congresses and symposiums in which the author took part:**

Apr. 11 2019, II International Scientific and Practical Conference "Modern Pediatric Dentistry and Orthodontics" - Department of Pediatric Dentistry and Orthodontics acad. I.P. Pavlova, St. Petersburg, ISBN (print edition) 978-5-93339-436-5 - *physical and mathematical methods of calculating the aligners topology using finite element analysis with weak spots identification to improve the efficiency of orthodontic treatment were presented.*

Sep. 17 2019, International Scientific-Practical Conference on the 60th Anniversary of the St. Petersburg State Medical University's Faculty of Dentistry, named after Acad. I.P. Pavlov - St. Petersburg - *modern diagnostic methods of the European Orthodontic Society were presented.*

Oct. 30 2019, "Modern methods of diagnosis, treatment and prevention of dental diseases": Symposium "Innovative digital technologies for diagnosis, treatment planning and monitoring of its results in dental practice" within the framework of the XVI scientific and practical conference "Modern methods of diagnosis, treatment and prevention of dental diseases" - St. Petersburg - *features of intraoral scanner use in orthodontics and paediatric dentistry with further application in orthodontic and orthopaedic treatment of complex patients were described.*

Oct. 2 2020, Physical and mathematical calculation of the topology of aligners at the III International Scientific and Practical Conference "Modern Paediatric Dentistry and Orthodontics" - St. Petersburg - *features of aligners topology during molar distalisation with finite element method and visualization of stresses and deformations of the aligners design were represented.*

Oct. 28 2020, "Dentistry of the Northern Capital": Symposium "Digital Dentistry" as part of the IV International Scientific and Practical Conference "Dentistry of the Northern Capital" - Online, St. Petersburg - *modern digital scanning, three-dimensional modelling and printing technologies for achieving the greatest efficiency of orthodontic treatment are described.*

Oct. 14 2021, "Bracket system vs aligners. Possible and Impossible" topic presented in the theses collection and at the international conference "Modern Paediatric Dentistry and Orthodontics: Difficult Dental Patient" - Zelenogorsk - *the results of aligners design capabilities are presented and the deviation factors from the designed treatment plan were visualized using the finite element method.*

Mar. 31 2022, "A two-stage technique for studying the position of the condyles of the temporomandibular joint" [16] topic presented in the theses collection and on the RUDN Interuniversity Conference "Actual Issues of Dentistry" - Department of Propaedeutic of Dental Diseases of the Medical Institute of the Peoples' Friendship University of Russia - Moscow - *methods of segmenting cranial bone structures from CT data and superimposition of the scanned teeth by an intraoral scanner to obtain combined models for the implementation of a digital protocol in orthodontic treatment were presented.*

Apr. 15 2022, "CBCT in orthodontics. How to get information that is not in the picture" topic presented in the theses collection and at the V International Scientific and Practical Conference "Modern Paediatric Dentistry and Orthodontics" - St. Petersburg - *the possibilities of obtaining and predicting the results of orthodontic treatment using*

*manual segmentation of cranial bone structures and three-dimensional models of dental arches were presented.*

Nov. 30 2022, XXVII National Russian scientific and practical conference of maxillofacial surgeons and dentists with international participation "New technologies in dentistry", St. Petersburg - *an innovative individualization of aligners topology using combined three-dimensional models of bone structures, dentition and aligners models was presented.*

### **The following are submitted for defence**

1. Objectivity of orthodontic treatment is achieved through the introduction of new digital technologies into the treatment process and the processing of the data obtained. Central occlusion dental arch models were created using an intraoral scanner following the scanning protocol. Virtual treatment plans for orthodontic patients with aligners were compiled.

2. Computerized tomography (CT) imaging is a four-dimensional voxel dataset with a range of densities on the Hounsfield scale from -1000 to 3000. To view the necessary information, a range corresponding to the density of the tissues of interest was selected. To create three-dimensional models of bone structures, the region contour was selected on each of the hundreds of layers in order to segment the range and create a shell. Manual segmentation took a long time (8-12 hours), manual area segmentation took 5-8 hours. Watershed segmentation took 1-2 hours; however, this method cannot be used to segment each tooth individually. To speed up the routine processing process, manual segmentation was performed, a neural network was trained, and as a result, an AI was created, which in turn is capable of creating an accurate composite three-dimensional model in 3-5 minutes.

To ensure the possibility of using segmentation using AI, supervised training of the neural network was performed. That is, a U-Net neural network model was trained based

on the results of annotated CT samples. A method for using AI for segmentation of cranial bone structures from CT data is presented.

3. In orthodontic treatment, the biotype of the oral mucosa plays a major role, as it has a significant impact on the choice of treatment tactics. When using clear aligners, the structure with a large surface area rests on the oral mucosa, and when the appliance is activated, additional pressure zones are created that can lead to gingival recession. A digital model of the oral mucosa biotype was created based on a combined three-dimensional model, including a segmented model of CT data and a processed model of dental scans. An analysis of oral mucosa thickness distribution across cranial bones was performed using combined 3D models.

4. In finite element analysis, a specific algorithm was created for each task - the design of a mathematical model. Due to the fact that no tasks on the deformation of aligner structures and the impact on the oral mucosa had been previously conducted, a new original design of a mathematical study of orthodontic aligner models was created.

5. Since the processes occurring during the treatment of orthodontic patients are extremely complex and cannot be seen, mathematical modelling was performed taking into account all the physical parameters of aligners. Three-dimensional models of aligners were created, the topology of aligners was analysed by finite elements, and the results were interpreted.

In most cases, it is recommended to use aligners with a high trimming. To minimize the risks of complications and to objectify the choice of the required type of trimming, a comparative mathematical analysis of the deformations of aligners with scalloped and straight trimming was performed using finite elements.

When creating aligners in the area of missing or extracted teeth, two standard methods are used - aesthetic and functional. To justify the possibility of combining both methods, a mathematical analysis of orthodontic structures with combined aesthetic components was performed using finite elements.

6. Digital orthodontic treatment protocol is complex and time-consuming. To optimize the work of an orthodontist and his team, a treatment protocol has been developed according to selected criteria. The new protocol allows, using segmentation with the help of AI, to create an individualized treatment plan; based on the global digital map of the oral mucosa, avoid unwanted complications; use aligners with improved force and aesthetic components. Ultimately, the digitization of the protocol leads to improved quality, time savings, and increased patient compliance during treatment.

## **Chapter 1: LITERATURE REVIEW**

### **1.1 Methods for assessing mucosal biotype**

Oral mucosa biotype determination using a dental probe is a rather traumatic procedure and it is performed using anaesthesia [255, 297]. The next method of determining the biotype is associated with obtaining an additional dose of radiation during a separate CT scan [48]. This information is extremely important in calculating the applied forces, in determining the possibility of oral mucosal support, and in predicting the treatment outcome.

Digitalization of orthodontic treatment involves data collection and processing, which should be obtained and prepared for further work. Next, algorithms for processing and interacting input data should be created using artificial intelligence to create a comprehensive automatic treatment plan and predict treatment [75, 98, 130, 143, 147, 214, 242, 244].

In modern dentistry, mucosa biotype determination is one of the key topics. Correct biotype determination influences both the treatment plan and the prevention of complications such as gingival recession.

Gingival recession is a common gingival disease with a variety of aetiologies, and is manifested by a displacement of gingiva vestibular margin in the apical direction with further exposure of the tooth root surface [10, 25].

Gingival biotype is defined as the thickness of the mucosa in the vestibular direction. Gingival biotype plays a key role in predicting success and preventing complications in orthodontic treatment [27]. Therefore, accurate planning is necessary to give predictable and stable results of the orthodontic treatment [7, 17, 155, 160].

Optimal periodontal health is maintained with a wide area of attached keratinized gingiva, which prevents the spread of inflammatory processes. In case of keratinized attached gingiva width reduction, it can lead to the development of destructive processes

and the occurrence of recession. A certain correlation between the width of the attached keratinized gingiva and the periodontal biotype has been identified [268].

Most authors and clinical orthodontists divide the gingival biotype into two types: thick and thin.

The thin gum biotype is characterized by high interdental papillae with point proximal contacts.

The average thickness of the attached gingiva is 1 mm.

The thick biotype is characterized by smoother gingival contours, interdental papillae are short and wide, and the average thickness is 1.5-2 mm [328].

However, a number of authors believe that there is a transitional biotype of gingiva - medium [241, 263]. These authors characterize it as transitional between thick and thin gingival biotypes with an average value of 1.5 mm. Maria N. et al. conducted studies in which they proved the impossibility to attribute the oral mucosa to a certain type, and introduced the definition of a mixed type that includes a combination of several phenotypes at once [107]. A thin gingival biotype presents the greatest difficulty in treatment planning and obtaining a stable aesthetic and functional result due to a small collagen content and a smaller keratinized attached area than in the thick phenotype [27, 151]. According to the authors, the true-thin gingival biotype occurs in two-thirds of patients [250].

Modern dentistry successfully uses a variety of methods to assess gingival biotype:

- histological methods,
- visual assessment and probing (invasive and non-invasive),
- ultrasonography,
- radiological,
- computed tomography data [1, 13, 35].



Fischer K. et al. found that it is possible to classify the periodontal biotype using scanning computed tomography, and this has clinical applications [105].

Barriviera M. et al. proposed to take CT measurements at specific points on the maxilla, from canines to second molars at distances of 2, 5, 8 and 12 mm. This non-invasive method gives an idea of the distribution of mucosal thickness on the upper jaw, but has a number of drawbacks that do not allow you to create a continuous distribution of measurements. To obtain this kind of CT data, the authors also used plastic retractors and a wooden spatula to isolate the palatal mucosa from the tongue and cheeks [48].

Wilmes B. suggested using a dental probe with a silicone stopper to invasively determine the thickness of the mucosa on the upper jaw before placing micro-implants needed for orthodontic fixation [297]. This method is local-point and traumatic, it also has a number of disadvantages when transferring measurements from a probe with a stopper.

Keratinized alveolar gingiva consists of free and attached parts. The boundary between the free and attached gingiva is the gingival groove bottom and the cement-enamel boundary. The attached part of the gingiva is fused to the tooth root cement and periosteum, and starts from the lower border of the gingival sulcus to the dental-alveolar junction.

In clinical practice, attached gingiva is evaluated by its colour texture, shape, gingival contours, and its biotype [23].

The histological structure of gingival biotypes with thick and thin biotypes differs, which in turn affects the planning of orthodontic treatment and consideration of the likelihood of complements. The thin biotype is characterized by capillaries and arterioles with narrow and moderate lumen, small spiky and granular cells. Thick biotype is characterized by wide lumen of vessels, pronounced layers of spiky and granular cells [18].

The main parameter of the gingival biotype, in addition to the thickness and height of the gingival papillae, is the attached gingiva thickness. According to various authors, the characteristics of thick and thin biotypes differ. The thin biotype is characterized by a gingiva that is less than 1 mm thick, while the thick biotype is more than 1 mm thick [216].

The thin biotype is up to 1.5 mm, the thick one is more than 2 mm [255].

In the clinical practice, special attention is paid to the thin gingival biotype; during orthodontic treatment, patients with a thick mucosa biotype can develop a local form of periodontitis; in the case of a thin biotype, the probability of recession is much higher, since loss of tooth-end attachment leads to marginal inflammation and resorption of the alveolar wall [24].

In the clinical practice, various methods of determining gingival thickness are used; however, all of them have a number of drawbacks and limitations.

One of the express methods proposed by Smirnova S., is a modification of the clinical method of gingival thickness measurement using a thin probe or endodontic instrument, for example, a reamer number 20 and a silicone stopper put on. After infiltration anaesthesia, the gingiva was punctured until the instrument reached the bone and the thickness was fixed with a silicone stopper. Then photo on millimetre paper was taken and gingival thickness was measured [19]. A similar methodology was proposed by Wilmes B. [297].

Amkhadova M. proposed an invasive method to determine the thickness of the attached soft tissues using an endodontic file (ISO 0.10) with a silicone stopper and application of 10% lidocaine spray anaesthesia. Measurements were taken at three points: in the edentulous area's apex, where the dental implant placement is expected; vestibular and orally on the attached keratinized mucosa apical to the first puncture 3 mm. The distance from the tip of the file to the silicone stopper was measured using an endodontic ruler. The biotype was considered thin at 1 mm or less.

Another clinical method for determining gingival thickness is a puncture within the attached gingiva 1-2 mm apical to the bottom of the gingival sulcus [18].

A minimally invasive method of biotype determination, which is often used by physicians of all specialties and does not require training, is to assess the degree of translucency of the periodontal probe through the gingiva. If the biotype is thick, the probe will not be translucent, if it is thin, indistinct contours will be visible [162]. This method of assessment does not take into account the transitional gingiva type, and there is no possibility to make quantitative measurements.

Using a specially designed series of Hu-Friedy COLORVUE BIOTYPE PROBE biotype probes made of white plastic with colour markings, Rasperini G. classified the gingival biotype into four types: thin, medium, thick and very thick. The essence of the method is to assess the translucency of the probe through the attached gingiva. A set of probes consists of white (without the probe tip colouring), with green and blue colouring. If a probe without colouring (white) is translucent, the biotype is considered thin. If green is translucent, then the biotype is medium. When blue colour is visible, the biotype is thick. If none of the probes is translucent, the biotype is classified as very thick [240].

Another way to determine the mucosa thickness is to use an ultrasound measuring device SDM (Austenal Medizintechnik, Cologne, Germany). The contact surface of the device - 4 mm moistened with water or oral liquid is put for 2-3 seconds to the place of mucous membrane thickness measurement, and measurements in the range from 0.5 to 6.0 mm are made. The error of measurements on the instrument scale was 0.1 mm [259].

In all of the above methods, there are progressive points in the approach to systematizing the study of gingival and oral mucosal biotypes. However, they require changes in CT study protocols. And the use of wooden spatulas, retractors, and tags makes it difficult to obtain the necessary universal data that will be used not only to study gingival biotype, but also to plan orthodontic treatment in general. Also, some methods

are painful and traumatic to the mucosa and lack sufficient visualization of soft tissue thickness distribution.

In all methods mentioned above, only separate one was used - probing or CT study. However, nowhere were two or more independent methods combined to obtain more data and systematize distributions. In most studies, measurements were performed only on the maxilla and the results obtained from it were interpolated to the tissues of the mandible as well.

### **1.2 Clear Aligner Therapy. Finite element analysis**

Aligners are removable orthodontic appliances made of clear transparent plastic by thermoforming. The term Clear Aligners Therapy (CAT) encompasses a wide range of removable appliances with different wearing styles, manufacturing and design methods, approaches to application and use in different clinical situations. Clear orthodontic appliances fully or partially cover the teeth's surface, unlike traditional orthodontic appliances and systems. Thus, aligners, by their design features, have the ability to treat a large number of orthodontic anomalies [295]. Initially, the CAT system was designed to correct small anomalies in tooth position. To this day, however, some clinicians continue to adhere to this concept and use aligners exclusively to bring orthodontic treatment to perfect occlusion in the final stages of treatment [54, 64, 91, 295]. More and more clinicians use additional retention elements, so-called attachments, consisting of composite material and fixed to the teeth through a special matrix of soft thin plastic according to a strict protocol [42, 95, 294].

Success in modern digital dentistry is largely driven by prediction, accurate calculations, and digital examination techniques. Despite the wide variety of orthodontic appliances available, most patients today prefer comfortable and aesthetic aligners [197, 226]

The shapes and sizes of the attachments are prescribed by the researchers. Currently, protocols have been created for each type of tooth movement as well as for

each specific task. Today, protocols for attachments are constantly being modified [42, 126, 272]. Initially, attachment design was simple, but since the use of finite element analysis (FEA), more and more types, shapes, and sizes of attachments have been introduced into treatment protocols [164].

Aligners can be divided into two types according to the type of manufacturing:

- 1) thermoformed aligners,
- 2) aligners made by direct printing on a 3D printer [158].

The plasticity index of 3DPIN material (29.4%) used in direct printing indicates the material brittleness, it was much lower than that of Invisalign (40.0-40.8%) and conventional thermoformed mouth guards (34.0-35.9%) (20-22), showing more elastic behaviour. At the same time, the relaxation index of the direct-printed material was much higher compared to Invisalign thermoformed materials, which is the reason for the rapid attenuation of orthodontic forces [62]. In addition to the worse physical properties compared to the thermoforming material, there are larger inaccuracies in the thickness of the aligners. This is due to the process of manufacturing clear aligners directly using 3D printing. In the process of printing the aligners on a 3D printer, it is not possible to guarantee a stable aligners thickness, which can negatively affect their clinical applicability [93].

According to the researchers, 3D printing technology is a suitable way to manufacture clear aligners and offers a number of advantages over the conventional thermoforming process. The currently published literature on direct-printed clear aligners shows that such a process is technically possible. However, a material ideally suited for this purpose does not yet exist. There is also a need to develop software adapted for this purpose. For this reason, no clinical studies using printed aligners have been conducted. Based on this, further in vitro and in vivo studies are needed to test these new technologies and materials. Particular attention should be paid to the cytotoxicity of printable resins. It is also necessary to calculate the clinical performance of directly printed clear aligners in

order to compare with the data obtained for thermoformed aligners [277]. Direct printing of clear aligners offers great opportunities to create modified topologies of aligner designs and the possibility of printing both functional and aesthetic aligners without compromising one or the other. This will be possible in the future if a suitable material with full biocompatibility and no cytotoxicity is created [103].

Clear aligners are currently the most technologically advanced part of orthodontics, but unfortunately, the least studied. The biomechanics of clear aligners are based on the biological processes of the body, but the principles of working with aligners differ from the traditional bracket technique. The treatment of patients with clear aligners utilizes virtual planning, which allows the clinician to determine the sequence of tooth movements leading to the final occlusion in the program before even one tooth is moved. This requires a paradigm shift in the thinking of the clinician, who must now "start at the end". Each treatment option can be visualized in terms of length of treatment, degree of difficulty in moving the teeth, and treatment outcomes.

The clinician and the patient can then choose the treatment option that best meets their goals [138, 272].

It is important to know and understand the principles of braces systems, archwire sequence order, the mechanics of the additional elements, but it is equally important to know and understand the principles of individualization of clear aligners. In order for treatment with aligners to be successful, an individualized approach is required. The clinician must take advantage of all possibilities to modify the aligners by adding structural elements during the clinical appointment [56–58].

In the process of creating a button or notch type retention element with a thermoforming tool, structural changes occur in the aligner itself where the elastics are attached. These deformations lead to an incorrect load distribution, which in turn slows down tooth movement and stresses the oral mucosa. These negative effects can be eliminated by adding additional structural reinforcements.

The mathematical calculation makes it possible to visualize the quantitative loads that are necessary for optimal tooth movement with the least amount of time.

The solution consists of many small interrelated problems, so-called finite elements, and is only an approximation, since the overall complex problem is too complex to compute. The finite element is accurate in modelling and adapts to the topology of the model under study, which is an effective method of engineering analysis. To date, this method has been widely used in medicine and is successfully used in calculations of individual aligner designs [111].

Using a mathematical model derived from the discretization of solids in CAD in three dimensions, finite element models contribute to the understanding of the biomechanics of orthodontic devices because they allow the estimation of stresses that occur in various tissue structures, such as the alveolar bone, periodontal ligament and teeth during treatment. Similarly, loading and displacement patterns can be determined using FE models depending on the device used [68, 134, 159, 205].

Bodily teeth movement in orthodontics has been widely studied and recognized as extremely complex because it implies that the applied force must pass through the centre of resistance of the tooth. Consequently, body movement of a tooth requires a complex system of forces and momentum forces to be applied to the tooth [176].

Orthodontic movement techniques based on thermoformed plastic aligners have demonstrated limitations in the configuration of complex force systems, such as extrusion of central incisors, rotation and tilt of canines, and body movement of teeth [174]. The need to overcome these limitations has led to the development of biomechanically "enhancing" composite attachments bonded to the tooth surface. These additions increase the biomechanical capabilities of aligners, allowing for more complex force systems, usually involving pairs of forces. The biomechanical nature of these innovative instruments must be understood in order to support protocols for their use and it must be evidence based. FEA models applied to new orthodontic techniques based on aligners

give better understanding of their theoretical efficiency, allowing for improved understanding in clinical settings.

To fully understand how thermoformed appliances work, two fundamental differences are needed to be known:

- In traditional orthodontic tooth repositioning, a force is applied to the bracket that transfers it to the tooth structures, creating a mechanical-biological chain of events that causes the tooth to shift.

- When teeth are relocated using aligners, an intentional, predetermined "mismatch" between the aligners and the teeth is set at each stage of treatment using a virtual model. The aligner corresponding to the new tooth position is placed on the dental arch, creating, with each mismatch, a system of forces that is directly transmitted to the tooth, creating a similar chain of events leading to the new tooth position [123].

Notably, a better understanding of material properties leads to the most accurate tooth movement sequencing and, as a result, more effective treatment. It has been shown that there is a wide variety of initial force mechanism systems during treatment with clear aligners. Because an aligner with a high initial force can be followed by an aligner with a low force, this results in inconsistent tooth movement. Furthermore, as aligner sequence order increases, deformations of aligners associated with force transfer also increase. There are studies showing that the orthodontic force generated by a thermoplastic material closely correlates with its hardness and modulus of elasticity; consequently, differences in the physical and chemical properties of clear aligners influence which aligner system the practitioner chooses.

The physical and material chemical properties have a direct influence on the treatment outcome. Patients who wore aligners made of harder material for two weeks of activation showed the best results for all parameters of tooth alignment and occlusion in general [33, 94].



It is also important to determine if the material properties change after use, as biofilm modification and oral environmental conditions can affect the hardness and material viscoelasticity. Because aligners are exposed to salivary enzymes, other oral byproducts, and various fluids during wear, and there is the possibility of damage caused by swallowing, speech, and bruxism [45, 65, 66, 230, 235]. The manufacture of clear aligners is based on the use of clear thermoplastic materials with suitable physical, chemical, and mechanical properties [82, 318].

The mechanical properties of polymers play a decisive role in the effectiveness of the therapeutic treatment. Low stiffness, good deformability, dimensional stability, and high biocompatibility are the conditions that the polymers used must meet. Orthodontic strength results from the aligners' deformation and from their elasticity. Therefore, orthodontic strength is directly dependent on the aligner material chemical composition, the arrangement and polymer chains orientation in it, the thickness of the aligner design, and the clinical protocol in which the amount of tooth movement is laid down [112, 127, 129, 148, 165, 171, 188, 190, 191, 253, 265]. The ideal aligner material should be clear, create sufficient mechanical force to induce orthodontic tooth movement in a strictly controlled manner, and at the same time it should not damage the surrounding periodontal tissues [112].

Polyethylene terephthalate glycol (PETG), Polycarbonate (PC) and Thermoplastic polyurethane (TPU) are mainly used to modify the properties of aligners [82, 129, 188, 193] PETG, a noncrystalline amorphous polyethylene terephthalate (PET) copolymer, has good mechanical properties, high wear resistance, dimensional stability and solvent resistance [29, 52, 82, 92, 116, 148, 188, 318].

The glycol group (G) is added to the main chain of the copolymerizing agent, which is a composition consisting of 31% mol 1,4-cyclohexylenedimethylene terephthalate (PCT) and 69 mol% PET. PETG has almost the same glass transition temperature ( $T_g$ ), deformation behaviour, and optical properties as PET, but it does not exhibit the

deformation-induced crystallization behaviour of PET at the production temperature [26, 138, 193, 235].

Polycarbonate (PC) has excellent mechanical strength, low water absorption and transparency, making it a very suitable material for orthodontic applications. Its properties are very similar to those of polymethyl methacrylate (PMMA), but polycarbonate has higher mechanical strength and can be used in a wider temperature range [318]. Polycarbonate is also highly clear in the visible light spectrum and offers higher light transmission than many types of glass [129].

Polyurethane (PU) is another flexible polymer, which is resistant to oil absorption and mechanical abrasion. Its properties are highly dependent on the raw materials which were used in production [55, 154, 177, 201, 202, 223, 252, 260].

Thermoplastic polyurethane (TPU) is one of the most universal engineering thermoplastics with elastomeric properties. TPU is easy to process, it has excellent physical properties, chemical resistance, abrasion resistance, adhesion properties [108, 194].

The mechanical properties of dental polymers are influenced by many factors, such as structural factors (molecular and crystalline structures, etc.) and environmental factors (temperature, humidity, etc.). The polymers used are usually either amorphous or semi-crystalline. Amorphous polymers usually appear clear because visible light can pass through them, whereas many semi-crystalline and crystalline polymers are opaque because they consist of a mixture of crystalline and amorphous phases with different refractive indices. The crystalline phase in semi-crystalline polymers can serve as a reinforcing mesh to improve mechanical properties in a wide range of applications. Low crystallinity polymers generally mean: high flexibility, high elasticity, good adaptation to tooth morphology. On the other hand, polymers have low tensile strength, low chemical resistance and stability [82]. Clinically, polymers with high flexibility and elasticity are more comfortable for patients when inserting or removing aligners. They also adapt better

to the complexity of tooth morphology and adhere perfectly to any surface. Compared to rigid material aligners, they also provide continuity of force reproduction during orthodontic treatment.

Eight thermoplastic materials used for orthodontic appliances are listed in table 1.

Table 1. Materials used in the manufacture of aligners

EVA	ethylene vinyl acetate copolymer
PE	polyethylene
PETG	polyethylene terephthalate glycol
PP	polypropylene
PC	polycarbonate
A+	copolyether
C+	copolymer of polypropylene and ethylene
PUR	polyurethane from methylenediphenyldiisocyanate and 1.6 hexanediol, additive

The tensile yield strength of the polymers under study can be distributed as follows:  $PC \geq PUR > PETG \geq A+ > PP \geq C+ > PE \geq EVA$ . This can be interpreted by the degree of crystallinity of the respective polymers. PC, PETG, A+, PUR as amorphous polymers show higher tensile yield strength than PP, C+, PE and EVA, which are semi-crystalline.

In addition to the structural influence on the mechanical properties, the glass transition temperature ( $T_g$ ) also plays an important role. Amorphous and semi-crystalline polymers, which behave similarly, have a lower  $T_g$ . Their mechanical behaviour is generally stiff and glassy. Above  $T_g$ , the behaviour of amorphous and semi-crystalline polymers changes partially. Amorphous polymers soften and can become flexible elastomers or even viscous liquids. Semi-crystalline polymers also soften and can become

flexible, depending on their degree of crystallinity [253]. Generally, the crystalline phase of a semi-crystalline polymer that is well above  $T_g$  can also disappear due to melting.

This means that the mechanical properties of polymers with  $T_g$  at room temperature can be strongly influenced by changes in temperature. Another factor affecting the properties of polymers is the molecular orientation of the polymer chains.

Thus, the mechanical properties of polymers depend on multiple factors, ranging from the phase state of the polymers (crystalline or amorphous), their water absorption capacity, their molecular orientation and their processing sequence, as well as their application conditions [28, 55].

A high modulus of elasticity is preferred for aligners because it increases the ability of aligners to transmit force under constant tension. In addition, materials with a higher modulus of elasticity can provide the same forces at a smaller size [31].

The thermoforming process affects the mechanical properties of clear aligners [31, 61, 253].

After thermoforming, the yield strength and modulus of elasticity of the polymers studied were found to decrease. The authors attribute this behaviour to a decrease in molecular weight due to heat treatment, molecules orientation and rapid cooling, preventing further polymers crystallization and causing residual stresses.

Ryu J. et al. investigated the effect of thermoforming on the physical and mechanical properties of clear mouthguard materials. They observed that the optical transparency, tensile strength and modulus of elasticity of the alignment materials decreases after the thermoforming process, while water absorption increases. Materials subjected to temperatures higher than their respective  $T_g$  can easily deform and reduce in thickness. The crystallinity of thermoplastic materials changes after thermoforming resulting in changes in mechanical properties.

Thus, these authors concluded that material properties such as transparency, water absorption and solubility, surface hardness, bending and elastic moduli as well as tensile and bending forces can change significantly after thermoforming [128, 254].

Although polyurethane is biocompatible, it is not an inert material as it is sensitive to heat, moisture and saliva enzymes. No by-products were detected after storage of Invisalign aligners in artificial saliva or ethanol solution for aging. In addition, no evidence of cytotoxicity or estrogenicity was detected at different aligners' eluents concentrations. This may be due to the material structure as it consists of polyurethane with the addition of methylene diphenyl diisocyanate and 1,6-hexanediol. The diphenyl structure provides stability and sufficient reactivity to form a polymer without any by-products. In addition, unlike the aromatic rings in bis-GMA, the polyurethane has short rigid parts connected by short flexible joints and long flexible parts. However, in vitro test conditions may have underestimated the chemical material stability.

Thus, a thorough literature analysis was carried out, the design of mathematical models available in studies by other authors was studied, in which most anatomical structures and elements (bone density difference - compact plate and porous bone tissue, paradental ligaments and homogeneity of tooth structure - without the enamel- dentin- cement division) were taken into account. Nevertheless, it has to be stated that the proposed variants do not fit the goals and objectives [84, 123].

### **1.3 Mucosa biotype significance in orthodontic treatment**

One of the main directions of modern dentistry is the oral mucosa biotype determination. This is important for developing an effective treatment plan and minimizing potential complications such as gingival recession.

Gingival recession is a common gingival disease with different aetiologies and is manifested by a gingiva vestibular margin displacement in the apical direction with further exposure of the tooth root surface.

Gingival biotype is defined as the mucosa thickness in the vestibular direction. Gingival biotype plays a key role in predicting success and preventing complications in orthodontic treatment [27]. Precise planning is therefore necessary, which gives predictable and stable results [7, 17, 155, 160]. If there is a wide area of keratinized attached gingiva, optimal periodontal health is maintained, preventing the spread of inflammation. If the keratinized zone of attached gingiva is not wide enough, it may lead to the development of destructive processes and the occurrence of recession. A certain correlation between the keratinized attached gingiva width and the periodontal biotype has been identified [268].

Most authors and clinical orthodontists divide the gingival biotype into two types: thick and thin.

The thin gingival biotype is characterized by high interdental papillae with local proximal contacts.

The average attached gingiva thickness is 1 mm.

The thick biotype is characterized by smoother gingival contours, interdental papillae are short and wide, and the average thickness is 1.5-2 mm [328].

However, a number of authors believe that there is a transitional biotype of gingiva - medium [241, 263]. Authors characterize it as transitional between the thick and thin gingival biotype with an average value of 1.5 mm. Maria N. et al. conducted studies in

which they proved the impossibility to attribute the oral mucosa to any particular type, and introduced the definition of a mixed type, which includes a combination of several phenotypes at once [107]. The thin gingival biotype presents the greatest difficulty in treatment planning and obtaining a stable aesthetic and functional result due to its low collagen content and a smaller keratinized attachment zone than in the thick phenotype [27, 151]. According to the authors, the true-thin gingival biotype occurs in two thirds of patients [250].

In addition to the standard methods for determining the mucosa biotype for the entire oral cavity, a number of authors have observed that the difference in mucosal thickness on the maxilla and mandible is different. After measurements, a significant difference was found between the thickness of mucosa on the maxilla and mandible [38, 86, 199, 215, 251, 289].

Thick and thin gingival biotypes exhibit differing histological structures, impacting orthodontic treatment planning and likelihood of complications. This issue is one of the most discussed and researched in the field of periodontics and affects all areas of dentistry. The methods for examining the gingival biotype also differ in each author according to their work and the possibilities of the least invasive and more efficient and provable way to determine the necessary correlations of complementation and gingival thickness. Also, depending on the need, different authors use gingival biotype classifications according to the procedures performed or out of personal preference, which in no way affects the manipulation performed by specialists [21, 50, 106, 109, 157, 161, 172, 207, 209, 262].

In clinical practice, special attention is paid to the thin gingival biotype; in orthodontic treatment, patients with a thick mucosal biotype may develop a local form of periodontitis; in the case of a thin biotype, recession is much more likely, as loss of tooth-end attachment leads to marginal inflammation and resorption of the alveolar wall.

“Colour-test №1”, which contains iodine, potassium iodide and base, is used to assess the degree of inflammation of the mucosa - the Schiller-Pisarev test. When the oral mucosa is inflamed, the amount of glycogen increases. The Schiller-Pisarev test is based on the ability of glycogen to stain when interacting with iodine-containing solutions

To characterize the inflammation, a specially developed colour grading was used: the test is negative if the gum turns light yellow; weakly positive - when stained in a light brown colour; positive - when stained in a dark brown colour.

#### Determining the Schiller-Pisarev test's numerical value

To determine the inflammatory process depth, Svrakov L. and Pisarev Yu. suggested lubricating the mucous membrane with iodine-iodide-potassium solution. In areas with deep damage of the connective tissue are being stained. This appears due to the accumulation of a large amount of glycogen in inflammation areas. The test is relatively sensitive and objective. When the inflammatory process reduces or stops, the colour intensity and its area is decreased.

When examining the patient, the gingiva is smeared with the specified solution. The degree of staining is determined and areas of intense gingival darkening are recorded in the examination chart, for objectification it can be expressed in numbers (points):

staining of gingival papillae - 2 points

gingival margin staining - 4 points

coloration of the alveolar gingiva - 8 points

The total score is divided by the number of teeth examined (usually 6). The iodine number is equal to the scores sum of each tooth divided by the number of teeth examined [278]. The evaluation of the Svrakov iodine number is shown in table 2.



Table 2. Schiller-Pisarev test digital value

mild inflammatory process	<2.3 points
moderate inflammatory process	=2.3-5.0 points
intense inflammation	=5.1-8.0 points

The Papillary-Marginal-Alveolar Index (PMA) indicates the severity of periodontal tissue inflammation. The index can be expressed in absolute numbers or as a percentage.

To determine the PMA gingival index, the gingiva is divided into three areas:

Papillary (P), Marginal (M), and Alveolar (A).

Numerical assessment of the inflammatory process is made as follows:

Inflammation of the papilla - 1 point;

Inflammation of the gingival margin - 2 points;

Inflammation of the alveolar gingiva - 3 points.

Evaluate the condition of the gingiva of each tooth.

$$PMA = \frac{[(\sum score) \times 100\%]}{3 \times (teeth amount)}$$

An index value of up to 30% indicates a mild inflammatory process; 30-60% indicates medium severity of gingivitis; more than 60% indicates a severe pathological process [115].

Before starting orthodontic treatment, it is necessary to ascertain the initial status of the orthodontic patient and his readiness for treatment. In most cases, if hygiene is unsatisfactory, the patient is taught oral hygiene and scheduled for the next visit to check hygiene indices. With poor oral hygiene during orthodontic treatment, complications

associated with inflammatory processes of the oral mucosa will occur. In addition, in the presence of oral mucosa inflammation, errors will inevitably occur in determining the oral mucosa biotype before the start of orthodontic treatment and, accordingly, in the choice of treatment tactics. According to Arsenina O. [2], only 10% of patients had an unsatisfactory status with signs of oral mucosa inflammation. At the same time, hyperaemia and gums swelling, bleeding during probing were noted. 27% of patients experienced periodontal complications during orthodontic treatment [8, 9, 11, 22, 40, 173, 178, 257, 296].

#### **1.4 Application of AI in segmentation of 3D models from CBCT data**

Cone Beam Computed Tomography (CBCT) is widely used in dentistry. It can record extensive information about the upper jaw and facial region. Thanks to the coordinates of voxels and grey value information, many details of the labelling can be effectively detected. CBCT has been used to detect bone density, resorption and enlargement in three dimensions. In implant dentistry, there are many methods to study bone repair and reconstruction [131]. In addition, periodontal conditions and tooth root shape are also attracting increasing attention [163]. The use of 3D segmentation and reconstruction technology is gradually being applied to restore the anatomical teeth structures and surrounding tissues.

The modern development of technology has made orthodontics one of the fastest growing fields of dentistry [204]. All of this has been made possible by the significant evolution of 3D imaging equipment and the development of image processing techniques.

The occurrence of aligners in 1997 has subsequently had a major impact on the development of orthodontics. These devices take into account the individual anatomy of the teeth and can perform tooth movement with optimal forces that are safe for the periodontium [203]. The teeth movements in this case are more physiological, and the

resulting therapeutic effect is most individualized and corresponds to the dental arches shape and the surrounding soft tissues.

The rise of artificial intelligence has captivated the global research community, marking the past decade as a pivotal era of technological progress. Artificial intelligence has been embraced enthusiastically in every industry, including dental science [221]. As the amount of patients' information and data grows exponentially, the need for advanced software to collect and store this data has become increasingly crucial.

The field of digital dentistry is experiencing significant growth due to the rise of AI in health care. With the continual advancement of AI technology, we can anticipate that AI will have a substantial impact on dentistry in the future, offering numerous advantages for dental clinics and patients alike. Moreover, recent studies indicate that AI may significantly affect job markets by replacing or repurposing certain professions. By implementing AI tools in dentistry, the occurrence of human errors and costs can be significantly reduced.

The use of a computer neural network (CNN) in orthodontic practice takes the treatment process to a higher level. The process of individualizing the aligners' topology is taking place.

Recent studies has shown that using convolutional neural networks in the case of computerized cephalometric analysis, the results are better than when performed manually by a radiologist or orthodontist [119, 184, 236]. Many studies on automatic identification of 19 cephalometric landmarks on x-ray cephalometric images have been described in the literature.

It is shown that AI can automatically find anatomical landmarks on X-ray cephalometric images with a very high accuracy. The use of CNN on panoramic images in the future may be superseded by more informative three-dimensional CBCT examinations. This is due to the fact that the accuracy of two-dimensional images is

lower, and the price difference between three-dimensional and two-dimensional radiological examinations is becoming smaller.

In preparation for orthodontic treatment, neural networks are used that can perform CBCT analysis and identify upper and lower jaw bone abnormalities, bone level, or the location of retained teeth. Digital model analysis is becoming increasingly important in orthodontics. Convergent neural networks are used to solve various tasks related to tooth segmentation and digital model analysis. Raith S. et al. [239] present a method to classify teeth with sufficient accuracy using an artificial neural network (ANN). This technique is also used in modern software.

Digital models of teeth obtained with an intraoral scanner are a single object, like a plaster model. Therefore, each tooth must be separated (segmented) is a software. Once the occlusal plane is determined, each tooth is aligned by moving and rotating according to established algorithms and tooth movement norms. Currently, artificial intelligence methods are used to automate the process of tooth segmentation and alignment in digital set-up programs [282]. The Autolign software (Diorco.Co., Yongin, South Korea) automatically segments teeth and determines the front axis of the clinical crown (FACC), the most prominent part of the central lobe on the front surface for incisors and premolars, and the buccal sulcus for molars [39]. Once the FACC of each tooth is determined and the occlusal plane and desired arch shape are set, the alignment of the teeth is done automatically by the software. This type of software requires the user to view the axes of each tooth, set the occlusal plane and determine the arch shape before alignment, which can be considered a semi-automatic method of creating a clinical set-up. Fully automated software automatically segments and aligns teeth based on intraoral scan data. Outcome Simulator Pro software (Align Technology, Inc., Arizona, USA). Ortho Simulation (Medit, Seoul, South Korea) is another example of fully automated set-up modelling software. Similar to Outcome Simulator Pro, Ortho Simulation is built into the Medit intraoral scanner software and uses scans obtained exclusively by Medit, i500 and i700 scanners. After importing the scan data, the clinician must identify the midlines of the

upper and lower teeth. The software then recognizes each tooth number and performs segmentation. With advances in artificial intelligence technology, digital set-up software is evolving rapidly, making it possible to automate previously manual tasks such as segmentation and tooth alignment. Previous studies have shown that digital set-up models performed manually by physicians have a high level of reliability [47, 149]. However, there have been no studies evaluating the effectiveness of automated programs for creating setups.

The digital set-up model can visualize the final occlusion of the orthodontic treatment, making accurate diagnosis and treatment planning possible. In complex cases, such as tooth retention, it can be used in combination with other types of patient data, such as clinical photographs, radiographs and CBCT. It can also be used to virtually simulate surgical procedures for patients with skeletal malocclusions who are about to undergo orthognathic surgery [290].

To automate the tedious tasks that clinicians must perform, modern CAD/CAM technology for the digital set-up has been supplemented by artificial intelligence algorithms. Tooth segmentation is the most important task for the reconstruction of a 3D tooth model. Since digital models use tooth segmentation techniques in which the mesiodistal width registration and the tooth approximal surface depends on the surface data, so areas that are not scanned can be registered inaccurately [150].

Close contacts between teeth, misalignment, and crowding can make automatic tooth segmentation time-consuming and difficult [185]. Advances have already been made in automatic segmentation algorithms using machine learning and deep learning. Kim T. et al [167] proposed an automatic segmentation tool with reconstruction of missing interdental data for intraoral scanner using generative-adversarial networks and reported a high level of accuracy obtained (figure 1, 2).



Figure 1 - Anterior segment crowding on a three-dimensional model of the mandibular dentition



Figure 2 - Missing data of interdental areas

In contrast to the rather large number of studies in the field of automated dental segmentation, little research is devoted to algorithms for automated tooth alignment. Fully automated software is stated only for consulting purposes.

A key problem is the heterogeneity of human morphology and different cultural norms of aesthetics, which can significantly influence the therapeutic process. Each patient has a different set of illnesses, uses different medications, suffers from genetic diseases, past trauma, and hospitalizations, leading to a variety of therapeutic combinations [203]. After collecting the patient's medical history, examining the patient, and performing additional studies such as diagnostic models, CBCT, and cephalometric radiographs, an individualized treatment plan is prepared. Sometimes the patient may not agree to the proposed treatment plan [245]. Then, the orthodontist may suggest an alternative treatment plan, which further increases the number of therapeutic combinations. Another problem is patient compliance. The resulting therapeutic effect

depends on the patient's cooperation and may not be sufficient due to poor oral hygiene, improper aligners use and care, and also due to insufficient long-term appliance wear [120].

Neural networks, inspired by the human brain's structure and function, are a collection of algorithms designed to uncover hidden patterns in data. These networks, composed of interconnected neurons, can be either organic, found in the human brain, or artificial, created through algorithms [292].

Most neural networks (NN) are limited to performing only one regression or classification task at a time. However, multiple NNs have the ability to simultaneously carry out multiple tasks of this nature. While in the majority of cases, the network will have a single output variable, in complex classification problems; it may involve multiple output units (which are then mapped to output variables during the post-processing stage). The artificial neural network (ANN) relies on various critical elements such as the unit's input and activation functions, network design, and the weight assigned to each input link [63].

If the initial two features remain fixed, the artificial neural network (ANN) behaviour is solely influenced by the current values of its weights. Initially, the weights of the training network are assigned random values, and subsequently, instances from the training set are exposed to the network at regular intervals. The input values for each instance are inputted into the input units, and the network output is compared to the desired output for that particular instance. Following this, the weights within the network are adjusted accordingly.

In order for the neural network to solve orthodontic problems effectively, an appropriate amount of patient data must be uploaded. In the case of rare anomalies, the amount of data available will not be sufficient for the AI to recognize them, which will take a long time for the neural network to be able to solve clinical problems at the same

level of efficiency as the orthodontist. The last problem in training a neural network is the time the orthodontist has to spend annotating DICOM, JPG, PNG, and STL files.

The current application of convolutional neural networks in orthodontics highlights the wide range of applications of deep learning methods. The results of our research indicate the significant superiority of deep learning methods in orthodontics over other high-performance algorithms. Based on these results, deep learning methods are expected to play an important role in the field of orthodontics in the future.

There are certain protocols for force calculation methods for the fabrication of aligners. These protocols also develop special elements for aligners, the so-called attachments, which are subject to continuous improvement [138, 272]. With the advent of new examination methods, computerization and data processing, treatment protocols are being developed that allow the best possible simulation of the hardware (aligners, beneslider, hirex) [297]. However, now, some examination techniques need to be refined.

In orthodontics and periodontics, there are methods to study the development of bone resorption and recession. Al-Zahrani M. et al. [36] and Chen Y. et al. [77] used CT data to analyse the progression of periodontal disease. The patient's alveolar bone might have resorption due to the disease progression and may result in the displacement or weakening of several teeth surrounding tissues. Thus, CBCT can provide information about bone tissue to help clinicians detect signs of periodontitis. Precise tooth segmentation can be used to analyse changes in periodontal disease such as periodontal ligament and bone resorption of a particular tooth.

In orthodontic treatment, physicians typically use medical imaging software such as MIMICS (Materialize, Belgium) and AMIRA (Thermo Fisher Scientific, France) to segment teeth and bone. According to the segmentation results, doctor can create several relevant clinical treatment plans. The software can implement automatic threshold segmentation based on grey density values, but automatic segmentation cannot



implement full tissue segmentation. Deep learning is a branch of artificial intelligence that has many advantages for fast and accurate data analysis.

There are three types of tooth segmentation methods: the threshold method, the active contour model method, and the neural network method [140]. The threshold method is based on different grey values between the tooth and the periodontal ligament. The main issue for this process is to obtain the optimal threshold differences; however, the optimal threshold for different samples is different. Therefore, for different samples, the optimal threshold should be re-examined. Heo H. et al. proposed an optimal threshold scheme for tooth segmentation [139]. However, the tissue near the tooth root is complex, making it difficult to distinguish alveolar bone from the root using a single threshold range. Akhoondali H. et al. proposed a fast and automatic segmentation method using the region augmentation method [30]. Since the grey values of cancellous bone and cortical bone close to the root are the same, the teeth cannot be segmented automatically. The active contour method is an interactive segmentation method based on contour reconstruction. Tooth contours are indicated by the shortest diagonal method or levelling algorithm, and the 3D tooth model is a reconstruction of the tooth contour [37, 46, 101, 113]. A study of tooth segmentation combining morphological features showed that the actual measured root mean square value is 0.39 mm, which is less than 0.4 mm [307].

Lee S. et al. [182] used a histogram-based method as a pre-processing step to calculate the average level of grey density in the bone and tooth regions. Simultaneously, they developed a posterior probability function (PPF) with CNN models to improve segmentation performance. The experimental results showed that the proposed method is better than the existing methods. In addition, Lee M. et al. examined the effect of metal artefacts during segmentation by adjusting the position of the teeth, marking all layers of two CBCT samples and five layers of other CBCT, and then sequentially moving to the teeth. The results showed that the used convolutional neural networks can reduce the area of mutual overlap between blocks [78].

Since the values of the Hounsfield units (HU) of different CBCT images are inconsistent, various methods of segmentation correction are used during segmentation [228]. This study used a U-net model to segment CBCT data for dental hard tissues, pulp cavity, cortical bone, and cancellous bone simultaneously. Generative adversarial networks (GANs) can be applied to medical images as training samples to eliminate the over-learning problem [76].

### **1.4.1 Deep learning**

Deep learning (DL) is a subset of machine learning that allows you to extract relevant features from data. These models are based on artificial neural networks with several consecutive layers: input, output and hidden layers to mimic the human brain functioning. DL is an important tool for data scientists because it allows them to make quick decisions and perform calculations. DL has now achieved high performance in a variety of applications, including the segmentation of cranial bone structures and individual teeth.

This section provides basic information about DL networks and model training methods. In addition, various metrics are described that are used to quantify the performance of automated segmentation algorithms.

### **1.4.2 Segmentation of medical images**

#### **1.4.2.1 Convolutional neural networks**

Convolutional Neural Networks (CNNs) are well-known deep neural networks used for image analysis. They have made great strides in the field of diagnostics. A typical CNN contains an input layer, a stack of functional layers, which typically includes convolutional layers, pooling layers, and fully connected layers, and an output layer. Basically, each convolution applies an  $n \times n$  kernel (for a two-dimensional input)

or an  $n \times n \times n$  kernel (for a three-dimensional input). This operation is especially useful for getting local templates, i.e. visual elements in images. The convoluted output then goes through batch normalization (BN) [152], followed by a non-linear activation function to perform feature map extraction, then down sampling by layer merging to capture a larger field of view. Further, fully connected layers are used to reduce the dimension of features and achieve high-level reasoning [117, 141, 152]. The final result is a fixed-size vector, where the shape of each element depends on the specific task (object localization, image classification, regression, patch-based segmentation, etc.). Increasing the depth (laying many hidden layers) may or may not significantly improve accuracy, depending on the problem complexity.

CNN can be used for image segmentation problems [169, 213, 321]. However, for this task, each input image must be patched and then the CNN must be trained to predict the class label of each patch's central pixel. The result is a pixel segmentation map for the entire image by sending patches at various positions in the CNN for classification. For reliable pixel segmentation, a fully convolutional neural network (FCN) is most commonly used.

#### **1.4.2.2 Fully convolutional neural networks**

Fully convolutional neural network (FCN) is a variant of CNNs that Long J. et al. [266] proposed for image segmentation. They are pioneering networks of the most advanced DL techniques for volumetric segmentation of medical images [146, 249, 321]. For example, Zhou X. et al. [321] segmented anatomical structures on 3D CT segmentation images of several 2D FCN slices and achieved promising results contrary to expert predictions by many. FCNs have an encoder-decoder architecture. The encoder converts the input image into a high-level representation object. The decoder then interprets these feature maps and extracts spatial information for pixel prediction. Compared to segmentation-based segmentation CNN, FCN is trained on entire images, without requiring region selection. To improve segmentation accuracy, many FCN

variants have been introduced. U-Net [247] is the most common FCN variant for biomedical image segmentation. It uses the missing connections between the up-sampling and down-sampling paths to recover from the loss of spatial context, providing accurate segmentation.

The promotion of U-Net has become a central event in the segmentation of medical images. Various works on image segmentation described in the literature are based on U-Net and its 3D variants (3D U-Net [79] and 3D V-Net [210]), which provide high segmentation accuracy [275, 300]. Based on FCN, Badrinarayanan V. et al. [43] proposed an encoder-decoder architecture called SegNet for image segmentation. While SegNet passes the maximum union indices to the layers with increasing sampling, FCN studies deconvolution filters to increase sampling (i.e. adds a relative map of objects from the encoding phase).

### **1.4.2.3 Recurrent neural networks**

Recurrent neural networks (RNNs) are artificial neural networks used to process sequential data, such as ultrasound image sequences and MRI [325]. RNNs store the previous output data and use their internal state to make a decision when processing the next input data. The fusion of RN and 2D FCN is widely used in the segmentation of medical images to improve the intersectional coherence of the generated segmentation [233].

### **1.4.2.4 Autoencoders**

Autoencoders (AE) are unsupervised neural networks, which are learning for compact hidden representations from input data. The architecture of a classical autoencoder contains two main networks: an encoder network that compresses the input data and produces code and a decoder network to reconstruct the data back into the input dimension using that code. Since the representations under study typically include useful information, a group of researchers have used autoencoders to extract common semantic

features and shape information from the raw data to guide heart image segmentation [219, 314]. Oktay O. et al. [219] developed a residual convolutional network model to recover 3D volumes from a full stack of 2D images for better image analysis.

#### **1.4.2.5 Generative-adversarial networks**

Generative-adversarial networks (GANs), proposed by Goodfellow I. et al. [124], are based on generating a model for creating new synthetic images. GANs in the learning process are taught to generate using two competing networks competing with each other: generator networks and discriminator networks. The generator is designed to artificially create fake images based on the random noise it receives, while the discriminator is used to determine whether the image is “real”. GANs are successfully applied to segmentation tasks. The segmentation network replaces the generator. The discriminator is necessary in order to distinguish the generated segmentation maps from the gold standard maps [196, 258]. Lau F. et al. [179] proposed ScarGAN to simulate a certain area of an object and artificially increase training sets using the GAN chain. Training U-Net with simulated tissue scans yielded more accurate test image segmentation (80.5% vs. 75.9%).

#### **1.4.2.6 Advanced building models**

Recently, a group of researchers have implemented advanced plotting modules to explore improved features for accurate image segmentation. These modules have been widely used to improve the efficiency of image segmentation in previous neural networks. Therefore, we can talk about three different types of modern methods:

- a) extended convolutional blocks for a multi-level set of functions (for example, deep control [181] initial modules [271], extended convolutional cores [312], extensive integration of spatial pyramids [72]);
- b) adaptive convolutional cores to capture the most relevant functions (for example, attention blocks [283], compression and excitation blocks [145]);

c) interlayer connections to restore previous functions in the following layers (for example, residual connections [135], dense connections [34]).

### 1.4.3 Training neural networks

The learning process is the most difficult stage in the dl methods due to the calculations complexity and the configuration required to perform them. This process requires a data set that includes paired images and fundamental truths, an optimizer and a loss function. The model training is aimed at obtaining the best network parameters to reduce the loss function.

#### 1.4.3.1 Gradient descent Optimizer

A deep network contains millions of parameters representing a mathematical solution to such a problem. The trained network adapts to the learning process according to a certain set of parameters by optimizing many network attributes. In particular, gradient descent is an optimization algorithm to reduce the loss function. Various gradient descent optimizers have been developed (for example, Momentum SGD [237] AdaGrad [90], Adam [168]).

#### 1.4.3.2 Loss functions

During the training process, the network error is reduced using the loss function, which evaluates how well the training algorithm matches the data set. For this purpose, a suitable loss function is required to design and configure the network. Given a series of paired images and labels  $\{(x_i; y_i): i = 1...; N\}$ , the network learns the mapping link  $x \rightarrow y$ . Thus, it predicts the result ( $\hat{y}$ ) as close as possible to the fundamental truth ( $y$ ).

**Mean Squared Error Loss (MSE)**, also known as L2 loss, is the default loss function for regression tasks such as image reconstruction, localization of teeth or bone pathologies. MSE is defined as:

$$L_{MSE} = \frac{1}{N} \sum_{i=1}^n (y_i - \hat{y}_i)^2,$$

where  $y_i$ ,  $\hat{y}_i$  denote the vectors of the gold standard and predicted values,  $N$  represents the number of dataset samples.

**Cross entropy (CE)** is the most commonly used loss function for image classification and segmentation tasks. With multiclass segmentation for each class, this loss resumes pixel-by-pixel probabilistic errors between the actual gold standard map and its relative predicted result.

Specifically, for image segmentation, several researchers used the soft-Dice loss function [210], which is so penalized for the discrepancy between the actual gold standard map and the corresponding predicted segmentation at the pixel level.

Moreover, various variants of cross-entropy and soft-Dice loss functions (for example, weighted cross-entropy loss [49, 156] and weighted soft-Dice loss [166, 309]) are widely used to solve class imbalance problems in medical image segmentation tasks in which the loss value is weighted taking into account infrequent categories. Several other DL networks use hybrid losses in which various loss functions are combined (for example, focal loss [73], soft-Dice loss and weighted cross entropy) to alleviate the problem of class imbalance and thus improve the quality of segmentation performance [310, 311].

### 1.4.3.3 Reduce over-fitting

**Weight initialization** [122, 136, 211] is an important concept choice, the purpose of which is to prevent the disappearance or output data explosion of level activations in the process of direct transmission of DL networks.

**Dropout** [141, 270], a regularization method that avoids retraining by randomly deleting some nodes in DL networks at each iteration of training, is one of the widely used functions to improve network efficiency.

**Data augmentation** [69, 317] is an effective method used in model training, where it increases the amount of input data by artificially generating training images by applying a set of affine transformations to existing data.

**Transfer learning** is a deep network method that aims to reuse a model pre-trained on existing large datasets, using its knowledge gained for this task. The model can converge quickly even with limited data. Several studies have shown the potential of transfer learning in improving the generalization ability of the network for cardiac ventricles segmentation [74, 99, 166].

#### 1.4.4 Evaluation indicators

Indicators such as quantitative accuracy, output time, and memory usage can be used to evaluate the effectiveness of segmentation methods. In addition, Dice similarity coefficient or Hausdorff distance are often used to assess geometric similarity, which have proven to be good indicators for assessing geometric similarity. In this task, the volume difference indicator was calculated to evaluate myocardium 3D segmentation in order to visualize the approach effectiveness in terms of volume. With the help of quantitative indicators, several methods can be compared against benchmarks (manual contouring), qualitative results are important for deciding which method is the best.

**1. Dice similarity coefficient (DSC)** is a fairly well known indicator when checking the segmentation of medical images. It is commonly used to calculate the similarity between predicted maps and gold standard maps. The range of its values is from 0 (mismatch) to 1 (excellent match).

$$DCS = 2 \frac{|P \cap G|}{|P| + |G|},$$

where P, G denote predicted maps and gold standard maps, respectively

**2. Hausdorff distance (HD)** [208] calculates the degree of similarity between two sets of points: the distance between two boundaries of the gold standard and the predicted



segmentation. This is an additional statistic to the DSC. HD identifies segmentations with large local differences, although they were well segmented. A lower HD value reflects a higher segmentation performance. The indicator is defined as follows:

$$HD = (\max_{p_i \in P} (\min_{g_j \in G} (d(p_i, g_j))), \max_{g_i \in G} (\min_{p_j \in P} (d(p_i, g_j)))) ,$$

where  $P = \{p_i : i = 1; \dots; N_p\}$ ,  $G = \{g_j : j = 1; \dots; N_g\}$  denote the predicted maps and gold standard maps, respectively,  $d$  represents the distance between  $p_i$  and  $g_j$ .

**3. Absolute Volume Difference (AVD)** measures the average difference across a whole set of slices between the predicted volume and the gold standard.

Thus, DL caused a research boom and became the engine of development in the field of image processing. Various neural networks and several methods of model training are described above. A brief overview of the estimated indicators for image segmentation is given.

### 1.4.5 Modern methods of segmentation of medical images

Segmentation of medical images, i.e. the separation of an image into several specific sets of organs or affected organs using medical imaging techniques, is one of the most important tasks in the analysis of medical images, which helps doctors in making a diagnosis and making important decisions. In previous years, many researchers have used DL-based networks to segment medical images [70, 110, 133, 212, 231, 249, 280, 301, 303, 313, 315, 322]. Automated segmentation has surpassed the accuracy of classical segmentation methods, including the threshold value method [302], the boundary-based method [80] and the region-based method [132].

Tao S. et al. proposed a method of segmentation of dental images using the U-Net network, the attention module, SAP and CE modules. The experimentally demonstrated upgraded network showed better performance and efficiency of segmentation, which

eventually led to clearer tooth contours, which contributed to better diagnostics. The proposed method is intended only for segmentation of dental images and is not applicable in other areas [276].

Complex segmentation of the cranial bone structures (lower jaw and upper jaw) on computed tomography (CT) is necessary for diagnosis and treatment planning during surgical interventions in the skull and face, in orthodontics, as well as in therapy and endodontics. Traditional manual segmentation is time-consuming and complex due to such craniofacial region bones properties as a variety of anatomical structures, due to the low contrast of soft tissues and due to distortions caused by metal structures. However, segmentation methods, including deep learning, require a large and consistent data set, which in turn creates difficulties in their clinical applications precisely because of the limited amount of data. Various studies have proposed deep learning approaches for automatic segmentation of the lower and upper jaws on CT images by combining multicentre datasets. In Park S. research. Four multicentre datasets obtained under different conditions were used to create a scenario in which the model was trained on one dataset and evaluated on other datasets. A hierarchical, parallel and multiscale residual data block for U-Net (HPMR-U-Net) was developed for the neural network [293]. To evaluate the performance, segmentation was performed with its own data set and with external data sets from multicenters in comparison with three other neural networks: U-Net, Res-U-Net and mU-Net. The results indicate that the performance of HPMR-U-Net segmentation is comparable with other models, with excellent data compatibility [224].

Before using the CT data, their pre-processing is applied. A deep learning approach is used to reduce the impact of artefacts created by metals (MAR) on dental CT images. It includes training a segmentation network for metallic objects, correcting projection data using a segmented area, merging corrected and original CT images, and replacing metallic areas in the original projection data. The proposed method surpasses traditional methods of post-processing of data based on segmentation of metals in the area of CT images [137].

### **1.4.5.1 Common DL architectures for medical image segmentation.**

2D U-Net. Based on the FCN architecture, Ronneberger O. et al. [247] proposed a U-Net network for segmentation of biomedical images. This model includes a U-channel consisting of two paths of analysis (narrowing) and synthesis (expansion), as well as pass-through connections connecting the layers of the narrowing path with their expanding counterparts to provide them with the most important high-resolution functions. The network architecture uses two 3x3 convolutions, followed by a reactivation function and a maximum merge operation to reduce the size of the hidden image. The process is repeated until a single feature vector is obtained that is useful for reconstructing an image with probabilistically classified pixels for accurate segmentation by including the transmitted output data during the analysis path. The proposed network simultaneously combines low-level object maps to improve accuracy with high-level object maps to extract complex objects.

Due to its outstanding efficiency, U-Net and its variants (integrating new modules and other concepts) are widely used in many areas of computer computing [49, 125, 316, 320, 326]. For example, Gordienko Y. et al. [125] used a U-Net-based network for lung segmentation using X-ray scanning. Their design provided fast and accurate image segmentation. Farrag N. et al. [102] compared several automated integrated systems for sample segmentation on native and contrast-enhanced T1 maps. These authors proved that the U-Net architecture achieved better results than Dense Nets and Attention Nets, which indicates the reliability of the U-Net-based method in clinical applications.

### **1.4.5.2 2.5D methods**

Some networks performing medical image segmentation are based on 2.5D approaches. These approaches take advantage of 3D segmentation by integrating (partial) 3D information to improve segmentation, taking into account that this avoids problems with high memory consumption. One of the most common methods involves using a 2D

CNN ensemble to analyse three orthogonal views from different directions (i.e., axial, coronary and sagittal views). [234]. This 2.5D approach has richer spatial information about neighboring pixels with lower computational costs than 3D [320]. These studies have demonstrated slightly improved accuracy compared to 2D. Since a 3D volume is a stack of adjacent 2D slices (a 2D image with adjacent slices), other alternatives have integrated information about adjacent slices to create a three-dimensional temporal context to improve segmentation performance. For example, Ganayem P. et al. [114] connected adjacent slices to the central one as different input channels. Some authors have investigated a 2.5D design system combining 2D and 3D methods [305, 308].

Zheng Q. [319] used a U-Net-based architecture that provides spatially consistent results for the entire volume by spreading segmentation across slices to perform 2D segmentation. Moeskops P. et al. [213] proposed a 2.5D approach to assess whether a single CNN can perform multiple segmentation tasks. The authors proved this concept using several methods (for example, brain MRI, breast MRI and CT heart angiography) for each of the three segmentation tasks. Their results showed that such a system could visualize a variety of anatomical structures using several methods without special training. Other 2.5D approaches offered hybrid image segmentation using the DL network combined with statistical shape modelling. For example, Wang C. and Smedby O. [291] correlated the output of orthogonal 2D U-Nets with a preliminary volumetric shape for a better outline.

### **1.4.5.3 Fully volumetric approaches (3D approaches)**

The following describes two modern networks based on 3D data processing. Most of the authors have expanded the basic idea of 2D approaches and modified it for a more multidimensional space [79, 88, 210]. Compared to 2D and 2.5D approaches, three-dimensional images can provide complete 3D information in various orientations, rather than in one or three orthogonal views. However, these 3D networks face major challenges

due to their increased need for resources, stemming from the larger spatial parameters within the model, ultimately limiting their applicability.

#### **1.4.5.4 3D U-Net**

One of the most well-known variants of the U-Net architecture, complementing it with the most complete information about spatial consistency, is 3D U-Net, proposed by Çiçek Ö. et al. [79]. The authors expanded the U-Net architecture by replacing 2D operations with their volumetric counterparts. The proposed algorithm provided dense volume segmentation based on the studied sparse 2D annotations. He tightly segmented the new data. Extensive results have demonstrated its effectiveness in complex and highly variable 3D structures.

The emergence of 3D U-Net is of great interest for the processing of three-dimensional images. Many volumetric segmentation methods reuse the three-dimensional U-Net model [49, 100, 153, 227, 309]. For example, Fahmy A. et al. [100] proposed a 3D model based on U-Net with a sliding window for processing large stacks of input data. Yang X. et al. [309] developed a fully automatic network for segmentation of the sample structure. Their network is similar to [79], but they replace (the concatenation operator) the union operator with the Residual Module Residual Unit (ResU). Deep control feedback and learning transfer are used to improve the learning process. Using the Similarity Coefficient of Multi-class Dice (Multi-class Dice Similarity Coefficient), this network has achieved promising results.

#### **1.4.5.5 V-Net**

In paper [210], a V-Net model is proposed for segmentation of MRI volume based on volumetric CNN. The contribution of the authors is the creation of a new objective function based on DSC. They also used 3D convolutions with a core size of 2x2x2 and a step of 2. Convolutions replaced unions with a predominantly smaller amount of memory. The non-linearities of PReLU [136] were used throughout the model. Similar to [247],

the features extracted from the compression path were extended to the decompression path to obtain detailed information, which gives a two-channel volumetric segmentation on the last convolution layer.

The experimental evaluation demonstrated that the V-Net model achieved good results in the data set of test tasks [187]. For example, Vesal S. et al. [285, 286] conducted numerous experiments and performed interesting comparisons of V-Net, 3D U-Net and several variants of the latter, including a multi-stage approach, for multiclass segmentation in the ACDC dataset. Gibson E. et al. [118] proposed an architecture based on deep learning, known as DenseVNet, with a large receptive field for segmentation of eight organs. Compared to [210], DenseVNet obtained significantly higher DSC scores for all organs.

#### **1.4.5.6 FCN-based segmentation**

Tran P. [279] used FCN [267]. Their automated FCN-based method has achieved significant segmentation efficiency compared to classical methods in terms of speed and accuracy. Many more advanced FCN-based studies have been developed to achieve significant improvements in segmentation efficiency. Indeed, a lot of research has been done to optimize the architecture of the model in order to improve the learning potential of functions for segmentation [83, 99, 156, 166, 183, 316, 323]. For example, [166] is offered a dense U-Net with initial modules to combine large-scale capabilities for accurate image segmentation with wide anatomical variability. In [233] Poodle R. et al. developed a repeating FCN (RFCN) based on GRU, a type of LSTM [142], and FCN networks to study image representations from 2D image stacks and perform segmentation. RFCN combines detection and segmentation into a unique architecture. In numerous papers [73, 156, 256, 309] several loss functions have been proposed (for example, weighted cross entropy loss, weighted Dice loss and focal loss) for better segmentation. Due to motion artefacts in cardiovascular magnetic resonance (CMR)

scanning that limit the applicability of 3D segmentation approaches [49], most FCN-based networks use 2D architectures that do a better job in these cases.

#### **1.4.5.7 Temporal and spatial consistency**

Since 2D networks are used to process each 2D slice of an entire volume, instead of 3D volume, the main disadvantage of using 2D segmentation networks is that they work in layers without studying intersectionality dependencies. Thus, 2D models may not be enough to segment teeth into sections where the boundaries are not strongly delineated. Numerous studies have used additional contextual information such as preliminary forms [71, 326] to overcome this problem and thus improve 2D FCN segmentation. Several other methodologies have used recurrent neural networks and multi-slice models (2.5D models) [227, 233, 320] to introduce spatial constraints to improve slice stack segmentation. These models are also used to extract spatiotemporal information on cardiac cycle frames to improve segmentation efficiency [238, 258, 298, 306].

#### **1.4.5.8 Anatomical limitations**

When using only standard loss functions in the learning process, it may not be possible to extract the features of the corresponding anatomical structures. Thus, in various works, the advantage of integrating anatomical constraints at the training stage for ideal model prediction has been studied. These constraints, presented in the form of regularization conditions to account for prior knowledge (for example, topology [81], contour [71] and shape [220, 311, 327]), force the model to produce more accurate segmentation results. For example, Oktay O. et al. [220] proposed an anatomically constrained neural network model that includes prior knowledge of CNN-based segmentation using an autocoding network. Its output data is forcibly aligned with the nonlinear compact representation underlying the anatomy. Zotti C. et al. [327] developed

a GridNet-based network that first integrates the shape of an object to aid kinetic segmentation. In contrast to these models, Painchaud N. et al. [222] developed a variational AE (VAE) to refine the network output by correcting anatomically implausible segmentation masks at the post-processing stage.

#### **1.4.5.9 Multi-stage models**

Various automated networks have been developed using a multi-stage pipeline, dividing the main task of segmentation into subtasks [186, 274, 287, 288, 299, 320]. An important step in the segmentation method is the automatic localization of the target structure in the MRI volume for segmentation of slices based on the localization result, which reduces computational complexity. For example, Vesal S. et al. [287] initially estimate the density of the map that localizes the structure of interest, then the second stage of modelling (segmentation) focuses on the regions of interest (ROI). Their network achieves better segmentation efficiency than previous segmentation methods based on convolutional neural networks. In addition, the Omega-Net developed by Vigneault D. et al. [288] includes several stages: first, the initial segmentation on the input image is achieved. Then the features studied at this initial stage are used to predict the parameters needed to transform the image into a canonical orientation. Finally, the transformed image is segmented.

#### **1.4.5.10 Hybrid approaches to segmentation**

Some approaches focus on DL fusion methods with traditional segmentation methods, such as deformable models [41, 206], graph-cut segmentation algorithms [195] and level set methods [89, 217] for better generalization. DL models are used to extract informative features and initialization stages in order to minimize dependence on manual interaction and achieve higher segmentation efficiency. The derived shape is integrated into deformable models to achieve a good compromise for a more accurate segmentation result. Similarly, Ngo T. et al. [217] applied the Deep Belief Network (DBN) to develop a level determination method for accurate segmentation.



## **Chapter 2. MATERIALS AND METHODS**

Research was conducted using software and modern medical equipment. An algorithm was developed and a flowchart was presented reflecting the stages of the Invisalign treatment protocol. Each stage was conducted independently: obtaining digital jaw models using an intraoral scanner, analysing CT data, photo protocol, determining the oral mucosa biotype. An oral mucosa digital map of each patient was compiled. The aligners' topology was analysed using the finite element method. The results obtained at the processing stage were combined into a unified model. The results of these studies became the basis for making changes to the stages of laboratory work. The developed treatment protocol contained optimized orthodontic structures and their three-dimensional models. Individual treatment plan modifications scaled with the orthodontist's assigned tasks. A modern comprehensive orthodontic treatment protocol is presented in figure 3. This flowchart represents a digital orthodontic treatment protocol with a workflow visualization and the ability to choose the sequence of studies to achieve the set goals.

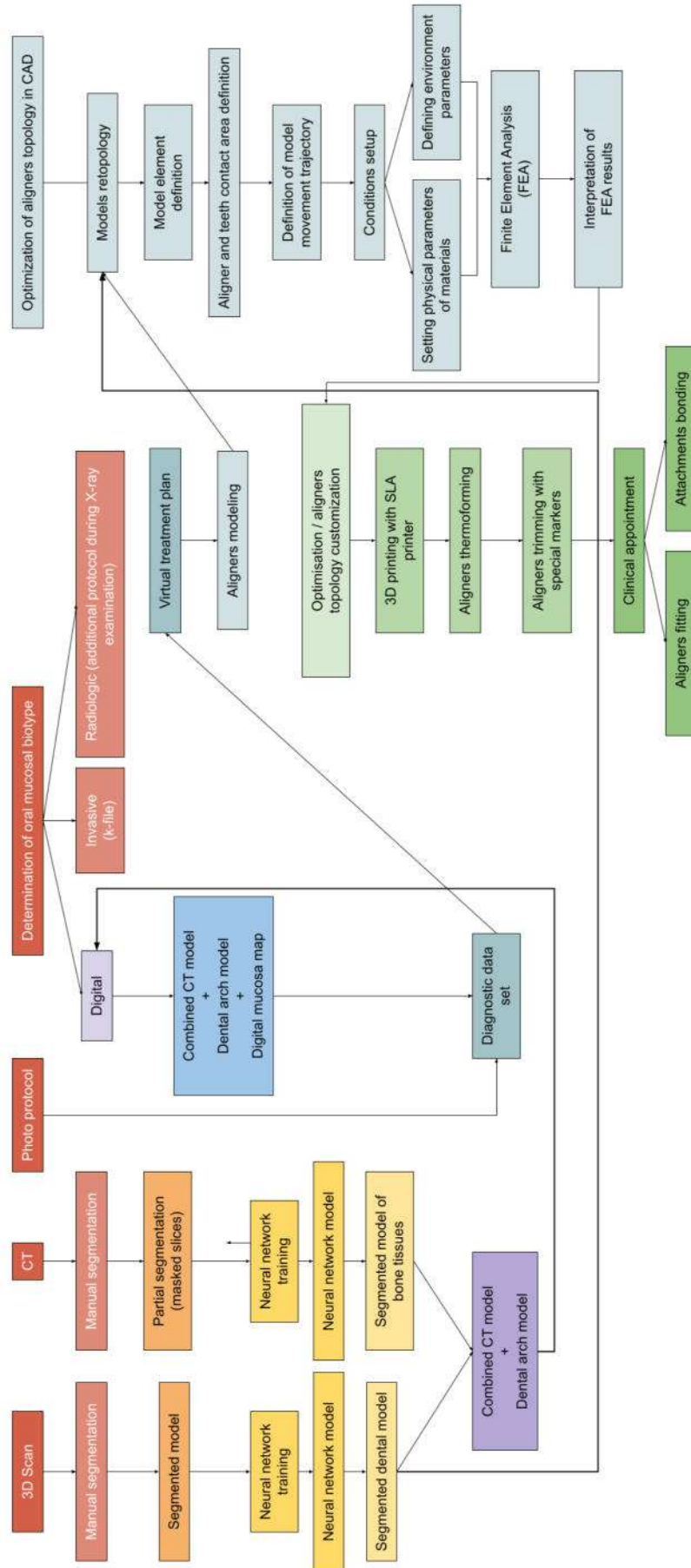


Figure 3 - Flowchart of the dissertation work

## **2.1 Protocol for obtaining three-dimensional models of dental arches**

Preparation for scanning was performed using proposed forms for patient data in digital form in the software 3Shape TRIOS Design studio (Copenhagen, Denmark) and Planmeca Romexis® CAD/CAM (Helsinki, Finland), in which patient data was filled in, an individual number was assigned, which is subsequently used in the study when working with anonymous data.

The preparation algorithm for the scanning equipment 3Shape trios 3, iTero® Element™, Planmeca Emerald S was performed, the scanning of two jaws was selected and the scanning process was performed.

The intraoral scanning was performed in accordance with the algorithm proposed by the manufacturers and the recommendations of specialists.

In connection with the peculiarity of obtaining, processing and optimizing the shell of three-dimensional models, it is imperative to perform a manual inspection of each model in the Meshmixer software. During which bridges of individual polygons were identified, removed and filled with a curved surface. This is an important criterion for the software, without which the process of processing and segmentation of models will be impossible.

The models have extraneous areas removed, and final edge processing was performed to continue working in the software.

The pre-setting of digital models of dental arches was performed according to the algorithm in accordance with the instructions of the software manufacturer. Manual segmentation and positioning of tooth axes are also performed according to the algorithms prescribed by the manufacturers of Maestro Ortho Studio 5 software.

Tooth movement modelling was performed segmentally according to algorithms for combining the movement of individual teeth.

The movement of one aligner step is limited to 0.25 mm of bodily movement or 2 degrees of rotation.

Combinable simultaneous tooth movements:

1. Rotation and uncontrolled inclination (TIP)
2. Rotation and mesio-distal movement
3. Rotation and intrusion
4. Vestibulo-oral movement and intrusion
5. Uncontrolled inclination and intrusion
6. Vestibulo-oral movement and mesio-distal movement
7. Uncontrolled inclination and mesio-distal movement
8. Vestibulo-oral movement and uncontrolled inclination

Incompatible movements:

1. Rotation and vestibulo-oral movement
2. Rotation and extrusion
3. Vestibulo-oral movement and extrusion
4. Uncontrolled inclination and extrusion
5. Mesial-distal movement and extrusion

Attachments were modelled according to the Invisalign protocols [Insider's Guide to Invisalign Treatment].

Additional elements are installed according to algorithms.

1. Movement of third molars
2. Elimination of diastema more than 6 mm
3. Elimination of crowding with lack of space more than 6 mm
4. Treatment of vertical incisor disocclusion more than 3.5 mm
5. Treatment of deep incisor occlusion of anterior teeth 2.5 mm
6. Closing of molars and canines by class II more than 5 mm

7. Elimination of closure of molars and canines by class III more than 4 mm
8. Closing of gaps after removal of molars and premolars.

Virtual models of aligners were created in Autodesk Meshmixer (Autodesk Inc., San Rafael, California). The trimming area was performed by selecting polygons with the brush tool and extruding the polygons by 1 mm. The model's polygons were then extruded, replicating the contact surfaces of the teeth, soft tissues, and aligner. To maintain these contact surfaces undistorted, manual smoothing of overhangs and individual polygon removal was performed.

The creation of pontics and reinforced beam pontics is carried out according to the same algorithms as the aligner modelling.

## **2.2 Creating 3D models for finite element analysis**

In the aligners' virtual model simulation, physical properties of the PET-G material were taken and entered into the ANSYS Workbench 2019 R1 software environment (ANSYS V.18; ANSYS Inc., Canonsburg, USA). Hyperplasticity properties were taken from the values given by the manufacturer for 22°C (Cristal PET-G; Bio-Art, Brazil). Density ( $1314.8 \text{ kg m}^{-3}$ ) and Poisson's ratio (0.31) were taken from the data table, isotropic elasticity was calculated from values of Young's modulus (2000 MPa) and tensile strength (26 MPa).

Mesh properties in the contact region were reduced by a global element size factor of 0.55 (1.65 mm), strain size factor (0.05) with a curvature capture function. Mesh properties that were not present in the contact region were modelled with larger elements. An element size of 3.0 mm was chosen with the minimum detail size that is resolved by the mesh (0.5 mm) and soft behaviour.

The physical properties characteristics of the materials, which were not specified by the manufacturer, were taken from scientific research data. Due to the fact that tabular values both in the literature and from the manufacturer of materials were not specified, the data were processed through a smart data tracer Easy Trace Pro (Easy Trace Group, Russia).

The grid size control element for the creation of work model elements depends on the shape of the dental models dimension.

The contact surfaces involved in contact calculations are described by the Definition: element size type of 1 mm, which is the minimum detail size that is allowed by the Defeature Size of 0.1 mm. Growth rate - the increase of the element edge length in each successive layer of elements is 1.5 by default. Curvature normal angle - the maximum allowable angle that can be covered by the edge of one element - default is 60 degrees. Local minimum size - The minimum size of a feature is 0.1 mm.

The path of aligner insertion is described by a general trajectory and may vary depending on the anatomy or anomaly of the dental arches.

### **2.3 Building a correlational model for the digital oral mucosa map**

Mucosa digital map modelling in Cloud Compare V2 is based on measurement of distances between polygon vertices of two models with specified parameters of colour grading scale. Floating colour grading does not give consistency of measurements, although numerically this does not play a significant role. However, this analysis utilizes the visual nature of the assessment, so fixed grading is mandatory before starting the analysis. It is also based on the oral mucosal biotype classification described in the literature.

Manual segmentation was performed according to specified algorithms and checked for artefacts and inaccuracies. The three-dimensional model should correspond

to the bone structures and should not go beyond the tissues of the person study. In addition, the model should not have holes in the bone tissues in the 3D shell and should be closed. Mimics inPrint 2.0 allows to create closed models. Using the thresholding method, an optimal value is selected and refined manually where artefacts are present. Due to the heterogeneous density of structures in a single CT study, a segmental selection of regions of interest is performed using Hounsfield thresholding. From the resulting masks, a model is created on each layer with predefined smoothing parameters and model shrinkage compensation. In Mimics Medical 21.0, the settings retained for interpretation of all studies.

Dental models and segmented CT models were merged in ProPlan CMF 3.0 with the models pre-aligned for ease of use. Only matching anatomical structures were marked with a brush, after which the models were statistically overlaid on the selected areas.

## **2.4 Neural network training**

Dragonfly software (v.2022.2, Objects Research Systems, Montreal, QC, Canada) was used to train the neural network. First, the digital parameters of the CT data stack were normalized into a 32-bit format with a floating-point number parameter. The original image was converted with a normalization parameter from 0 to 1, with the minimum and maximum intensity parameters on the Hounsfield scale set manually. Anything that does not fall within the specified parameter gets a value of 0. This normalization is unique for each CT study, so it is necessary to manually set the boundaries of interest. The frames (frames) with masks of the selected layer are created before training. The training frame was segmented according to the same criteria as the creation of masks during manual segmentation. A separate layer was created for each anatomical structure - for the bone tissue of the upper jaw, for the lower jaw, for the dentition of the upper and lower jaws. After the masks were created, it is necessary to set a background layer that fills all the

space unmarked by the masks. To train the neural network, a deep learning model with a four-layer U-Net architecture (4 levels U-Net in model parameter) was created.

After that, the prediction of the selected layer was performed and then the model was trained. After adding frames with prediction correction, the model is retrained. Training quality is validated by both the model's performance metrics and predictions on the selected layer.

The trained model was used to segment the CT under AI control and small adjustments are made to achieve the best result. The resulting segmented models are then exported from the software in stl format.

## **2.5 Laboratory phase**

Preparation of three-dimensional models for printing on a 3D printer in Photon Workshop V2 was performed by adding a three-dimensional model simultaneously with adjustment of printing parameters, which were defined according to the selected resin and are described in the manufacturer's documentation. Before starting printing, the printing platform was calibrated. After printing was completed, all models were washed of excess resin and the model was exposed to UV light in an ultraviolet chamber.

The resin parameters allow aligner thermoforming without destroying the model.

- 1) Stiffness - 79 Shore D
- 2) Viscosity (25°C) - 552 MPa\*s
- 3) Density in liquid state - 1.1 g/cm<sup>3</sup>
- 4) Density in solid state - 1.184 g/cm<sup>3</sup>
- 5) Shrinkage - 7.1%
- 6) Tensile strength - 23.4 MPa
- 7) Elongation at break - 14.2%



Thermoforming of Cristal PET-G plastic aligners (Bio-Art, Brazil) was performed by applying release silicone to the model immediately before forming and creating a vacuum under the model using Bio-art PlastVac P7.

Aligner trimming and polishing edges corresponds to the standard algorithms of constructive fabrication and should not have sharp edges, cracks and scratches.

Pontic filling was performed by applying bond to the inner pontic surface, a thin layer of composite according to the patient's teeth colour and UV lamp exposure for 30 seconds.

## 2.6 Clinical and diagnostic appointment

### 2.6.1 Photo protocol and diagnosis

The photo protocol and diagnostics were performed in accordance with the requirements prescribed in the Flexiligner completion form shown in the figures 4 - 8.

Figure 4 - Flexiligner form

План лечения			
Текущая ситуация в полости рта:			
1. Сужение:	Верхняя челюсть: <input type="radio"/> да <input type="radio"/> нет	Нижняя челюсть: <input type="radio"/> да <input type="radio"/> нет	
2. Скудность:	Верхняя челюсть: <input type="radio"/> да <input type="radio"/> нет	Нижняя челюсть: <input type="radio"/> да <input type="radio"/> нет	
3. Перекрестное соотношение:	<input type="radio"/> да <input type="radio"/> нет	<input type="checkbox"/> в переднем отделе <input type="checkbox"/> в боковом отделе	<input type="checkbox"/> односторонний <input type="checkbox"/> двусторонний
4. Соотношение клыков по Энглю:	СПРАВА: <input type="radio"/> I класс <input type="radio"/> II класс <input type="radio"/> III класс	СЛЕВА: <input type="radio"/> I класс <input type="radio"/> II класс <input type="radio"/> III класс	
5. Соотношение 1-ых моляров по Энглю:	СПРАВА: <input type="radio"/> I класс <input type="radio"/> II класс <input type="radio"/> III класс	СЛЕВА: <input type="radio"/> I класс <input type="radio"/> II класс <input type="radio"/> III класс	
6. Соотношение резцов по вертикали:	<input type="radio"/> нейтральный (1/3) <input type="radio"/> глубокий <input type="radio"/> открытый <input type="radio"/> прямой		
7. Смещение центральной линии:	<input type="radio"/> да <input type="radio"/> нет	<input type="checkbox"/> на верхней челюсти <input type="checkbox"/> на нижней челюсти	
8. Есть ли наклон окклюзионной плоскости (Наклон относительно зрачковой линии):	<input type="radio"/> Да <input type="radio"/> Нет		
9. Есть ли пародонтологический статус:	<input type="radio"/> Да <input type="radio"/> Нет Резорбция костной ткани более 1/3 длины корня, не предполагает корпусные перемещения.		
10. Особенности:	Выберите особенность и отметьте соответствующие зубы: <input type="checkbox"/> Зуб удалён <input type="checkbox"/> - Имплантат <input type="checkbox"/> - Винир/коронка		
	<p>Upper arch: 1.8 1.7 1.6 1.5 1.4 1.3 1.2 1.1   2.1 2.2 2.3 2.4 2.5 2.6 2.7 2.8 Lower arch: 4.8 4.7 4.6 4.5 4.4 4.3 4.2 4.1   3.1 3.2 3.3 3.4 3.5 3.6 3.7 3.8</p>		
План лечения:			
Пожалуйста, внимательно относитесь к процедуре заполнения анкеты! Отмеченные вами ниже клинические предпочтения будут использоваться для формирования технического задания и изготовления 3d-диагностики.			
11. Лечим зубные дуги:	<input type="radio"/> Обе <input type="radio"/> Верхнюю <input type="radio"/> Нижнюю		
12. Центральная линия:	Верхняя центральная линия: <input type="radio"/> не менять <input type="radio"/> сдвинуть вправо <input type="radio"/> сдвинуть влево	Оцените фотографии пациента: если при открытии рта (фото с ретрактором и широко открытым ртом, Энгля) центр нижней челюсти выравнивается с верхним, то можно предположить, что у пациента есть функциональное смещение нижней челюсти и корпусно центральную линию на нижней челюсти смещать НЕ нужно.	Нижняя центральная линия: <input type="radio"/> не менять <input type="radio"/> сдвинуть вправо <input type="radio"/> сдвинуть влево  За счёт: <input type="checkbox"/> смещенной зубо (коронки или виниры/лэзын) <input type="checkbox"/> изменение положения НЧ (отметьте в пункте 19)

Figure 5 - Flexiligner form

13. Устранить скученность за счёт:	<input type="checkbox"/> расширения <input type="checkbox"/> сепарации <input type="checkbox"/> апрайтинга <input type="checkbox"/> дистализации <input type="checkbox"/> удаления <input type="checkbox"/> протрузии																		
14. Перекрестное соотношение боковых зубов:	<input type="radio"/> отсутствует <input type="radio"/> не менять <input type="radio"/> скорректировать <ul style="list-style-type: none"> <li><input type="checkbox"/> Гиперкоррекция движений</li> <li><input type="checkbox"/> Эластические межчелюстные тяги (кнопка-кнопка)</li> <li><input type="checkbox"/> Эластические межчелюстные тяги (кнопка-МИ)</li> </ul>																		
15. Расширение:	<input type="radio"/> не делать расширение <input type="radio"/> 3-3 (в области клыков) <input type="radio"/> 5-5 (в области клыков и премоляров) <input type="radio"/> 6-6 (в области клыков, премоляров и 1-ых моляров) <input type="radio"/> 7-7 (по всей дуге) <div style="border: 1px solid #ccc; padding: 5px; margin-top: 10px;">             За счёт             <table style="width: 100%; border-collapse: collapse;"> <tr> <td style="width: 50%; border-right: 1px solid #ccc; padding: 5px;">Верхний зубной ряд:</td> <td style="padding: 5px;">Нижний зубной ряд:</td> </tr> <tr> <td style="border-right: 1px solid #ccc; padding: 5px;"><input type="checkbox"/> торк</td> <td style="padding: 5px;"><input type="checkbox"/> торк</td> </tr> <tr> <td style="border-right: 1px solid #ccc; padding: 5px;"><input type="checkbox"/> корпусно</td> <td style="padding: 5px;"><input type="checkbox"/> корпусно</td> </tr> </table> <p>Объём расширения всей зубной дуги</p> <input type="radio"/> 1-2 мм.  <input type="radio"/> 2-3 мм.  <input type="radio"/> 3-4 мм.           </div>	Верхний зубной ряд:	Нижний зубной ряд:	<input type="checkbox"/> торк	<input type="checkbox"/> торк	<input type="checkbox"/> корпусно	<input type="checkbox"/> корпусно												
Верхний зубной ряд:	Нижний зубной ряд:																		
<input type="checkbox"/> торк	<input type="checkbox"/> торк																		
<input type="checkbox"/> корпусно	<input type="checkbox"/> корпусно																		
16. Сепарации:	<input type="checkbox"/> при возможности, отложить начало проведения сепараций до этапа нивелирования (раунд триппинг) <input type="checkbox"/> применить сепарации с 1 шага <input type="checkbox"/> во фронтальном отделе <input type="checkbox"/> в области премоляров <input type="checkbox"/> в области моляров <input type="checkbox"/> в области искусственных коронок <input type="checkbox"/> в области молочных зубов (при их наличии) <input type="checkbox"/> на усмотрение лаборатории																		
17. Допускаете ли Вы использование микроимплантатов (МИ) в данном кейсе:	<input type="radio"/> Да <input type="radio"/> Нет <input type="radio"/> По рекомендации лаборатории (Какие локализации чаще используете в практике)																		
18. 8-ые зубы:	<p style="color: red; text-align: center;"><b>Внимание! По умолчанию недистопированные 8 зубы и зубы, находящиеся в контакте покрываются элайнером!</b></p> <table style="width: 100%; border-collapse: collapse; text-align: center;"> <tr> <td style="width: 33%;"></td> <td style="width: 33%; border-right: 1px solid #ccc;"> <input type="radio"/> Планируется удаление  <input type="radio"/> Не планируется удаление  <input type="radio"/> Удаление по рекомендации лаборатории           </td> <td style="width: 33%; border-right: 1px solid #ccc;"> <input type="radio"/> Планируется удаление  <input type="radio"/> Не планируется удаление  <input type="radio"/> Удаление по рекомендации лаборатории           </td> </tr> <tr> <td></td> <td style="border-right: 1px solid #ccc;">1.8</td> <td style="border-right: 1px solid #ccc;">2.8</td> </tr> <tr> <td></td> <td style="border-right: 1px solid #ccc;"> <input type="radio"/> Планируется удаление  <input type="radio"/> Не планируется удаление  <input type="radio"/> Удаление по рекомендации лаборатории           </td> <td style="border-right: 1px solid #ccc;"> <input type="radio"/> Планируется удаление  <input type="radio"/> Не планируется удаление  <input type="radio"/> Удаление по рекомендации лаборатории           </td> </tr> <tr> <td></td> <td style="border-right: 1px solid #ccc;">4.8</td> <td style="border-right: 1px solid #ccc;">3.8</td> </tr> </table>		<input type="radio"/> Планируется удаление <input type="radio"/> Не планируется удаление <input type="radio"/> Удаление по рекомендации лаборатории	<input type="radio"/> Планируется удаление <input type="radio"/> Не планируется удаление <input type="radio"/> Удаление по рекомендации лаборатории		1.8	2.8		<input type="radio"/> Планируется удаление <input type="radio"/> Не планируется удаление <input type="radio"/> Удаление по рекомендации лаборатории	<input type="radio"/> Планируется удаление <input type="radio"/> Не планируется удаление <input type="radio"/> Удаление по рекомендации лаборатории		4.8	3.8						
	<input type="radio"/> Планируется удаление <input type="radio"/> Не планируется удаление <input type="radio"/> Удаление по рекомендации лаборатории	<input type="radio"/> Планируется удаление <input type="radio"/> Не планируется удаление <input type="radio"/> Удаление по рекомендации лаборатории																	
	1.8	2.8																	
	<input type="radio"/> Планируется удаление <input type="radio"/> Не планируется удаление <input type="radio"/> Удаление по рекомендации лаборатории	<input type="radio"/> Планируется удаление <input type="radio"/> Не планируется удаление <input type="radio"/> Удаление по рекомендации лаборатории																	
	4.8	3.8																	
19. Коррекция в сагиттальной плоскости:	<input type="checkbox"/> Не менять <input type="checkbox"/> Ортогнатическая хирургия <input checked="" type="checkbox"/> Предположение возможного смещения нижней челюсти Байт-Джамп (конструктивный прикус - лаборатория меняет положение нижней челюсти по отношению к верхней до начала лечения, ориентируясь на данные, которые вы предоставили: <b>обязательные фотографии, скриншоты суставов</b> ) <p style="color: blue; font-size: small;"><i>Внимание! Использование межчелюстных тяг и удаление 8 зубов обязательно!</i></p> <input type="checkbox"/> использовать регистрат прикуса (вы определили новое предполагаемое положение нижней челюсти любым доступным в клинике способом) <input type="checkbox"/> переднее смещение (класс II\1, II\2) <input type="checkbox"/> боковое смещение (боковое смещение нижней челюсти с коррекцией центральной линии при симметричных классах смыкания) <input type="checkbox"/> смещение с ротацией (смещение нижней челюсти с коррекцией центральной линии при асимметричных классах смыкания) <input type="checkbox"/> вертикальное смещение (коррекция высоты прикуса за счёт смещения нижней челюсти в результате экструзии/интрузии зубов при изменении торка или апрайте)  <input checked="" type="checkbox"/> Дистализация <p style="color: red; font-size: small;"><b>Внимание! Выбирая данный пункт Вы соглашаетесь на удаление зубов мудрости в сегменте дистализации!</b></p> <ul style="list-style-type: none"> <li>• последовательная (до 2мм + межчелюстные тяги) в секторах:               <table style="display: inline-table; vertical-align: middle;"> <tr><td>1</td><td><input type="checkbox"/></td><td>2</td></tr> <tr><td>4</td><td><input type="checkbox"/></td><td>3</td></tr> </table> </li> <li>• смешанная/последовательная (от 3мм + межчелюстные тяги + МИ) в секторах:               <table style="display: inline-table; vertical-align: middle;"> <tr><td>1</td><td><input type="checkbox"/></td><td>2</td></tr> <tr><td>4</td><td><input type="checkbox"/></td><td>3</td></tr> </table> </li> <li>• групповая по Вергаре (межчелюстные тяги + МИ) в секторах:               <table style="display: inline-table; vertical-align: middle;"> <tr><td>1</td><td><input type="checkbox"/></td><td>2</td></tr> <tr><td>4</td><td><input type="checkbox"/></td><td>3</td></tr> </table> <ul style="list-style-type: none"> <li><input type="radio"/> в IZC (подскуловой гребень)</li> <li><input type="radio"/> в Buccal Shelf (щёчный выступ)</li> </ul> </li> </ul>	1	<input type="checkbox"/>	2	4	<input type="checkbox"/>	3	1	<input type="checkbox"/>	2	4	<input type="checkbox"/>	3	1	<input type="checkbox"/>	2	4	<input type="checkbox"/>	3
1	<input type="checkbox"/>	2																	
4	<input type="checkbox"/>	3																	
1	<input type="checkbox"/>	2																	
4	<input type="checkbox"/>	3																	
1	<input type="checkbox"/>	2																	
4	<input type="checkbox"/>	3																	

Figure 6 - Flexiligner form

Мезиализация

- последовательная (до 2мм + межчелюстные тяги) в секторах: 1  2   
4  3
- закрытие постэкстракционных промежутков (power arm + MI или power arm + power arm) в секторах: 1  2   
4  3   
*(обязательно оценить соотношение коронки с гайморовой пазухой и объемом ануляции коронки, объем перевешивания не более 5 мм)*
- групповая (межчелюстные тяги + MI) в секторах: 1  2   
4  3

20. Планируете ли замену/установку:

Выберите особенность и отметьте соответствующие зубы:

Планируется удаление ? Удаление по рекомендации лаборатории

Не перемещать зуб  Не ставить аттачменты

- пломба  - имплантат  - винир/коронка

Если планируется поднятие высоты прикуса в боковых отделах или замена объемных пломб, отметьте их на схеме. Мы оставим место для будущих реставраций.

21. При несоответствии ширины резцов и клыков по Болтону предпочтительнее:

- оставить промежутки дистальнее боковых резцов
- оставить промежутки дистальнее и мезиальнее боковых резцов
- сепарация антагонистов
- при сепарации нижних резцов более 0,3 мм раскрыть тремы в области верхних боковых резцов

22. Выравнивание фронтальных зубов:

Выравнивание фронтальных верхних зубов:

- по режущему краю
  - Боковые резцы на одном уровне с центральными
  - Боковые резцы на 0.5 мм короче центральных
- по десневому краю

Взять зубы за эталон:

Выравнивание фронтальных нижних зубов:

- по режущему краю
- по десневому краю

Взять зубы за эталон:

Выравнивание по десневому краю подразумевает, что режущие края зубов могут быть на разном уровне и планируется дальнейшая реставрация в этой области. ?

23. Соотношение резцов по сагиттали:

Верхняя челюсть:

- не менять
- менять
  - корпусно (ретракция/протракция)
  - торк (ретрузия/протрузия)

Нижняя челюсть:

- не менять
- менять
  - корпусно (ретракция/протракция)
  - торк (ретрузия/протрузия)

24. Коррекция окклюзионной плоскости (кривая Шпее, кант):

- заполнить схему
- на усмотрение лаборатории

Ингрузия  Экструзия

Figure 7 - Flexiligner form




25. Обрезка элайнеров:		<input type="radio"/> высокая *	<input type="radio"/> комбинированная	<input type="radio"/> низкая
				
		при незначительных изменениях пародонта	при локальных изменениях пародонта	при генерализованных изменениях пародонта
		* Рекомендовано лабораторией	Укажите зону низкой обрезки (номера зубов):	
		<input type="text"/>		
26. Применить виртуальную эластичную цепочку (Уплотнение аппроксимальных контактов):		Гиперкоррекция в случаях лечения с закрытием трем		
		<input type="radio"/> нет		
		<input type="radio"/> да, 3-3		
		<input type="radio"/> да, 6-6		
27. Последовательность перемещения зубов:		<input type="radio"/> по протоколам лаборатории		
		<input type="radio"/> напишите свои предпочтения:		
		<input type="text"/>		

Figure 8 - Flexiligner form

In the order form, the patient's dental scan files are uploaded for evaluation by the laboratory specialists. The laboratory then informs on whether the 3D models are of acceptable or unacceptable quality.

The patient's data were entered into the form: surname, first name, middle name and date of birth.

Photos were taken during the clinical appointment are uploaded to the form in the diagnostics section according to the protocol specified in the protocol: profile photo, photo to determine the exposure of incisors - full-face with "Emma", full-face with smile, full-face with retractor and open mouth, intraoral photos - occlusal view of the upper and lower dentition, lateral view of occlusion on the left, right and frontal view, orthopantomogram.

The individualized treatment plan was filled out according to the goals and objectives for each individual patient following the protocol provided in the forms. Where indicated items should be noted:

### **Description of the current oral situation:**

1. Presence of deficiency of the maxilla and/or mandible

2. Crowding on the maxilla and/or mandible
  3. Presence of a crossbite
  4. Angle's classification of the canines:
    - Right side: class I, class II, class III
    - Left side: class I, class II, class III
  5. Angle's classification of 1st molars:
    - Right side: class I, class II, class III
    - Left side: class I, class II, class III
  6. Vertical incisor ratio: neutral (1/3), deep bite, open, underbite
  7. Centre line displacement
  8. Occlusal plane inclination (inclination relative to the pupils axis).
  9. Presence of periodontal status
  10. Treatment features: extracted tooth; implant; veneer/crown
- Treatment plan:**
11. Which jaw will be treated, upper jaw, lower jaw or both.
  12. Centreline:
    - Upper centre line: do not change, shift right or left
    - Lower centre line: do not change, shift right or left
  13. Eliminate crowding by: expansion, separation, uprighting, distalization, extraction, protrusion.
  14. Cross-relationship of lateral teeth: absent, not changed, corrected
  15. Expansion:
    - No expansion

- 3-3 (in the canine area)
- 5-5 (in the canine and premolar area)
- 6-6 (in the area of canines and premolars and 1st molars)
- 7-7 (across the arch)

16. Interproximal reduction:

- if possible, postpone the start of separation until the levelling phase (round tripping)
- apply IPR from stage 1
- in the anterior region
- in the premolars
- in the area of molars
- in the area of artificial crowns
- in the area of deciduous teeth (if any present)
- according to the laboratory's discretion

17. Whether is allowed the use of microimplants (MI) in this case:

- yes
- no
- as recommended by the laboratory

18. 8th teeth - 1.8; 2.8; 3.8; 4.8:

By default, non-dystopic 8 teeth and teeth in contact are covered with aligners!

- planned extraction
- extraction is not planned
- extraction on the recommendation of the laboratory

19. Correction in the sagittal plane:

- Do not change



- Orthognathic surgery
- Suggestion of possible mandibular shift Bite-Jump (constructive bite - laboratory changes the position of the lower jaw in relation to the upper jaw before treatment, focusing on the data provided: mandatory photos, screenshots of TMJ)

The use of intermaxillary traction and extraction of 8 teeth is mandatory.

- use a bite registration (you have determined the new position of the mandible by any method available in the clinic)
- anterior displacement (class II/1, II/2)
- lateral displacement (lateral displacement of the mandible with correction of the centre line in symmetrical occlusion classes)
- rotation displacement (mandibular displacement with correction of the central line in asymmetrical occlusion classes)
- vertical displacement (correction of bite height due to shifting of the mandible as a result of extrusion/intrusion of teeth in case of torque or uprighting changes)
- Distalization
  - Sequential (up to 2mm + intermaxillary traction) in sectors
  - Mixed/sequential (from 3mm + intermaxillary traction + MI) in sectors
    - in the IZC (The infrazygomatic crest)
    - in the Buccal Shelf
- Mesialization
  - sequential (up to 2 mm + intermaxillary traction) in the sectors;
  - closure of postextraction gaps (power arm + MI or power arm) (it is obligatory to evaluate the position of roots with maxillary sinus and

the amount of root angulation, the amount of movement should not exceed 5 mm)

- intermaxillary group traction + MI) in the sectors

20. Whether placement/replacement is planned: Picking out the features and marking the corresponding teeth on the scheme:

- Planned extraction
- Extraction as recommended by the laboratory
- Do not move the tooth
- Do not place attachments
- Filling
- Implant
- Veneer/crown

If it is planned to raise the bite height in the lateral areas or replace bulk fillings, mark them on the scheme. The laboratory will leave space for future restorations.

21. In the case of Bolton's discrepancy in the width of incisors and canines, the following is preferable:

- leave spaces distally above the lateral incisors
- leave spaces distally and mesially above the lateral incisors
- antagonists separation
- when the lower incisors are separated by more than 0.3 mm, tremas are opened in the area of the upper lateral incisors

22. Alignment of the frontal teeth and which tooth is taken as a reference:

- Alignment of frontal upper teeth: on the incisal or gingival margin
- Alignment of frontal lower teeth: on the incisal or gingival margin

Gingival alignment implies that the incisal edges of the teeth may be at different levels and further restoration is planned in this area.

23. Change in sagittal incisor ratio:

Maxilla: change / do not change

Mandible: change / do not change

24. Completion of occlusal plane correction scheme (Curve of Spee, edging) or at the laboratory's choice

25. Aligners trimming:

- High for minor periodontal changes
- Combined in localized periodontal changes
- Low in generalized periodontal changes

26. Apply virtual elastic chain (Sealing of the approximal contacts):

Hypercorrection in cases of treatment with tremas closure: no, 3-3, 6-6

- Sequence of tooth movement: according to laboratory protocols or orthodontist's preference.

### **2.6.2 Evaluation of oral soft tissue inflammation**

The iodine test is a diagnostic and assessment method for the gums state based on the ability of the iodine-iodide-potassium solution to stain areas of glycogen accumulation. In the areas of deep connective tissue damage, where glycogen is most abundant, staining occurs in an intense blue colour. Visually assessing the gums allows for determining the degree of inflammation.

To perform the test, the gums were smeared with the solution and the degree of staining is assessed. Areas of intense gums coloration were recorded in the examination chart. To objectify the results, a scoring scale was used:

Gum papilla staining: 2 points

Gingival margin staining: 4 points

Alveolar mucosa staining: 8 points

The iodine number is the points sum obtained in the assessment of the gums for each tooth, divided by the number of teeth examined.

Evaluation of Svrakov's iodine number values:

- Mild inflammatory process:
  - PMA index is less than 2.3 points indicates a mild inflammation of the periodontal tissues.
  - Inflammatory changes may be insignificant and do not cause pronounced clinical symptoms.
- Moderately expressed inflammatory process:
  - PMA index value from 2.3 to 5.0 points indicates a moderately expressed inflammation of the periodontal tissues.
  - Inflammatory changes may be more pronounced and lead to the development of clinical symptoms, such as bleeding gums, swelling, hyperaemia.
- Intense inflammatory process:
  - PMA index from 5.1 to 8.0 points indicates an intense inflammation of the periodontal tissues.
  - Inflammatory changes may be pronounced and lead to the development of destructive processes in the periodontal tissues, such as gingivitis, periodontitis.

The papillary-marginal-alveolar index (PMA) is a quantitative assessment of the severity of inflammation in periodontal tissues. The index can be expressed as a percentage of the number of teeth with inflammation.

To determine the PMA gingival index, the gingiva was divided into three areas:

Papillary (P), marginal (M), and alveolar (A).

A point scale is used to quantify the inflammatory process in the gums.

1 point - inflammation of the papilla;

2 points - inflammation of the gingival margin;

3 points - inflammation of the alveolar gingiva.

The scoring is performed on each tooth.

$$\text{PMA} = \frac{[(\sum \text{point score}) \times 100\%]}{3 \times (\text{number of teeth})}$$

Index values of up to 30% indicate a mild severity of the inflammatory process; 30-60% - moderate severity of gingivitis; more than 60% - severe degree of the pathological process.

Before the start of orthodontic treatment, it was necessary to verify the initial status of the orthodontic patient and his readiness for treatment. In most cases, if hygiene is unsatisfactory, the patient is taught oral hygiene and the next visit is scheduled to check the hygiene indices. With poor oral hygiene during orthodontic treatment, complications associated with inflammatory processes of the oral soft tissues will occur. Also, with the presence the oral soft tissues inflammation, errors will inevitably occur in determining the oral soft tissues biotype before the start of orthodontic treatment and, accordingly, the choice of treatment tactics.

## Chapter 3. RESULTS

### 3.1 Protocol for obtaining three-dimensional dentition models

During the clinical appointment, the patient undergoes a standardized photo protocol and mandatory professional oral hygiene after examination. Only then are their teeth scanned, with patient data automatically recorded in the scanner software. This is critical for creating an accurate working model of the teeth, as soft plaque can disrupt the scan and negatively impact aligner fit. The given digital diagnostic model demonstrates the difference in surface roughness with and without proper oral hygiene (figure 9, 10).

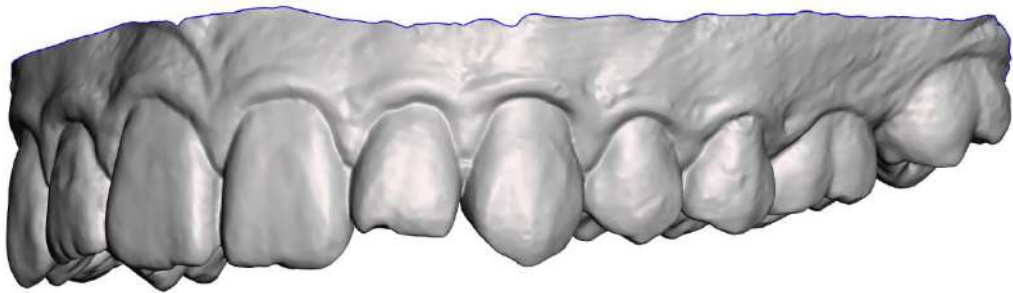


Figure 9 - Three-dimensional model of the upper dentition without oral hygiene

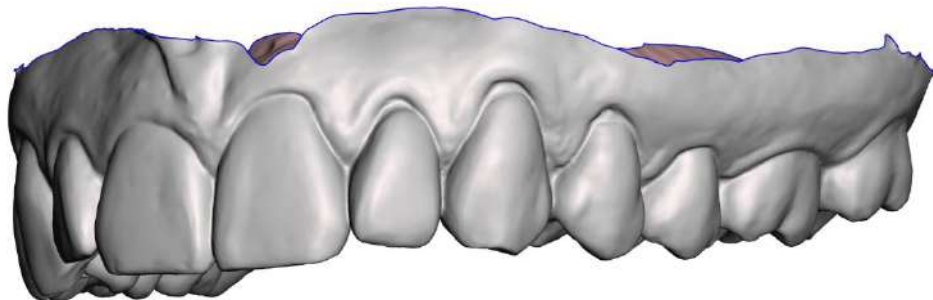


Figure 10 - Three-dimensional model of the upper dentition after oral hygiene

Following complete oral cavity sanitation and professional oral hygiene, the dentition of the upper and lower jaws is scanned according to protocol. Scanning begins

at the distal surface of the molars, with the tip directed at a 40-50 degree angle from the lingual/palatal surface of the teeth, as shown in figure 11.

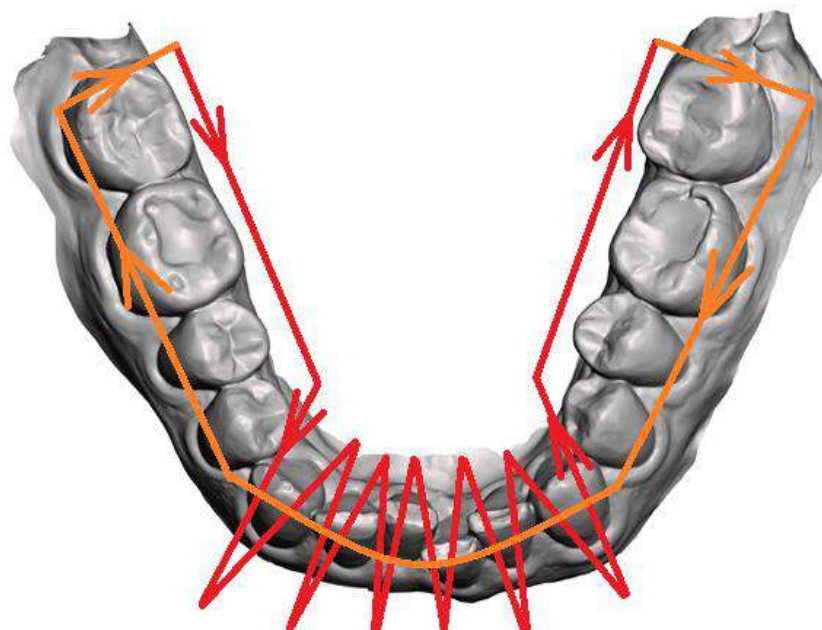


Figure 11 - Algorithm for scanning with an intraoral scanner

Having obtained upper and lower jaw dentition models, a model of the dentition in central occlusion was required. Subsequently, the combined models of the upper and lower jaw dentition should be aligned along these surfaces (figure 12).

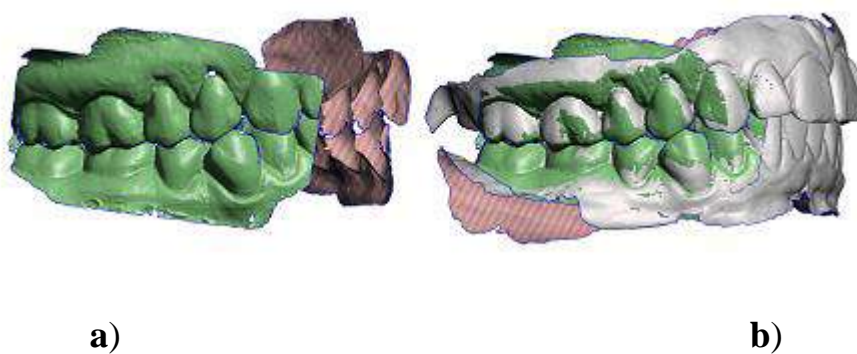


Figure 12 - Three-dimensional model in central occlusion (a), superimposed models of the upper and lower dentition on the occlusal model (b)

After alignment, it was necessary to remove artefacts, which were not process by the artificial intelligence of the scanner software (figure 13).

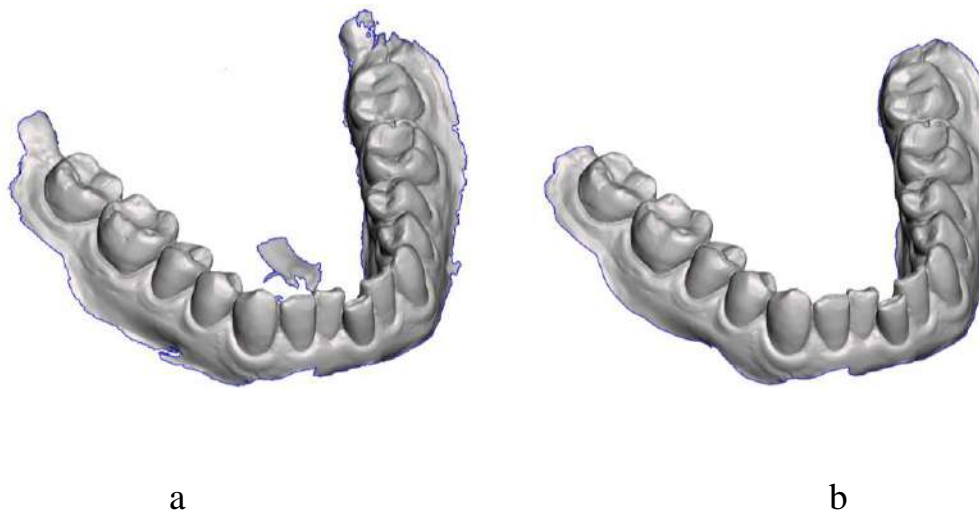


Figure 13 - Artefacts removal on a three-dimensional model of the dentition before (a) and after (b)

Then, to plan orthodontic treatment, occlusal planes were set in the software, and virtual bases of the jaw models were added (figure 14).

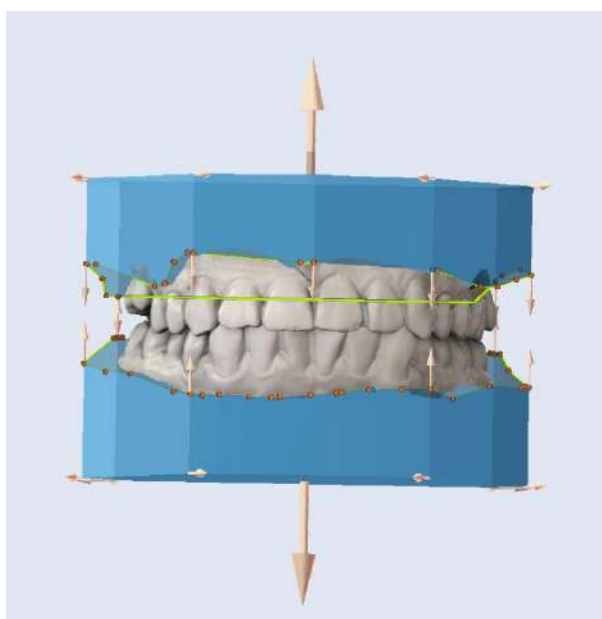


Figure 14 - Adding a virtual base on the dentition model



After the models have been processed, the teeth were segmented manually or automatically using AI. Root models of the teeth are added, if segmented CT data was available. The roots were matched to the segmented models of the individual teeth. In the absence of segmented tooth root models, the tooth axes were aligned (figure 15).

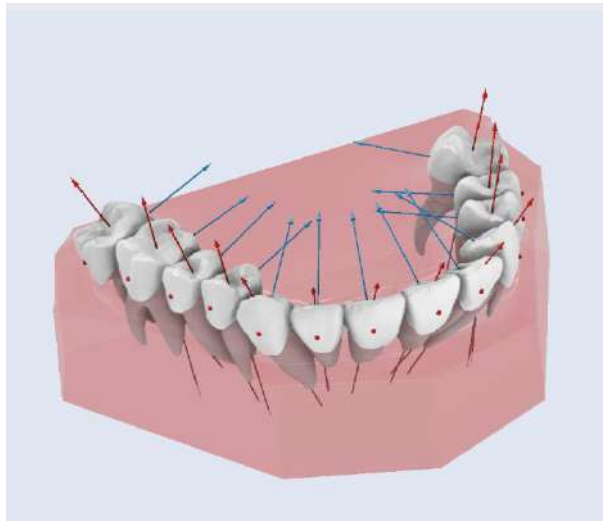


Figure 15 – Each tooth virtual axes orientation

Once the dental models were obtained, a treatment plan was made with a staging by moving each individual tooth to the planned position (figure 16).

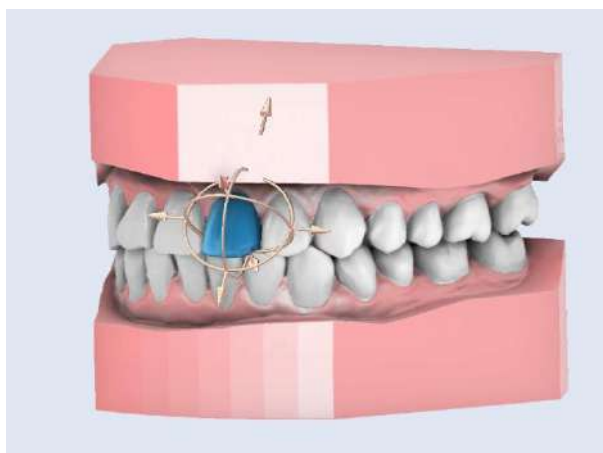


Figure 16 - Manipulator of the highlighted tooth to set its position

### **3.1.1 Protocol for obtaining three-dimensional dentition models**

After complete oral sanitation and professional hygiene, dental scans of the upper and lower jaw rows are performed according to the protocol recommended by the manufacturer.

The three-dimensional models of the dentition were manually processed and visually inspected for artefacts that need to be removed.

After the models were processed, teeth were segmented manually or automatically using AI. The individual segmented models of each tooth were matched to the tooth root models from the CT scan. If no tooth root models were available, the axes of each tooth were aligned and virtual tooth root models were modelled.

### 3.2 CT data segmentation

There are criteria for data selection for segmentation: 8x12, 15x17 CT scans of the upper and lower jaw, three-dimensional models of the dental rows obtained by an intraoral scanner with a difference of no more than four months in the absence of inflammatory processes of the oral mucosa.

For the study, the directions of segmentation of bone structures and individual teeth were chosen by various methods to obtain the most stable result. Also, major criteria was the availability of the method in daily practice.

AI (artificial intelligence) or NN (neural networks) segmentation further assisted patients in preparing a digital treatment plan and achieving precise control over root positions (figure 17). In the current work, the following options for segmenting the cranial bone structures and individual teeth were possible:

1. Manual segmentation
2. Manual area segmentation
3. Watershed segmentation
4. Automatic with the help of AI (NN)

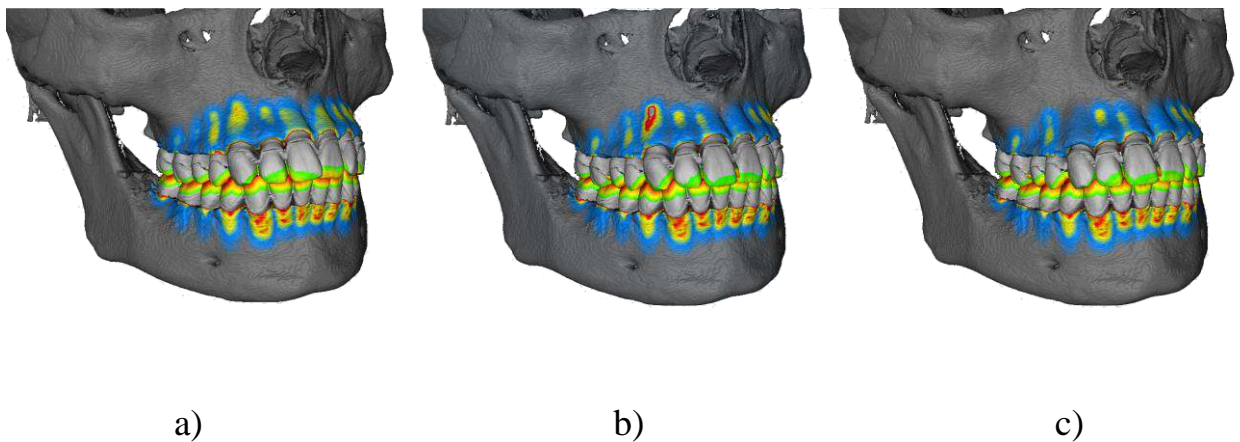


Figure 17 - (a) Pre-treatment; (b) without root correction; (c) after root correction

This list highlights the most advanced segmentation method using AI. However, it will work properly when the data has been prepared, that is, the segmentation model has already been trained. This method gives the most stable result in research, which least of all depends on the human factor in processing input data.

Each of the methods is available to clinicians, however, the criteria for processing and obtaining data should be considered:

1. The manual method takes a lot of time and numerous errors are possible.
2. Manual area segmentation is a relatively fast method that requires traditional processing after highlighting contrasting areas of masks (figure 65, 66).
3. Watershed method is the fastest; however, it lacks the possibility of segmentation of individual teeth.
4. AI – in the presence of a trained model, segmentation occurs automatically and takes several seconds. In its absence, training takes a long time, but still it takes less time than manual segmentation.

### **3.2.1 Manual segmentation of CT data**

For the manual method, the first step was the processing of CBCT and segmentation of bone structures according to the Hounsfield scale to create a three-dimensional model without the use of filters and image modifications. Each dicom dataset was processed in Mimics inPrint 2.0 and Mimics PRO Plan CMF 3.0 software [20, 51].

The masks of each layer were finalized manually to ensure maximum accuracy in further work. The resulting 3D models were smoothed with compensation with shrink

compression, and the contours of the models were evaluated for possible errors during processing (figure 18).

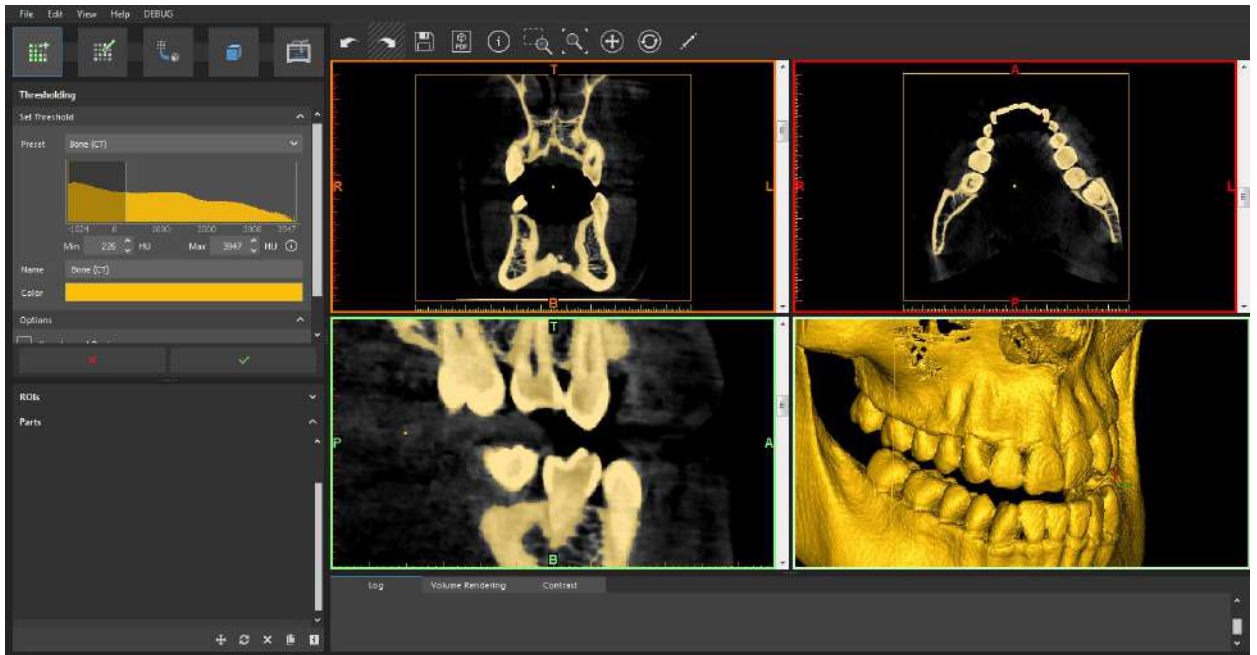


Figure 18 - Manual processing of CBCT by the threshold values method on the Hounsfield scale

### **Processing, smoothing, combining.**

The three-dimensional models of the maxilla and mandible were divided into separate models after processing (figure 19). A key point in the preparation of the data was the matching the scanned dental models with the obtained bone structure models from CT scans. Due to the fact that the models geometry only partially matched (tooth enamel was the common part, which was manually precisely processed) and the mismatched part of bone tissue on first set of models and mucosa on the second set, then standard global or local alignment tools often gave a matching error.



Figure 19 - Dividing the 3D models into upper and lower jaw

The control analysis in the Geomagic Control X software (3D Systems, Rock Hill, SC) proves that "extra" data in the form of mismatching geometries parts of the models (teeth roots, bone tissue and oral mucosa) during the comparison gives a large error in the analysis methodology and can lead to incorrect results (figure 20, 21).

The tool that eliminates matching errors works on the "brush" principle, which highlights only necessary parts of the models that are involved in matching process with different geometries. A comparative analysis is presented in the illustration (figure 22 - 26) shows the comparison of results obtained by the pre-alignment method with automatic aligning and the manual labelling method. The obtained results are visually examined on slices of the initial CT with contour lines of 3D models. Red colour of models and contour lines corresponds to the matching using the "brush" tool, blue colour denotes models matched by automatic method of global or local registration within the minimum value of 1 mm with preliminary approximate aligning of models. Yellow colour indicates

models obtained by segmentation using the Hounsfield scale and additional manual processing. Thus, the analysis showed that the result obtained by the automatic alignment differs from the result obtained by the selective method using the “brush” tool.

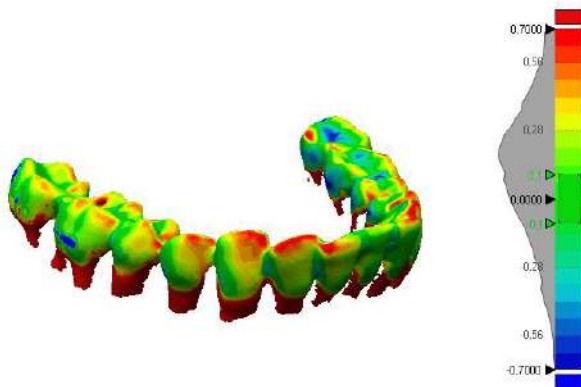


Figure 20 - Automatic comparison of segmented models from the CBCT and scanned dental models

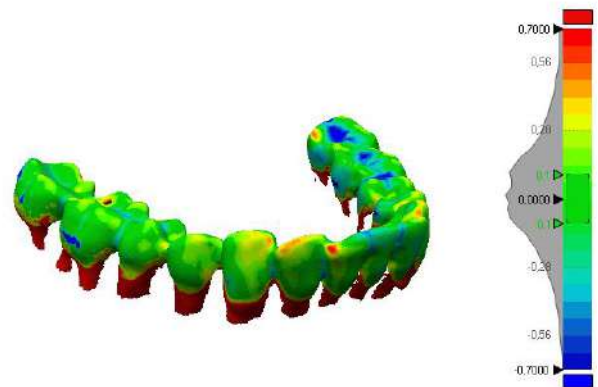


Figure 21 - Marker alignment of segmented models from CBCT and scanned dental models

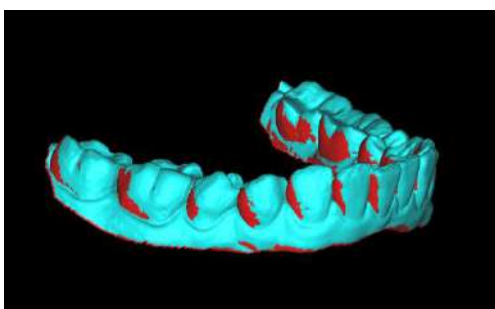


Figure 22 - Three-dimensional comparison of automatic and manual alignment of the teeth using the marking of the areas of interest. The blue colour is automatic alignment, the red colour is manual alignment

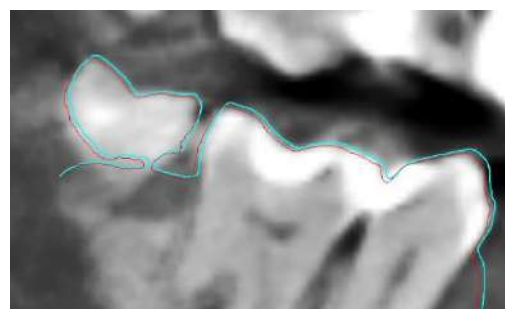


Figure 23 - Marked areas guide contour comparison of automatic and manual tooth alignment. The blue colour is automatic alignment, the red colour is manual alignment



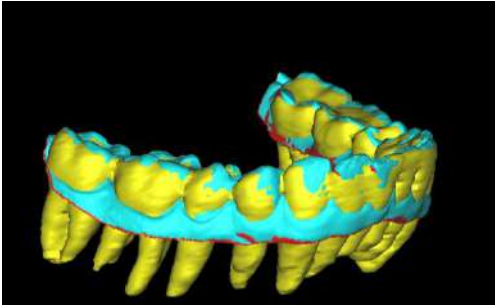


Figure 24 - Three-dimensional comparison of the position of the dental rows in automatic and manual mode by marking the areas of interest with the position of segmented CT tooth models. Blue colour - automatic alignment, red colour - manual alignment, yellow colour - segmented CT tooth model

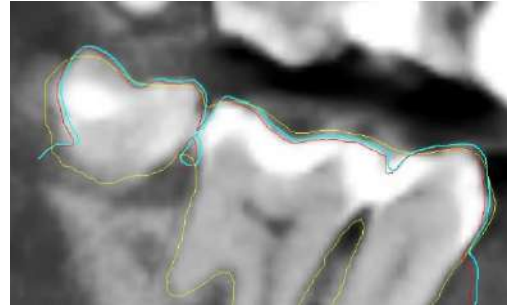


Figure 25 - Contour comparison of the position of the dental rows in automatic and manual mode by marking the areas of interest with the position of segmented CT tooth models. Blue colour - automatic alignment, red colour - manual alignment, yellow colour – segmented CT tooth models

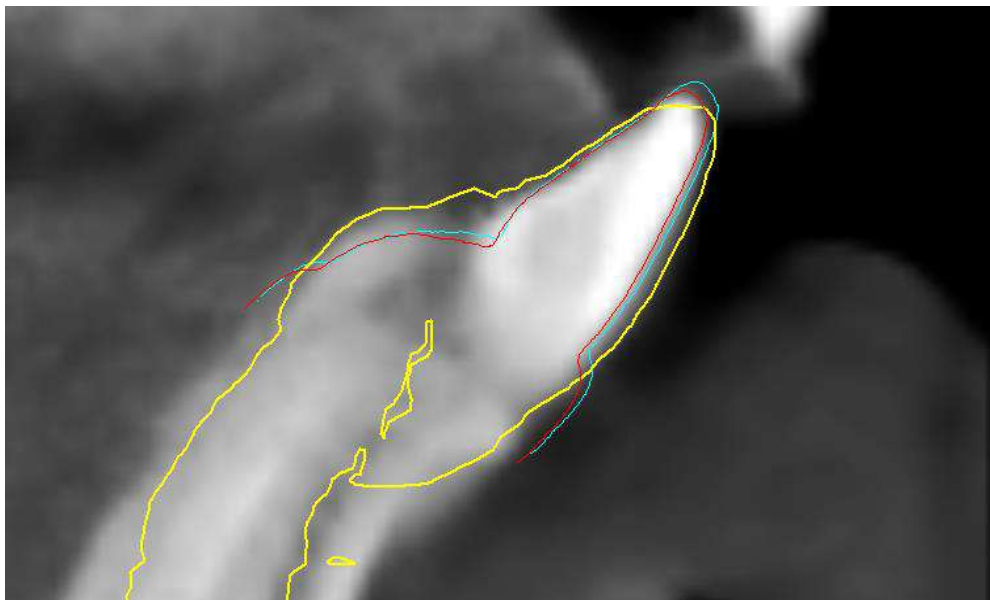


Figure 26 - Contour comparison of the automatic and manual alignment of the teeth by marking the areas of interest with the position of the segmented CT tooth models. Blue indicates automatic alignment, red indicates manual alignment, yellow indicates segmented CT tooth models



In the Mimics Proplan CMF 3.0 software the brush tool was used to select the aligning areas and the scanned 3D dental models were moved (figure 27, 28).

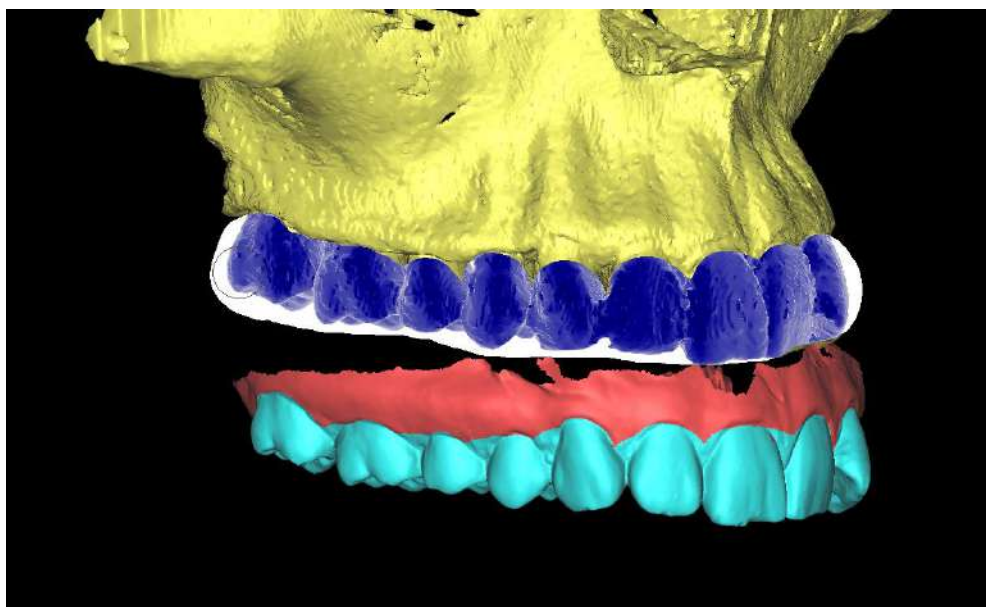


Figure 27 - Method of selecting an area of interest for matching required areas with the brush tool

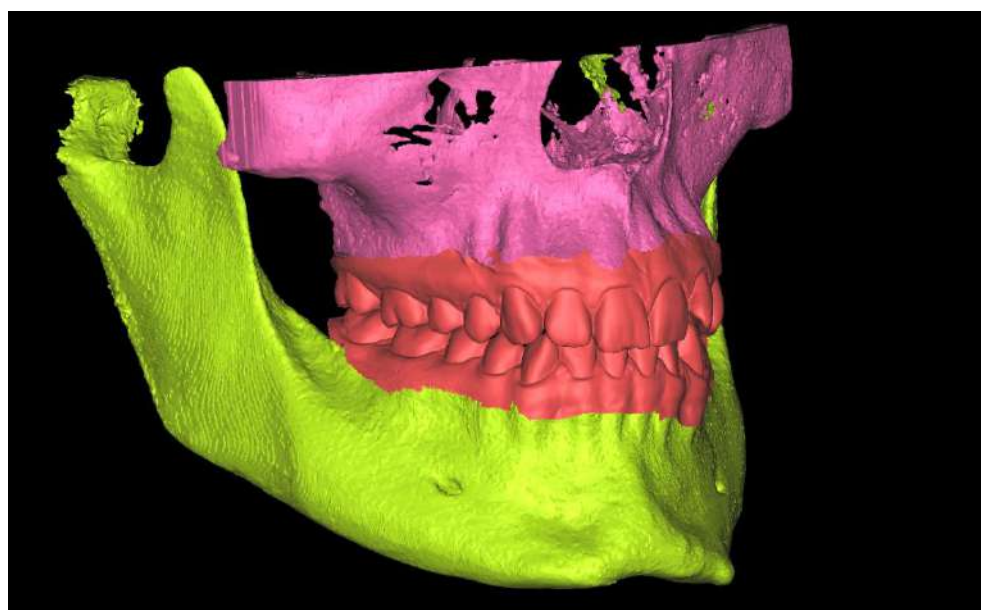


Figure 28 - Aligned model of scanned dental models and segmented CT models

After this function was performed, models were prepared and tooth tissue was removed from the analysis by segmentation of the model set. The crown parts of the teeth were removed from a threshold segmented CT models (figure 29).

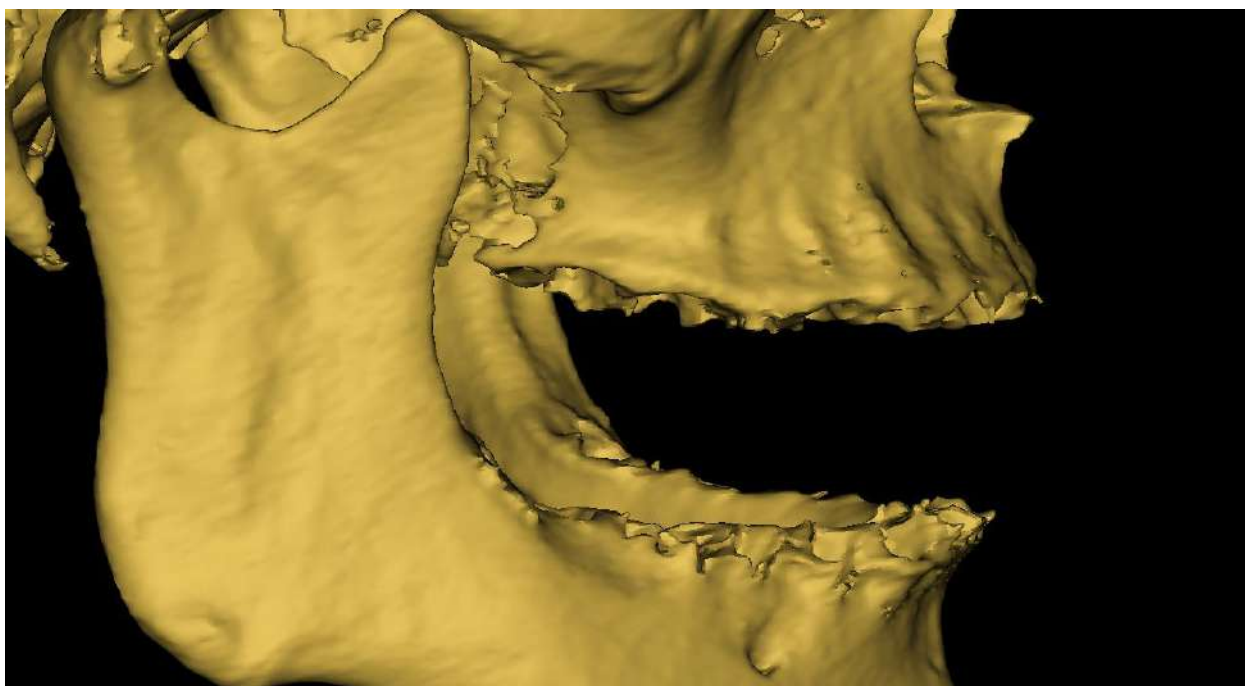


Figure 29 - Segmented model of bone structures without teeth

For the stability and repeatability of the result of processing models without repeating geometry, the factors affecting the processing of three-dimensional models were removed from the method, namely, instead of manual segmentation, processing using computer algorithms was chosen.

Segmentation of the teeth and soft tissues in the models obtained by intraoral scanning was performed by trimming the gingival contour and smoothing the selection line. Two separate models of the teeth and soft tissues were created (figure 30 - 32).

Processing of the combined models: teeth trimming, gingiva, tooth extraction on the 3D CT models.

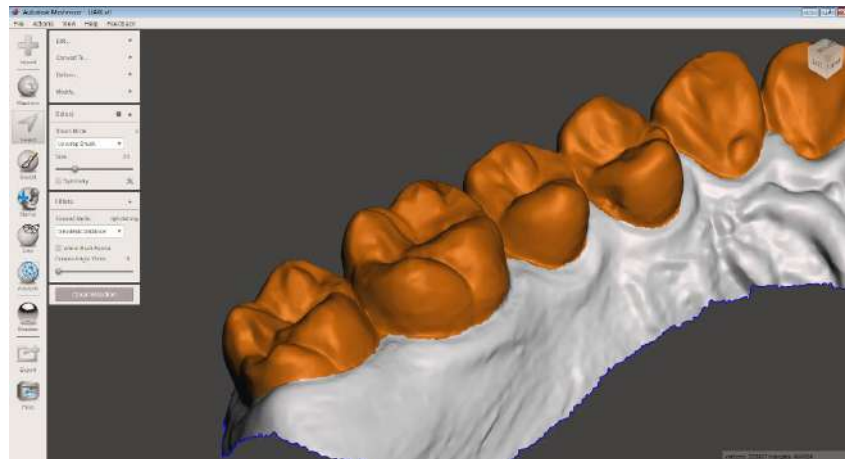


Figure 30 - Segmentation of teeth on a three-dimensional dental model

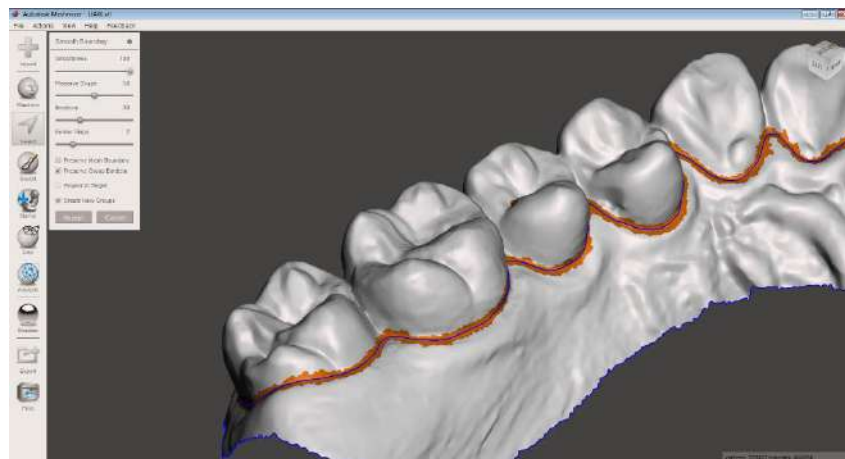


Figure 31 - Smoothing the contours of the selected dentition model

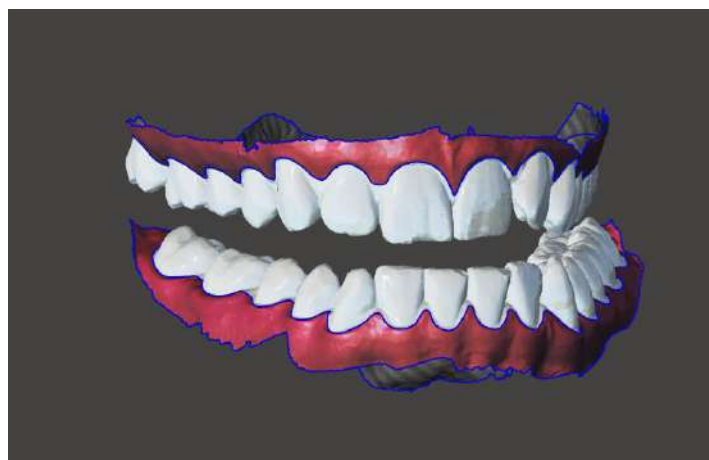


Figure 32 - Separate tooth and soft tissue models in the assembled model

On the next step of processing and removing excess information on the 3D models, the area around the teeth is constructed, in particular around the segmented teeth without soft tissue and with a fixed boundary along the gingival margin, which does not affect the amount of information removed by Boolean operations. After segmentation of the teeth, the separate model by duplication was copied and a mathematical extrusion operation of 1 mm was performed, which gave sufficient coverage and the model filling planes converged at a slight angle in the centre (figure 33, 34).

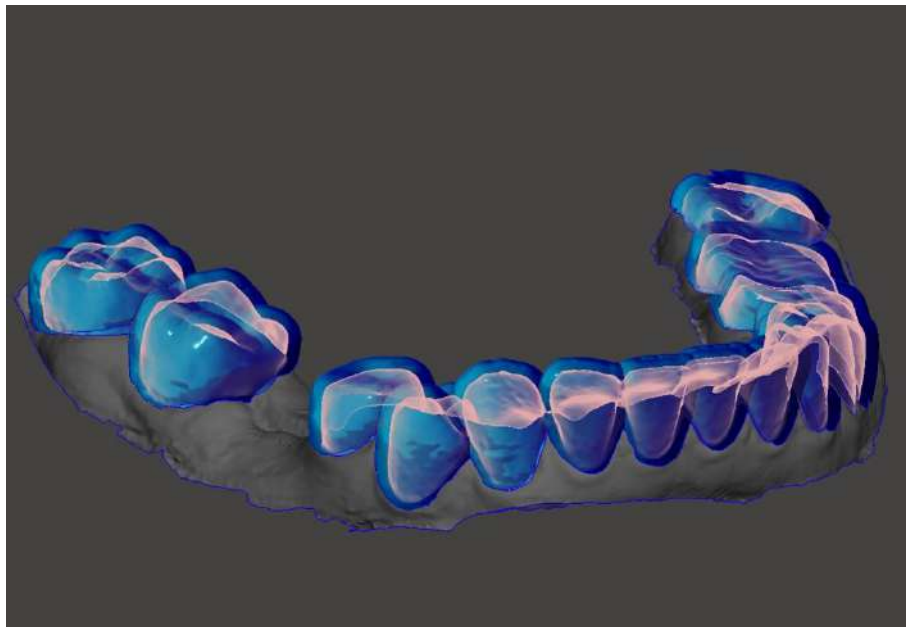


Figure 33 - Extrusion of the segmented tooth model by 1 mm

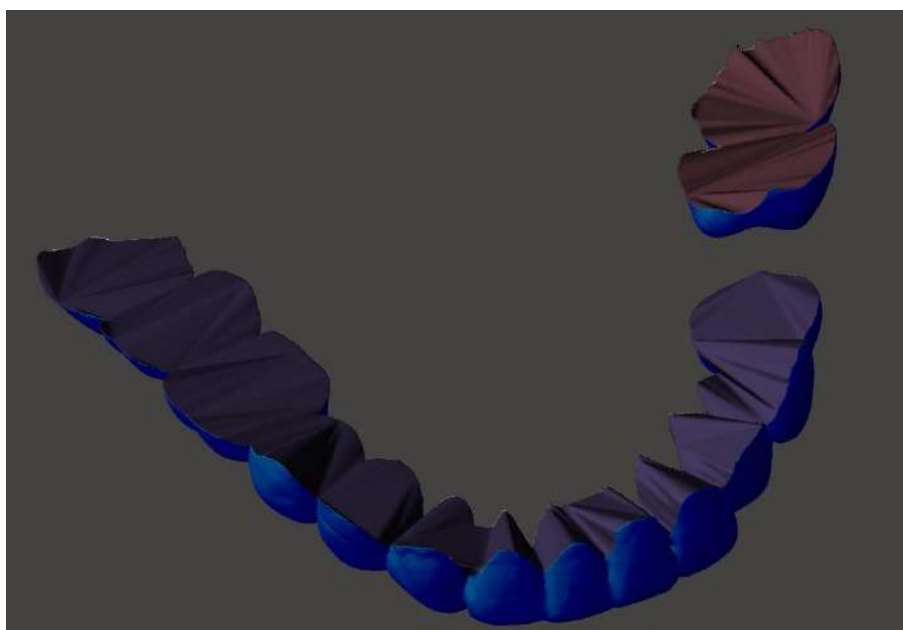


Figure 34 - Closing the contours of the segmented model

To perform Boolean functions with three-dimensional objects, solid models were created from upper and lower jaw shells and segmented closed models of the upper and lower arches of dental models (figure 35).

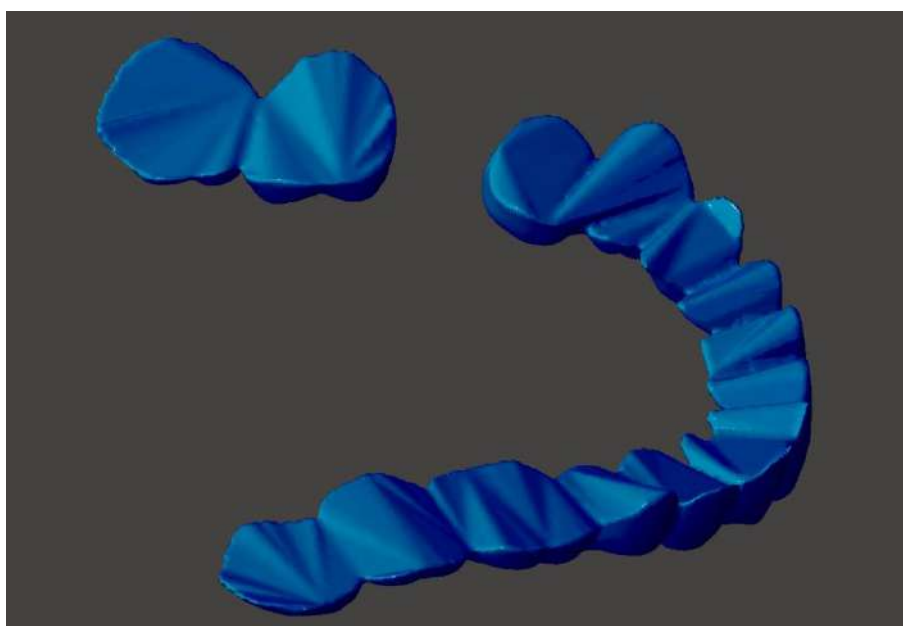


Figure 35 - Converting a shell into a solid model



After executing the Boolean functions, the models were automatically refined to close and correct geometry errors (figure 36 - 39).

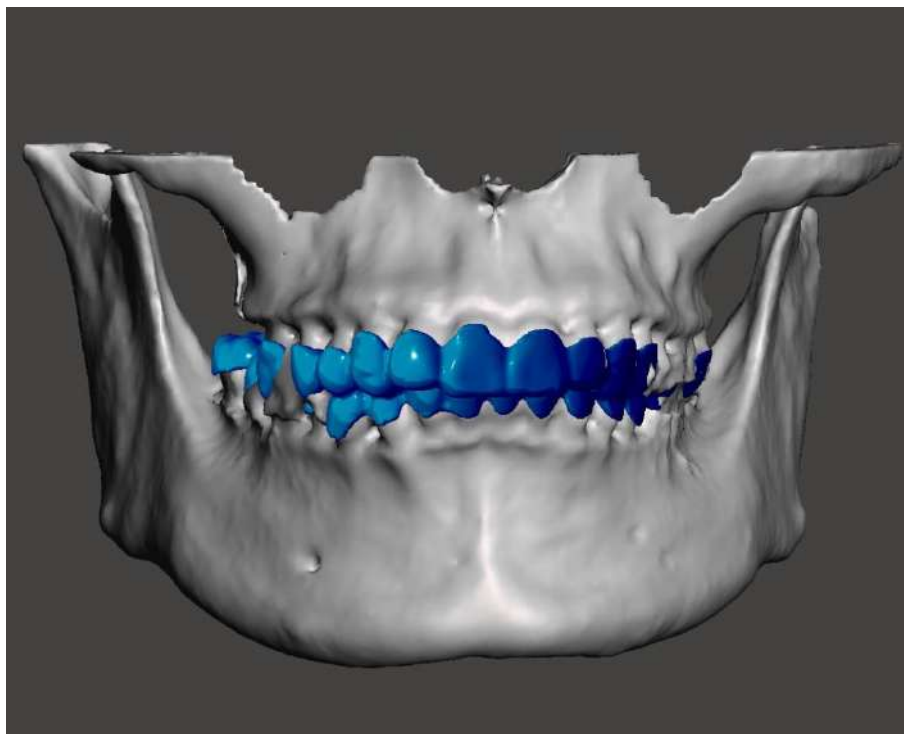


Figure 36 - Models before the Boolean function

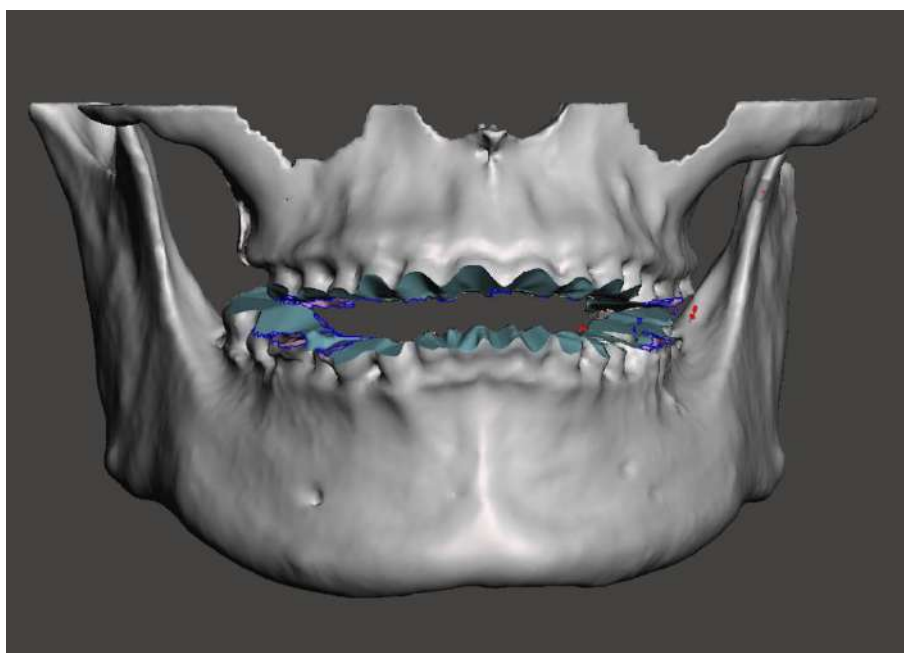


Figure 37 - Three-dimensional model of the mandible and maxilla after performing the Boolean operation

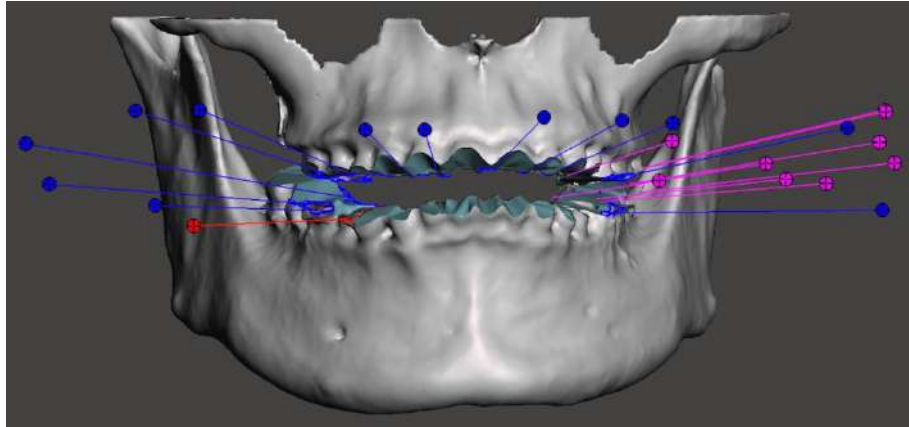


Figure 38 - Automatic geometry error correction

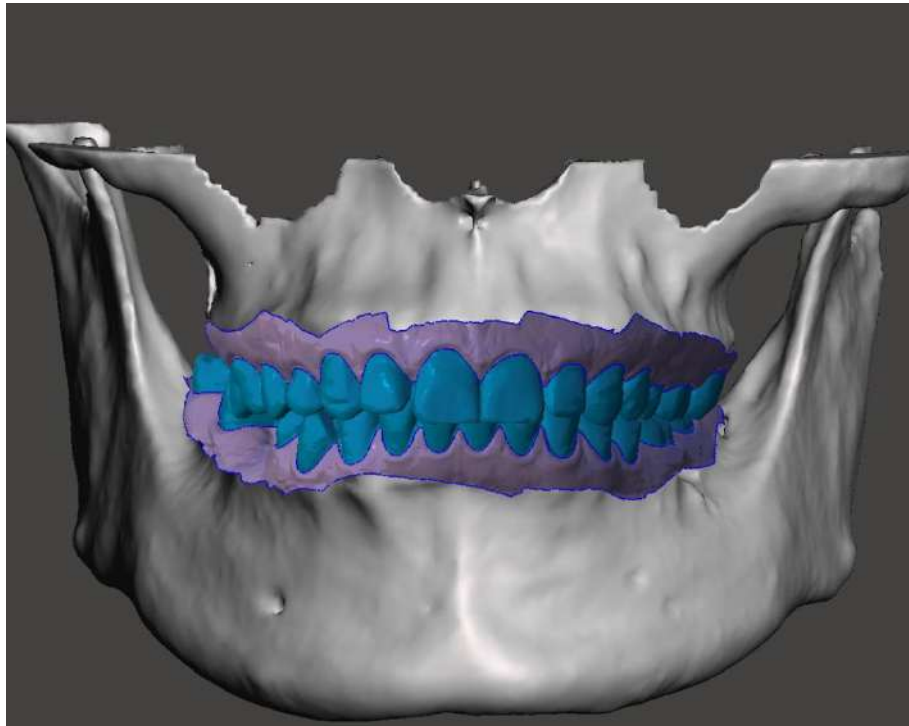


Figure 39 - Assembled 3D model, ready for analysis

### 3.2.2 Creating a digital model of the mucosa biotype

After obtaining the processed models, the distribution scale was adjusted for absolute values in the Cloud Compare software (figure 40, 41). Segmented dental, bone,

and soft tissue models were imported into the software and the selected shells were analysed (figure 42).

Data processing in Cloud Compare, customization, colour systematization.

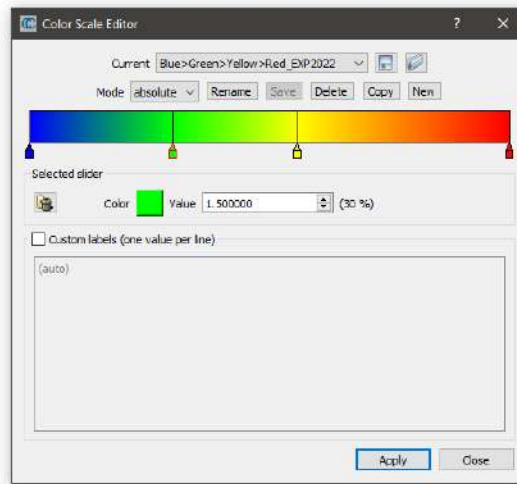


Figure 40 - Medium mucosa biotype values

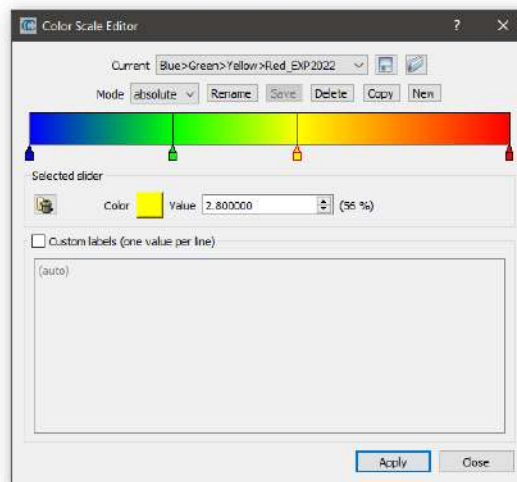


Figure 41 - Thick mucosa biotype values

A systematic approach to examining the models obtained and creating distance maps is an important step and forms a further distribution into groups according to colour



gradation. Relative scale values distribute the colour palette evenly and with the same oral mucosal thickness on different models will give different colours, which in turn will give an erroneous allocation to groups of oral mucosal biotypes.

The absolute values of the colour grading scale were used for systematization and this scheme was applied to all the studied models.

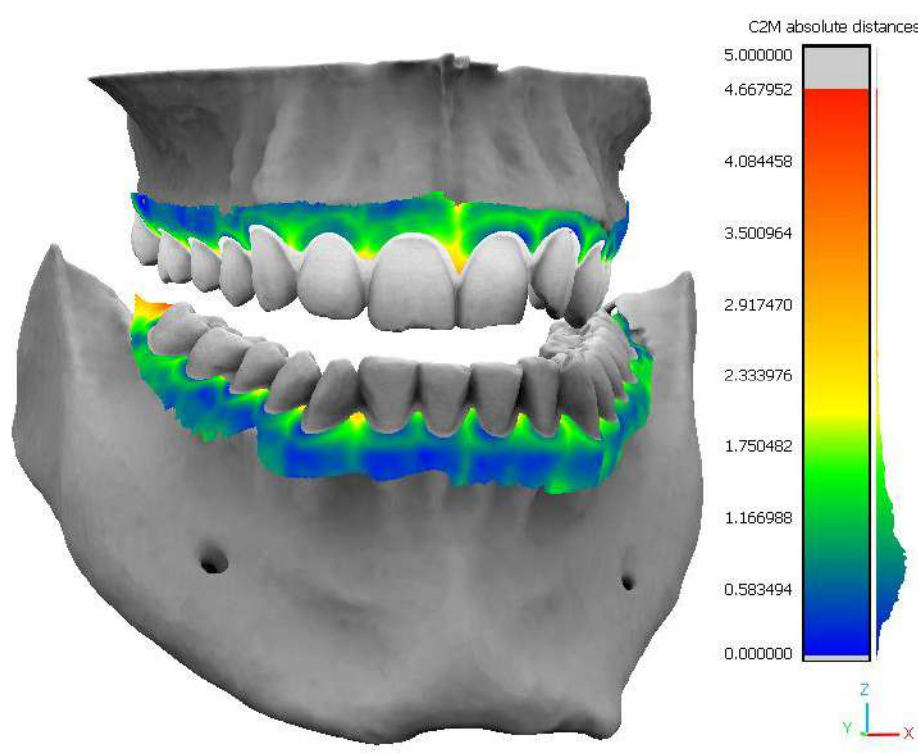


Figure 42 - Soft tissue thickness map

Based on the data obtained, the entire analysis area can be divided into three zones (figure 43):

1. Vestibular surface from teeth 18 to 28 and 38 to 48.
2. Oral surface from teeth 15 to 25 and 35 to 45.
3. Oral surface from teeth 18 to 15, 28 to 25, 38 to 35, 48 to 45.

This segmentation into zones can be seen in the distribution graph (figure 44).

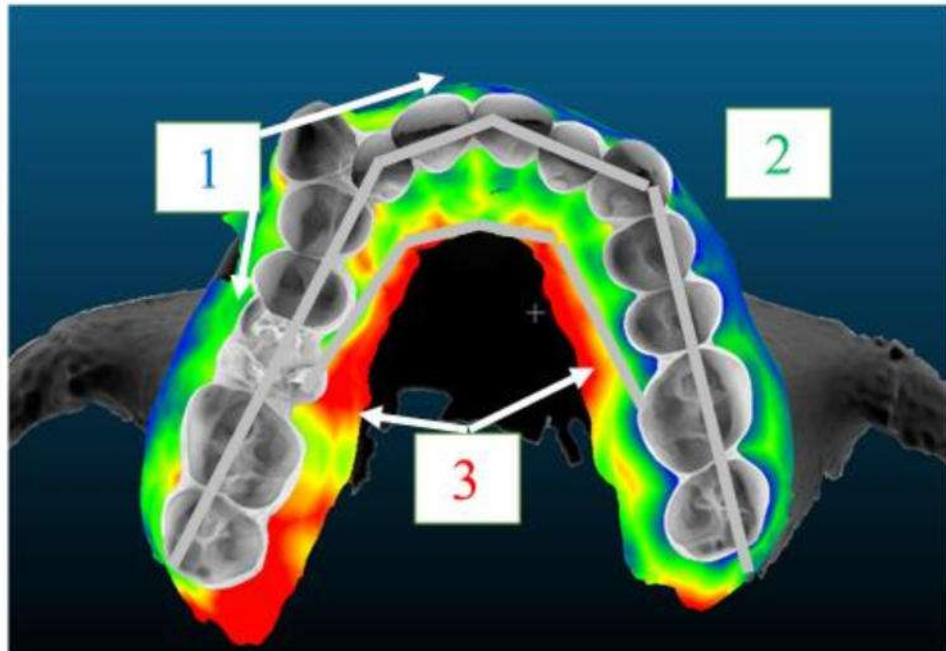


Figure 43 - Distribution of mucosal thickness into zones

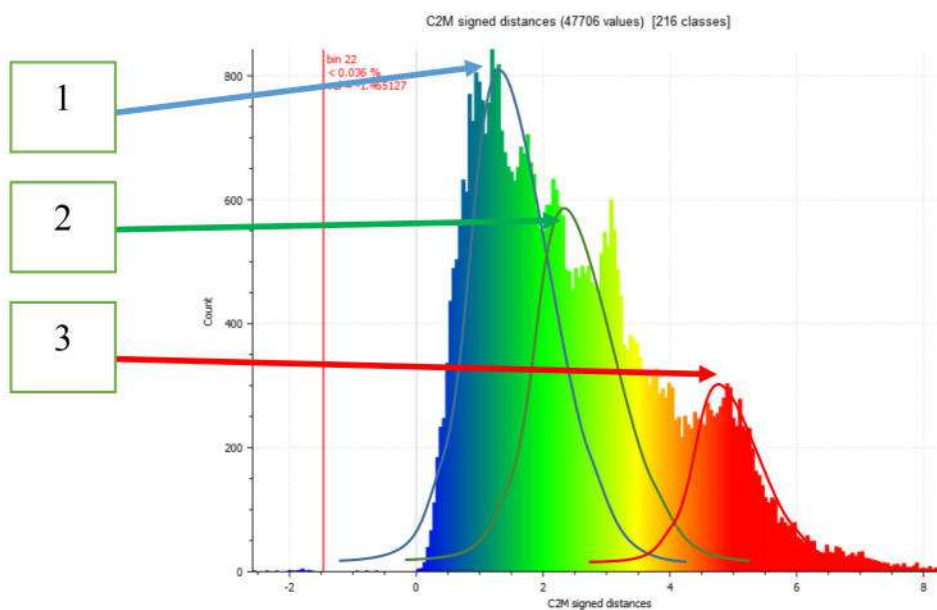


Figure 44 - Areas of mucosal thickness distribution

The analysis of the distribution shows three overlapping dispersions corresponding to the zones described above. By plotting the distributions and interpolating them on the control measurements taken in the oral cavity by mucosa translucency, different patterns of both distributions were obtained, characteristic of the three biotypes of oral mucosa.

Control measurements were made in a traditional way, using a periodontal probe and assessing the translucency of the attached gingiva. The qualitative data collected helped to separate the quantitative data into primary groups, and to carry out an analysis to pinpoint the mucosal biotype and interpolate the quantitative data into qualitative data (figure 45).

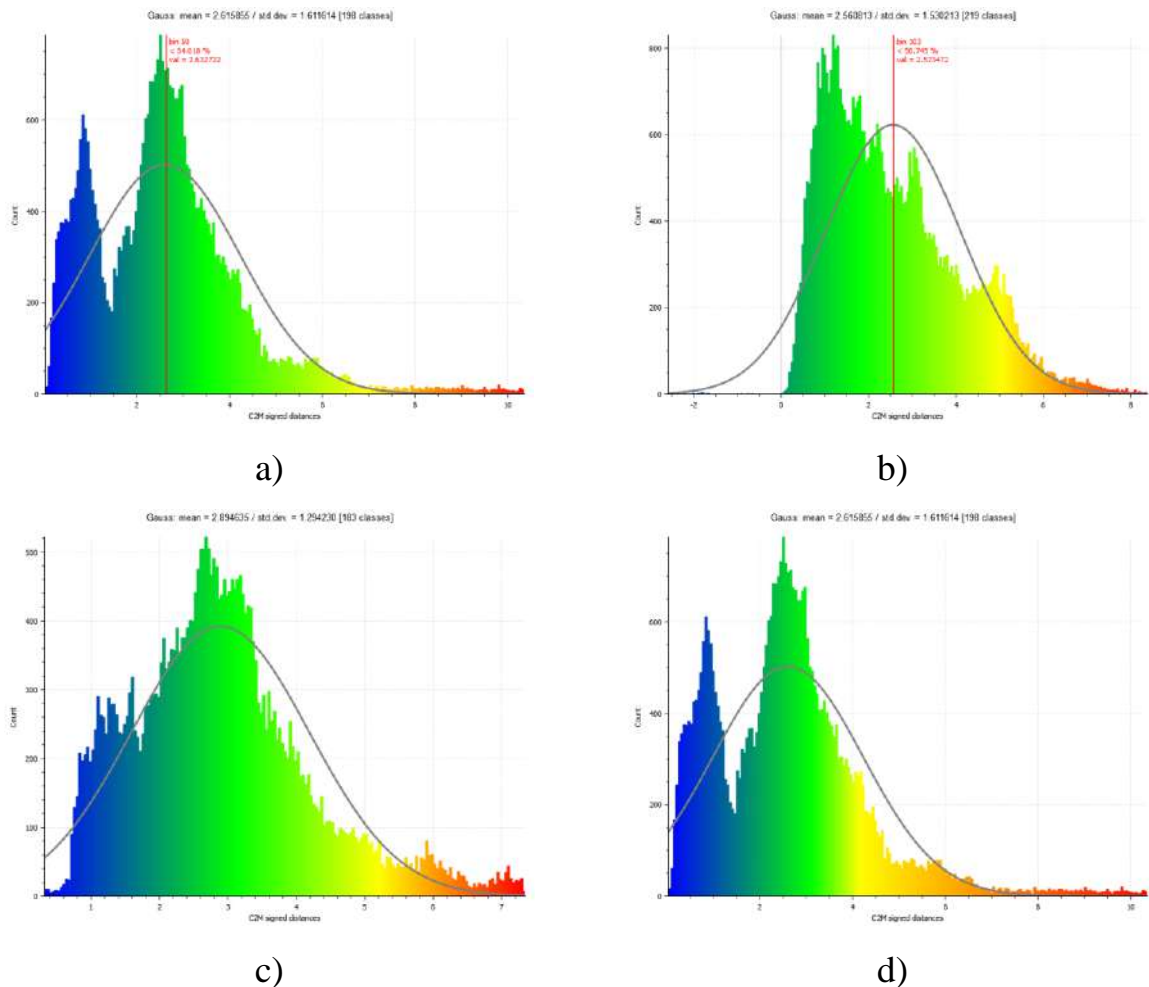


Figure 45 - Interpretation of the normal distribution in the graph of mucosal thickness distribution areas, indicating a shift towards the mucosa biotype thickness (a), (b), (c), (d)

### 3.2.3 CT data segmentation methodology choice

It is possible to obtain the segmentation result from CT scans using different methods. When working with a small amount of CT, manual segmentation can be used. With the development of tools for selecting the necessary masks, the processing speed increases significantly, but when a large number of layers are processed, the precision of the result decreases. A comparison was made on how much the choice of segmentation method affects the measurements result. Two approaches to segmentation were to be considered: manual and automatic using AI algorithms (figure 46 - 49).

With AI segmentation

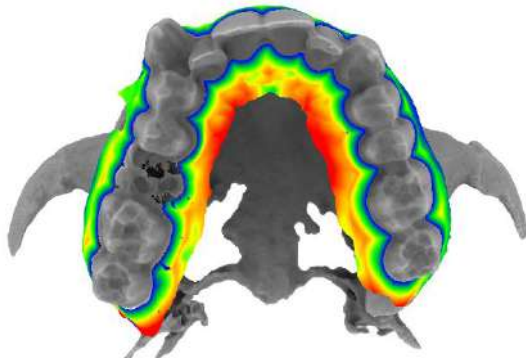


Figure 46 - Distribution of upper jaw mucosa thickness on the automatically segmented model

Without AI segmentation

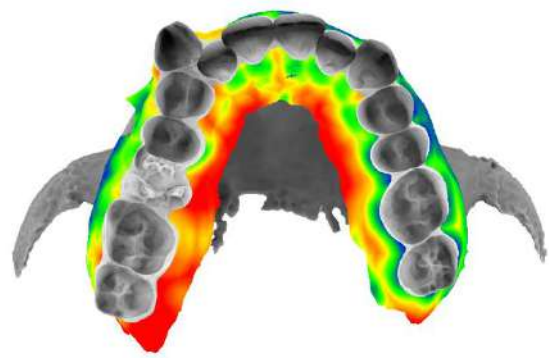


Figure 47 - Distribution of upper jaw mucosa thickness on the had segmented model

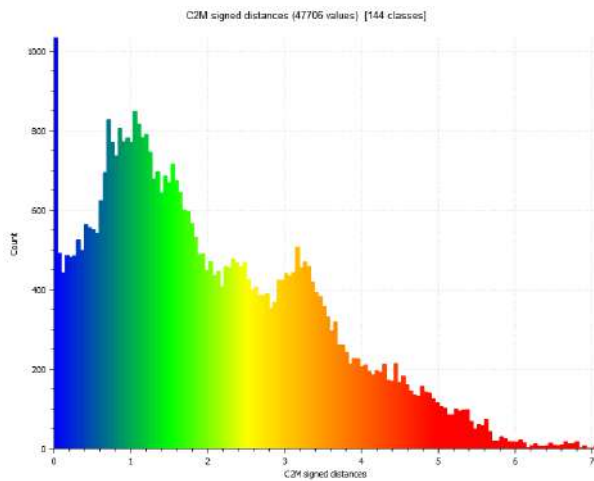


Figure 48 - Distribution graph of upper jaw mucosa thickness on the automatically segmented model

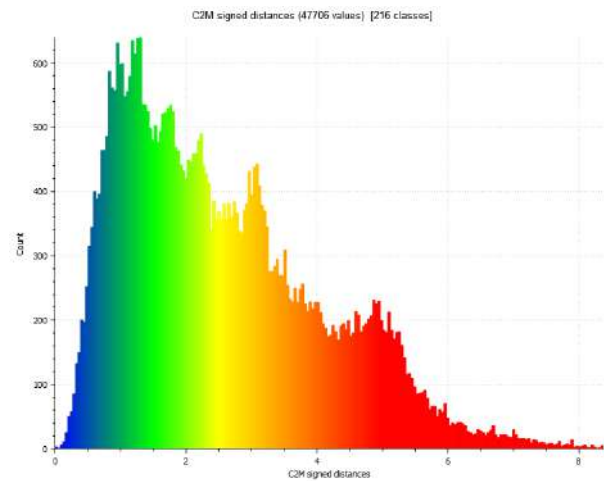


Figure 49 - Distribution graph of upper jaw mucosa thickness on the hand segmented model

In order to achieve a stable result with the lowest error when processing CT data - creating masks of each layer and generating the 3D model grid, automatic segmentation algorithms were used instead of manual segmentation. The final result of manual and automatic segmentation remained the same. However, the papillary sheath can be noted in the graph of mucosal thickness distribution in automatic segmentation (figure 50).

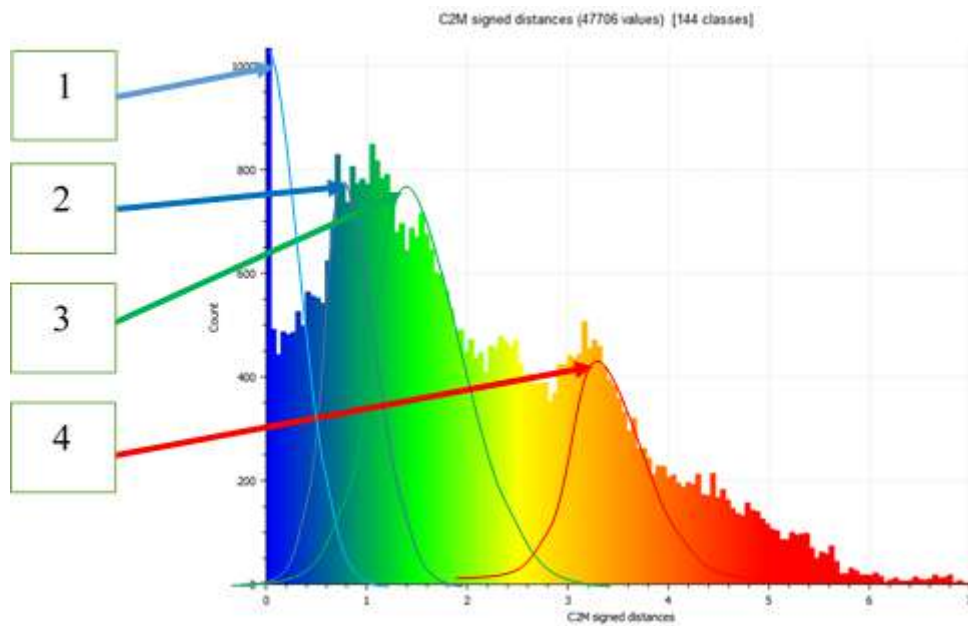


Figure 50 - Areas of mucosal thickness distribution on the graph with AI automatic segmentation

Examples of oral mucosa thickness distribution in different patients graphs are shown below, visualisation of CT data on three-dimensional models, correlation analysis of mucosa definition by gingival translucency, staining of mucosa with “Colour-test №1” and distribution of mucosa thickness on three-dimensional models for different classifications of mucosa (figure 51 - 59).

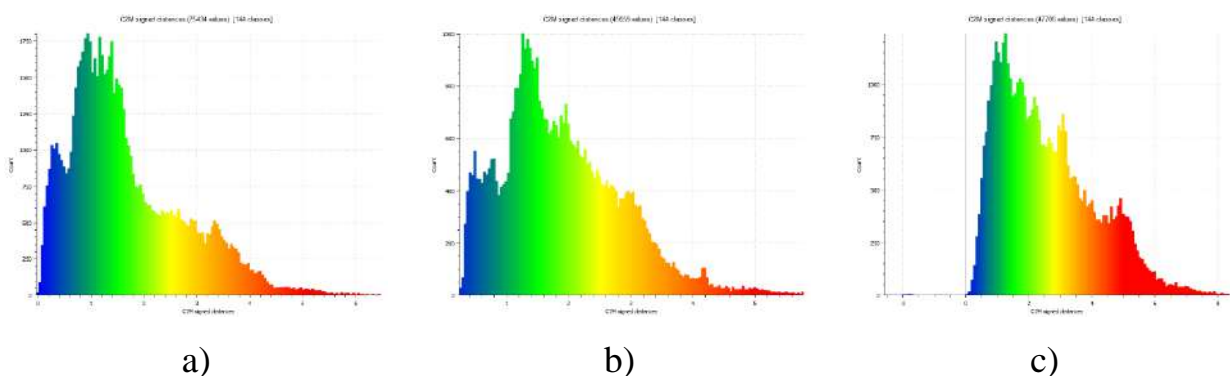


Figure 51 - Distribution of mucosa thickness on the maxilla on the segmented model by manual method. Thin (a), medium (b), thick (c) gingival biotype



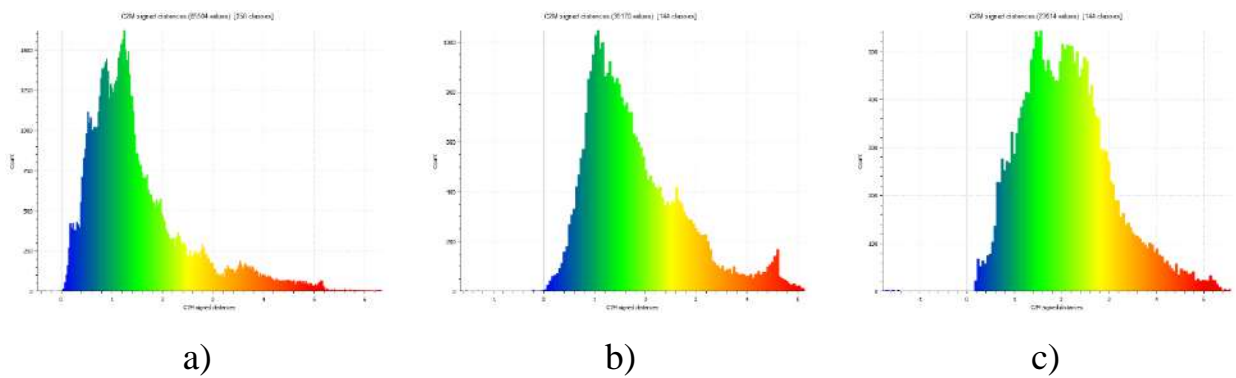


Figure 52 - Distribution of mucosa thickness on the mandible on the segmented model by manual method. Thin (a), medium (b), thick (c) gingival biotype

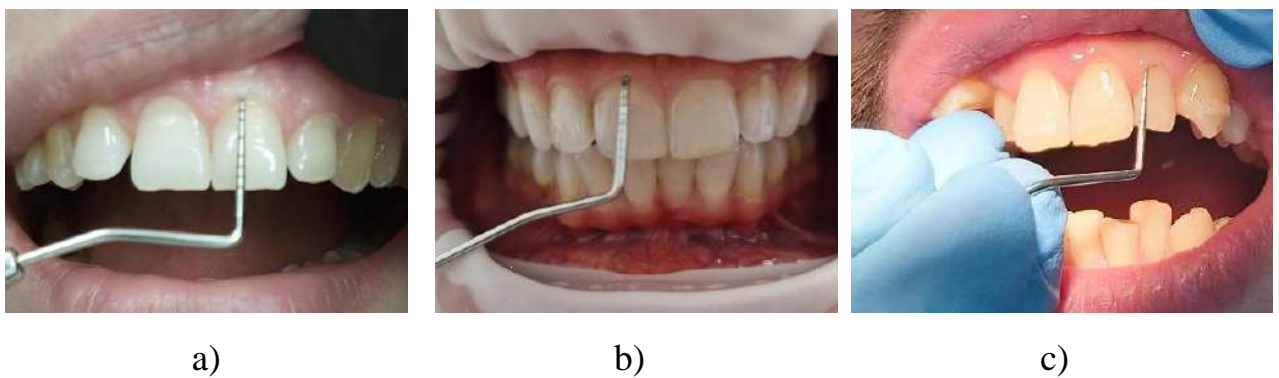


Figure 53 - Determination of gingival biotype by the probe translucence method. Thin (a), medium (b), thick (c) gingival biotype

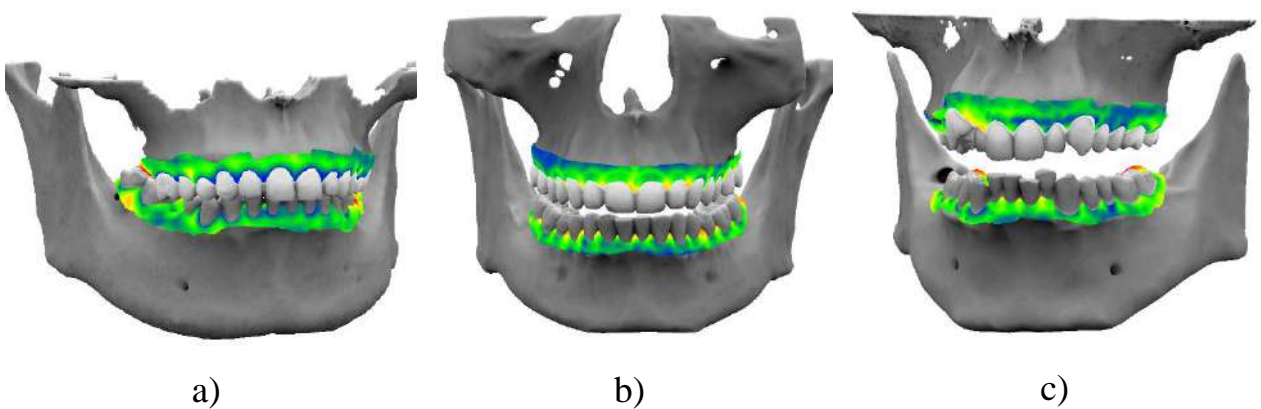


Figure 54 - Three-dimensional deviations map for determining the gingival biotype. Thin (a), medium (b), thick (c) gingival biotype

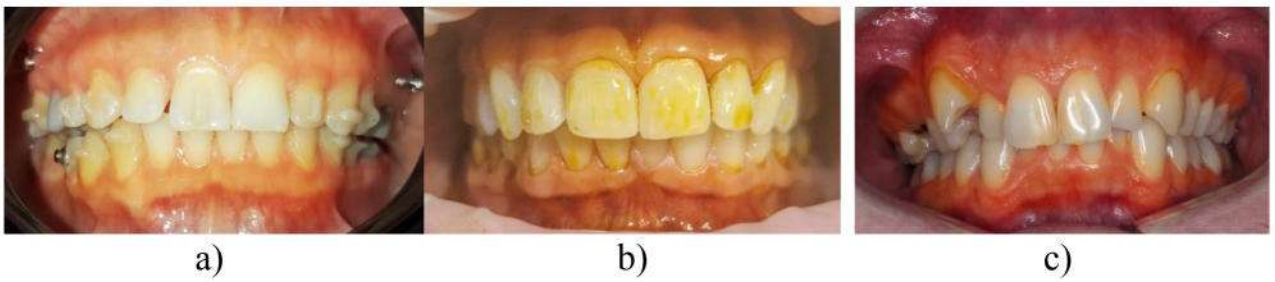


Figure 55 - Determination of inflammation using "Colour-test №1". Thin (a), medium (b), thick (c) gingival biotype

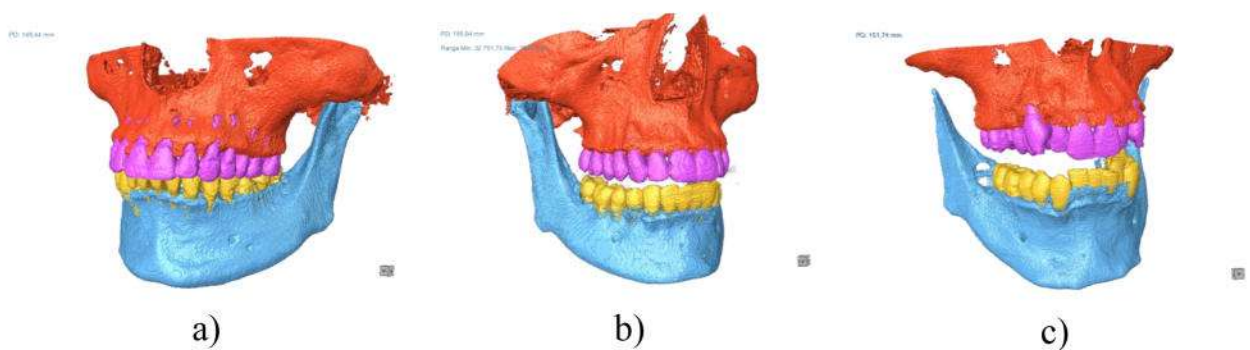


Figure 56 - 3D model of bone structures and dentition from CT using AI segmentation. Thin (a), medium (b), thick (c) gingival biotype

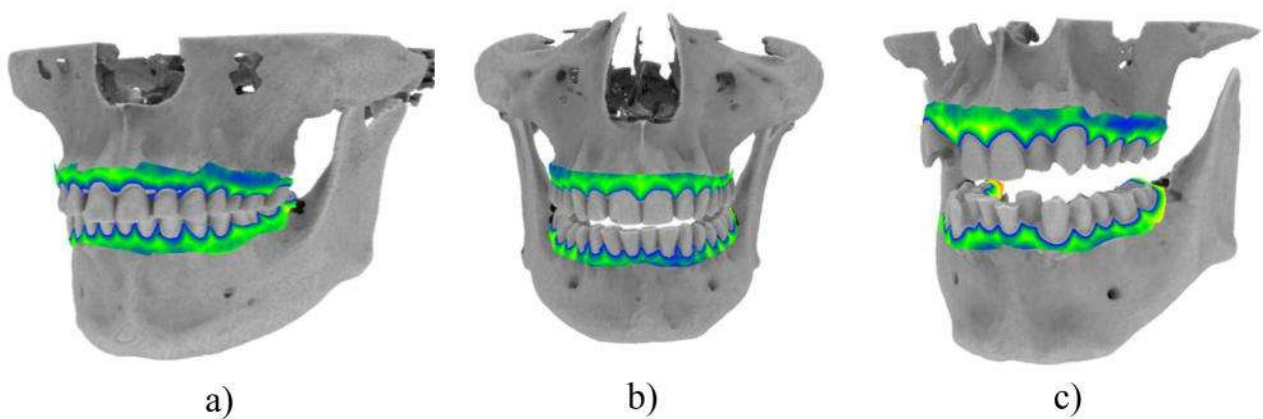


Figure 57 – Gingiva thickness distribution on a 3D AI-segmented model. Thin (a), medium (b), thick (c) gingival biotype



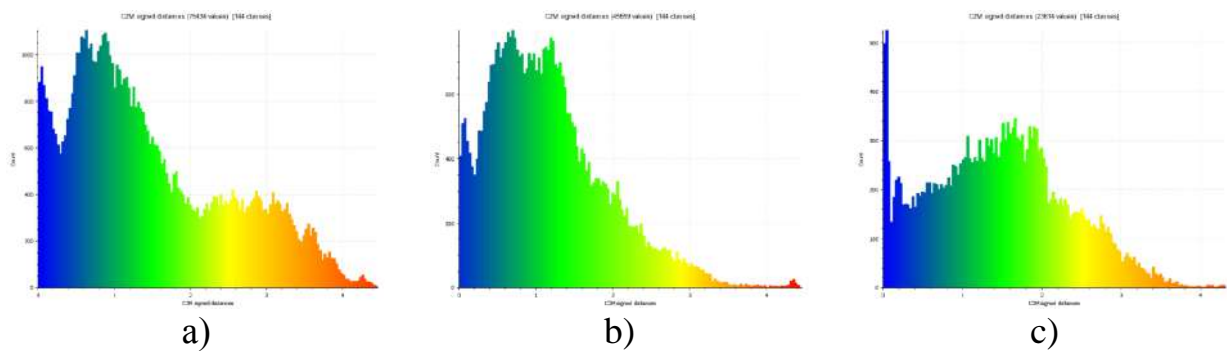


Figure 58 - Distribution of gingiva thickness on a 3D AI-segmented model of the maxilla. Thin (a), medium (b), thick (c) gingival biotype

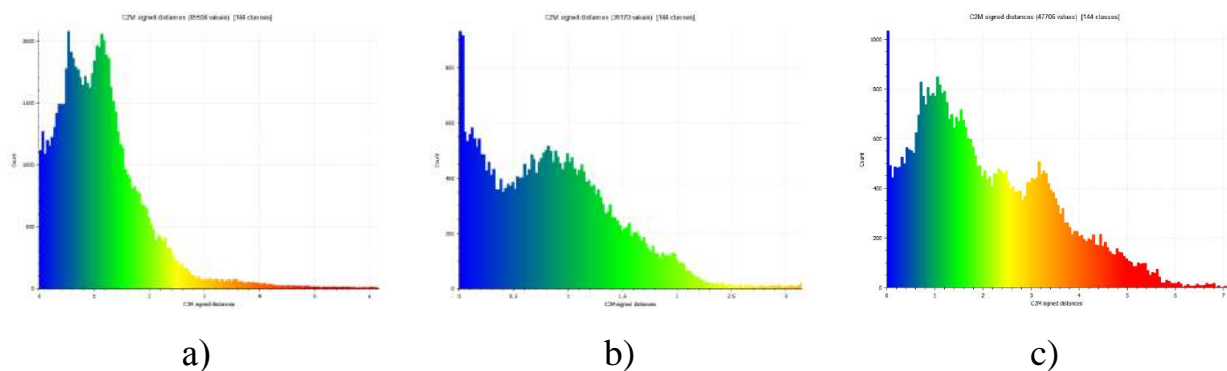


Figure 59 - Gingival thickness distribution in an AI-segmented 3D mandible model. Thin (a), medium (b), thick (c) gingival biotype

The conducted studies showed that the dispersion analysis of zone distribution revealed three types of oral mucosa - thin, thick and mixed in accordance with traditional periodontal probe examinations. Mucosa with signs of inflammatory processes was excluded from the study.

### 3.2.4 CT data segmentation

This study consisted of a theoretical part, where the deformation distributions of the aligners were calculated, and a clinical part, where the obtained data was tested during clinical appointments.

The obtained data from CT segmentation in the form of three-dimensional models of the maxilla and mandible was the starting point for further studies, such as the creation of three-dimensional models of the dentition using intraoral scanning, the planning of various orthodontic designs, and the determination of the possibility of using implants and templates (figure 60).



Figure 60 - Three-dimensional model of the maxilla and mandible after manual segmentation

### 3.3 AI Segmentation

Data collection and pre-processing was used in segmentation. The data used in the study were obtained using a CBCT and processed in Dragonfly software (v.2022.2, Objects Research Systems, Montreal, QC, Canada) normalized the HU value of the CBCT data was set to 0-1.

#### 3.3.1 Normalization of CT data

To reduce the amount of data to be processed, pre-processing was performed. This involved normalizing the data to a standard range.

In CBCT, images are represented using Hounsfield units (HU) [229]. HU is a dimensionless unit universally used in computed tomography (CT) to express CT numbers resulting from the linear transformation of measured attenuation coefficients [144]. The results are based on arbitrarily given densities of air and pure water. They range from -1000 HU for air and over 3000 for metals [121]. In this study, normalization was performed using a linear function:

$$y = mx + b,$$

where:  $x$  refers to the HU obtained with the CBCT machine, with a minimum value (-1000) and a maximum value (3000-20000), which depended on various machine and scanning parameters as well as the irradiation dose;

$y$  is the target HU value in the range 0-1. In these data, the mean HU value was 0.16. The standard deviation value was 0.15.

The probability map of the CBCT HU distribution is shown in figure 61, and after normalization, the HU probability distribution map is shown in figure 62.

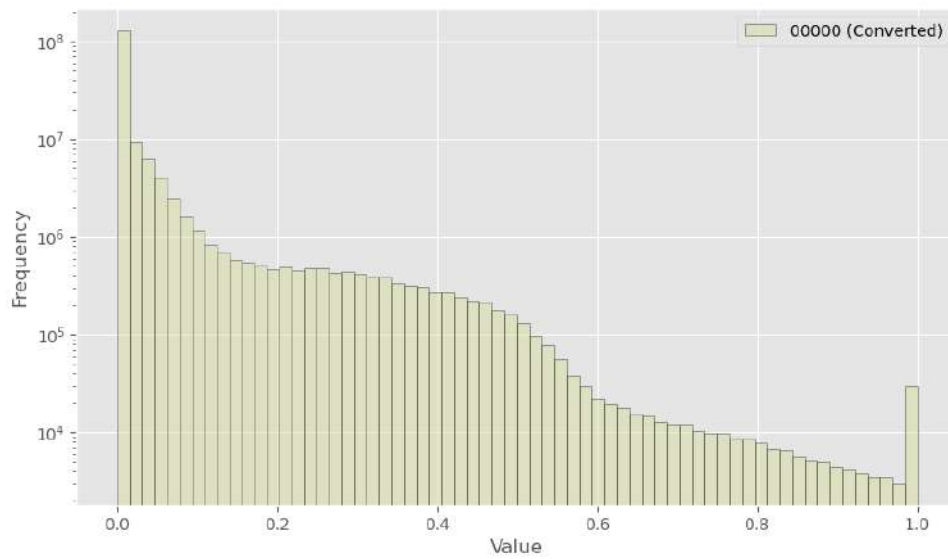


Figure 61 - Probability of CBCT HU distribution map

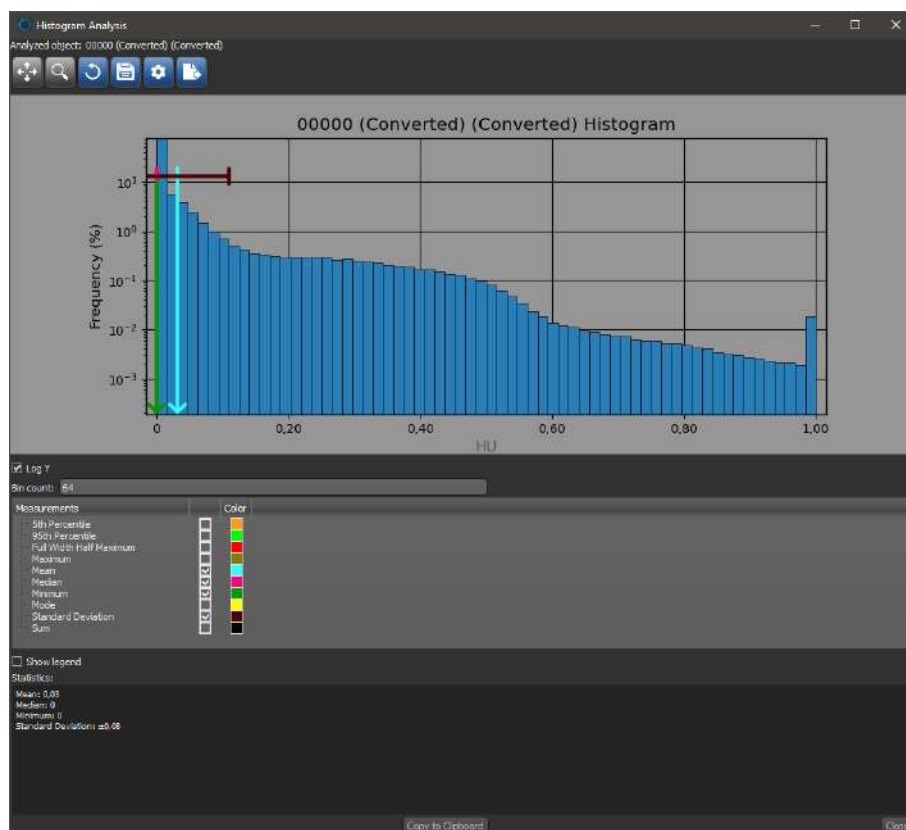


Figure 62 - Probability of CBCT HU distribution map after normalization

### 3.3.2 Annotation of CT layers data

The purpose of semantic image segmentation was to label each pixel in the image with the appropriate representation class. The output itself is a high-resolution image (usually the same size as the input image) in which each pixel is assigned to a particular class. Each image was labelled with five different colours that were used to represent the five classes (upper dentition, lower dentition, upper jaw, lower jaw and background) (figure 63). The images were normalized as shown in the top image in figure 64 and the manually labelled result is shown in the bottom image in figure 64.

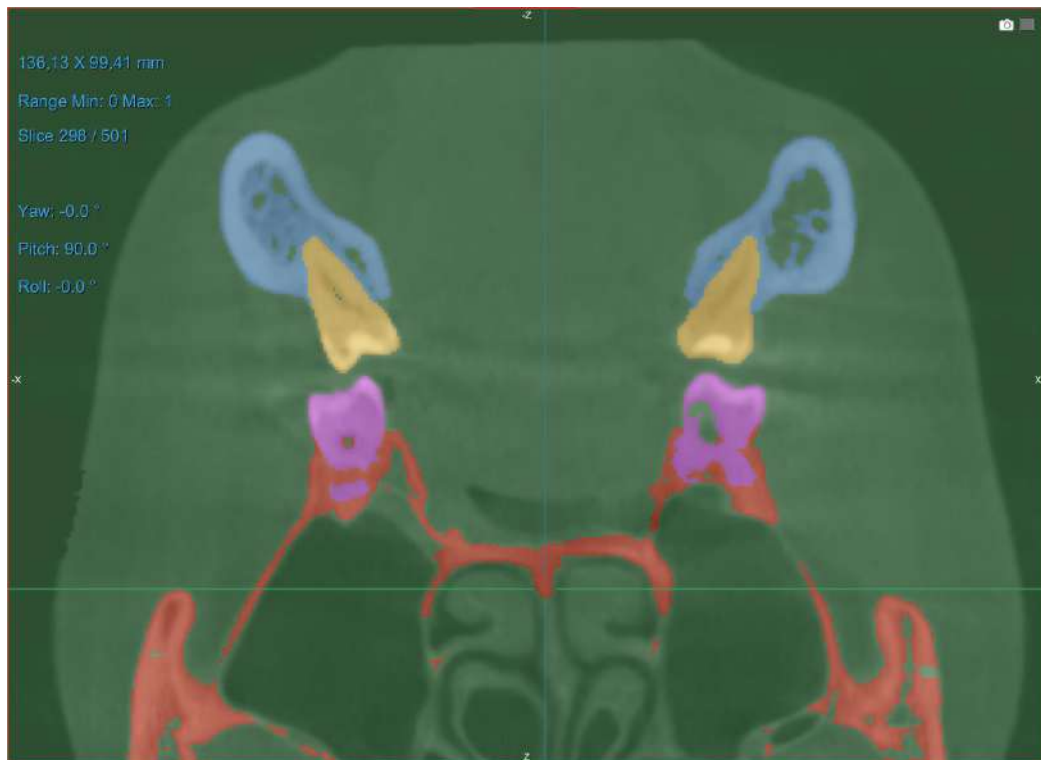


Figure 63 - Semantic segmentation of the CBCT. The image is divided into five classes, in which the upper dentition is purple

### 3.3.3 Increasing the amount of AI training data

Data augmentation is a method of artificially creating more training samples to increase the diversity of training data. This can be achieved by applying affine transformations (e.g. rotating and scaling), moving vertically and horizontally to the original labelled samples. The image brightness was randomly changed by specifying the luminance factor due to different HU values in different CBCT data. The luminance coefficient was chosen randomly in the range  $[-0,2]$ . The luminance variation allows the model to perform a generalization over all trained images at different luminance levels. The data was augmented 10 times using different factors.

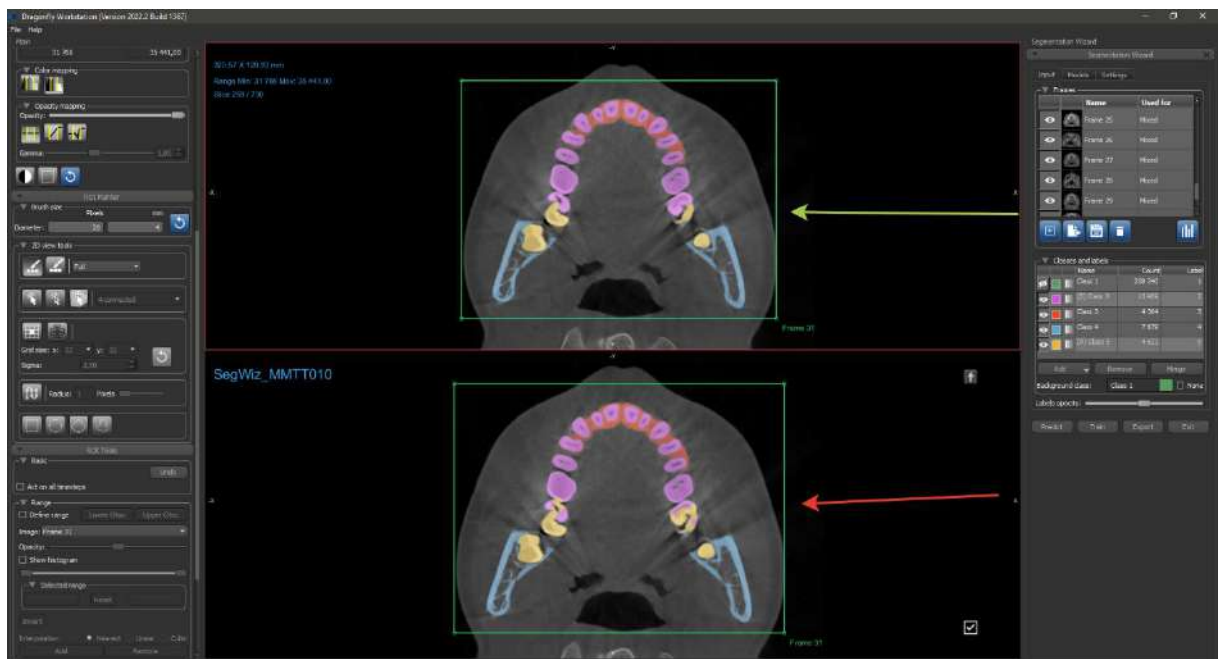


Figure 64 - Annotation result of the CBCT sample

### Manual segmentation in U-Net training

Manual segmentation is used to create anchor layers, which is used to train the neural network and, if necessary and if a large number of errors occur, is supplemented with additional correction layers with masks (figure 65, 66).

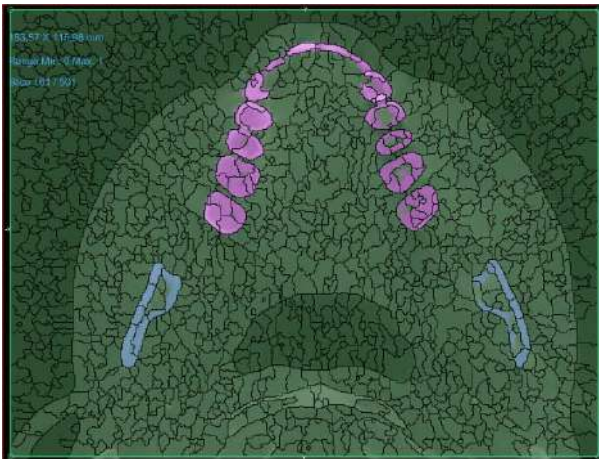


Figure 65 - Manual segmentation of maxilla and mandible in preparation for a training model. Purple is the dentition of the upper jaw. Blue - lower jaw bone structure, green - background

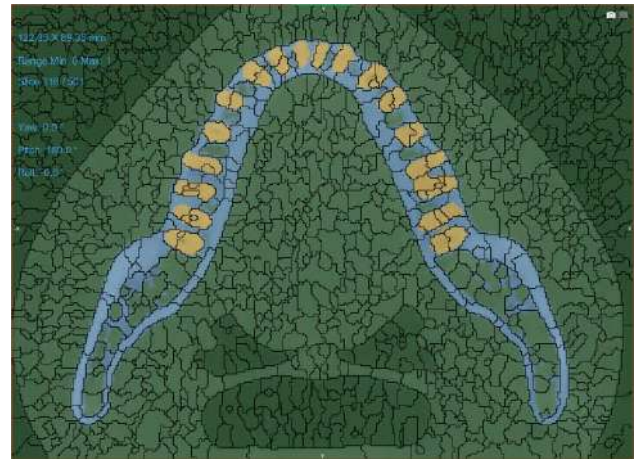


Figure 66 - Manual segmentation of maxilla and mandible in preparation for a training mode. Yellow is the dentition of the mandible. Blue - lower jaw bone structure, green - background

### 3.3.4 Semantic segmentation of images using U-net

The aim of this step was to label each pixel in the image with the appropriate class. The 2D U-net model consists of encoding and decoding parts [248]. The training parameters in U-net were as follows: number of layers in the model = 4, patch size = 64, packet size = 32 and loss function = cube loss. Training was performed using 100 epochs; however, it was terminated if there was no improvement in the “loss value” for 10 consecutive epochs. The overall structure of the network is illustrated in figure 67.

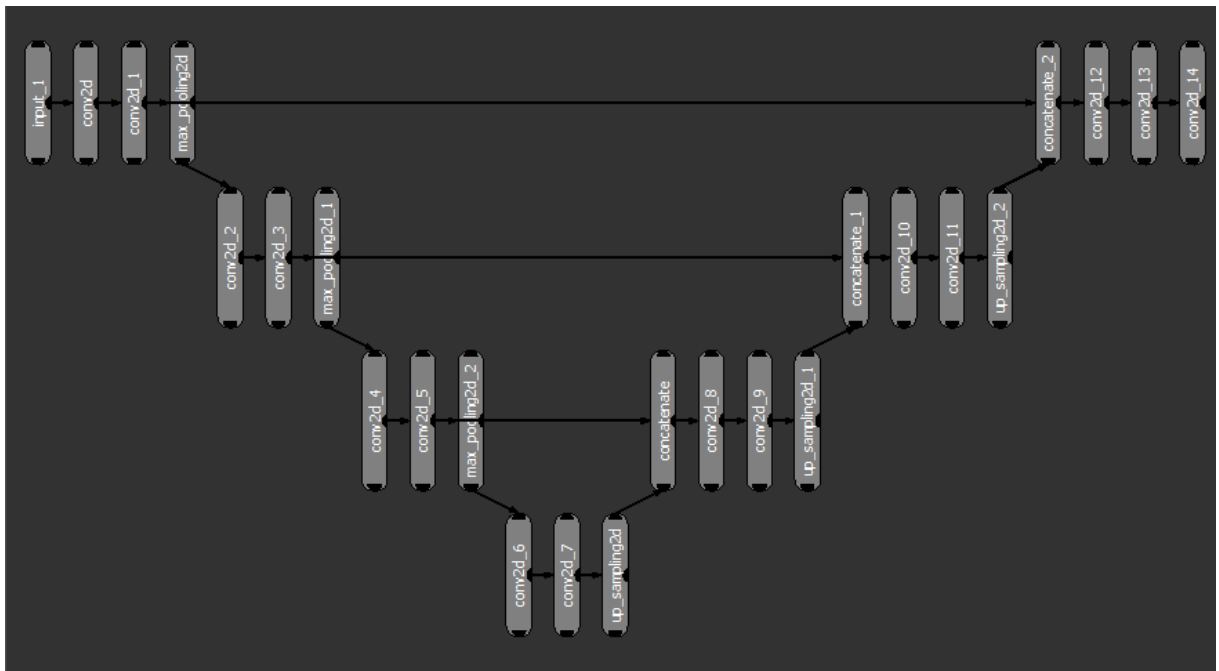


Figure 67 - 2D U-net architecture

Image noise was removed from the ROI, smoothed the data and created a 3D model reconstruction based on the ROI. Small unrelated noise, which was less than  $0.8 \text{ nm}^3$ , was eliminated. The final ROI was then converted into “grid” data (figure 68).



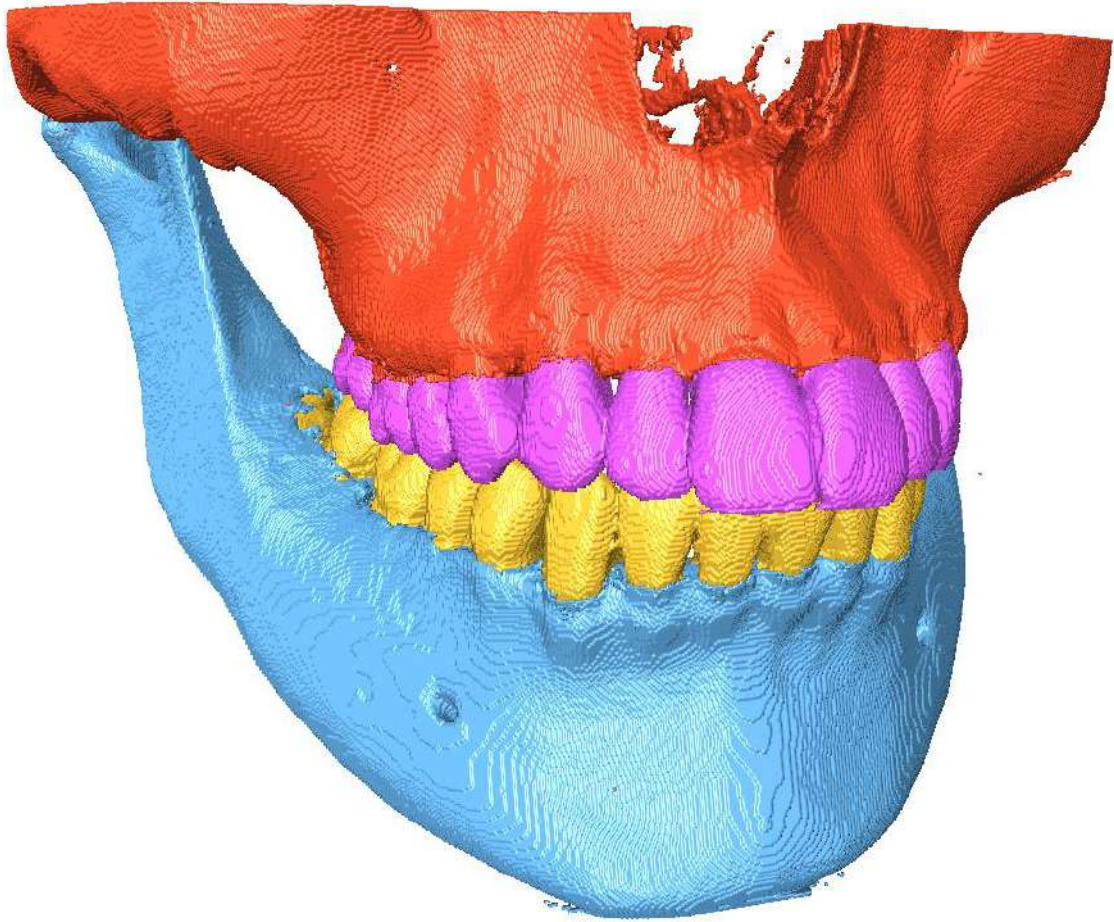


Figure 68 - Result of the 3D model after final U-Net neural network training

**Normalization is important for image pre-processing.** If the image is not pre-processed, the network will diverge during training, causing the loss function value to reach infinity. Normalization was done by linear change, and the resulting value was in the range 0 to 1. If the normalized range is different, the result will be affected. However, as the amount of data increases during training, the trained U-net model can be used in the new CBCT.

Gan Y. et al. [113] proposed a method to extract the connected tooth and alveolar bone region from CT images using a global convex level set model. However, this method can only be used in patients whose teeth are in the open bite position. In this study, U-net

combined with data magnification method is proposed to achieve automatic segmentation of different tissues in a closed bite.

In this study, the image segmentation efficiency was significantly improved by training the network by manually labelling five images. Subsequently, by increasing the data volume, fully automatic segmentation and identification of multiple tissues in the oral cavity can be performed. The accuracy of automatic segmentation can be increased, which will significantly improve automated diagnostics in dentistry.

### **3.3.5 AI based CT segmentation**

Created working layers to train the U-Net neural network by preparing and processing input CT data.

The neural network was trained, and as a result, an automatic algorithm for segmenting bone structures and dental radii from CT data was created.

Deviation control analysis was performed on selectively taken models (figure 69), by which segmentation errors could be detected. The result obtained with segmentation accuracy control is effective with a large amount of data in a short period of time (figure 70).

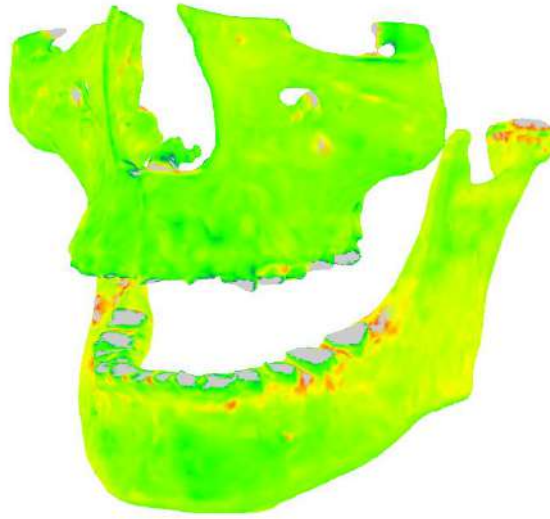
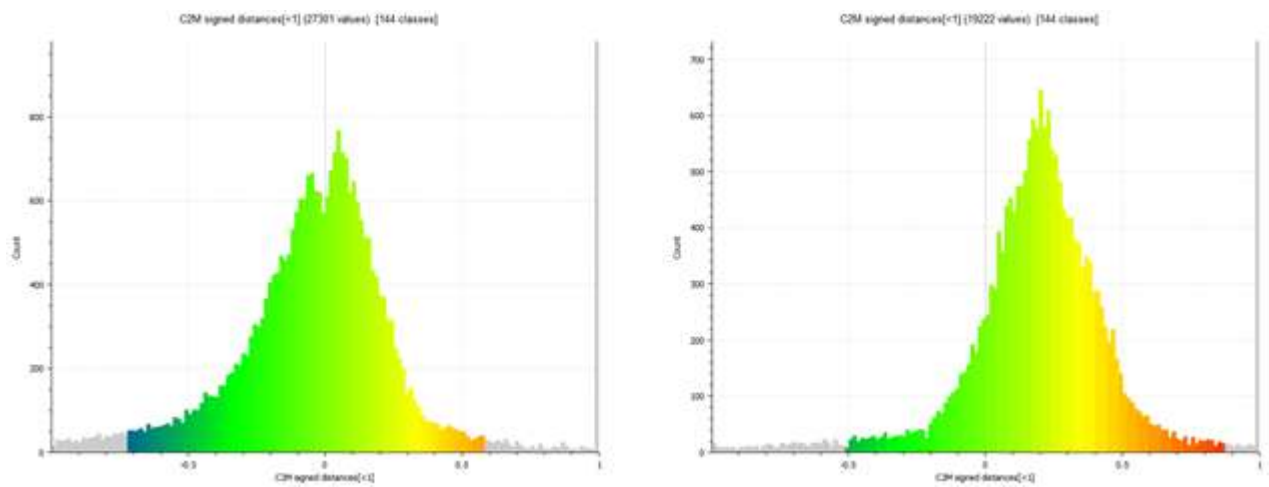


Figure 69 - Deviation map of jaw models segmented manually and by AI



a)

b)

Figure 70 - deviation map of maxilla (a) and mandibula (b) models

When training the AI model to segment the structures under study, errors occur, which are eliminated at subsequent stages of training the neural network model. Comparative analysis of segmentation by manual and automatic methods shows the best performance and fewer segmentation errors.

### 3.4 Creating a correlation model of the mucosa digital map

To create a correlation model, an examination of patients before or during orthodontic treatment was carried out. The presence of inflammatory processes was determined using the "Colour-test №1". The staining occurs due to the reaction of an increased amount of glycogen with iodine-containing solutions. Thus, only patients without any signs of inflammatory processes of the mucosa were taken into the work, which allows to create three-dimensional models of soft tissues and make an objective digital map of the gingival mucosa [6].

After the CT data was segmented manually or automatically it was merged through the reference models of the dental rows with connected soft tissue models.

A method for determining the mucosa biotype with a check for the presence of inflammation of the mucosa (figure 71 - 90).



Figure 71 - PMA "Colour-test №1"



Figure 72 - PMA "Colour-test №1"

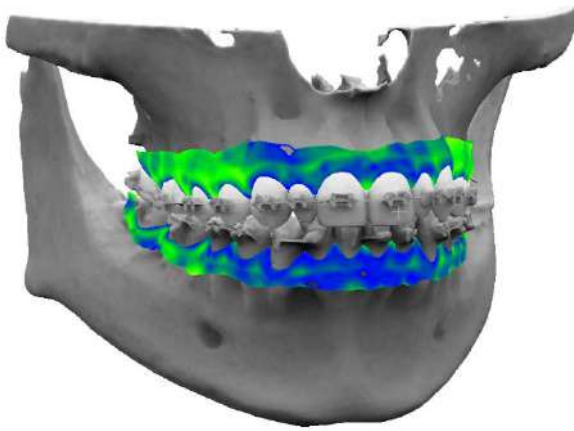


Figure 73 - Mucosa thickness map on a three-dimensional model. The medium biotype of the mucosa

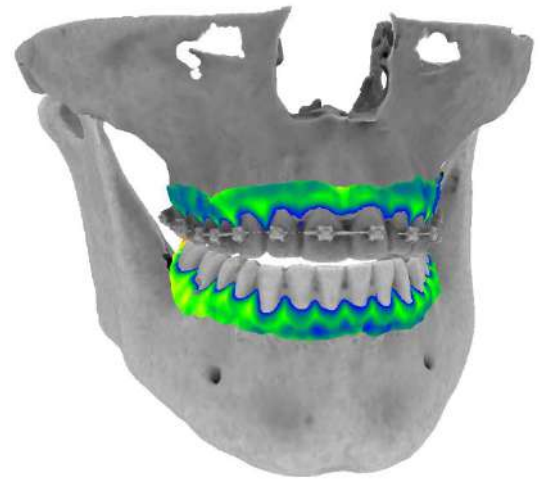


Figure 74 - Mucosa thickness map on a three-dimensional model. Medium/thick biotype of the mucosa

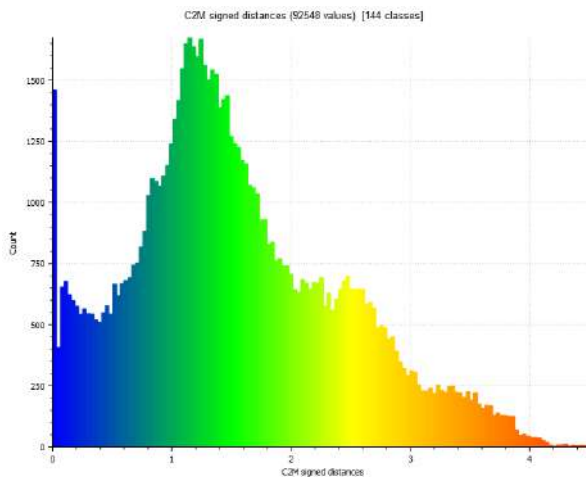


Figure 75 - Mucosa thickness distribution on the upper jaw. Medium biotype of the mucosa (maxilla)

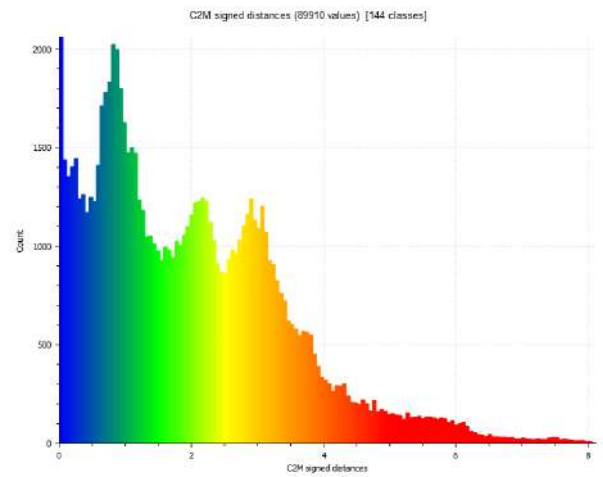


Figure 76 - Mucosa thickness distribution on the upper jaw. Medium/thick biotype of mucosa (maxilla)



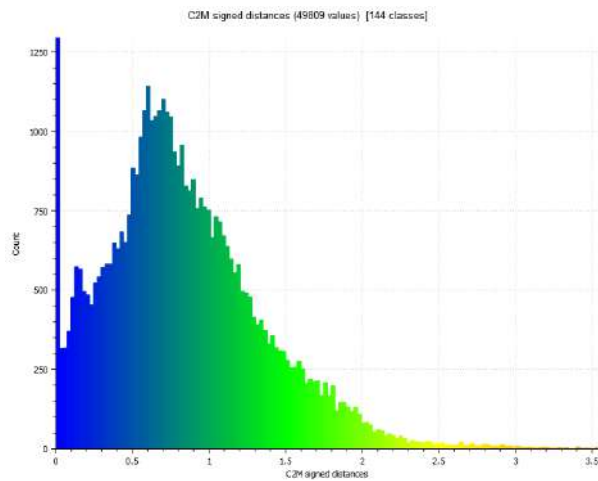


Figure 77 - Mucosa thickness distribution on the upper jaw. Medium biotype of the mucosa (mandible)

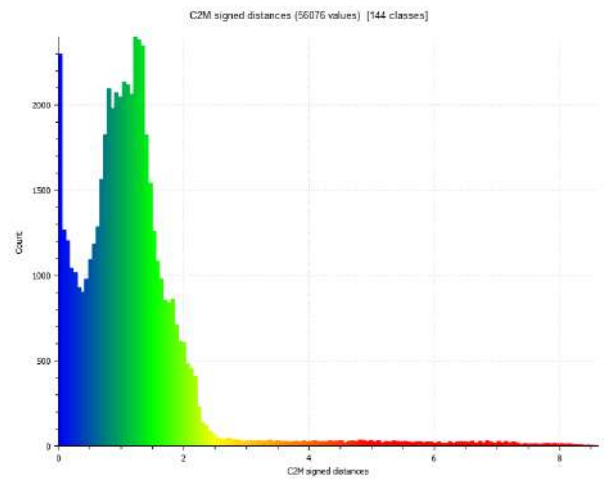


Figure 78 - Mucosa thickness distribution on the upper jaw. Thin biotype of the mucosa (mandible)

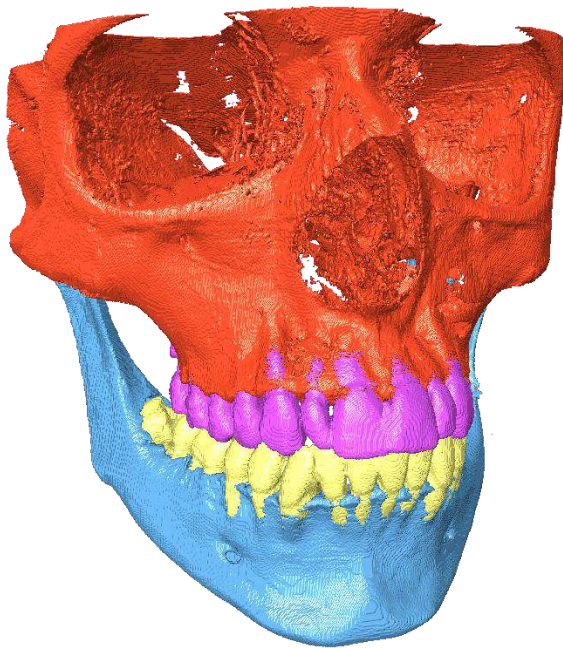


Figure 79 - Three-dimensional model of bone tissues and dentition using AI

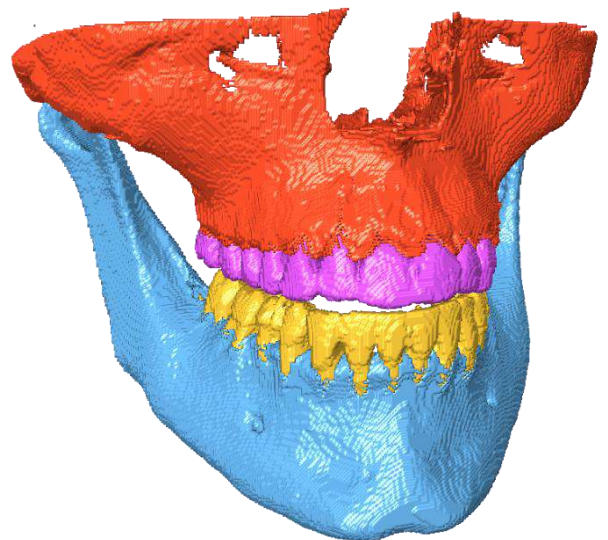


Figure 80 - Three-dimensional model of bone tissues and dentition using AI



Figure 81 - PMA "Colour-test №1"



Figure 82 - PMA "Colour-test №1"

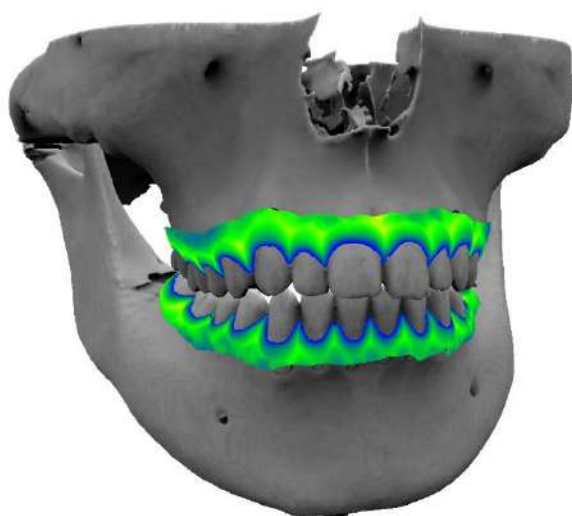


Figure 83 - Mucosa thickness map on a three-dimensional model. Medium/thick mucosa biotype

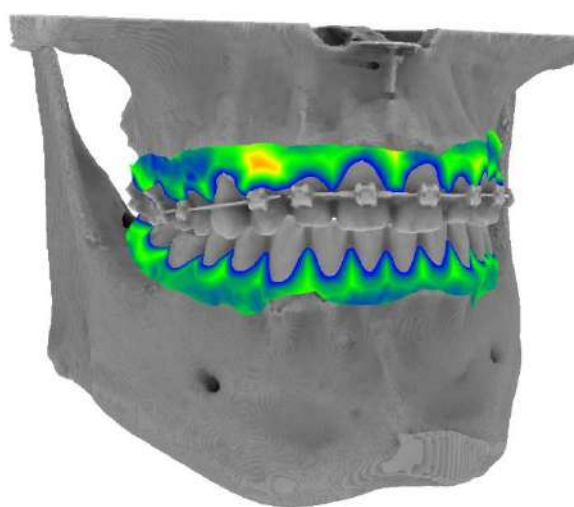


Figure 84 - Mucosa thickness map on a three-dimensional model. Medium/thick mucosa biotype

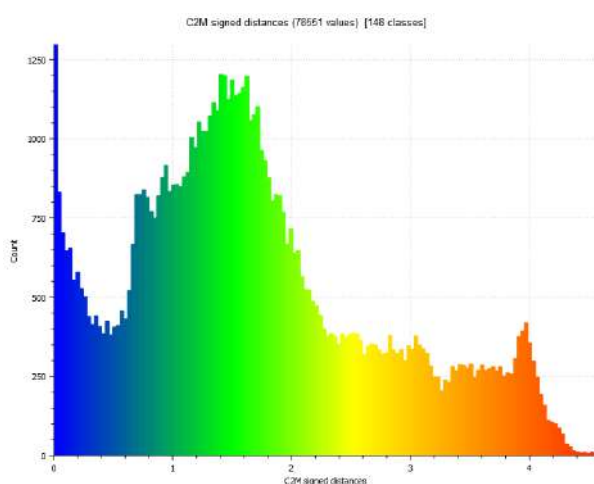


Figure 85 - Mucosa thickness distribution on the upper jaw. Medium/thick biotype of the mucosa (maxilla)

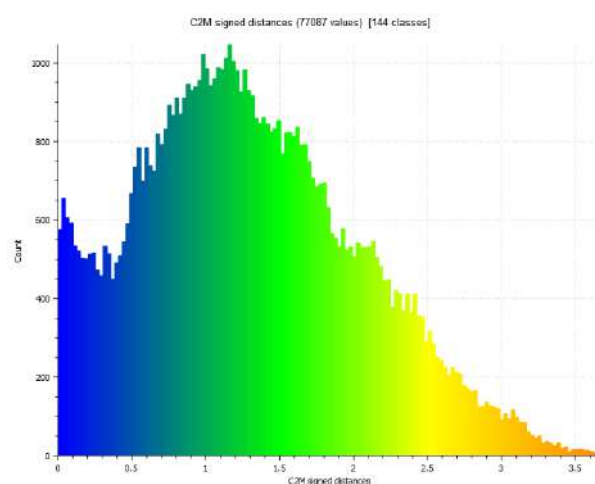


Figure 86 - Mucosa thickness distribution on the upper jaw. Medium biotype of the mucosa (maxilla)

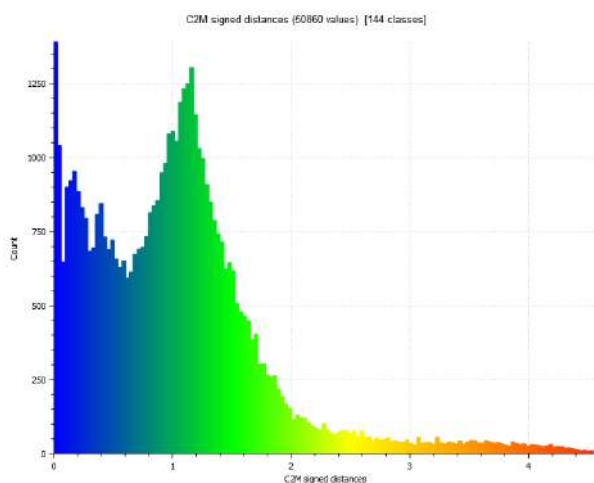


Figure 87 - Mucosa thickness distribution on the upper jaw. Medium/thin biotype of the mucosa (mandible)

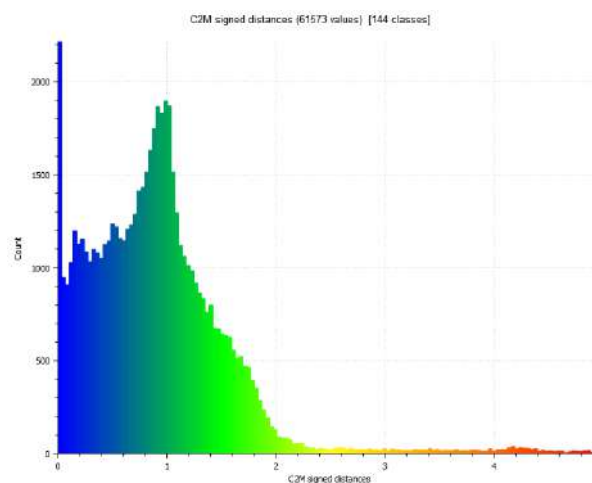


Figure 88 - Mucosa thickness distribution on the upper jaw. Medium biotype of the mucosa (mandible)

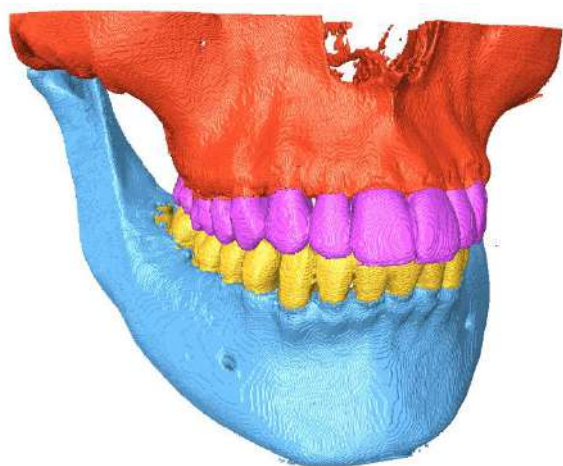


Figure 89 - 3D model of bone tissue and dentition using AI

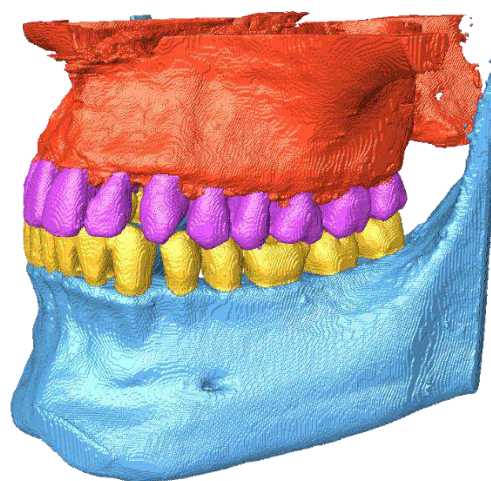


Figure 90 - 3D model of bone tissue and dentition using AI

After data collection and the mucosa thickness map creation was completed, it became possible to talk about method objectivity not only in general, but also in terms of individual details. In the area of the frenulum, it is possible to determine objectively the need of frenuloplasty, soft tissue hypertrophy, as in figure 84 in the area of tooth 1.3 local fibromatosis can be seen.



Increase in the number of colour maps allows using this technique according to a simplified algorithm without using the probe illumination techniques or invasive methods of local gingival biotype determination. An obligatory item of objectification is the use of "Colour-test №1".

"Colour-test №1" - is designed to detect inflammatory processes in the soft tissues of the oral cavity (Schiller-Pisarev test). The test is an objective test for assessing the degree of periodontal disease and the effectiveness of the treatment, it can be used to determine the prevalence of inflammation and the boundaries of surgical intervention during gingivectomy, curettage of periodontal pockets, to identify subgingival dental deposits.

#### Composition and main properties

The properties of "Colour-test №1", which includes iodine, potassium iodide and a base, are determined by the ability of glycogen (the amount of which increases with inflammation) to give colour in the process of interaction with iodine-containing solutions. When applying "Colour-test №1" to the soft tissues of the oral cavity, the inflamed areas are stained.

#### Mode of application

Apply liquid "Colour-test №1" to the gingival margin. According to the degree of staining of the inflamed mucosa (from light brown to dark brown), one can judge the degree of inflammation in the gum.

If there is no staining, then the sample is considered negative.

Data on the oral mucosa state were verified using a qualitative reaction "Colour-test №1". In the presence of inflammation, the data were not taken into account. The study involved only those with no signs of oral mucosa inflammation. Thus, the mucosa biotype erroneous determination was excluded.

### 3.4.1 Oral mucosa digital map correlation modelling

A new convenient and illustrative scheme of oral gingival thickness distribution is proposed, which can be evaluated globally (figure 91), considering the whole model, as well as locally (figure 92).

When applying the new technique, the protocols of radiological studies are not changed.

The great advantage of the proposed technique is its non-invasiveness. The proposed technique clearly shows the full distribution of mucosa thickness over the whole surface with the possibility of virtual local probing to obtain the numerical value of the mucosal thickness.

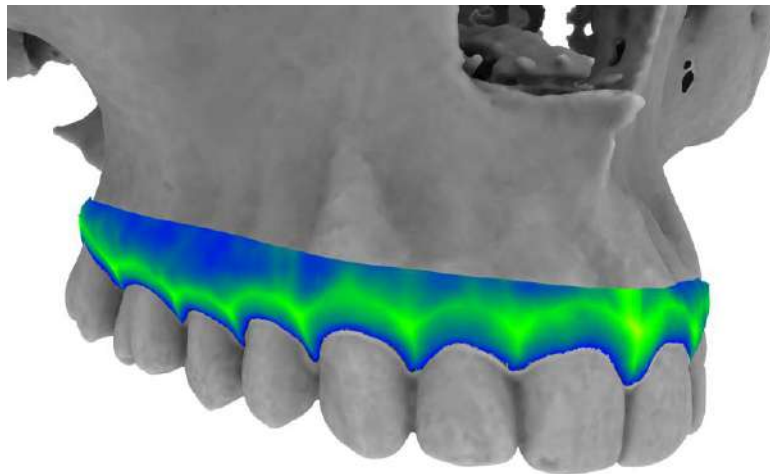


Figure 91 - Global mucosa thickness distribution map on a 3D model

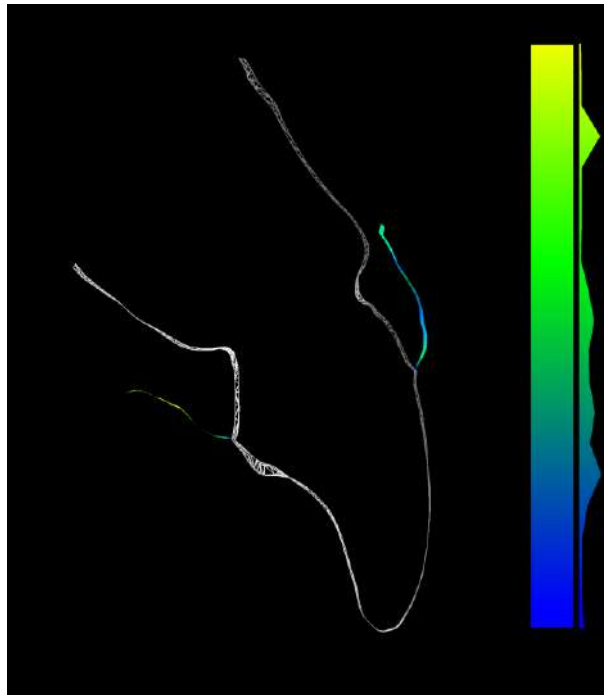


Figure 92 - Slice of the bone and mucosa with a colour map

### 3.5 Creating 3D models for FEA

The basic principles of biomechanics are based on average values and do not take into account the individual characteristics of each patient. In the case when there is no individualization of the patient's orthodontic treatment, some of the physical properties of the aligners are lost [96]. For this purpose, it is necessary to obtain a visual mapping of deformations and stresses in the aligner using calculations in physical and mathematical software packages. The results obtained are used to optimize the aligner design. However, these studies should be treated critically, since the physical and mechanical models are simplified and do not take into account a number of parameters.

The physical properties of PET-G material were taken in the simulation of the aligners' virtual model and entered into the ANSYS software workspace (ANSYS V.18; ANSYS Inc., Canonsburg, USA). Hyperplasticity properties are taken at 22°C from the

values given by the manufacturer (Cristal PET-G; Bio-Art, Brazil). Density ( $1314.8 \text{ kg m}^{-3}$ ) and Poisson's ratio (0.31) were taken from the data table, isotropic elasticity was calculated from Young's modulus (2000 MPa) and tensile strength (26 MPa) values (Figure 93).

	A	B	C	D	E
	Property	Value	Unit		
	Material Field Variables	Table			
	Density	0,0475	lb in <sup>-3</sup>		
	Isotropic Elasticity				
	Derive from	Young's Modulus an...			
6	Young's Modulus	2E+08	Pa		
7	Poisson's Ratio	0,4			
8	Bulk Modulus	3,3333E+08	Pa		
9	Shear Modulus	7,1429E+07	Pa		
10	Uniaxial Test Data	Tabular			
11	Scale	1			
12	Offset	0	Pa		
13	Shear Test Data	Tabular			
14	Has Lateral Strain	No			
15	Scale	1			
16	Offset	0	Pa		

Figure 93 - Physical properties of PET-G material

The grid properties of the contact area were reduced by a global element size factor of 0.55 (1.65 mm), a strain size factor (0.05) with a curvature capture option. Mesh properties that were not present in the contact area were modelled with larger elements. An element size of 3.0 mm was chosen with the minimum part size allowed by the mesh (0.5 mm) and a soft behaviour.

Material physical properties characteristics, which were not specified by the manufacturer, were taken from research data [60, 92]. Due to the fact that tabulated values were not specified in the literature or by the material manufacturer, the data were therefore processed through the Easy Trace Pro intelligent data tracer (Easy Trace Group, Russia).

A project was created based on a raster chart file (Figure 94), units and coordinate origins were specified, and the total distance in pixels along the x and y-axes was set.

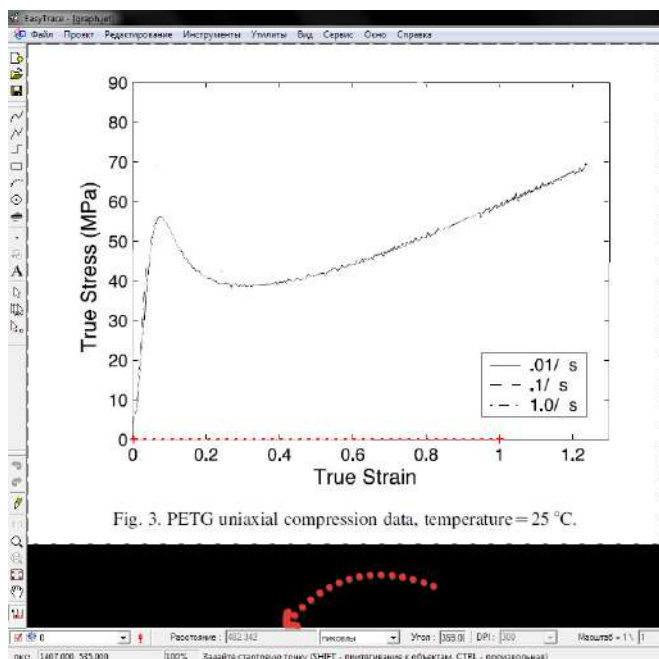


Figure 94 - Processing raster data from scientific articles into tabular values

This was followed by tracing the line of the graph and converting to a tabular format (figure 95, 96)

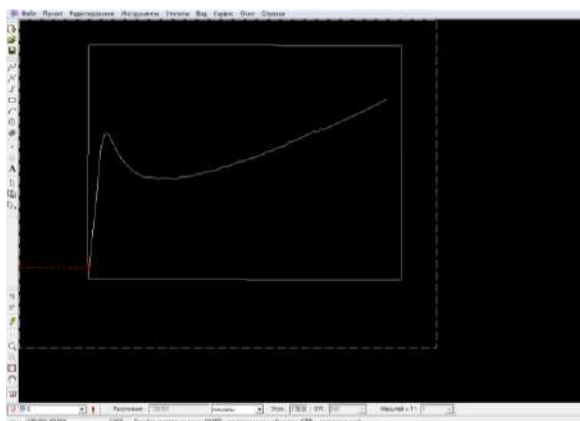


Figure 95 - Tracing graph data by selected colour

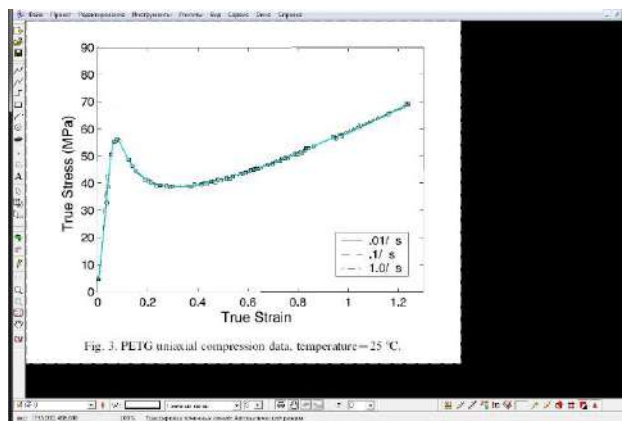


Figure 96 - Graph overlay tracing

The resulting trace data were converted to tabular values and corrected to zero position in LibreOffice Calc software, (figure 97) then a graph was plotted to verify that the trace and calculations were correct (figure 98).

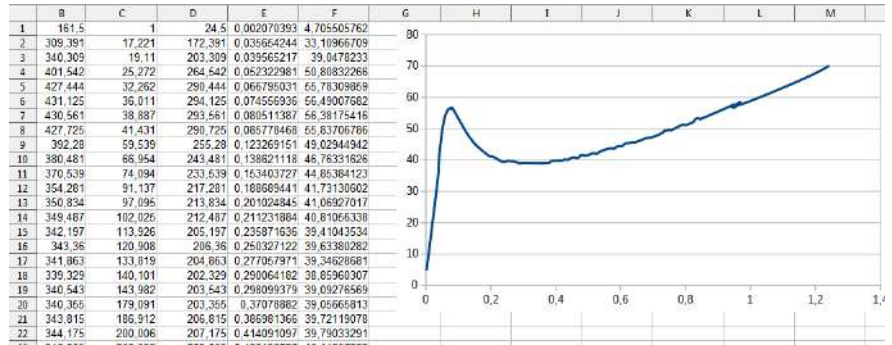
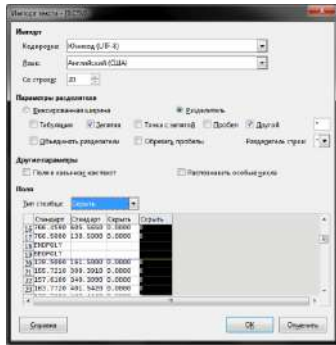


Figure 97 - Tabular data filter

Figure 98 - Correction of raw data after processing and plotting

The data was transferred to the ANSYS environment (Figure 90).

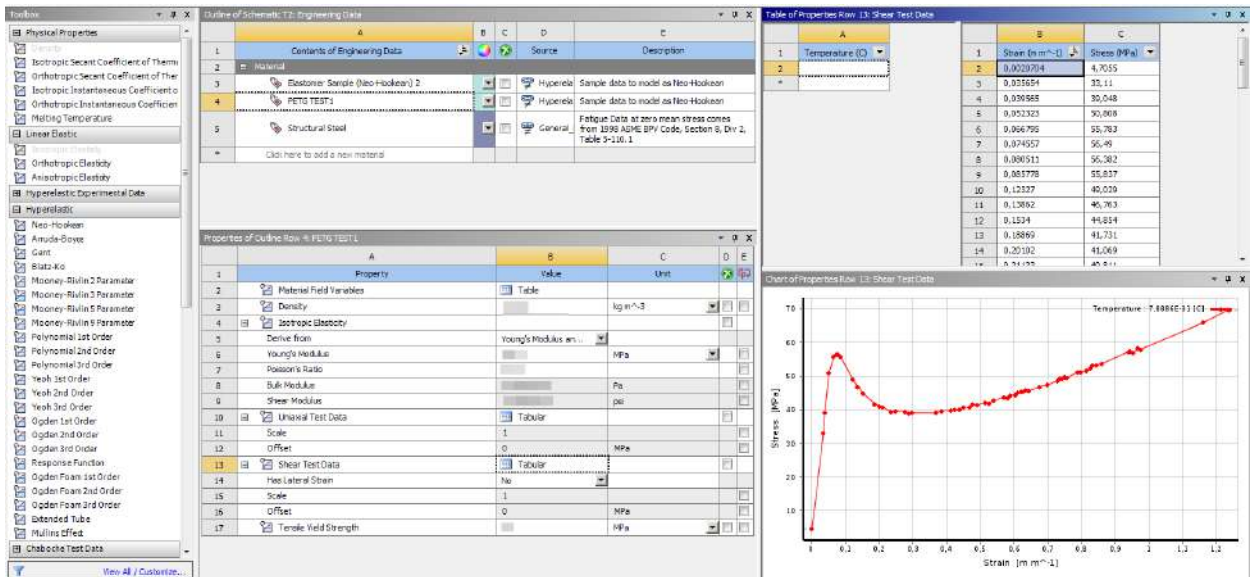


Figure 99 - Material properties data added to the ANSYS engineering environment

For this study, the patients' mouths were scanned using a Planmeca Emerald™ intraoral scanner (Planmeca, Helsinki, Finland) and 3D dental models were created (figure 100).

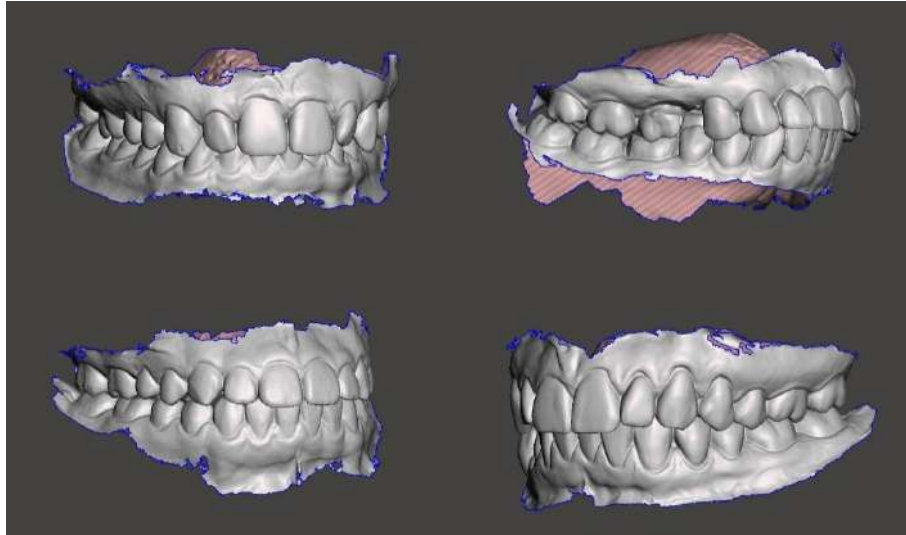


Figure 100 - Three-dimensional dental models obtained with an intraoral scanner

From these, patients with different treatment protocols on aligners were selected. A virtual planning was performed for each with the Maestro 3D Ortho Studio software (AGE Solutions, Pontedera, Italy) (Figure 101).

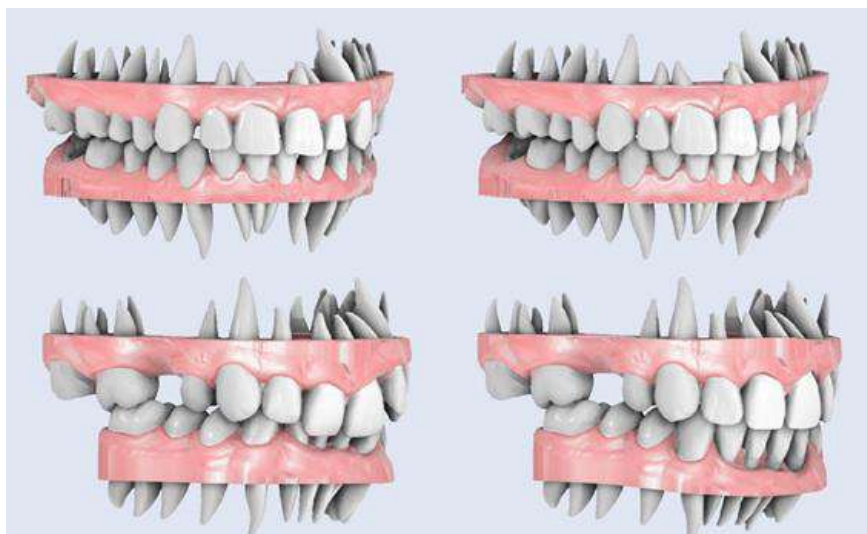


Figure 101 - Creating a treatment plan in Maestro Ortho Studio V5



The original models were pre-processed and shells errors were fixed in Autodesk Meshmixer software (Autodesk Inc., San Rafael, CA). The virtual models of the aligners were created by extrusion with a 1 mm extrusion of selected borders and smoothing overhanging edges (Figure 102, 103).

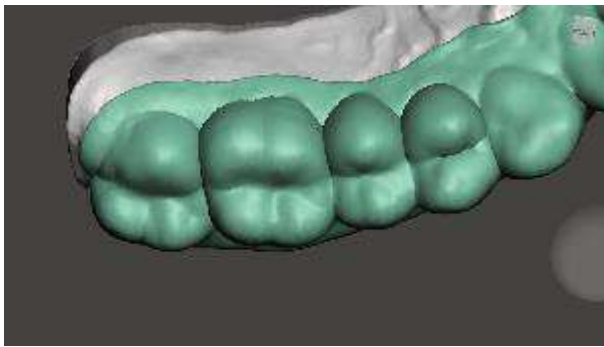


Figure 102 - Extrusion of the selected virtual aligners by 1 mm

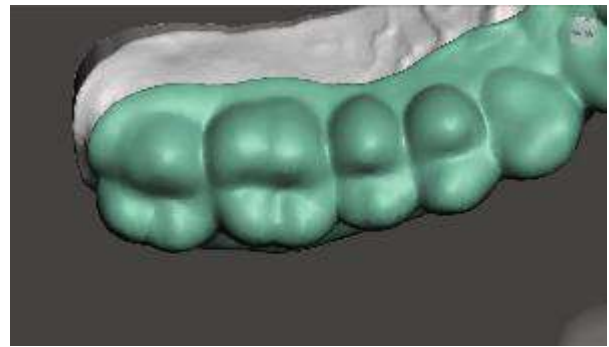


Figure 103 - Smoothing out the overhanging edges of the virtual aligner design

The intermediate stages "before" and "after" are taken as the basis for the virtual modelling of the aligners (figure 104).



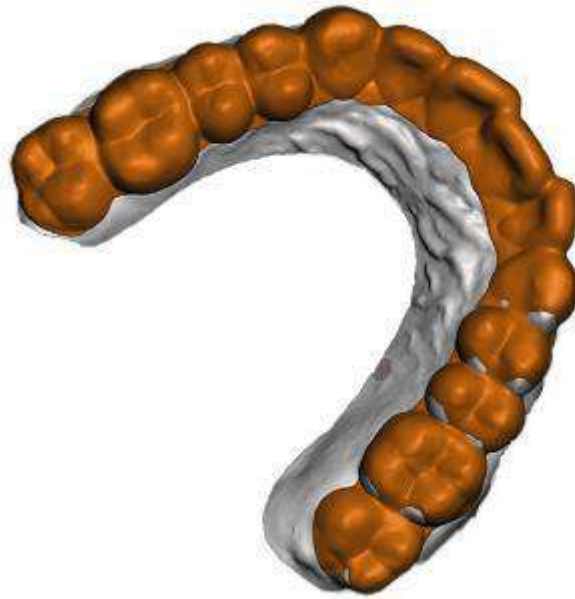


Figure 104 - Aligner model with the desired movement (top) and the initial dentition model (bottom)

To expedite the mathematical model's calculation, simplifications were made to areas irrelevant to aligner operation. Element dimensions were chosen considering both anatomical topology importance and the software's maximum allowable virtual mesh elements (Figure 105, 106) [97, 198].

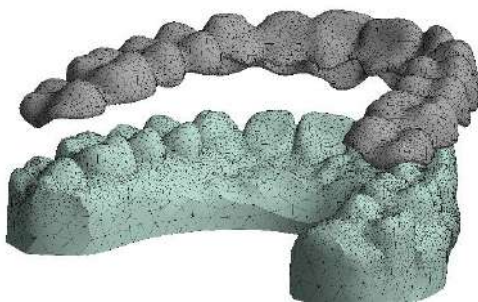


Figure 105 - General view of the model and view of elements

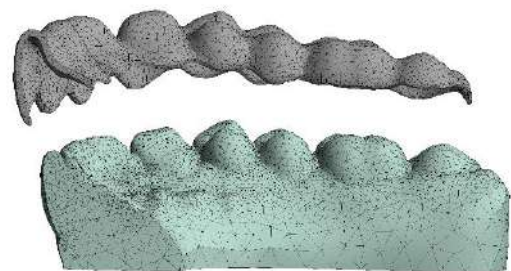


Figure 106 - Assembly model cut and element dimensions view

The contact surface has been enlarged on the base model for possible overlap with the sliding aligner model (figure 107 - 109).



Figure 107 - Aligner contact surface

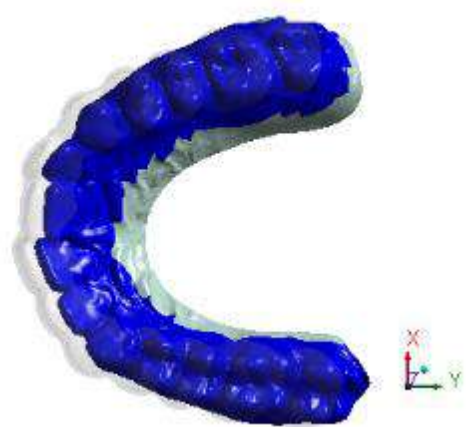


Figure 108 - Contact surface of the dentition model

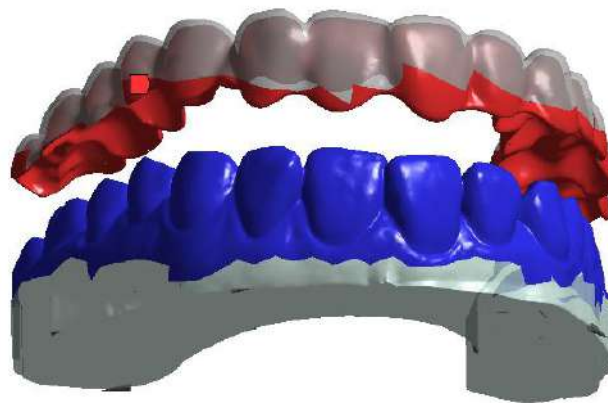


Figure 109 - Contact surfaces of the aligner and the dentition

Since none of the load modelling methods mentioned earlier in the literature was suitable for this task, a new technique for fitting the aligner was developed, taking into account its trimming and the shape of the dentition. In the new method, the movements

of both the aligner and the dentition were selected in such a way that the edges of the aligner structure were not deformed from contact with the model of the dentition, and the model movement path simulated a real trajectory, fitting the aligner on the dentition (figure 110).

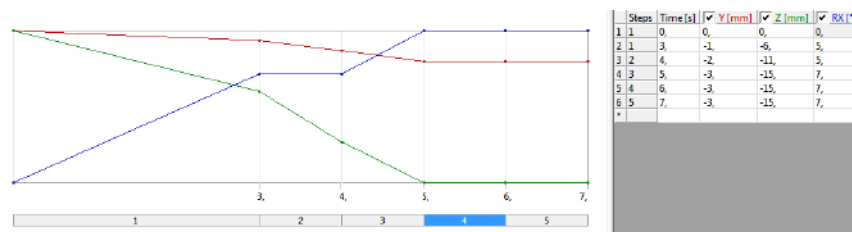


Figure 110 - Combining the design of the aligner with the movement of the dentition model. Red line - movement along the Y axis, green line - movement along the Z axis, blue line - rotation along the X axis

A short-term force (10 N) was applied to the aligner at the 6 seconds mark over the entire surface to evenly distribute the load and then removed, thus obtaining a load in the aligner fitted on the dentition (figure 111).

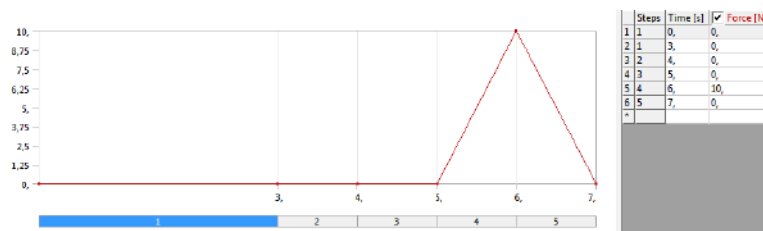


Figure 111 - Short-term application of force at the 6 second mark

The general vector of movements and loads is shown in figure 112.

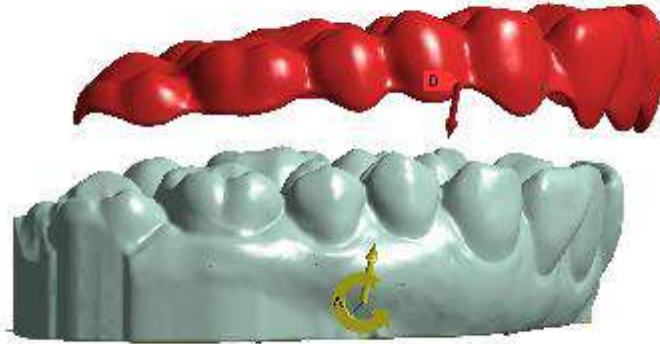


Figure 112 - General vector of movements of the aligner and the dentition

### 3.5.1 Reverse modelling

To create aligner topology analysis models with an aesthetic component, various types of beam connections were developed and analysed, suitable for modification with an aesthetic component. Designs for aligners and basic dentition models, adapted from previously developed designs, were used in the study for each clinical case, considering their physical parameters and required tasks.

Bodily tooth movement with negative tipping was compared with equal tooth movement with a given pitch but different aligner design topology.

For the study control set of aligners, a standard type of beam connection was selected to obtain structural reinforcement and increased elasticity and analysed for deformation, strain and stress in the structure.

In order to efficiently and quickly create a design of a mathematical model suitable for the goals and objectives of creating calculations for a beam structure and its modification with an aesthetic pontic, a simulation modelling approach was chosen with

the movement of the teeth one step ahead, by moving the teeth, and not the aligner model (figure 113).

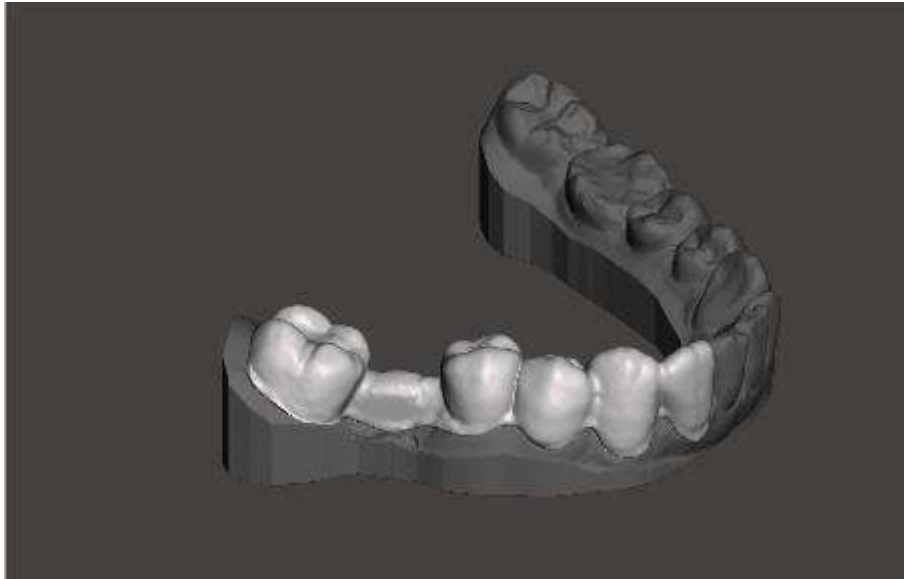


Figure 113 - Partial virtual aligner with beam reinforcement modelling

The modelled parts of the structure were processed in the ANSYS mechanical program for further analysis (figure 114).

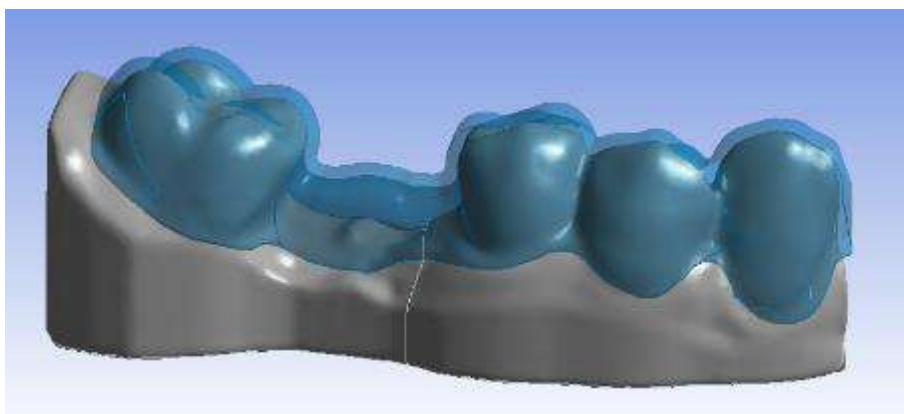


Figure 114 - Virtual shell of beam-reinforced aligner part

A comparison set of aligners included standard clinical aesthetic solutions, for which a pontic was created in the area where the tooth was directly missing (figure 115).

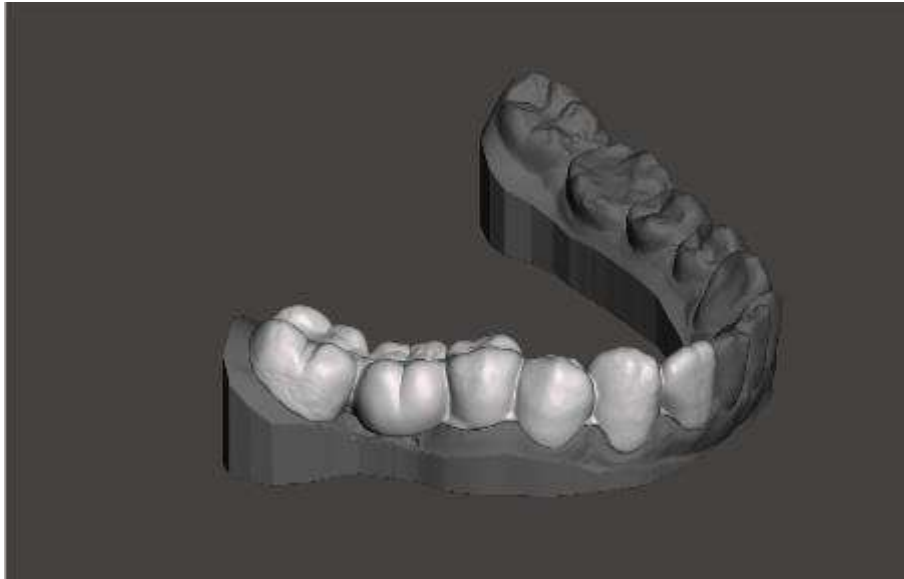


Figure 115 - Partial virtual aligner model with an aesthetic pontic modelling

The resulting models were also processed in the Ansys Mechanical software and load and deformation calculations were carried out (figure 116).

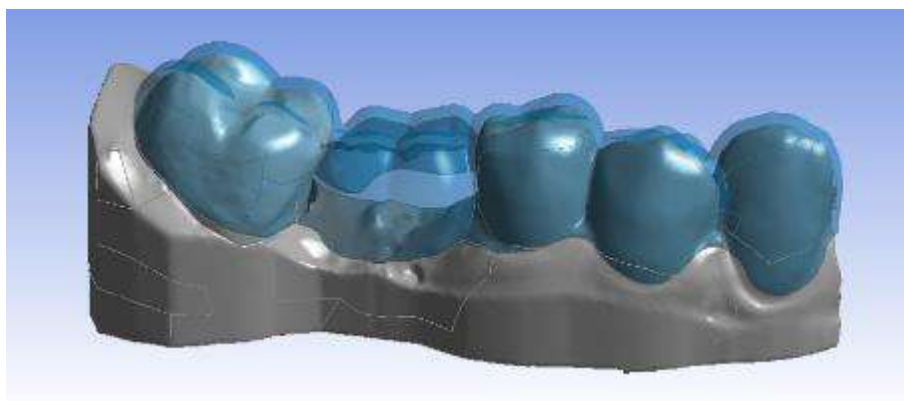


Figure 116 - Virtual shell of the aligner part with aesthetic pontic

For the reverse design, an individual tooth model was created with a fixed movement step, and movements were applied in the analysis model with the same step (figure 117).

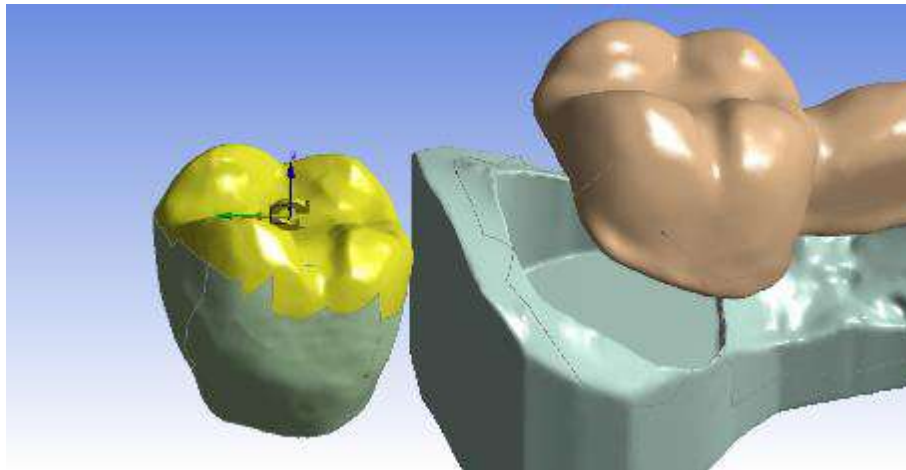


Figure 117 - Reverse modelling of tooth movement (distalization and distal tipping)

Finite element analysis showed the weaknesses of both designs, as well as their possible modification by strengthening. In the case of beam reinforcement, large bending deformations on a relatively small surface are noticeable, which indicates a low efficiency in the transfer of orthodontic forces and the stage of possible destruction of the structure (figure 118).



Figure 118 - Elastic shear deformation with beam reinforcement



When using a pontic, the load is transferred over a larger area and more evenly distributed over the design of the aligner; however, the excessive plasticity of this solution leads to a loose fit of the aligner to the teeth surfaces and supporting attachments (figure 119).

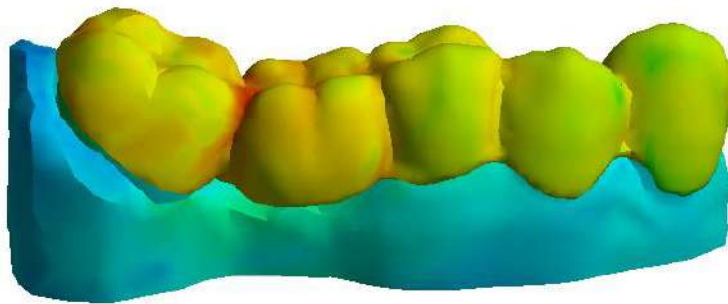


Figure 119 - Elastic shear deformation with pontic

According to the results of the analysis by finite elements, the main disadvantages of both designs were identified.

In the first design, with the use of a pontic, when the aligner is activated, compression occurs in the mesio-distal direction, which leads to deformation and expansion in the vestibulo-oral direction not only in the area of the missing tooth, but also in the area of neighbouring teeth. In turn, this leads to the fact that in the presence of such a deformity, the aligner does not fit snugly in the attachment area, which may cause loss of anchorage, which leads to a deviation from the planned treatment plan and treatment plan correction is required (figure 120).



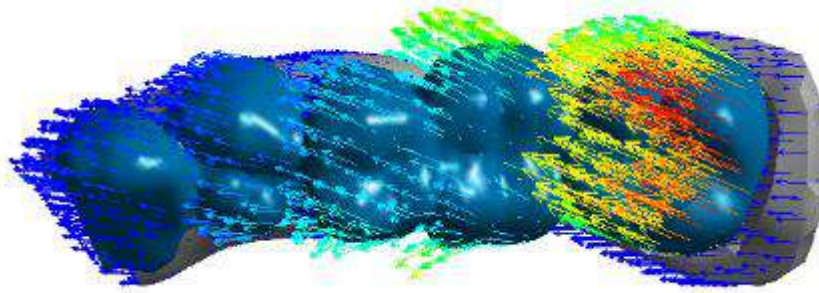


Figure 120 - Aligner deformation vectors with aesthetic pontic

In the second design, when a standard solution (beam connection) is used, an excessive load on the mucosa occurs, which in turn can lead to impaired wound healing at the site of tooth extraction and to microcirculation disorders in the gums at the site of excessive pressure from the liner design (figure 121, 122).

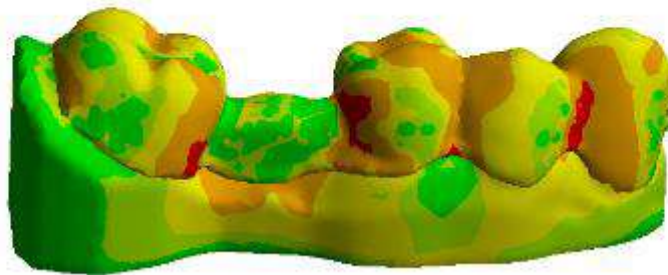


Figure 121 - Pressure on the mucosa with beam connection in the area of tooth 46

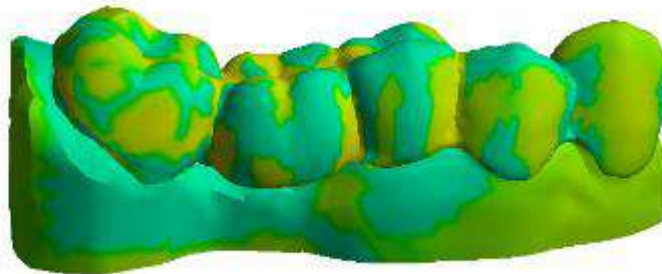


Figure 122 - Pressure on the mucosa with a pontic in the area of tooth 46

Based on the analysis of structures such as "beam" and "pontic", it was decided to modify them. That is, to get a new design that would include both the aesthetics and the functions of both types of connections. By removing the load from the gums where the tooth was lost and preserving the aligner's power structure, this decision also improved the structure's aesthetics, typically boosting patient motivation during treatment.

### 3.5.2 Preclinical modelling of tooth movement

According to the results of finite element calculations, the aligner topology strongly influences its resistance to deformation. Unforeseen deformations in the aligner redirect forces from the lateral structure surfaces to the occlusal surface, which in turn affects the predictability of treatment, and may lead to deviation from the initial virtual treatment plan, as well as the need for additional corrections during the clinical appointment.

Visual analysis of the data reveals areas of greatest structural tension, physical properties, and pressure (applied forces) on individual teeth and the entire arch. Visualization of stresses in the aligner design helps to determine the optimal form of cutting in certain places, individual for each clinical case, as well as to increase the

strength of the structure, its resistance to wear, micro cracks and breakage (figure 123, 124).

Visualization of the stress data generated in the aligner design during activation gives complete control over the load on the teeth, the distribution of orthodontic force and its direction on each tooth involved in movement and anchorage (figure 125, 126).

Studies have shown that when the structure is reinforced with additional PET-G material in the most loaded areas, better structural stability is provided and excessive deformations are reduced. Because excessive deformations cause incorrect application of force to the moved teeth in addition to a weak distribution of forces on the anchorage teeth. Insufficient resistance of the aligner to excessive deformations leads to incorrect distribution of forces on the dentition and deviations from the planned tooth movements.

Preclinical modelling of tooth movement has shown that in complex clinical cases, an individual approach to the process of orthodontic treatment is required, which requires the creation of a modified aligner topology. Thus, carrying out such calculations allows modifying the aligner, and thereby reducing the treatment time compared to the treatment time with a standard aligner. In a long-time treatment, only a small correction will be required or any treatment plan corrections will not be required. Aligners with a straight cut are more resistant to deformation and retain their original shape; as a result, design forces are applied to the teeth. The best force distribution was observed when using a straight cut aligner. The forces were directed to the lateral surfaces of the teeth, while when trimming the aligner along the gingival margin, slight deformations were observed, and the forces were redirected to the occlusal surface.



Figure 123 - Elastic aligner deformation with scalloped margin



Figure 124 - Elastic aligner deformation with straight Cut

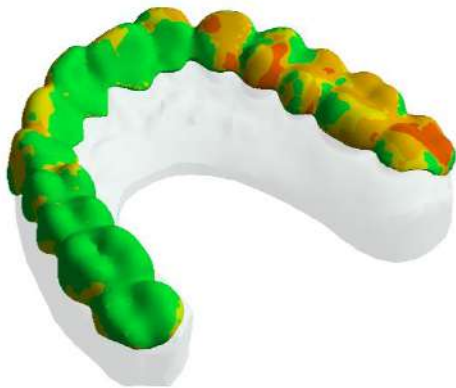


Figure 125 - Aligner shear stress with scalloped margin



Figure 126 - Straight cut aligner shear Stress

The topology of straight-cut aligners, compared to with scalloped margin trimming, demonstrates a redistribution of elastic deformity at the deformity site and further correct distribution of forces applied to the teeth.

Preclinical modelling of tooth movement allows in complex clinical cases to obtain individual optimal variants of aligner modifications. This method of modifying and optimizing the manufacture of aligners is extremely important and relevant in modern orthodontics. The computational power of finite element analysis makes it possible to

simulate the physical properties of the aligner that were predicted only theoretically, without taking into account individualization. Some virtual simplifications do not affect the result or their consideration goes beyond the evaluation and diagnostic requirements. To mimic real device behaviour, uneven virtual aligner thickness was manually adjusted (virtual model thickness was corrected based on real aligner sidewall measurements) (Figure 127, 128). However, other physical and chemical properties that reduce the aligners' strength should also be taken into account. The study was carried out in order to clearly understand how aligners could be modified to reduce treatment time and improve treatment control. On virtual models, the need of an individual approach was demonstrated without the use of standard protocols and with the possibility of choosing only one specific type of trimming of the aligners.



Figure 127 - Uneven anterior aligner thickness

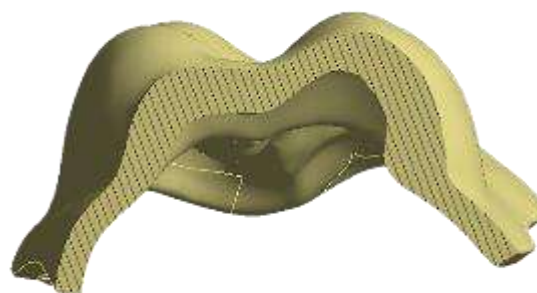


Figure 128 - Uneven aligner thickness in the posterior region

Aligner model wall thickness has been manually reduced to recreate better physical behaviour during FEA.

Straight cut aligners have shown the best stability and predictability in relation to the planned models at every stage. When trimming along the gingival margin, the design is highly deformed during initial activation and poorly distributes pressure on the teeth, which leads to deviation from the steps planned in the virtual setup.

The options for constructing mathematical calculations proposed in the literature were not suitable for performing the assigned tasks. As a result of the analysis, it was concluded that simplifications in virtual models does not affect the whole pattern and its demonstration for understanding the distribution of forces, strains and stresses in the appliance.

Preclinical simulations of tooth movement have shown that scalloped aligners can be drastically deformed, resulting in a change in the direction of tooth movement. This, in turn, will cause a deviation from the treatment plan and will lead to the need for its adjustment. Scalloped aligners deform in areas with the least amount of material or in the thickest area, which may go unnoticed by the orthodontist. To avoid this, pre-clinical modelling should be done and areas of interest should be reinforced with additional PET-G material.

A comparison was made of deformed aligner models with a straight and scalloped trimming (figure 129). Aligners with gingival trim showed less resistance to deformation. Forces directed to the occlusal and lateral surfaces of the teeth, perpendicular to the occlusal plane, imitated the presence of attachments with a uniform attachment area over the entire surface. This simplification of the model was made to exclude possible additional deformations arising from attachments when analysing the topology of aligners in certain places of interest, and to create the possibility of generalizing the mathematical model.

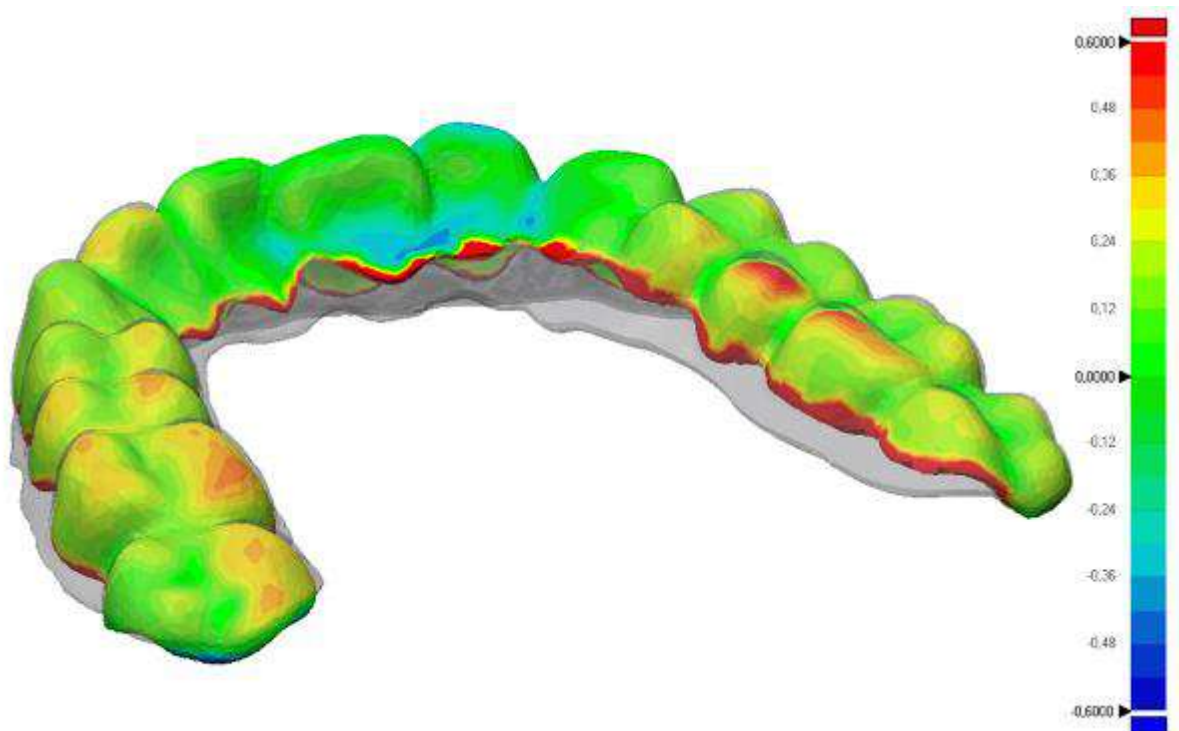


Figure 129 - Deviation map showing the difference in deformities between high and gingival margins

### 3.5.3 Three-dimensional models creation for FEA

Using the three-dimensional models of the dentition obtained by the intraoral scanner, virtual treatment plans for orthodontic patients on aligners were set up and virtual models of aligners were created. This complex was placed in the ANSYS software environment, in which an architecture for calculating the deformations of the aligners was formed (figure 130). The architecture developed in this way allows the placement of 3D models of dentition and aligners without re-creating the environment and quickly obtaining the results of finite element analyses (figure 131).



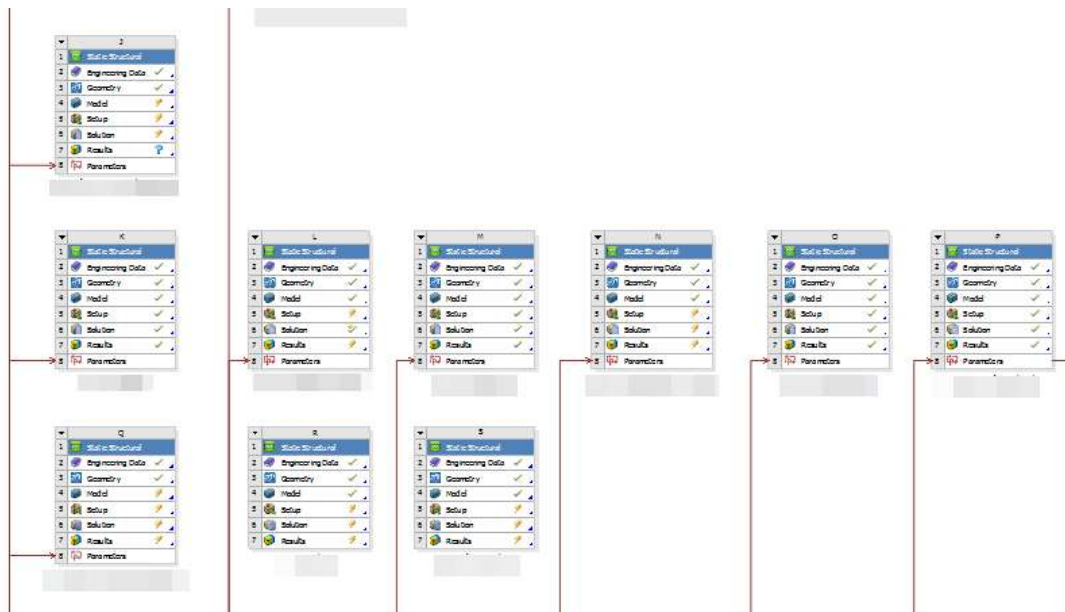


Figure 130 - Structure of models in ANSYS Workbench



Figure 131 - Architecture of ANSYS Workbench for each model

A new original design of orthodontic aligners' mathematical model was developed, different from the design used by other researchers and not previously described in the literature. The developed basic design algorithm was subjected to modifications for each clinical case separately. The modified aligners' effectiveness was determined by the degree of deformation and load distribution of the entire aligner design.

The CAD system was used to calculate the deformations of the aligners and to visualise the load and strain distribution maps. This visualisation clearly showed the areas of the aligners' design that need to be reinforced.



Based on the results of mathematical analysis, the methodology of scalloped and straight trimming of aligners depending on the gingival biotype was justified. In case of a thin gingival biotype, scalloped trimming of the applied aligners is used. Aligners are reinforced with high trimming in areas requiring active movement of individual teeth (traction, mesio-distal movements, rotations).

A comparative analysis of the existing standard techniques for the fabrication of orthodontic aligners with additional reduction of the trimming edges in those cases where there are periodontal changes has been carried out.

The findings indicate the following results of the study:

- 1) Aligners trimming individualisation according to the clinical situation and the defined gingival biotype is important.
- 2) Aligners beam elements modification with the use of aesthetic pontics is necessary.
- 3) Achieved an increase in structural strength by modifying the topology of the aligners.
- 4) Increased the efficiency of orthodontic treatment on aligners.
- 5) Achieved a reduction in the number of revisions during treatment with aligners.
- 6) Achieved improved aesthetics without compromising durability.
- 7) Achieved aligners' topology optimisation without loss of function.
- 8) Developed a new concept of models for CAD analysis.
- 9) Three-dimensional models of scanned dentition were processed.
- 10) Created virtual models of aligners with modified topology.
- 11) Developed mathematical study design in engineering software.
- 12) Processed and optimised three-dimensional models for CAD work.
- 13) Material properties for aligners with certain physical properties were selected and used in the practical part of the study. Their physical and chemical coefficients were established from the data of different sources. Further, these data were imported into the working environment of Ansys engineering software.

- 14) The calculations of different variants of modifications in the topology of the aligners for each patient were carried out.
- 15) Conclusions were drawn for modifying and improving the topology of the aligners in each clinical case.
- 16) General characteristics of modification of aligner topology in similar clinical cases are developed.

### 3.6 Clinical and laboratory methods

The development of the treatment plan was carried out in the Maestro Ortho Studio V5 software, taking into account the set clinical goals and objectives. An example of the development of a treatment plan according to selected criteria is presented, in which it is possible to use optimization and improvement of the topology of a set of aligners (figure 132, 133).

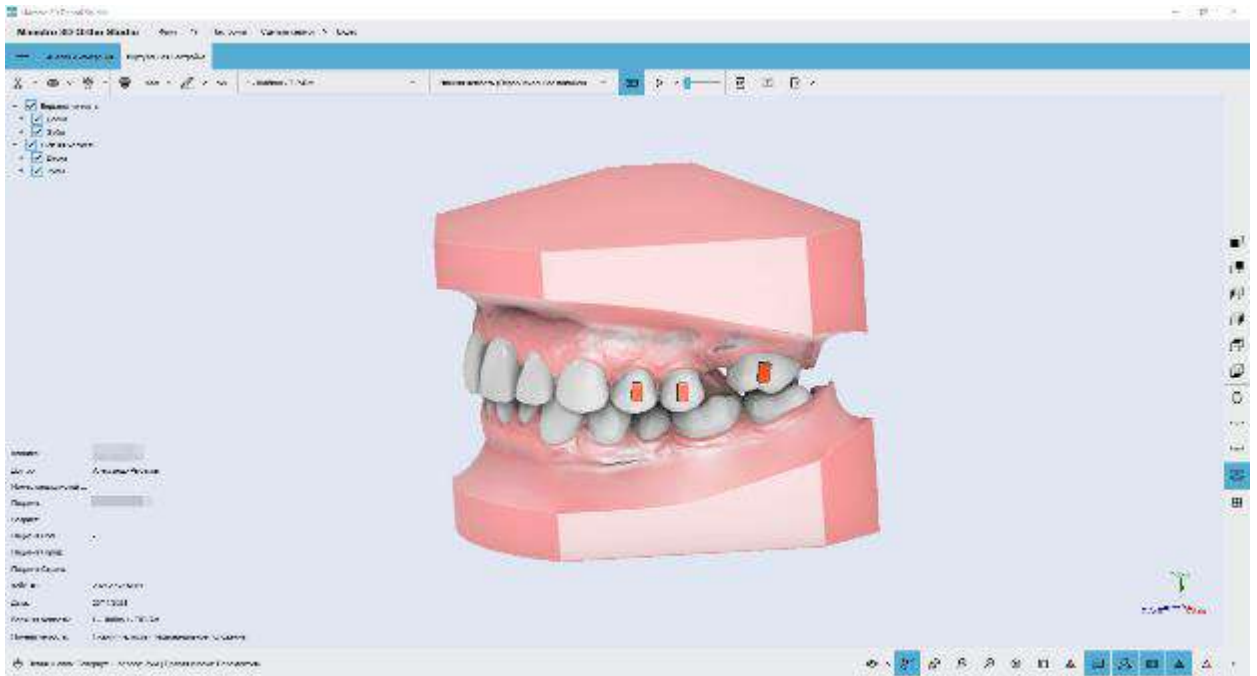


Figure 132 - Development of a treatment plan using attachments, starting position

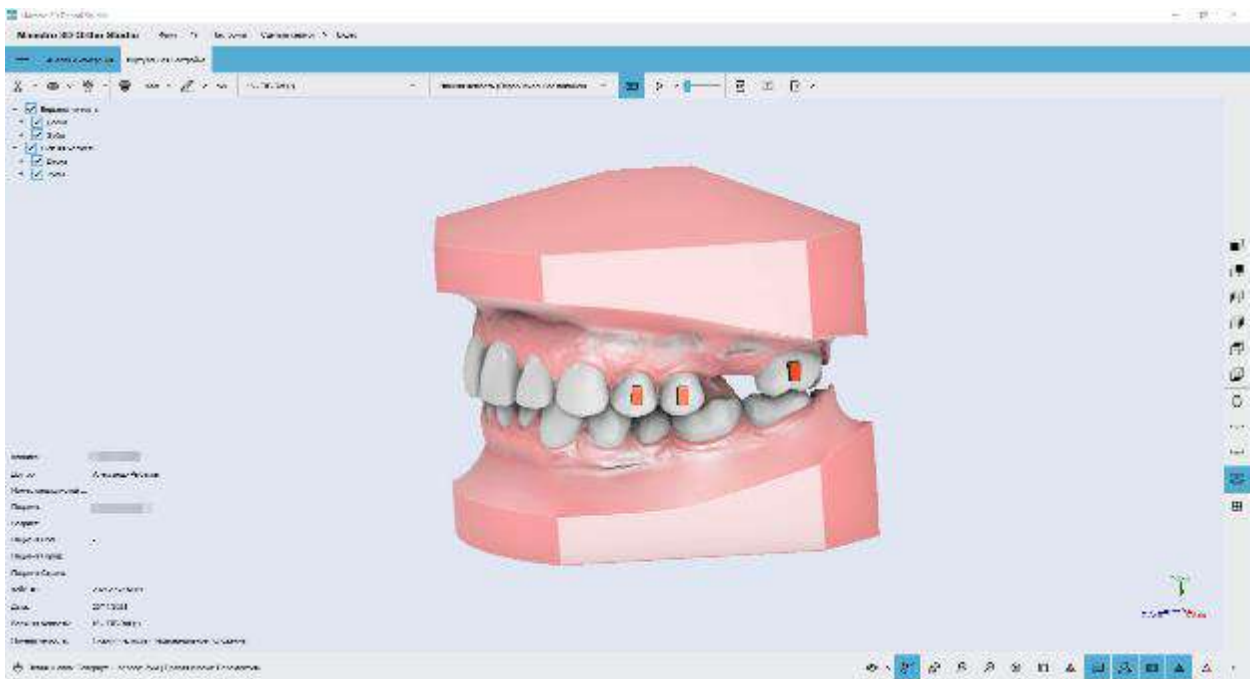


Figure 133 - Development of a treatment plan using attachments, final position

Treatment planning took place taking into account the clinical goals and objectives of each patient, all the norms of restriction and the norms of movement of each tooth, the order and combination of movements were performed in accordance with the physiological capabilities of the body and the aligner design physical property (figure 134).

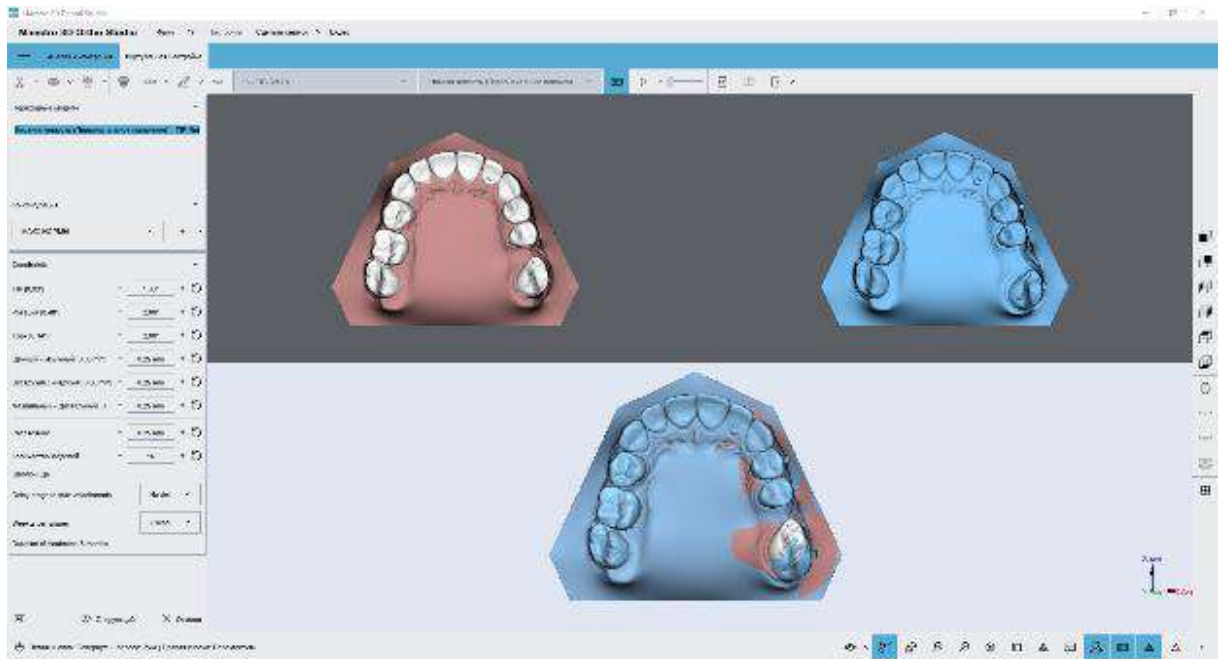


Figure 134 - Building models with limitations of tooth movements

In a number of clinical cases, after creating a number of models in the traditional way with the help of reinforcement with a beam element, modified aesthetic elements were introduced, along with functional ones (figure 135,136).

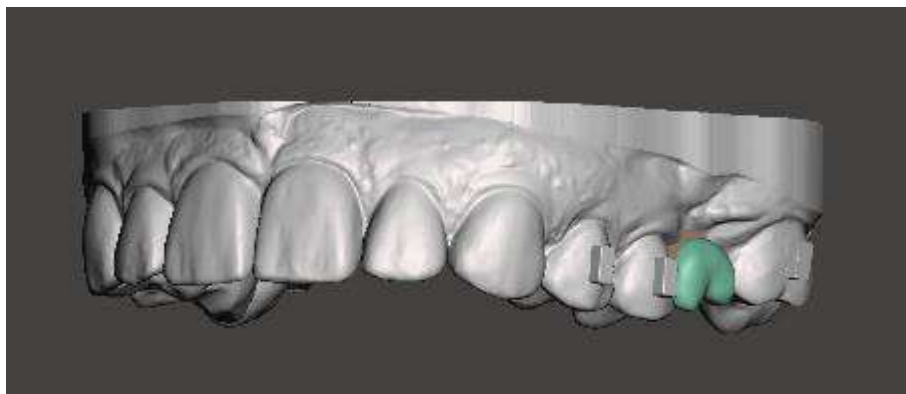


Figure 135 - Beam connection modification by adding a partial pontic

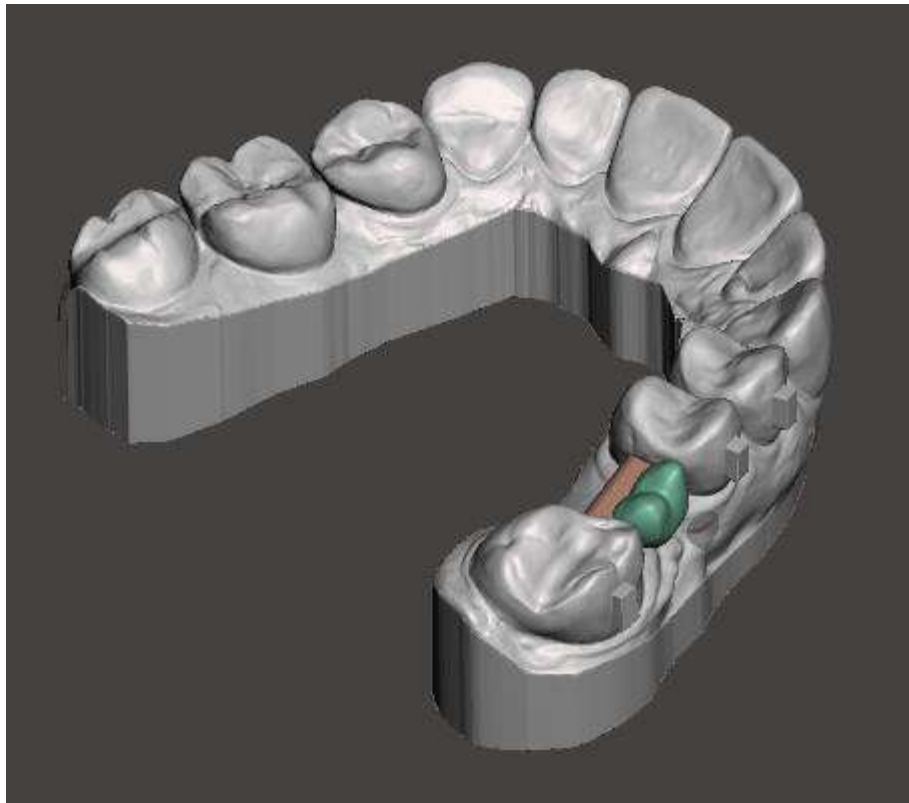


Figure 136 - Selecting the shape and size of a partial pontic when modelling the modification of a beam connection

The resulting models were processed in the Photon Workshop V2 software and sent to the SLA printer based on the LCD display for stereolithographic printing of 3D models Anycubic Photon S (figure 137).

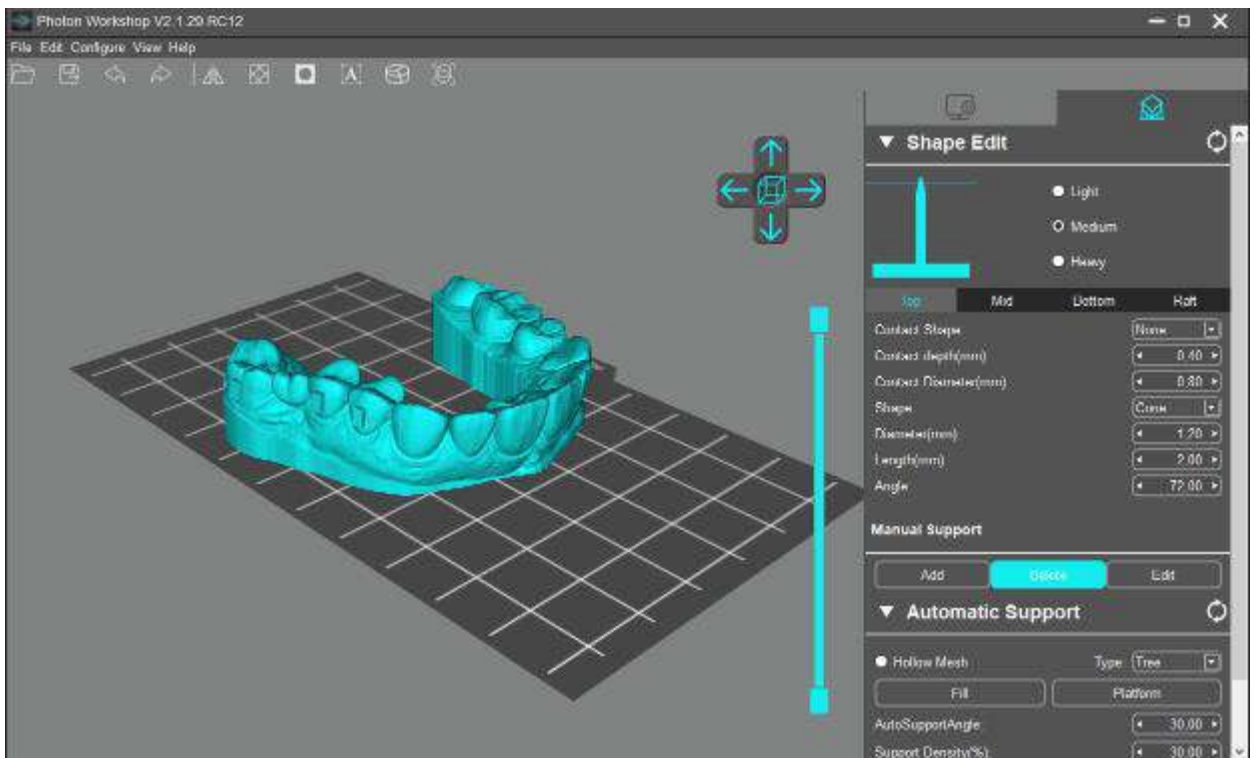


Figure 137 - Photon Workshop V2 Software Workspace

The printed models were processed in isopropanol and exposed in a UV chamber for 45 minutes (figure 138).

Aligners were fabricated using a vacuum former. Next, trimming was performed taking into account the topology and extending the edges in places with the highest load (figure 139).



Figure 138 - Printed 3D model on the Anycubic Photon S 3D SLA printer after processing in isopropanol and UV cure



Figure 139 - Printed thermoformed and trimmed aligner



At the initial stages of treatment, the appliances were created with modified trimming and were made without functional changes in topology, and also had no aesthetic changes (figure 140, 141).

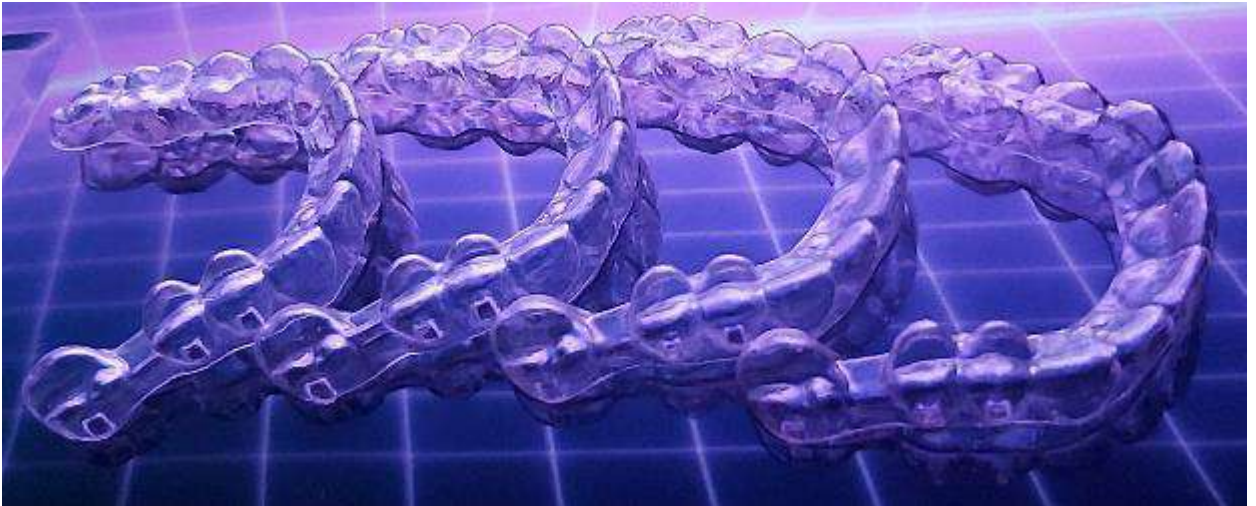


Figure 140 - Beam-reinforced aligner set without aesthetic component



Figure 141 - Aligner template with standard bar reinforcement

The aesthetic pontic aligners were then treated with bonding and a thin layer of flowable composite. The composite colour was selected according to the patient's teeth colour (figure 142).



Figure 142 - Applying a pontic with a flowable composite material

After applying each layer, exposure to a UV lamp was carried out for 15 seconds. After applying the last layer, the translucency of the layers was assessed. The final exposure was carried out for 30 seconds (figure 143).

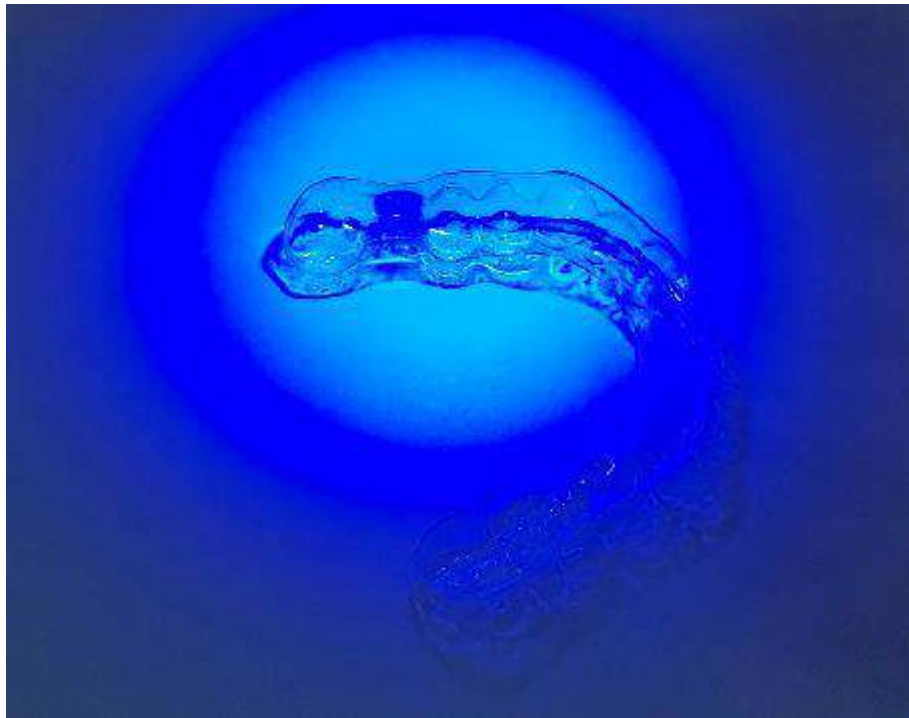


Figure 143 – Composite layers of pontic curing with UV light

Comparison of aligner designs with and without aesthetic-functional topology modification (figure 144).



Figure 144 - Aligner with and without beam reinforcement and aesthetic component

Clinical examples of the initial stages of treatment without changes in the aligners' topology were performed using aligners manufactured in the clinic as well as Flexiligner designed aligners (figure 145 - 150).

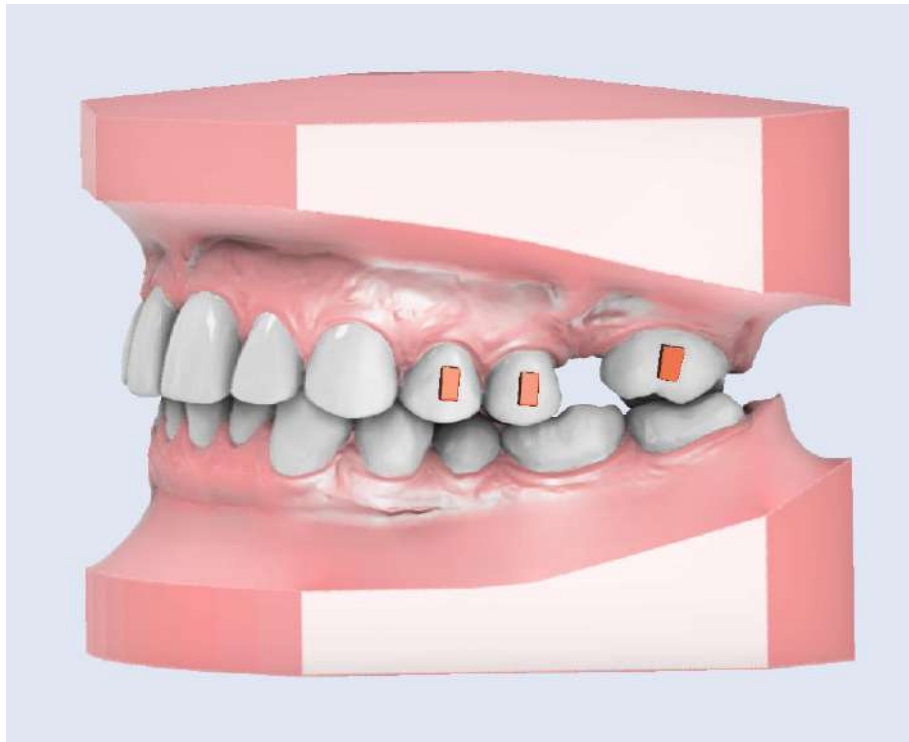


Figure 145 - Virtual treatment plan step #1





Figure 146 - Aligners without modification of the aesthetic component, made by the author

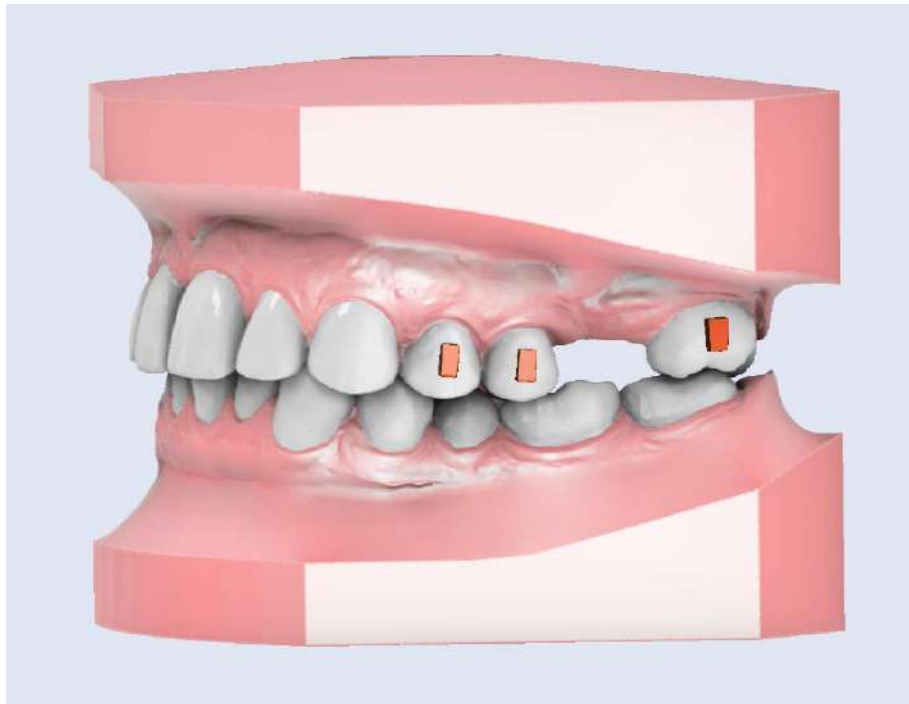


Figure 147 - Virtual treatment plan step #16



Figure 148 - After finishing distal tipping in step #16



Figure 149 - Standard aligner trimming protocol treatment (Flexiligner) Step #1



Figure 150 - Aligners without an aesthetic component, made according to the standard Flexiligner protocol at the stage of treatment

### **3.6.1 Treatment protocol with aligners**

After working with virtual models and calculating the required aligners' topology, step-by-step models of the patient's dentition were printed on an SLA printer according to the treatment plan, and the aligners with modified topology were fabricated by thermoforming on the printed models. Aligners trimming was performed according to the marks on the 3D model in accordance with the trimming modification.

Patients with modified aligners experienced no breakage despite excessive loading during removal and wear. An example of irreversible deformation of an aligner (figure 151).



Figure 151 - Irreversible deformation of aligner with standard design

Modified aligner topology eliminated patient complaints about aligner pressure where teeth are missing, achieving unsupported load distribution on the mucosa. In the areas of high load and aesthetic requirements (premolar areas), the result also corresponded to the virtual treatment plan.

The flowchart (Figure 3) shows all the steps involved in the development of the treatment protocol with aligners, while the flowchart for clinicians (Figure 152) shows a ready-made recommended protocol for the management of patients with aligners.

The set of actions presented in this paper allows us to combine the patient's clinical data into a single array and make the treatment process as individualised as possible by automating it. The result of each step is both an independent dataset and the basis for the next one. For example, segmented models from CT scans are independent digital objects for planning surgical and orthodontic manipulations. However, for modelling aligners, the segmented model is one of the steps in the work. In turn, the flowchart shown in figure



152 is an optimized map for orthodontists working with the digital protocol. It will help the clinician increase efficiency and save time when seeing patients as well as managing laboratories involved in the fabrication of aligners.

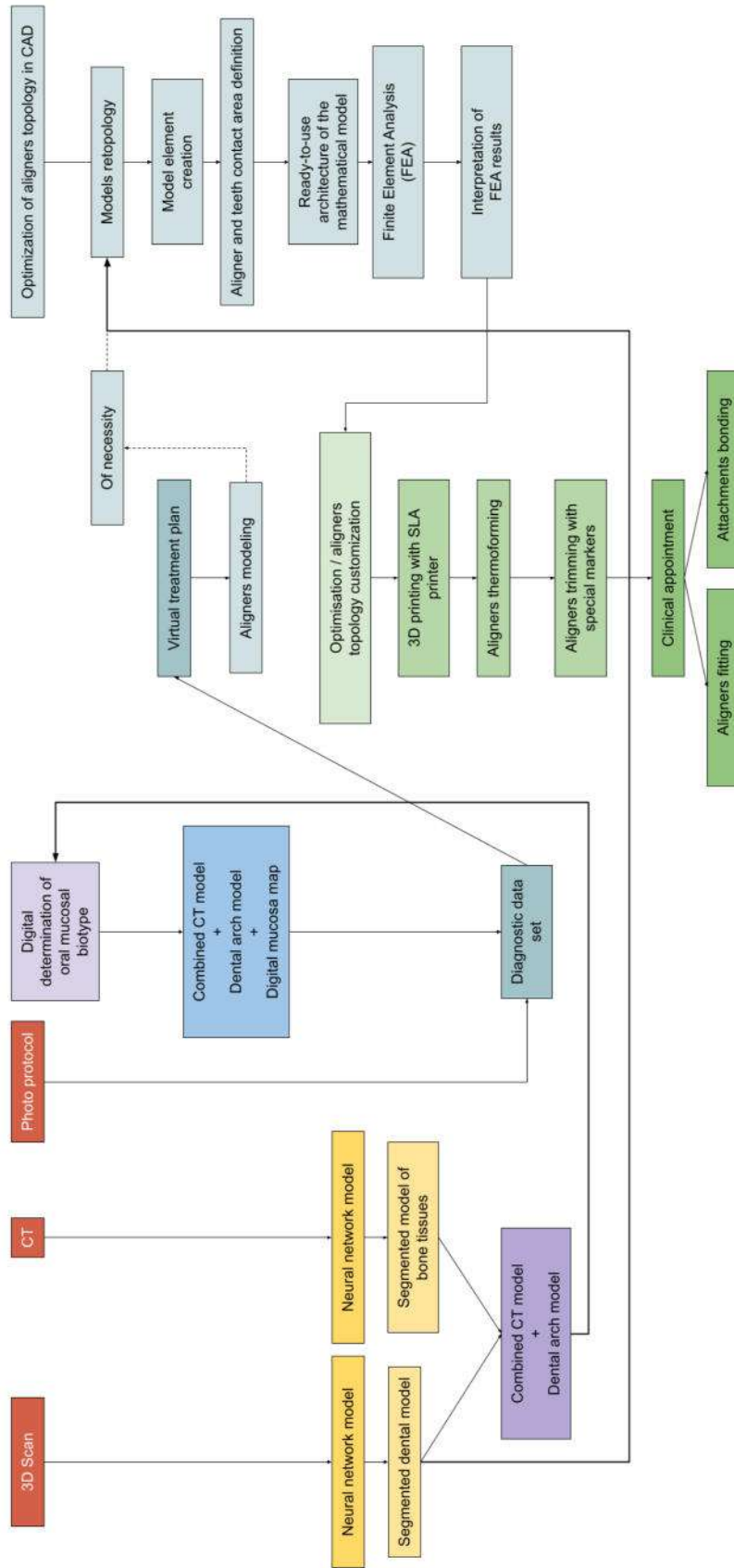


Figure 152 - Flowchart of work for orthodontists

## SUMMARY

Various malocclusions have a very high prevalence, indicating the need to find an effective orthodontic treatment with no recurrence [5, 32].

There are various methods of bite correction. Obviously, the most technologically advanced ones, i.e. those that use digital technology to make them completely predictable, are now taking centre stage. At the moment, such a technique is the treatment with aligners [104, 170, 192].

The aligners' introduction in 1997 has had a major impact on the development of orthodontics. These appliances take into account the teeth individual anatomy and can move the teeth with optimal forces that are safe for the periodontium. The movements of the teeth are more physiological and the resulting treatment effect is more individualised and corresponds to the shape of the dental arches and the surrounding soft tissues.

With the use of modern digital technologies and their combinations [85, 180, 304] it is possible to analyse and predict the risks of complications in detail. If the topology of the aligner is incorrectly chosen, excessive forces may be applied to the moving tooth or excessive pressure may be exerted on the gingiva, especially on gingiva with a thin biotype, which may lead to recession. Hence, in order to avoid complications in the form of gingival recession, an accurate and simple method of determining the biotype of the oral mucosa is essential [232].

Protocols, which are currently used with aligners, are insufficiently studied and may not take into account all the influence of oral mucosal biotype on the final outcome.

**Aim of the study:** effectiveness improvement of orthodontic patients' complex treatment with clear aligners.

One of the most important topics in modern dentistry is to determine the gingival biotype. This is important for developing an effective treatment plan and minimising potential complications such as gingival recession.

In clinical practice, special attention is given to the thin gingival biotype; during orthodontic treatment, patients with a thick gingival biotype may develop a localised form of periodontitis; in the case of a thin biotype, the likelihood of recession is much higher, as loss of gingival attachment leads to marginal inflammation and resorption of the alveolar wall.

Before starting the orthodontic treatment, it is important to ascertain the initial status of the orthodontic patient and their readiness for treatment. In most cases, if hygiene is poor, the patient should be educated on oral hygiene and scheduled for a follow-up visit to check hygiene indices. If oral hygiene is poor during orthodontic treatment, complications related to inflammation of the gingiva will occur. Also, in the presence of inflammation of the gingiva before orthodontic treatment, errors in determining the gingival biotype and the choice of treatment tactics will inevitably occur.

The use of a convolutional neural network (CNN) in orthodontic practice takes the treatment process to a higher level. This creates exceptional possibilities for individualising the aligners' topology.

Recent studies show that when convolutional neural networks are used in the case of computerised cephalometric analysis, the results are better than when performed manually by a radiologist or orthodontist [119, 184, 236].

Neural networks can analyse CT and identify upper and lower jaw bone pathologies, bone levels or the location of retained teeth.

Converged neural networks are also used for various tasks related to tooth segmentation and digital model analysis.

The digital models of the teeth obtained by the intraoral scanner are a single object, similar to a plaster model. Therefore, each tooth must be divided (segmented) in software.

Fully automated software automatically segments and aligns teeth based on intraoral scan data.

Tooth segmentation is an important step for reconstructing a 3D tooth model. Advances have been made in automatic segmentation algorithms using machine learning and deep learning. The results of these studies indicate the significant superiority of deep learning methods in orthodontics over other high-performance algorithms.

Segmentation using AI (artificial intelligence) or NS (neural networks) is further used to work with patients to create a digital treatment plan and to precisely control the position of tooth roots.

At the first stage of the work progress for this study, the patients' oral cavity was scanned using a Planmeca Emerald™ intraoral scanner (Planmeca, Helsinki, Finland) and three-dimensional dental models were created. The models were processed and manually segmented into individual models of each tooth and soft tissues.

In the second stage of the work progress, patients CT data was obtained, manual CT segmentation was performed, and AI was applied in CT segmentation. The following variants of segmentation of cranial bone structures and individual teeth are presented in this work:

1. Manual segmentation
2. Smart grid tool
3. WaterShed
4. Automatic with AI

For the manual method, the first step is to process the CBCT data and segment the hard bone and teeth tissues using the Hounsfield scale to create a 3D model without the use of filters and image modifications. Each dataset in dicom format was processed in Mimics inPrint 2.0 and Mimics PRO Plan CMF 3.0 software.

When using AI, with the presence of a trained model, segmentation is automatic and takes a few seconds. In the absence of such a model, the training takes a long time, but it is much shorter than the manual method.

The data used in the study were acquired using a CBCT machine and processed in Dragonfly software (v.2022.2, Objects Research Systems, Montreal, QC, Canada). The HU values of the CBCT data were normalised to standardise the training of the neural network.

Pre-processing was required to reduce the amount of computed data. After normalisation, semantic segmentation of CBCT was performed. Next, data augmentation was performed, which is a method of artificially creating more training samples to increase the diversity of the training data. Manual segmentation was performed with U-Net training and the final result was semantic segmentation of images using U-net.

In this study, the efficiency of image segmentation was significantly improved by training the network by manually marking five images. In the future, by expanding the amount of data, fully automatic segmentation and identification of multiple tissues in the oral cavity can be performed. By doing so, the accuracy of automatic segmentation will be improved, which will significantly improve automated diagnosis in dentistry.

At the third stage of the course of work, after processing of CT data, segmentation of bone structures and segmentation of teeth and oral mucosa on three-dimensional models of dental rows, all data were superimposed and compared into a single whole. This made it possible to obtain separate layers of bone tissue, soft tissues of the oral cavity and reference teeth. Determination of distances from the surface of the mucosa model to the bone structures and combined tooth models determined the aggregate mucosal thickness colour map, and the zone distribution and graphical data allowed analysis to determine the gingival biotype.

The conducted studies showed that the dispersion analysis of distribution zone revealed three types of oral mucosa - thin, thick and mixed, which corresponds to traditional studies using a periodontal probe test. The result of the work was the creation of a correlation model of the mucosal thickness digital map. A new method for obtaining a digital map of gingival biotype was proposed.

At the fourth stage, the development of orthodontic treatment plans for patients was made in Maestro Ortho Studio V5 software. Clinical goals and objectives for each patient were taken into account during treatment planning. All restriction, norms of movement of each tooth, order and combination of tooth movements were performed according to the physiological capabilities of the organism and aligner design and materials physical properties.

Since the basic principles of biomechanics are based on average values, the individual characteristics of each specific patient are not taken into account. When the individualisation of the orthodontic treatment of the patient is absent, some aligners physical properties are lost [96]. The aim was to obtain a visual representation of deformations and stresses in the aligner by using calculations in physics and mathematics software packages, and to use the results for optimising the aligner design.

In the fifth step, the physical properties of the PET-G material were taken and implemented into the working environment of ANSYS software (ANSYS V.18; ANSYS Inc., Canonsburg, USA) in the modelling of the virtual aligner model.

Since none of the methods previously reported in the literature were suitable for this task, a new technique was developed to fit the aligner appliance on the tooth arch. In the new method, the movements of both the aligner and the dentition were selected in such a way that the edges of the aligner do not deform from contact with the teeth models, and the model creates a realistic trajectory of the aligner fit on the dentition.

In order to create models for analysing the topology of an aligner with an aesthetic component, different types of beam joints suitable for modification with an aesthetic component were developed and analysed. The study design with specific aligner physical parameters and the base model of the dentition was taken from the previously developed one and modified to suit the required task for each clinical case separately.

For the investigated control set of aligners, in order to obtain reinforcement and increase the elasticity of the structure, a standard type of beam connection was selected and analysed for deformation and stress in the appliance structure.

Orthodontic designs with aesthetic components obtained from the simulations were processed in ANSYS mechanical software for further analysis.

The comparative set of aligners included standard clinical solutions with aesthetics in mind by creating a pontic in the area where the tooth was missing.

Finite element mathematical analysis has shown the weaknesses of the beam and pontic type structures, as well as possible ways to modify them.

Based on the analysis of both designs, it was decided to modify them. That is, to obtain a new design that would incorporate both the aesthetics and functions of both types of connections. This solution made it possible to relieve the gingival load in the area of the lost tooth without disturbing the aligner force structure, in addition to improving the aesthetic component of the design, which usually leads to increased patient motivation in the treatment process.

According to the results of finite element analysis, the topology of the aligner has a strong effect on its resistance to deformations. Unforeseen deformations in the aligner redirect forces from the lateral surfaces of the structure to the occlusal surface, which in turn affects the predictability of treatment and can lead to deviations from the initial virtual treatment plan, as well as the need for additional adjustments during the clinical appointment.

From the visual analysis of the obtained data, it is possible to make a conclusion about the areas of maximum stress of the structure, its physical properties and the pressure (applied forces) on each tooth and the entire arch as a whole. Visualisation of the stresses in the structure of the aligner helps to determine the optimal form of trimming in certain places, which are individual for each clinical case, as well as to increase the strength of the structure, its resistance to wear, microcracks and breakage.



Straight trimmed aligners showed better stability and predictability with regard to predicted outcomes at each step. When trimming along the gingival margin, the design is highly deformed during initial activation and poorly distributes pressure on the teeth, resulting in deviations from the steps planned in the virtual set-up.

In the sixth step of the progression, the obtained dental models were processed in Photon Workshop V2 software and then sent to an LCD-based SLA printer Anycubic Photon S for 3D models stereolithographic printing.

The 3D printed models were washed in isopropanol and cured in an UV light chamber for 45 minutes.

The aligners were fabricated using a vacuum former. Next, topological trimming was performed and the edges were extended in the most stressed areas.

In the initial stages of treatment, orthodontic structures were created with modified trimming and were made without functional changes in topology, and were not aesthetically modified.

The aligners with aesthetic pontics were then treated by applying bond and a thin layer of liquid-flow composite. The colour of the composite was matched to the colour of the patient's teeth.

Clinical examples of initial treatment phases without changes to the topology of the aligners were performed with the production of the aligners in the clinic as well as orders from Flexiligner.

In addition to the high demands placed on the aesthetics of aligners, the designs of aligners must also fulfil their direct function. In finite element studies, it has been confirmed that in aligners there is additional stress on the upper and middle thirds of the incisors on the vestibular surface [84, 200, 324].

This effect was also confirmed in the study, but it could not be avoided completely. The effect can be reduced by adding reinforcing ribs on the vestibular side and increasing

the height of the aligner in the anterior region on the palatal and vestibular sides. When performing treatment with aligners with extraction or primary and secondary adentia, the aligner is subjected to increased physical demands in addition to aesthetic properties. Therefore, combined pontic designs have been developed in the course of this work. A pontic is placed on the cheek or vestibular side and a bar reinforcement is placed on the lingual or palatal side. According to FEA calculations, this type of aesthetic pontic modelling distributes the loads as with a bar connection alone, but with an aesthetic pontic. This results in a minimal complications probability and better control of tooth movement.

For the new orthodontic treatment protocol, a method of obtaining an individual gingival biotype map is proposed in order to individualise the amount of trimming of aligners with the least changes in their physical properties and to ensure an individual approach to achieve the best planned result. The gingival biotype map will also be very useful in dental surgery; it will greatly facilitate the work of surgeons when placing orthodontic mini-implants. The digital mucosal biotype map reduces the time of clinical appointments and does not require additional procedures, including invasive ones, to obtain the necessary information about the thickness of the oral mucosa in problematic points. The biotype map also provides not only the possibility of selecting the overall trimming of the aligners for both jaws, but also individualisation for each jaw separately.

The proposed new protocols significantly reduce the likelihood of orthodontic treatment complications due to patient noncompliance and violation of protocols for wearing aligners and elastics.

A solution to another problem in the use of aligners, non-physiological pressure on the patient's oral mucosa, has been proposed. When using removable appliances (usually partial removable dentures), the masticatory load is distributed through the denture base to the mucosa and bone tissue, which is a major disadvantage. Since the oral mucosa does not have morphological structures that can absorb the pressure, the mucosa is compressed,

which in turn leads to circulatory disorders in these areas. A similar situation occurs with prolonged use of aligners, when an aligner support is placed in place of a lost tooth [3, 12, 14, 15]. Using finite element analysis, the places of excessive pressure on the mucosa when the aligner is activated are clearly visible. By altering the aligner's topology or structurally reinforcing specific areas, it becomes possible to lessen or eliminate pressure on the mucosa during aligner deformations, as demonstrated by the author's study. A new protocol for modifying the aligner topology using finite element analysis has been developed.

Stress data visualisation generated in the aligner structure during activation gives full control over the load on the teeth, the distribution of orthodontic forces and the direction of these forces on each tooth involved in movement and anchorage.

However, the mass use of the finite element method as a mandatory protocol in orthodontic treatment directly by clinicians is a matter of time, as it faces the problem of increasing computing power. At present, the finite element method is used by most companies manufacturing aligners, but the data is closed and does not affect the protocols of orthodontic patient management, it only helps to choose the thickness and hardness of the material from which the aligners are made.

All the goals and objectives set in the paper were successfully fulfilled. The study proposes a new mandatory orthodontic treatment protocol using AI-assisted automatic segmentation to monitor the position of tooth roots and better predict treatment. In terms of complications prevention, this provides the safest approach (dehiscence and fenestration). This protocol also provides a more complete picture of the choice of position and shape of the attachments to achieve the planned orthodontic treatment outcome.

## CONCLUSIONS

1. Using three-dimensional models of dental arches obtained by an intraoral scanner, virtual treatment plans for orthodontic patients with aligners were created.
2. Computed tomography (CT) data of orthodontic patients was obtained. Data segmentation was performed using manual segmentation, watershed segmentation, area segmentation, and using a trained U-Net neural network. A comparative analysis of the methods was performed and the most technologically advanced segmentation method using AI with great potential for further application was selected.
3. A new algorithm for creating a digital map of the oral mucosa biotype was developed. The algorithm combines digital data from three-dimensional models obtained with an intraoral scanner and segmented bone structures from CT scans using AI. The absence of inflammatory processes in the oral mucosa of orthodontic patients was assessed using the PMA index with the use of the "Colour-test №1". A comparative analysis of the oral mucosa biotype determination using the traditional method and the developed digital maps was performed.
4. A new original design of mathematical models of orthodontic aligners was developed, which is different from the design used by other researchers and has not been described in the literature before. The general developed design algorithm was modified for each clinical case separately. The efficiency was determined by the degree of deformation and the distribution of load on the entire aligner structure.
5. A comparative analysis of existing standard methods for manufacturing orthodontic aligners, taking into account the additional trimming of the edges in areas with changes in the periodontium was performed. Using the computer-aided design system, the aligners' deformations calculations were obtained and maps of the loads distribution and deformations were presented. Such visualization clearly showed the areas in the aligners design that need to be strengthened.

Based on the mathematical analysis results, the methods of using scalloped and straight aligners trimming depending on the gingival biotype were justified. With a

thin gingival biotype, a scalloped aligners trimming is used. Aligners must be strengthened with a high cut in places of active movement of individual teeth (traction, mesio-distal movements, rotations).

According to the results of the finite element analysis of orthodontic structures with combined aesthetic components, it was proved that the obtained structure has improved physical and aesthetic properties.

6. A digital protocol for orthodontic treatment with aligners was developed according to the selected criteria. Based on the trained neural network model, finite element analysis and digital maps of the oral mucosa, a new orthodontic treatment protocol was proposed, the use of which leads to further individualization and optimization of orthodontic treatment. The protocol allows to improve the quality, save time and increase patient compliance during treatment.

## CLINICAL GUIDELINES

A new mandatory protocol for orthodontic treatment has been proposed, utilizing automatic segmentation to meticulously control root positions and predict treatment outcomes. Notably, this approach offers the safest method for preventing complications like dehiscence and fenestration. Additionally, the protocol provides a comprehensive overview for selecting attachment positioning and shape to achieve optimal treatment results.

For a new orthodontic treatment protocol, an individual mucosa biotype map is needed in order to individualize the amount of aligners trimming with the least changes in their physical properties and provide an individual approach to achieve the best planned result. The mucosa biotype map will also be very useful in dental surgery; it will greatly facilitate the work of surgeons when installing orthodontic mini-implants. The oral mucosa digital map biotype reduces the time of clinical admission and does not require additional procedures, including invasive ones, to obtain the necessary information about the oral mucosa thickness at problem points. Also, the biotype map provides not only the possibility of choosing a common aligner trim for both jaws, but also individualization for each jaw separately.

The proposed new protocols significantly reduce the likelihood of orthodontic treatment complications due to patient compliance and violations of the protocols for wearing aligners and elastics.

The use of the finite element method as a mandatory protocol in orthodontic treatment directly by the doctor is a matter of time and increasing computing power. To date, the finite element method is used by most companies manufacturing aligners, however, the data is confidential and does not affect the protocols for managing an orthodontic patient in any way, but only helps to choose the thickness and stiffness of the material from which the aligners are made.

With the introduction of the above methods into practice and with the greater use of AI in each of these processes, today the orthodontist can already plan treatment with a completely predictable result and with the least dependence on patient compliance.

**LIST OF ABBREVIATIONS**

AI: Artificial Intelligence

CAD: Computer Aided Design Systems

CAT: Clear Aligner Therapy

CBCT: Cone Beam Computed Tomography

CNN: Convolutional Neural Network

CT: Computed Tomography

DL: Deep Learning

FCN: Fully Convolutional Network

FEA: Finite Element Analysis

GAN: Generative adversarial network

PET-G: Polyethylene terephthalate glycol

RFCN: Region-based Fully Convolutional Network

RNN: Recurrent neural network



**BIBLIOGRAPHY**

1. Arsenina, O. I. Orthodontic treatment of a patient with thin gingival biotype and occlusion anomalies / O. I. Arsenina, A. I. Grudyanov, A. G. Nadtochiy [et al.] // Stomatology. - 2020. - Vol. 99. - № 1. - P. 89-94. [In Russian]
2. Arsenina, O. I. Diagnosis and treatment of inflammatory processes in the periodontium arising during orthodontic treatment / O. I. Arsenina, O. A. Frolova, O. V. Petrunina // The Dental Institute. - 2005. - Vol. 1. - № 26. - P. 50-55. [In Russian]
3. Bagryantseva, N. V. Improvement of methods of temporary prosthetics of patients with partial and complete loss of teeth at the stages of dental implantation: dissertation .... Candidate of medical sciences: 14.01.14 / N. V. Bagryantseva. - Nizhny Novgorod, 2020. - 225 p. [In Russian]
4. Volkova, M. N. Diseases of the oral mucosa / M. N. Volkova, Y. P. Chernyavsky, N. A. Sakharuk, E. R. Elenskaya. - Vitebsk, 2016. - 236 p. [In Russian]
5. Vorobyev, M. V. Frequency of dental anomalies in children and factors affecting their occurrence / M. V. Vorobyev, Sh. F. Dzhuraeva, M. V. Moseeva, A. A. Tropina // Scientific Review. Medical Sciences. - 2022. - № 6 2022. - P. 7-11. [In Russian]
6. Hancharyk, I. N. Indirect braces bonding using the new Russian orthodontic adhesive / I. N. Hancharyk, N. A. Sokolovich, A. V. Rybakov [et al.] // The Dental Institute. – 2023. – T. 4 (101). – P. 52-54. [In Russian]
7. Denisova, E. G. Periodontal biotypes and gingival recession: hygienic aspects / E. G. Denisova, I. I. Sokolova. - 2015. - Vol. 4. - № 69. - P. 143-147. [In Russian]
8. Iordanishvili, A.K. Oral hygiene, the condition of periodontal tissues and ways to improve them in young people undergoing orthodontic treatment / A.K. Iordanishvili, K.A. Kerimkhanov, L.N. Soldatova, V.F. Chernysh. – 2015. [In Russian]

9. Iordanishvili, A.K. Diseases of organs and tissues of the oral cavity in young people / A.K. Iordanishvili, A.S. Soldatkina // Institute of Dentistry. – 2015. – No. 3. – P. 38-41. [In Russian]
10. Karneeva T.V. Gingival recession and its main causes / Karneeva T.V. // Health Care of the Far East. - 2019. - № 4. - P. 54-56. [In Russian]
11. Kolesnik, K. A. Clinical assessment of the condition of periodontal tissues in adolescents with exogenous constitutional obesity / K. A. Kolesnik, G. V. Zherdeva // Institute of Dentistry. – 2015. – No. 2. – P. 74-75. [In Russian]
12. Komlev, S. S. New technologies in the complex treatment of patients with partial and complete absence of teeth: dissertation .... Doctor of medical sciences: 14.01.14 / S. S. Komlev. - 2020. - 297 p. [In Russian]
13. Kopetsky, I. S. Periodontal biotype: anatomical features and interrelation with surrounding tissues / I. S. Kopetsky, L. V. Pobozhieva, Y. V. Shevelyuk, A. I. Kopetskaya. - 2020. - Vol. 26. - № 2. - P. 114-119. [In Russian]
14. Korotkikh, N. G. Fundamentals of rehabilitation of stomatological patients of surgical practice by the method of dental implantation / N. G. Korotkikh, N. E. Mitin, L. P. Nabatchikova, L. B. Filimonova. - Methodical recommendations for students of dental faculty, interns, clinical residents, 2013. - 33 p. [In Russian]
15. Poroshin, A. V. Orthopaedic treatment with complete removable prostheses with fixation on mini-implants / A. V. Poroshin, D. V. Mikhailchenko, A. A. A. Aleshechkin, A. Y. Maiboroda // Volgograd Scientific Medical Journal. - 2013. - № 4. - P. 50-51. [In Russian]
16. Rybakov, A. V. Two-step Methodology of Investigating the Position of the Temporomandibular Joint condyles : abstract of the interuniversity conference of RUDN " Relevant issues of stomatology " / A. V. Rybakov, N. A. Sokolovich. - Moscow, 2022. - 114-115 p. [In Russian]

17. Sarkisyan, V. M. Variants of the gingival structure at different biotypes / V. M. Sarkisyan, O. V. Zayratyants, A. M. Panin, M. G. Panin // Dental Forum. - 2011. - No. 5. - 2011. - P. 105-106. [In Russian]
18. Sarkisyan, V. M. Morphological features of the gingiva of different biotypes / V. M. Sarkisyan, O. V. Zayrtiyants, A. M. Panin, M. G. Panin // Periodontology. - 2012. - Vol. 1. - № 62. - P. 26-29. [In Russian]
19. Smirnova, S. S. Modification of the clinical method of gingival thickness measurement and experimental substantiation of its effectiveness / S. S. Smirnova, G. I. Ron, I. E. Valamina [et al.] // Bulletin of the Ural Medical Academic Science. - 2010. - № 2. - P. 100-102. [In Russian]
20. Sokolovich, N. A. Temporomandibular joint position assessment technique / N. A. Sokolovich, A. V. Rybakov, A. A. Saunina [et al.] // The Medical Alliance. – 2023. – T. 11. – № 1.
21. Tarasenko, S. V. Index assessment of periodontal condition in patients with rheumatoid arthritis / S. V. Tarasenko, A. A. Makarevich // Russian Journal of Dentistry // Russian Journal of Dentistry. - 2018. - Vol. 22. - № 4. - P. 199-202. [In Russian]
22. Ulitovsky, S. B. Study of the prevalence of periodontal diseases in orthodontic patients / S. B. Ulitovsky, A. V. Shevtsov // Parodontologiya. - 2020. - Vol. 25. - № 1. - P. 37-41. [In Russian]
23. Zur, O. Plastic and aesthetic surgery / O. Zur, M. Hürzeler. - 2014. - 847 p. [In Russian]
24. Shashurina, S. V. Improvement of methods of surgical treatment of gingival recessions: dissertation .... Candidate of medical sciences: 14.01.14 / S. V. Shashurina. - Tver, 2017. - 281 p. [In Russian]

25. Scherbakov, A. S. Gingival recessions: etiopathogenesis, features of treatment planning and prevention / A. S. Scherbakov, M. B. Kuznetsova, S. I. Vinogradova [et al.] // Verkhnevolzhskiy Medical Journal. - 2012. - Vol. 10. - № 1. - P. 6. [In Russian]
26. Abdallah, M. N. Biomaterials used in orthodontics: Brackets, archwires, and clear aligners / M. N. Abdallah, T. Lou, J. M. Retrouvey, S. Suri // Advanced Dental Biomaterials. – 2019.
27. Abraham, S. Gingival biotype and its clinical significance - A review / S. Abraham, K. T. Deepak, R. Ambili [et al.] // Saudi Journal for Dental Research. – 2014. – Vol. 5. – № 1. – P. 3-7.
28. Ahn, H. W. Effects of aging procedures on the molecular, biochemical, morphological, and mechanical properties of vacuum-formed retainers / H. W. Ahn, H. R. Ha, H. N. Lim, S. Choi // Journal of the Mechanical Behavior of Biomedical Materials. – 2015. – Vol. 51.
29. Ahn, H. W. A new type of clear orthodontic retainer incorporating multi-layer hybrid materials / H. W. Ahn, K. A. Kim, S. H. Kim // Korean Journal of Orthodontics. – 2015. – Vol. 45. – № 5.
30. Akhoondali, H. Rapid automatic segmentation and visualization of teeth in CT-scan data / H. Akhoondali, R. A. Zoroofi, G. Shirani // Journal of Applied Sciences. – 2009. – Vol. 9. – № 11.
31. Alexandropoulos, A. Chemical and mechanical characteristics of contemporary thermoplastic orthodontic materials / A. Alexandropoulos, Y. S. Al Jabbari, S. Zinelis, T. Eliades // Australian orthodontic journal. – 2015. – Vol. 31. – № 2.
32. Alhammadi, M. S. Global distribution of malocclusion traits: A systematic review / M. S. Alhammadi, E. Halboub, M. S. Fayed [et al.] // Dental Press Journal of Orthodontics. – 2018. – Vol. 23. – № 6. – P. 40.e1.

33. Al-Nadawi, M. Effect of clear aligner wear protocol on the efficacy of tooth movement: A randomized clinical trial / M. Al-Nadawi, N. D. Kravitz, I. Hansa [et al.] // *Angle Orthodontist*. – 2021. – Vol. 91. – № 2.
34. Alom, M. Z. Inception recurrent convolutional neural network for object recognition / M. Z. Alom, M. Hasan, C. Yakopcic [et al.] // *Machine Vision and Applications*. – 2021. – Vol. 32. – № 1.
35. Alves, P. H. M. Measurement properties of gingival biotype evaluation methods / P. H. M. Alves, T. C. L. P. Alves, T. A. Pegoraro [et al.] // *Clinical Implant Dentistry and Related Research*. – 2018. – Vol. 20. – № 3. – P. 280-284.
36. Al-Zahrani, M. S. Comparison of Cone Beam Computed Tomography-Derived Alveolar Bone Density Between Subjects with and without Aggressive Periodontitis / M. S. Al-Zahrani // *Journal of clinical and diagnostic research*. – 2017.
37. Amorim, P. H. J. Reconstruction of Panoramic Dental Images Through Bézier Function Optimization / P. H. J. Amorim, T. F. Moraes, J. V. L. Silva [et al.] // *Frontiers in Bioengineering and Biotechnology*. – 2020. – Vol. 8.
38. Anand, P. S. Width and thickness of the gingiva in periodontally healthy individuals in a central Indian population: a cross-sectional study / P. S. Anand, A. Bansal, B. R. Shenoi [et al.] // *Clinical Oral Investigations*. – 2022. – Vol. 26. – № 1. – P. 751-759.
39. Andrews, L. The concept and appliance / L. Andrews // *the concept and appliance*. – 1989.
40. Arita, M. Consideration of the AM method in PMA index / M. Arita, S. Yamada, H. Tanoi [et al.] // *Koku Eisei Gakkai zasshi*. – 1972. – Vol. 22. – № 2. – P. 264-268.

41. Avendi, M. R. A combined deep-learning and deformable-model approach to fully automatic segmentation of the left ventricle in cardiac MRI / M. R. Avendi, A. Kheradvar, H. Jafarkhani // *Medical Image Analysis*. – 2016. – Vol. 30.
42. Ayidaga, C. Effects of Variable Composite Attachment Shapes in Controlling Upper Molar Distalization with Aligners: A Nonlinear Finite Element Study / C. Ayidaga, B. Kamiloglu // *Journal of Healthcare Engineering*. – 2021. – Vol. 2021.
43. Badrinarayanan, V. SegNet: A Deep Convolutional Encoder-Decoder Architecture for Image Segmentation / V. Badrinarayanan, A. Kendall, R. Cipolla // *IEEE Transactions on Pattern Analysis and Machine Intelligence*. – 2017. – Vol. 39. – № 12.
44. Bai, Y. X. Patients with anterior spaces caused by periodontal disease treated with aligner technique / Y. X. Bai, B. Yang, Q. Dai [et al.] // *Zhonghua kou qiang yi xue za zhi = Zhonghua kouqiang yixue zazhi = Chinese journal of stomatology*. – 2009. – Vol. 44. – № 7.
45. Bargellini, A. Short Term Evaluation of the Effects of Orthodontic Clear Aligners on Sleep Bruxism Activity / A. Bargellini, T. Castroflorio, F. Casasco [et al.] // *Iranian Journal of Orthodontics*. – 2016. – Vol. 12. – № 2.
46. Barone, S. CT segmentation of dental shapes by anatomy-driven reformation imaging and B-spline modelling / S. Barone, A. Paoli, A. V. Rationale // *International Journal for Numerical Methods in Biomedical Engineering*. – 2016. – Vol. 32. – № 6.
47. Barreto, M. S. Reliability of digital orthodontic setups / M. S. Barreto, J. Faber, C. J. Vogel, T. M. Araujo // *The Angle Orthodontist*. – 2016. – Vol. 86. – № 2. – P. 255-259.
48. Barriviera, M. A new method to assess and measure palatal masticatory mucosa by cone-beam computerized tomography / M. Barriviera, W. R. Duarte, A. L. Januário [et al.] // *Journal of Clinical Periodontology*. – 2009. – Vol. 36. – № 7. – P. 564-568.

49. Baumgartner, C. F. An exploration of 2D and 3D deep learning techniques for cardiac MR image segmentation / C. F. Baumgartner, L. M. Koch, M. Pollefeys, E. Konukoglu // *Lecture Notes in Computer Science (including subseries Lecture Notes in Artificial Intelligence and Lecture Notes in Bioinformatics)*. – 2018. – Vol. 10663 LNCS.

50. Bednarz, W. Ultrasonic biometer and its usage in an assessment of periodontal soft tissue thickness and comparison of its measurement accuracy with a bone sounding method / W. Bednarz, A. Zielińska // *Dental and Medical Problems*. – 2011. – Vol. 48. – № 4. – P. 481-489.

51. Belikova, K. Deep negative volume segmentation / K. Belikova, O. Y. Rogov, A. Rybakov [et al.] // *Scientific Reports*. – 2021. – Vol. 11. – № 1. – P. 16292.

52. Bernard, G. Colorimetric and spectrophotometric measurements of orthodontic thermoplastic aligners exposed to various staining sources and cleaning methods / G. Bernard, P. Rompré, J. R. Tavares, A. Montpetit // *Head and Face Medicine*. – 2020. – Vol. 16. – № 1.

53. Bilello, G. Accuracy evaluation of orthodontic movements with aligners: a prospective observational study / G. Bilello, M. Fazio, E. Amato [et al.] // *Progress in Orthodontics*. – 2022. – Vol. 23. – № 1.

54. Borda, A. F. Outcome assessment of orthodontic clear aligner vs fixed appliance treatment in a teenage population with mild malocclusions / A. F. Borda, J. S. Garfinkle, D. A. Covell [et al.] // *Angle Orthodontist*. – 2020. – Vol. 90. – № 4. – P. 485-490.

55. Boubakri, A. Investigations on hygrothermal aging of thermoplastic polyurethane material / A. Boubakri, K. Elleuch, N. Guermazi, H. F. Ayedi // *Materials and Design*. – 2009. – Vol. 30. – № 10.

56. Bowman, S. J. Creative adjuncts for clear aligners, part 1: Class II treatment / S. J. Bowman, F. Celenza, J. Sparaga [et al.] // J Clin Orthod. – 2015. – Vol. 49. – № 2. – P. 83-94.

57. Bowman, S. J. Creative adjuncts for clear aligners, part 2: Intrusion, rotation, and extrusion / S. J. Bowman, F. Celenza, J. Sparaga [et al.] // J Clin Orthod. – 2015. – Vol. 49. – № 3. – P. 162-172.

58. Bowman, S. J. Creative adjuncts for clear aligners, part 3: Extraction and interdisciplinary treatment / S. J. Bowman, F. Celenza, J. Sparaga [et al.] // Journal of clinical orthodontics : JCO. – 2015. – Vol. 49. – № 4. – P. 249-262.

59. Bowman, S. J. Improving the predictability of clear aligners / S. J. Bowman // Seminars in Orthodontics. – 2017. – Vol. 23. – № 1.

60. Brown, R. A. Large Strain Deformation of PETG at Processing Temperatures / R. A. Brown. – 2000.

61. Bucci, R. Thickness of orthodontic clear aligners after thermoforming and after 10 days of intraoral exposure: a prospective clinical study / R. Bucci, R. Rongo, C. Levatè [et al.] // Progress in Orthodontics. – 2019. – Vol. 20. – № 1.

62. Can, E. In-house 3D-printed aligners: effect of in vivo ageing on mechanical properties / E. Can, N. Panayi, G. Polychronis [et al.] // European journal of orthodontics. – 2022. – Vol. 44. – № 1.

63. Caruana, R. An Empirical Comparison of Supervised Learning Algorithms / R. Caruana, A. Niculescu-Mizil // Proceedings of the 23rd international conference on Machine learning - ICML '06. – 2006. – Vol. 2006. – P. 161-168.

64. Carvajal-Flórez, A. Orthodontic treatment outcomes obtained by application of a finishing protocol / A. Carvajal-Flórez, D. M. Barbosa-Lis, O. A. Zapata-Noreña [et al.] // Dental Press Journal of Orthodontics. – 2016. – Vol. 21. – № 2. – P. 88-94.



65. Castroflorio, T. Effects of clear aligners on sleep bruxism: Randomized controlled trial / T. Castroflorio, A. Bargellini, A. Lucchese [et al.] // *Journal of Biological Regulators and Homeostatic Agents*. – 2018. – Vol. 32. – № 2.

66. Castroflorio, T. Effects on sleep bruxism activity of clear aligners detected with nocturnal instrumental recordings / T. Castroflorio, A. Bargellini, A. Lucchese [et al.] // <https://trialssearch.who.int/Trial2.aspx?TrialID=ISRCTN12654415>. – 2017.

67. Castroflorio, T. Predictability of orthodontic tooth movement with aligners: effect of treatment design / T. Castroflorio, A. Sedran, S. Parrini [et al.] // *Progress in Orthodontics*. – 2023. – Vol. 24. – № 1.

68. Cattaneo, P. M. The finite element method: A tool to study orthodontic tooth movement / P. M. Cattaneo, M. Dalstra, B. Melsen // *Journal of Dental Research*. – 2005. – Vol. 84. – № 5.

69. Chen, C. Improving the Generalizability of Convolutional Neural Network-Based Segmentation on CMR Images / C. Chen, W. Bai, R. H. Davies [et al.] // *Frontiers in Cardiovascular Medicine*. – 2020. – Vol. 7.

70. Chen, C. Multi-task Learning for Left Atrial Segmentation on GE-MRI / C. Chen, W. Bai, D. Rueckert // *Lecture Notes in Computer Science (including subseries Lecture Notes in Artificial Intelligence and Lecture Notes in Bioinformatics)*. – 2019. – Vol. 11395 LNCS.

71. Chen, C. Learning Shape Priors for Robust Cardiac MR Segmentation from Multi-view Images / C. Chen, C. Biffi, G. Tarroni [et al.] // *Lecture Notes in Computer Science (including subseries Lecture Notes in Artificial Intelligence and Lecture Notes in Bioinformatics)*. – 2019. – Vol. 11765 LNCS.

72. Chen, L. C. Rethinking Atrous Convolution for Semantic Image Segmentation Liang-Chieh / L. C. Chen, G. Papandreou, I. Kokkinos [et al.] // *IEEE Transactions on Pattern Analysis and Machine Intelligence*. – 2018. – Vol. 40. – № 4.

73. Chen, M. FR-NET: Focal loss constrained deep residual networks for segmentation of cardiac MRI / M. Chen, L. Fang, H. Liu // Proceedings - International Symposium on Biomedical Imaging. – 2019. – Vols. 2019-April.

74. Chen, S. Med3D: Transfer Learning for 3D Medical Image Analysis / S. Chen, K. Ma, Y. Zheng. – 2019.

75. Chen, S. Machine learning in orthodontics: Introducing a 3D auto-segmentation and auto-landmark finder of CBCT images to assess maxillary constriction in unilateral impacted canine patients / S. Chen, L. Wang, G. Li [et al.] // Angle Orthodontist. – 2020. – Vol. 90. – № 1. – P. 77-84.

76. Chen, X. Generative Adversarial U-Net for Domain-free Medical Image Augmentation / X. Chen, Y. Li, L. Yao [et al.]. – 2021. – P. 1.

77. Chen, Y. Automatic Segmentation of Individual Tooth in Dental CBCT Images from Tooth Surface Map by a Multi-Task FCN / Y. Chen, H. Du, Z. Yun [et al.] // IEEE Access. – 2020. – Vol. 8. – № April 2022. – P. 97296-97309.

78. Chung, M. Pose-aware instance segmentation framework from cone beam CT images for tooth segmentation / M. Chung, M. Lee, J. Hong [et al.] // Computers in Biology and Medicine. – 2020. – Vol. 120.

79. Çiçek, Ö. 3D U-net: Learning dense volumetric segmentation from sparse annotation / Ö. Çiçek, A. Abdulkadir, S. S. Lienkamp [et al.] // Lecture Notes in Computer Science (including subseries Lecture Notes in Artificial Intelligence and Lecture Notes in Bioinformatics). – 2016. – Vol. 9901 LNCS.

80. Çiğla, C. Region-based image segmentation via graph cuts / C. Çiğla, A. A. Alatan // Proceedings - International Conference on Image Processing, ICIP. – 2008.

81. Clough, J. R. Explicit Topological Priors for Deep-Learning Based Image Segmentation Using Persistent Homology / J. R. Clough, I. Oksuz, N. Byrne [et al.] //

Lecture Notes in Computer Science (including subseries Lecture Notes in Artificial Intelligence and Lecture Notes in Bioinformatics). – 2019. – Vol. 11492 LNCS.

82. Condo', R. Mechanical properties of 'two generations' of teeth aligners: Change analysis during oral permanence / R. Condo', L. Pazzini, L. Cerroni [et al.] // *Dental Materials Journal*. – 2018. – Vol. 37. – № 5.

83. Cong, C. Invert-U-Net DNN segmentation model for MRI cardiac left ventricle segmentation / C. Cong, H. Zhang // *The Journal of Engineering*. – 2018. – Vol. 2018. – № 16.

84. Cortona, A. Clear aligner orthodontic therapy of rotated mandibular round-shaped teeth: A finite element study / A. Cortona, G. Rossini, S. Parrini [et al.] // *The Angle Orthodontist*. – 2020. – Vol. 90. – № 2. – P. 247-254.

85. Cui, Z. Toothnet: Automatic tooth instance segmentation and identification from cone beam ct images / Z. Cui, C. Li, W. Wang // *Proceedings of the IEEE Computer Society Conference on Computer Vision and Pattern Recognition*. – 2019. – Vols. 2019-June. – № 3. – P. 6361-6370.

86. Cuny-Houchmand, M. Gingival Biotype Assesement: Visual Inspection Relevance And Maxillary Versus Mandibular Comparison / M. Cuny-Houchmand, S. Renaudin, M. Leroul [et al.] // *The Open Dentistry Journal*. – 2013. – Vol. 7. – № 1. – P. 1-6.

87. D'Antò, V. The Predictability of Transverse Changes in Patients Treated with Clear Aligners / V. D'Antò, R. Valletta, L. Di Mauro [et al.] // *Materials*. – 2023. – Vol. 16. – № 5.

88. Dou, Q. Automatic lesion detection with three-dimensional convolutional neural networks / Q. Dou, H. Chen, J. Qin, P.-A. Heng // *Biomedical Information Technology*. – 2020.

89. Duan, J. Deep Nested Level Sets: Fully Automated Segmentation of Cardiac MR Images in Patients with Pulmonary Hypertension / J. Duan, J. Schlemper, W. Bai [et al.] // Lecture Notes in Computer Science (including subseries Lecture Notes in Artificial Intelligence and Lecture Notes in Bioinformatics). – 2018. – Vol. 11073 LNCS.

90. Duchi, J. Adaptive subgradient methods for online learning and stochastic optimization / J. Duchi, E. Hazan, Y. Singer // Journal of Machine Learning Research. – 2011. – Vol. 12.

91. Duong, T. Finishing with invisalign. / T. Duong, E. Kuo // Progress in orthodontics. – 2006. – Vol. 7. – № 1.

92. Dupaix, R. B. Finite strain behavior of poly(ethylene terephthalate) (PET) and poly(ethylene terephthalate)-glycol (PETG) / R. B. Dupaix, M. C. Boyce // Polymer. – 2005. – Vol. 46. – № 13. – P. 4827-4838.

93. Edelmann, A. Analysis of the thickness of 3-dimensional-printed orthodontic aligners / A. Edelmann, J. D. English, S. J. Chen, F. K. Kasper // American Journal of Orthodontics and Dentofacial Orthopedics. – 2020. – Vol. 158. – № 5.

94. Eliades, T. Orthodontic aligner treatment: a review of materials, clinical management, and evidence / T. Eliades, A. E. Athanasiou. – 2021. – 186 p.

95. Eliades, T. The use of attachments in aligner treatment: Analyzing the ‘innovation’ of expanding the use of acid etching–mediated bonding of composites to enamel and its consequences / T. Eliades, S. N. Papageorgiou, A. J. Ireland // American Journal of Orthodontics and Dentofacial Orthopedics. – 2020. – Vol. 158. – № 2.

96. Elkholy, F. Forces and moments delivered by PET-G aligners to an upper central incisor for labial and palatal translation / F. Elkholy, T. Panchaphongsaphak, F. Kilic [et al.] // J Orofac Orthop. – 2015. – Vol. 76. – № 6. – P. 460-475.

97. Erke Wang, T. N. Back to elements-tetrahedra vs. hexahedra / T. N. Erke Wang, R. Rauch // Proceedings of the 2004 international ANSYS conference. – 2004.

98. Faber, J. Artificial intelligence in orthodontics / J. Faber, C. Faber, P. Faber // APOS Trends in Orthodontics. – 2019. – Vol. 9. – № 4. – P. 201-205.

99. Fahmy, A. S. Automated analysis of cardiovascular magnetic resonance myocardial native T1 mapping images using fully convolutional neural networks / A. S. Fahmy, H. El-Rewaidy, M. Nezafat [et al.] // Journal of cardiovascular magnetic resonance : official journal of the Society for Cardiovascular Magnetic Resonance. – 2019. – Vol. 21. – № 1.

100. Fahmy, A. S. Three-dimensional deep convolutional neural networks for automated myocardial scar quantification in hypertrophic cardiomyopathy: A multicenter multivendor study / A. S. Fahmy, U. Neisius, R. H. Chan [et al.] // Radiology. – 2020. – Vol. 294. – № 1.

101. Fan, Y. Marker-based watershed transform method for fully automatic mandibular segmentation from CBCT images / Y. Fan, R. Beare, H. Matthews [et al.] // Dentomaxillofacial Radiology. – 2019. – Vol. 48. – № 2.

102. Farrag, N. A. Evaluation of fully automated myocardial segmentation techniques in native and contrast-enhanced T1-mapping cardiovascular magnetic resonance images using fully convolutional neural networks / N. A. Farrag, A. Lochbihler, J. A. White, E. Ukwatta // Medical physics. – 2021. – Vol. 48. – № 1. – P. 215-226.

103. FayyazAhamed, S. Cytotoxic evaluation of directly 3D printed aligners and Invisalign / S. FayyazAhamed, S. M. Kumar, R. K. Vijayakumar [et al.] // European Journal of Molecular and Clinical Medicine. – 2020. – Vol. 7. – № 5.

104. Fiori, A. Predictability of crowding resolution in clear aligner treatment / A. Fiori, G. Minervini, L. Nucci [et al.] // Progress in Orthodontics. – 2022. – Vol. 23. – № 1.

105. Fischer, K. R. Gingival biotype revisited — novel classification and assessment tool / K. R. Fischer, A. Künzlberger, N. Donos [et al.]. – 2017.

106. Fischer, K. R. Gingival biotype revisited—novel classification and assessment tool / K. R. Fischer, A. Künzlberger, N. Donos [et al.] // *Clinical Oral Investigations*. – 2018. – Vol. 22. – № 1. – P. 443-448.

107. Fischer, K. R. On the relationship between gingival biotypes and gingival thickness in young Caucasians / K. R. Fischer. – 2014. – № 2009. – P. 865-869.

108. Frick, A. Characterization of TPU-elastomers by thermal analysis (DSC) / A. Frick, A. Rochman // *Polymer Testing*. – 2004. – Vol. 23. – № 4. – P. 413-417.

109. Fu, J.-H. Tissue Biotype and Its Relation to the Underlying Bone Morphology / J.-H. Fu, C.-Y. Yeh, H.-L. Chan [et al.] // *Journal of Periodontology*. – 2010. – Vol. 81. – № 4. – P. 569-574.

110. Fu, M. Hierarchical combinatorial deep learning architecture for pancreas segmentation of medical computed tomography cancer images / M. Fu, W. Wu, X. Hong [et al.] // *BMC Systems Biology*. – 2018. – Vol. 12.

111. Fuhrer, R. S. A comparative finite element analysis of maxillary expansion with and without midpalatal suture viscoelasticity using a representative skeletal geometry / R. S. Fuhrer, D. L. Romanyk, J. P. Carey // *Sci Rep*. – 2019. – Vol. 9. – № 1. – P. 8476.

112. Fujiyama, K. Analysis of pain level in cases treated with Invisalign aligner: Comparison with fixed edgewise appliance therapy / K. Fujiyama, T. Honjo, M. Suzuki [et al.] // *Progress in Orthodontics*. – 2014. – Vol. 15. – № 1.

113. Gan, Y. Tooth and Alveolar Bone Segmentation From Dental Computed Tomography Images / Y. Gan, Z. Xia, J. Xiong [et al.] // *IEEE Journal of Biomedical and Health Informatics*. – 2018. – Vol. 22. – № 1. – P. 196-204.

114. Ganaye, P. A. Removing segmentation inconsistencies with semi-supervised non-adjacency constraint / P. A. Ganaye, M. Sdika, B. Triggs, H. Benoit-Cattin // *Medical Image Analysis*. – 2019. – Vol. 58.
115. Genina, E. A. Phototherapy of gingivitis: Pilot clinical study / E. A. Genina, V. A. Titorenko, V. V. Tuchin [et al.] // *Journal of Innovative Optical Health Sciences*. – 2011. – Vol. 4. – № 4. – P. 437-446.
116. Gerard Bradley, T. Do the mechanical and chemical properties of Invisalign™ appliances change after use? A retrieval analysis / T. Gerard Bradley, L. Teske, G. Eliades [et al.] // *European Journal of Orthodontics*. – 2016. – Vol. 38. – № 1.
117. Gheller, C. Deep learning based detection of cosmological diffuse radio sources / C. Gheller, F. Vazza, A. Bonafede // *Monthly Notices of the Royal Astronomical Society*. – 2018. – Vol. 480. – № 3.
118. Gibson, E. Automatic Multi-Organ Segmentation on Abdominal CT with Dense V-Networks / E. Gibson, F. Giganti, Y. Hu [et al.] // *IEEE Transactions on Medical Imaging*. – 2018. – Vol. 37. – № 8.
119. Gilmour legilmou, L. Locating Cephalometric X-Ray Landmarks with Foveated Pyramid Attention / L. Gilmour legilmou, ualbertaca Nilanjan Ray nray. – 2020.
120. Gkantidis, N. The orthodontic–periodontic interrelationship in integrated treatment challenges: a systematic review / N. Gkantidis, P. Christou, N. Topouzelis // *Journal of Oral Rehabilitation*. – 2010. – Vol. 37. – № 5. – P. 377-390.
121. Glide-Hurst, C. Changes realized from extended bit-depth and metal artifact reduction in CT / C. Glide-Hurst, D. Chen, H. Zhong, I. J. Chetty // *Medical Physics*. – 2013. – Vol. 40. – № 6. – P. 061711.

122. Glorot, X. Understanding the difficulty of training deep feedforward neural networks / X. Glorot, Y. Bengio // *Journal of Machine Learning Research*. – 2010. – Vol. 9.
123. Gomez, J. P. Initial force systems during bodily tooth movement with plastic aligners and composite attachments: A three-dimensional finite element analysis / J. P. Gomez, F. M. Peña, V. Martínez [et al.] // *Angle Orthodontist*. – 2015. – Vol. 85. – № 3. – P. 454-460.
124. Goodfellow, I. Generative adversarial networks / I. Goodfellow, J. Pouget-Abadie, M. Mirza [et al.] // *Communications of the ACM*. – 2020. – Vol. 63. – № 11.
125. Gordienko, Y. Deep learning with lung segmentation and bone shadow exclusion techniques for chest X-ray analysis of lung cancer / Y. Gordienko, P. Gang, J. Hui [et al.] // *Advances in Intelligent Systems and Computing*. – 2019. – Vol. 754.
126. Goto, M. A method for evaluation of the effects of attachments in aligner-type orthodontic appliance: Three-dimensional finite element analysis / M. Goto, W. Yanagisawa, H. Kimura [et al.] // *Orthodontic Waves*. – 2017. – Vol. 76. – № 4.
127. Hahn, W. The influence of occlusal forces on force delivery properties of aligners during rotation of an upper central incisor / W. Hahn, B. Engelke, K. Jung [et al.] // *Angle Orthodontist*. – 2011. – Vol. 81. – № 6.
128. Hallmann, L. Effect of Dental Thermoplastic Materials on the Clinical Effectiveness of Clear Aligner / L. Hallmann, M. Gerngroß // *Austin Journal of Dentistry*. – 2021. – Vol. 8. – № 1. – P. 40-42.
129. *Handbook of Polycarbonate Science and Technology*. – 1999.
130. Hansa, I. Outcomes of clear aligner treatment with and without Dental Monitoring: A retrospective cohort study / I. Hansa, V. Katyal, D. J. Ferguson, N. Vaid // *American Journal of Orthodontics and Dentofacial Orthopedics*. – 2021. – Vol. 159. – № 4. – P. 453-459.



131. Hasan, I. Radiographic evaluation of bone density around immediately loaded implants / I. Hasan, M. Dominiak, A. Blaszczyzyn [et al.] // *Annals of Anatomy*. – 2015. – Vol. 199. – P. 52-57.
132. Hasan, M. K. DSNet: Automatic dermoscopic skin lesion segmentation / M. K. Hasan, L. Dahal, P. N. Samarakoon [et al.] // *Computers in Biology and Medicine*. – 2020. – Vol. 120.
133. Havaei, M. Brain tumor segmentation with Deep Neural Networks / M. Havaei, A. Davy, D. Warde-Farley [et al.] // *Medical Image Analysis*. – 2017. – Vol. 35.
134. Hayashi, K. A novel method for the three-dimensional (3-D) analysis of orthodontic tooth movement - Calculation of rotation about and translation along the finite helical axis / K. Hayashi, Y. Araki, J. Uechi [et al.] // *Journal of Biomechanics*. – 2002. – Vol. 35. – № 1.
135. He, K. Deep residual learning for image recognition / K. He, X. Zhang, S. Ren, J. Sun // *Proceedings of the IEEE Computer Society Conference on Computer Vision and Pattern Recognition*. – 2016. – Vols. 2016-Decem.
136. He, K. Delving deep into rectifiers: Surpassing human-level performance on imagenet classification / K. He, X. Zhang, S. Ren, J. Sun // *Proceedings of the IEEE International Conference on Computer Vision*. – 2015. – Vol. 2015 Inter. – P. 1026-1034.
137. Hegazy, M. A. A. U-net based metal segmentation on projection domain for metal artifact reduction in dental CT / M. A. A. Hegazy, M. H. Cho, M. H. Cho, S. Y. Lee // *Biomedical Engineering Letters*. – 2019. – Vol. 9. – № 3. – P. 375-385.
138. Hennessy, J. Clear aligners generations and orthodontic tooth movement / J. Hennessy, E. A. Al-Awadhi // *Journal of Orthodontics*. – 2016. – Vol. 3125. – № January. – P. 1-9.

139. Heo, H. Segmentation of tooth in CT images for the 3D reconstruction of teeth / H. Heo, O.-S. Chae // *Image Processing: Algorithms and Systems III*. – 2004. – Vol. 5298.
140. Heo, M.-S. Artificial intelligence in oral and maxillofacial radiology: what is currently possible? / M.-S. Heo, J.-E. Kim, J.-J. Hwang [et al.] // *Dentomaxillofacial Radiology*. – 2021. – Vol. 50. – № 3.
141. Hinton, G. E. Improving neural networks by preventing co-adaptation of feature detectors / G. E. Hinton, N. Srivastava, A. Krizhevsky [et al.]. – 2012.
142. Hochreiter, S. Long Short-Term Memory / S. Hochreiter, J. Schmidhuber // *Neural Computation*. – 1997. – Vol. 9. – № 8. – P. 1735-1780.
143. Hou, D. The effect of digital diagnostic setups on orthodontic treatment planning / D. Hou, R. Capote, B. Bayirli [et al.] // *American Journal of Orthodontics and Dentofacial Orthopedics*. – 2020. – Vol. 157. – № 4. – P. 542-549.
144. Hounsfield, G. N. Computed medical imaging. Nobel lecture, Decemberr 8, 1979 / G. N. Hounsfield // *Journal of Computer Assisted Tomography*. – 1980. – Vol. 4. – № 5. – P. 665-674.
145. Hu, J. Squeeze-and-Excitation Networks / J. Hu, L. Shen, S. Albanie [et al.] // *IEEE Transactions on Pattern Analysis and Machine Intelligence*. – 2020. – Vol. 42. – № 8.
146. Hu, P. Automatic abdominal multi-organ segmentation using deep convolutional neural network and time-implicit level sets / P. Hu, F. Wu, J. Peng [et al.] // *International Journal of Computer Assisted Radiology and Surgery*. – 2017. – Vol. 12. – № 3.
147. Hung, H.-C. Applications of Artificial Intelligence in Orthodontics / H.-C. Hung, Y.-C. Wang, Y.-C. Wang // *Taiwanese Journal of Orthodontics*. – 2020. – Vol. 32. – № 2.

148. Ihssen, B. A. Effect of in vitro aging by water immersion and thermocycling on the mechanical properties of PETG aligner material / B. A. Ihssen, J. H. Willmann, A. Nimer, D. Drescher // *Journal of Orofacial Orthopedics*. – 2019. – Vol. 80. – № 6.

149. Im, J. Comparison of virtual and manual tooth setups with digital and plaster models in extraction cases / J. Im, J. Y. Cha, K. J. Lee [et al.] // *American Journal of Orthodontics and Dentofacial Orthopedics*. – 2014. – Vol. 145. – № 4. – P. 434-442.

150. Im, J. Accuracy and efficiency of automatic tooth segmentation in digital dental models using deep learning / J. Im, J. Y. Kim, H. S. Yu [et al.] // *Scientific Reports*. – 2022. – Vol. 12. – № 1. – P. 1-11.

151. Imber, J. C. Treatment of Gingival Recession: When and How? / J. C. Imber, A. Kasaj // *International Dental Journal*. – 2021. – Vol. 71. – № 3. – P. 178-187.

152. Ioffe, S. Batch normalization: Accelerating deep network training by reducing internal covariate shift / S. Ioffe, C. Szegedy // *32nd International Conference on Machine Learning, ICML 2015*. – 2015. – Vol. 1.

153. Isensee, F. Automatic Cardiac Disease Assessment on cine-MRI via Time-Series Segmentation and Domain Specific Features : *Lecture Notes in Computer Science* / F. Isensee, P. Jaeger, P. M. Full [et al.]. – 2017. – Vol. 10663.

154. Jaggy, F. ATR-FTIR analysis and one-week stress relaxation of four orthodontic aligner materials / F. Jaggy, S. Zinelis, G. Polychronis [et al.] // *Materials*. – 2020. – Vol. 13. – № 8.

155. Jalladaud, M. How to analyze periodontal morphotypes in order to reduce the risk of periodontal recession / M. Jalladaud, M. Lahmi, C. Lallam. – 2017. – P. 95-103.

156. Jang, Y. Automatic segmentation of LV and RV in cardiac MRI / Y. Jang, Y. Hong, S. Ha [et al.] // *Lecture Notes in Computer Science (including subseries Lecture Notes in Artificial Intelligence and Lecture Notes in Bioinformatics)*. – 2018. – Vol. 10663 LNCS.

157. Jepsen, S. Periodontal manifestations of systemic diseases and developmental and acquired conditions: Consensus report of workgroup 3 of the 2017 World Workshop on the Classification of Periodontal and Peri-Implant Diseases and Conditions / S. Jepsen, J. G. Caton, J. M. Albandar [et al.] // Journal of periodontology. – 2018. – Vol. 89. – P. S237-S248.

158. Jindal, P. Mechanical and geometric properties of thermoformed and 3D printed clear dental aligners / P. Jindal, M. Juneja, F. L. Siena [et al.] // American Journal of Orthodontics and Dentofacial Orthopedics. – 2019. – Vol. 156. – № 5.

159. Jones, M. L. A validated finite element method study of orthodontic tooth movement in the human subject / M. L. Jones, J. Hickman, J. Middleton [et al.] // Journal of Orthodontics. – 2001. – Vol. 28. – № 1.

160. Joshi, N. Gingival Biotype and Gingival Bioform : Determining Factors for Periodontal Disease Progression and Treatment Outcome / N. Joshi, M. C. Agarwal, E. Madan [et al.]. – 2016. – Vol. 4. – № 3. – P. 220-225.

161. Joshi, N. Gingival Biotype and Gingival Bioform: Determining Factors for Periodontal Disease Progression and Treatment Outcome / N. Joshi, M. Chandra, E. Madan [et al.] // International Journal of Scientific Study. – 2016. – Vol. 4. – № 3. – P. 220-225.

162. Kan, J. Y. K. Dimensions of Peri-Implant Mucosa: An Evaluation of Maxillary Anterior Single Implants in Humans Case series / J. Y. K. Kan, K. Rungcharassaeng, K. Umezumi, J. C. Kois. – 2003. – № April. – P. 18-20.

163. Kapila, S. D. CBCT in orthodontics: Assessment of treatment outcomes and indications for its use. Vol. 44 / S. D. Kapila, J. M. Nervina. – 2015.

164. Karras, T. Efficacy of Invisalign attachments: A retrospective study / T. Karras, M. Singh, E. Karkazis [et al.] // American Journal of Orthodontics and Dentofacial Orthopedics. – 2021. – Vol. 160. – № 2.

165. Ke, Y. A comparison of treatment effectiveness between clear aligner and fixed appliance therapies / Y. Ke, Y. Zhu, M. Zhu // BMC Oral Health. – 2019. – Vol. 19. – № 1.

166. Khened, M. Fully convolutional multi-scale residual DenseNets for cardiac segmentation and automated cardiac diagnosis using ensemble of classifiers / M. Khened, V. A. Kollerathu, G. Krishnamurthi // Medical Image Analysis. – 2019. – Vol. 51.

167. Kim, T. Tooth Segmentation of 3D Scan Data Using Generative Adversarial Networks / T. Kim, Y. Cho, D. Kim [et al.] // Applied Sciences 2020, Vol. 10, Page 490. – 2020. – Vol. 10. – № 2. – P. 490.

168. Kingma, D. P. Adam: A method for stochastic optimization / D. P. Kingma, J. L. Ba // 3rd International Conference on Learning Representations, ICLR 2015 - Conference Track Proceedings. – 2015.

169. Kleesiek, J. ilastik for Multi-modal Brain Tumor Segmentation / J. Kleesiek, A. Biller, G. Urban [et al.] // BraTS Challenge Manuscripts, MICCAI 2014. – 2014.

170. Ko, H. C. Recommendations for clear aligner therapy using digital or plaster study casts / H. C. Ko, W. Liu, D. Hou [et al.] // Progress in Orthodontics. – 2018. – Vol. 19. – № 1.

171. Kohda, N. Effects of mechanical properties of thermoplastic materials on the initial force of thermoplastic appliances / N. Kohda, M. Iijima, T. Muguruma [et al.] // Angle Orthodontist. – 2013. – Vol. 83. – № 3.

172. Kolte, R. Assessment of gingival thickness with regards to age, gender and arch location / R. Kolte, A. Kolte, A. Mahajan // Journal of Indian Society of Periodontology. – 2014. – Vol. 18. – № 4. – P. 478-481.

173. Kononova, O. V. Features of treatment of patients with generalized periodontitis with manifestations of psychoemotional stress / O. V. Kononova, A. V.

Borysenko, V. M. Batig, M. I. Sheremet // Romanian Journal of Stomatology. – 2019. – Vol. 65. – № 4. – P. 371-375.

174. Kravitz, N. D. How well does Invisalign work? A prospective clinical study evaluating the efficacy of tooth movement with Invisalign / N. D. Kravitz, B. Kusnoto, E. BeGole [et al.] // American Journal of Orthodontics and Dentofacial Orthopedics. – 2009. – Vol. 135. – № 1.

175. Kundal, S. Aligners: The Science of Clear Orthodontics / S. Kundal // International Journal of Dental and Medical Specialty. – 2020. – Vol. 7. – № 1.

176. Kusy, R. P. Influence of force systems on archwire-bracket combinations / R. P. Kusy // American Journal of Orthodontics and Dentofacial Orthopedics. – 2005. – Vol. 127. – № 3.

177. Kwon, J. S. Force delivery properties of thermoplastic orthodontic materials / J. S. Kwon, Y. K. Lee, B. S. Lim, Y. K. Lim // American Journal of Orthodontics and Dentofacial Orthopedics. – 2008. – Vol. 133. – № 2.

178. Lachapelle, D. Measurement of Gingivitis among School-Age Children in Brantford, Sarnia, and Stratford, using the P-M-A Index / D. Lachapelle, J. Sévigny, J.-M. Brodeur, C. Couture // Canadian Journal of Public Health. – 1990. – Vol. 81. – № 5. – P. 370-375.

179. Lau, F. ScarGAN: Chained Generative Adversarial Networks to Simulate Pathological Tissue on Cardiovascular MR Scans / F. Lau, T. Hendriks, J. Lieman-Sifry [et al.] // Lecture Notes in Computer Science (including subseries Lecture Notes in Artificial Intelligence and Lecture Notes in Bioinformatics). – 2018. – Vol. 11045 LNCS. – P. 343-350.

180. Lechuga, L. Cone Beam CT vs. Fan Beam CT: A Comparison of Image Quality and Dose Delivered Between Two Differing CT Imaging Modalities / L. Lechuga, G. A. Weidlich // Cureus. – 2016. – Vol. 8. – № 9.

181. Lee, C. Y. Deeply-supervised nets / C. Y. Lee, S. Xie, P. W. Gallagher [et al.] // *Journal of Machine Learning Research*. – 2015. – Vol. 38.
182. Lee, S. Automated CNN-Based tooth segmentation in cone-beam CT for dental implant planning / S. Lee, S. Woo, J. Yu [et al.] // *IEEE Access*. – 2020. – Vol. 8. – P. 50507-50518.
183. Li, J. Dilated-inception net: Multi-scale feature aggregation for cardiac right ventricle segmentation / J. Li, Z. L. Yu, Z. Gu [et al.] // *IEEE Transactions on Biomedical Engineering*. – 2019. – Vol. 66. – № 12.
184. Li, W. Structured Landmark Detection via Topology-Adapting Deep Graph Learning / W. Li, Y. Lu, K. Zheng [et al.] // *Lecture Notes in Computer Science (including subseries Lecture Notes in Artificial Intelligence and Lecture Notes in Bioinformatics)*. – 2020. – Vol. 12354 LNCS. – P. 266-283.
185. Lian, C. Deep Multi-Scale Mesh Feature Learning for Automated Labeling of Raw Dental Surfaces from 3D Intraoral Scanners / C. Lian, L. Wang, T. H. Wu [et al.] // *IEEE Transactions on Medical Imaging*. – 2020. – Vol. 39. – № 7. – P. 2440-2450.
186. Liao, F. Estimation of the Volume of the Left Ventricle From MRI Images Using Deep Neural Networks / F. Liao, X. Chen, X. Hu, S. Song // *IEEE Transactions on Cybernetics*. – 2017. – Vol. 49. – № 2.
187. Litjens, G. Evaluation of prostate segmentation algorithms for MRI: The PROMISE12 challenge / G. Litjens, R. Toth, W. van de Ven [et al.] // *Medical Image Analysis*. – 2014. – Vol. 18. – № 2.
188. Liu, C. L. Colour stabilities of three types of orthodontic clear aligners exposed to staining agents / C. L. Liu, W. T. Sun, W. Liao [et al.] // *International Journal of Oral Science*. – 2016. – Vol. 8. – № 4.

189. Lombardo, L. Predictability of orthodontic movement with orthodontic aligners: a retrospective study / L. Lombardo, A. Arreghini, F. Ramina [et al.] // *Progress in Orthodontics*. – 2017. – Vol. 18. – № 1.

190. Lombardo, L. Stress relaxation properties of four orthodontic aligner materials: A 24-hour in vitro study / L. Lombardo, E. Martines, V. Mazzanti [et al.] // *Angle Orthodontist*. – 2017. – Vol. 87. – № 1.

191. Lombardo, L. MicroCT X-ray comparison of aligner gap and thickness of six brands of aligners: an in-vitro study / L. Lombardo, M. Palone, M. Longo [et al.] // *Progress in Orthodontics*. – 2020. – Vol. 21. – № 1.

192. Long, H. An objective system for appraising clear aligner treatment difficulty: clear aligner treatment complexity assessment tool (CAT–CAT) / H. Long, Z. Wu, X. Yan [et al.] // *BMC Oral Health*. – 2020. – Vol. 20. – № 1.

193. Lu, Q. W. Comparing the compatibility of various functionalized polypropylenes with thermoplastic polyurethane (TPU) / Q. W. Lu, C. W. Macosko // *Polymer*. – 2004. – Vol. 45. – № 6.

194. Lu, Q. W. Comparing the compatibility of various functionalized polypropylenes with thermoplastic polyurethane (TPU) / Q. W. Lu, C. W. Macosko // *Polymer*. – 2004. – Vol. 45. – № 6. – P. 1981-1991.

195. Lu, X. Graph cut segmentation of the right ventricle in cardiac MRI using multi-scale feature learning / X. Lu, X. Chen, W. Li, Y. Qiao // *ACM International Conference Proceeding Series*. – 2019.

196. Luc, P. Semantic Segmentation using Adversarial Networks / P. Luc, C. Couprie, S. Chintala, J. Verbeek. – 2016.

197. Luis, F. The insider's Guide to Invisalign Treatment / F. Luis, G. Moncayo.



198. Madenci, E. The Finite Element Method and Applications in Engineering Using ANSYS®. Vol. 3 / E. Madenci, I. Guven. – Boston, MA : Springer US, 2015. – 54-67 p.
199. Malpartida-Carrillo, V. Periodontal phenotype: A review of historical and current classifications evaluating different methods and characteristics. Vol. 33 / V. Malpartida-Carrillo, P. L. Tinedo-Lopez, M. E. Guerrero, [et al.]. – John Wiley and Sons Inc, 2021.
200. Mampieri, G. Treatment of impacted canines with aligners: An alternative and viable option / G. Mampieri, T. Castroflorio, A. Conigliaro, A. Giancotti // Clinical Case Reports. – 2021. – Vol. 9. – № 9.
201. Martin, D. J. Thermoplastic polyurethane (TPU)-based polymer nanocomposites / D. J. Martin, A. F. Osman, Y. Andriani, G. A. Edwards // Advances in Polymer Nanocomposites: Types and Applications. – 2012.
202. Martina, S. In vitro cytotoxicity of different thermoplastic materials for clear aligners / S. Martina, R. Rongo, R. Bucci [et al.] // Angle Orthodontist. – 2019. – Vol. 89. – № 6.
203. Masella, R. S. The neuroanatomic basis of facial perception and variable facial discrimination ability: Implications for orthodontics / R. S. Masella, M. Meister // American Journal of Orthodontics and Dentofacial Orthopedics. – 2007. – Vol. 132. – № 3. – P. 293-301.
204. Math, M. V. Bridging to medicine / M. V. Math, Y. R. Kattimani, R. M. Khadkikar // British Dental Journal 2016 220:10. – 2016. – Vol. 220. – № 10. – P. 500-500.
205. McGuinness, N. Stresses induced by edgewise appliances in the periodontal ligament--a finite element study. / N. McGuinness, A. N. Wilson, M. Jones [et al.] // Angle Orthodontist. – 1992. – Vol. 62. – № 1.

206. Medley, D. O. Segmenting the left ventricle in cardiac in cardiac MRI: From handcrafted to deep region based descriptors / D. O. Medley, C. Santiago, J. C. Nascimento // Proceedings - International Symposium on Biomedical Imaging. – 2019. – Vols. 2019-April.

207. Memon, S. A comparative evaluation of the reliability of three methods of assessing gingival biotype in dentate subjects in different age groups: An in vivo study / S. Memon, J. R. Patel, R. Sethuraman [et al.] // Journal of Indian Prosthodontist Society. – 2015. – Vol. 15. – № 4. – P. 313-317.

208. Menze, B. H. The Multimodal Brain Tumor Image Segmentation Benchmark (BRATS) / B. H. Menze, A. Jakab, S. Bauer [et al.] // IEEE Transactions on Medical Imaging. – 2015. – Vol. 34. – № 10.

209. MG, N. Newman and Carranza's Clinical Periodontology / N. MG. – Elsevier Health Sciences, 2014. – 635-648 p.

210. Milletari, F. V-Net: Fully convolutional neural networks for volumetric medical image segmentation / F. Milletari, N. Navab, S. A. Ahmadi // Proceedings - 2016 4th International Conference on 3D Vision, 3DV 2016. – 2016.

211. Mishkin, D. All you need is a good init / D. Mishkin, J. Matas // 4th International Conference on Learning Representations, ICLR 2016 - Conference Track Proceedings. – 2016.

212. Moccia, S. Development and testing of a deep learning-based strategy for scar segmentation on CMR-LGE images / S. Moccia, R. Banali, C. Martini [et al.] // Magnetic Resonance Materials in Physics, Biology and Medicine. – 2019. – Vol. 32. – № 2.

213. Moeskops, P. Deep learning for multi-task medical image segmentation in multiple modalities / P. Moeskops, J. M. Wolterink, B. H. M. van der Velden [et al.] // Lecture Notes in Computer Science (including subseries Lecture Notes in Artificial Intelligence and Lecture Notes in Bioinformatics). – 2016. – Vol. 9901 LNCS.

214. Morris, R. S. Accuracy of Dental Monitoring 3D digital dental models using photograph and video mode / R. S. Morris, L. N. Hoye, M. H. Elnagar [et al.] // American Journal of Orthodontics and Dentofacial Orthopedics. – 2019. – Vol. 156. – № 3. – P. 420-428.

215. Müller, H. P. Gingival phenotypes in young male adults / H. P. Müller // Journal of Clinical Periodontology. – 1997. – Vol. 24. – № 1. – P. 65-71.

216. Müller, H. P. Masticatory mucosa in subjects with different periodontal phenotypes / H. P. Müller, A. Heinecke, N. Schaller, T. Eger // Journal of Clinical Periodontology. – 2000. – Vol. 27. – № 9. – P. 621-626.

217. Ngo, T. A. Combining deep learning and level set for the automated segmentation of the left ventricle of the heart from cardiac cine magnetic resonance / T. A. Ngo, Z. Lu, G. Carneiro // Medical Image Analysis. – 2017. – Vol. 35.

218. Nimwegen, W. G. van. Immediate placement and provisionalization of implants in the aesthetic zone with or without a connective tissue graft: A 1-year randomized controlled trial and volumetric study / W. G. van Nimwegen, G. M. Raghoobar, E. G. Zuiderveld [et al.] // Clinical Oral Implants Research. – 2018. – Vol. 29. – № 7. – P. 671-678.

219. Oktay, O. Multi-input cardiac image super-resolution using convolutional neural networks / O. Oktay, W. Bai, M. Lee [et al.] // Lecture Notes in Computer Science (including subseries Lecture Notes in Artificial Intelligence and Lecture Notes in Bioinformatics). – 2016. – Vol. 9902 LNCS.

220. Oktay, O. Anatomically Constrained Neural Networks (ACNNs): Application to Cardiac Image Enhancement and Segmentation / O. Oktay, E. Ferrante, K. Kamnitsas [et al.] // IEEE Transactions on Medical Imaging. – 2018. – Vol. 37. – № 2.

221. Ossowska, A. Artificial Intelligence in Dentistry-Narrative Review / A. Ossowska, A. Kusiak, D. Świetlik // International Journal of Environmental Research and Public Health. – 2022. – Vol. 19. – № 6. – P. 3449.

222. Painchaud, N. Cardiac MRI Segmentation with Strong Anatomical Guarantees / N. Painchaud, Y. Skandarani, T. Judge [et al.] // Lecture Notes in Computer Science (including subseries Lecture Notes in Artificial Intelligence and Lecture Notes in Bioinformatics). – 2019. – Vol. 11765 LNCS.

223. Papadopoulou, A. K. Changes in roughness and mechanical properties of Invisalign® appliances after one- and two-weeks use / A. K. Papadopoulou, A. Cantele, G. Polychronis [et al.] // Materials. – 2019. – Vol. 12. – № 15.

224. Park, S. Deep Learning-Based Automatic Segmentation of Mandible and Maxilla in Multi-Center CT Images / S. Park, H. Kim, E. Shim [et al.] // Applied Sciences (Switzerland). – 2022. – Vol. 12. – № 3.

225. Pasciuti, E. Deep Bite Treatment with Aligners: A New Protocol / E. Pasciuti, G. Coloccia, A. D. Inchingolo [et al.] // Applied Sciences (Switzerland). – 2022. – Vol. 12. – № 13. – P. 6709.

226. Patini, R. Clear aligners' effects on aesthetics: Evaluation of facial wrinkles / R. Patini, P. Gallenzi, S. Meuli [et al.] // Journal of Clinical and Experimental Dentistry. – 2018. – Vol. 10. – № 7. – P. e696-e701.

227. Patravali, J. 2D-3D fully convolutional neural networks for cardiac MR segmentation / J. Patravali, S. Jain, S. Chilamkurthy // Lecture Notes in Computer Science (including subseries Lecture Notes in Artificial Intelligence and Lecture Notes in Bioinformatics). – 2018. – Vol. 10663 LNCS.

228. Pauwels, R. CBCT-based bone quality assessment: Are Hounsfield units applicable? Vol. 44 / R. Pauwels, R. Jacobs, S. R. Singer, M. Mupparapu. – 2015.

229. Pauwels, R. CBCT-based bone quality assessment: are Hounsfield units applicable? / R. Pauwels, R. Jacobs, S. R. Singer, M. Mupparapu // *Dento Maxillo Facial Radiology*. – 2015. – Vol. 44. – CBCT-based bone quality assessment. – № 1. – P. 20140238.

230. Pereira, N. C. Frequency of awake bruxism behaviour in orthodontic patients: Randomised clinical trial: Awake bruxism behaviour in orthodontic patients / N. C. Pereira, P. V. P. Oltramari, P. C. R. Conti [et al.] // *Journal of Oral Rehabilitation*. – 2021. – Vol. 48. – № 4.

231. Pereira, S. Brain Tumor Segmentation Using Convolutional Neural Networks in MRI Images / S. Pereira, A. Pinto, V. Alves, C. A. Silva // *IEEE Transactions on Medical Imaging*. – 2016. – Vol. 35. – № 5.

232. Pernet, F. Long-term evaluation of lower incisors gingival recessions after orthodontic treatment / F. Pernet, C. Vento, N. Pandis, S. Kiliaridis // *European Journal of Orthodontics*. – 2019. – Vol. 41. – № 6. – P. 559-564.

233. Poudel, R. P. K. Recurrent fully convolutional neural networks for multi-slice MRI cardiac segmentation / R. P. K. Poudel, P. Lamata, G. Montana // *Lecture Notes in Computer Science (including subseries Lecture Notes in Artificial Intelligence and Lecture Notes in Bioinformatics)*. – 2017. – Vol. 10129 LNCS.

234. Prasoon, A. Deep feature learning for knee cartilage segmentation using a triplanar convolutional neural network / A. Prasoon, K. Petersen, C. Igel [et al.] // *Lecture Notes in Computer Science (including subseries Lecture Notes in Artificial Intelligence and Lecture Notes in Bioinformatics)*. – 2013. – Vol. 8150 LNCS.

235. Pratto, I. Thermal and mechanical characterization of thermoplastic orthodontic aligners discs after molding process / I. Pratto, M. C. A. Busato, P. R. S. Bittencourt // *Journal of the Mechanical Behavior of Biomedical Materials*. – 2022. – Vol. 126.

236. Qian, J. CephaNet: An improved faster r-cnn for cephalometric landmark detection / J. Qian, M. Cheng, Y. Tao [et al.] // Proceedings - International Symposium on Biomedical Imaging. – IEEE Computer Society, 2019. – Vols. 2019-April. – P. 868-871.

237. Qian, N. On the momentum term in gradient descent learning algorithms / N. Qian // Neural Networks. – 1999. – Vol. 12. – № 1.

238. Qin, C. Joint learning of motion estimation and segmentation for cardiac MR image sequences / C. Qin, W. Bai, J. Schlemper [et al.] // Lecture Notes in Computer Science (including subseries Lecture Notes in Artificial Intelligence and Lecture Notes in Bioinformatics). – 2018. – Vol. 11071 LNCS.

239. Raith, S. Artificial Neural Networks as a powerful numerical tool to classify specific features of a tooth based on 3D scan data / S. Raith, E. P. Vogel, N. Anees [et al.] // Computers in Biology and Medicine. – 2017. – Vol. 80. – P. 65-76.

240. Rasperini, G. Influence of Periodontal Biotype on Root Surface Exposure During Orthodontic Treatment: A Preliminary Study / G. Rasperini, R. Acunzo, P. Cannalire, G. Farronato // The International Journal of Periodontics & Restorative Dentistry. – 2017. – Vol. 35. – № 5. – P. 655-675.

241. Rathee, M. Prevalence of Gingival Biotypes among Young Dentate North Indian Population: A Biometric Approach / M. Rathee, P. L. Rao, M. Bhoria // International Journal of Clinical Pediatric Dentistry. – 2016. – Vol. 9. – № 2. – P. 104-108.

242. Real, A. Del. Use of automated artificial intelligence to predict the need for orthodontic extractions / A. Del Real, O. Del Real, S. Sardina, R. Oyonarte // Korean Journal of Orthodontics. – 2022. – Vol. 52. – № 2. – P. 102-111.

243. Ren, L. The predictability of orthodontic tooth movements through clear aligner among first-premolar extraction patients: a multivariate analysis / L. Ren, L. Liu, Z. Wu [et al.] // *Progress in Orthodontics*. – 2022. – Vol. 23. – № 1.

244. Retrouvey, J.-M. The role of AI and machine learning in contemporary orthodontics / J.-M. Retrouvey // *APOS Trends in Orthodontics*. – 2021. – Vol. 11. – № 1. – P. 74-80.

245. Roberts-Harry, D. Orthodontics. Part 2: Patient assessment and examination I / D. Roberts-Harry, J. Sandy // *British Dental Journal* 2003 195:9. – 2003. – Vol. 195. – № 9. – P. 489-493.

246. Robertson, L. Effectiveness of clear aligner therapy for orthodontic treatment: A systematic review. Vol. 23 / L. Robertson, H. Kaur, N. C. F. Fagundes, [et al.]. – 2020.

247. Ronneberger, O. U-net: Convolutional networks for biomedical image segmentation / O. Ronneberger, P. Fischer, T. Brox // *Lecture Notes in Computer Science (including subseries Lecture Notes in Artificial Intelligence and Lecture Notes in Bioinformatics)*. – 2015. – Vol. 9351.

248. Ronneberger, O. U-net: Convolutional networks for biomedical image segmentation / O. Ronneberger, P. Fischer, T. Brox // *Lecture Notes in Computer Science (including subseries Lecture Notes in Artificial Intelligence and Lecture Notes in Bioinformatics)*. – 2015. – Vol. 9351.

249. Roth, H. R. Deeporgan: Multi-level deep convolutional networks for automated pancreas segmentation / H. R. Roth, L. Lu, A. Farag [et al.] // *Lecture Notes in Computer Science (including subseries Lecture Notes in Artificial Intelligence and Lecture Notes in Bioinformatics)*. – 2015. – Vol. 9349.

250. Rouck, T. De. The gingival biotype revisited: transparency of the periodontal probe through the gingival margin as a method to discriminate thin from thick gingiva / T. De Rouck, R. Eghba, K. Collys [et al.]. – 2009. – № February. – P. 428-433.

251. Rouck, T. De. The gingival biotype revisited: Transparency of the periodontal probe through the gingival margin as a method to discriminate thin from thick gingiva / T. De Rouck, R. Eghbali, K. Collys [et al.] // *Journal of Clinical Periodontology*. – 2009. – Vol. 36. – № 5. – P. 428-433.

252. Russo, P. Thermoplastic polyurethane films reinforced with carbon nanotubes: The effect of processing on the structure and mechanical properties / P. Russo, M. Lavorgna, F. Piscitelli [et al.] // *European Polymer Journal*. – 2013. – Vol. 49. – № 2.

253. Ryokawa, H. The mechanical properties of dental thermoplastic materials in a simulated intraoral environment / H. Ryokawa, Y. Miyazaki, A. Fujishima [et al.] // *Orthodontic Waves*. – 2006. – Vol. 65. – № 2.

254. Ryu, J. H. Effects of thermoforming on the physical and mechanical properties of thermoplastic materials for transparent orthodontic aligners / J. H. Ryu, J. S. Kwon, H. B. Jiang [et al.] // *Korean Journal of Orthodontics*. – 2018. – Vol. 48. – № 5.

255. Sala, L. Comparative in vitro study of two methods for gingival biotype assessment / L. Sala, R. Alonso-Pérez, R. Agustin-Panadero [et al.] // *Journal of Clinical and Experimental Dentistry*. – 2018. – Vol. 10. – № 9. – P. e858-e863.

256. Sander, J. Towards increased trustworthiness of deep learning segmentation methods on cardiac MRI / J. Sander, B. D. de Vos, J. M. Wolterink, I. Išgum. – 2019.

257. Sandler, H. C. Testing the uniformity of the P-M-A index as a measurement of periodontal disease / H. C. Sandler // *Journal of Dental Research*. – 1952. – Vol. 31. – № 3.

258. Savioli, N. A Generative Adversarial Model for Right Ventricle Segmentation / N. Savioli, M. S. Vieira, P. Lamata, G. Montana. – 2018.

259. Schaller, N. Ultrasonic determination of thickness of masticatory mucosa / N. Schaller, T. Eger // *Pathology*. – 1999. – P. 248-253.



260. Schuster, S. Structural conformation and leaching from in vitro aged and retrieved Invisalign appliances / S. Schuster, G. Eliades, S. Zinelis [et al.] // American Journal of Orthodontics and Dentofacial Orthopedics. – 2004. – Vol. 126. – № 6.

261. Sfondrini, M. F. New Materials and Techniques for Orthodontics / M. F. Sfondrini, A. Scribante // Materials. – 2023. – Vol. 16. – № 5.

262. Shah, H. K. Gingival Biotype Classification, Assessment, and Clinical Importance: A Review / H. K. Shah, S. Sharma, S. Shrestha // Journal of Nepalese Society of Periodontology and Oral Implantology. – 2020. – Vol. 4. – № 2. – P. 83-88.

263. Shah, R. Prevalence of gingival biotype and its relationship to clinical parameters / R. Shah, N. K. Sowmya, D. S. Mehta // Contemporary Clinical Dentistry. – 2015. – Vol. 6. – № 5. – P. S167-S171.

264. Shaikh, K. Artificial Intelligence in Dentistry / K. Shaikh, S. V. Bekal, H. F. A. Marei, [et al.]. – Springer Nature Switzerland AG, 2022. – 209 p.

265. Shalish, M. Adult patients' adjustability to orthodontic appliances. Part I: A comparison between Labial, Lingual, and Invisalign™ / M. Shalish, R. Cooper-Kazaz, I. Ivgi [et al.] // European Journal of Orthodontics. – 2012. – Vol. 34. – № 6.

266. Shelhamer, E. Fully Convolutional Networks for Semantic Segmentation / E. Shelhamer, J. Long, T. Darrell // IEEE Transactions on Pattern Analysis and Machine Intelligence. – 2017. – Vol. 39. – № 4.

267. Shi, B. An End-to-End Trainable Neural Network for Image-Based Sequence Recognition and Its Application to Scene Text Recognition / B. Shi, X. Bai, C. Yao // IEEE Transactions on Pattern Analysis and Machine Intelligence. – 2017. – Vol. 39. – № 11.

268. Singh, J. Correlation of gingival thickness with gingival width, probing depth, and papillary fill in maxillary anterior teeth in students of a dental college in Navi Mumbai

/ J. Singh, V. Rathod, P. Rao [et al.] // Contemporary Clinical Dentistry. – 2016. – Vol. 7. – № 4. – P. 535-538.

269. Smith, J. M. Predictability of lower incisor tip using clear aligner therapy / J. M. Smith, T. Weir, A. Kaang, M. Farella // Progress in Orthodontics. – 2022. – Vol. 23. – № 1.

270. Srivastava, N. Dropout: A simple way to prevent neural networks from overfitting / N. Srivastava, G. Hinton, A. Krizhevsky [et al.] // Journal of Machine Learning Research. – 2014. – Vol. 15.

271. Szegedy, C. Going deeper with convolutions / C. Szegedy, W. Liu, Y. Jia [et al.] // Proceedings of the IEEE Computer Society Conference on Computer Vision and Pattern Recognition. – 2015. – Vols. 07-12-June.

272. Tai, S. Clear aligner technique / S. Tai. – 2018.

273. Takahashi, S. On current trends in orthodontics / S. Takahashi // Japanese dental journal. – 1961. – Vol. 14.

274. Tan, L. K. Convolutional neural network regression for short-axis left ventricle segmentation in cardiac cine MR sequences / L. K. Tan, Y. M. Liew, E. Lim, R. A. McLaughlin // Medical Image Analysis. – 2017. – Vol. 39.

275. Tao, Q. Deep learning-based method for fully automatic quantification of left ventricle function from cine MR images: A multivendor, multicenter study / Q. Tao, W. Yan, Y. Wang [et al.] // Radiology. – 2019. – Vol. 290. – № 1.

276. Tao, S. Tooth CT Image Segmentation Method Based on the U-Net Network and Attention Module / S. Tao, Z. Wang // Computational and Mathematical Methods in Medicine. – 2022. – Vol. 2022.

277. Tartaglia, G. M. Direct 3D printing of clear orthodontic aligners: Current state and future possibilities. Vol. 14 / G. M. Tartaglia, A. Mapelli, C. Maspero, [et al.]. – 2021.

278. Tenovuo, J. Concentration of Thiocyanate and Ionizable Iodine in Saliva of Smokers and Nonsmokers / J. Tenovuo, K. K. Makinen // *Journal of Dental Research*. – 1976. – Vol. 55. – № 4. – P. 661-663.

279. Tran, P. V. A Fully Convolutional Neural Network for Cardiac Segmentation in Short-Axis MRI / P. V. Tran. – 2016.

280. Trullo, R. Joint segmentation of multiple thoracic organs in CT images with two collaborative deep architectures / R. Trullo, C. Petitjean, D. Nie [et al.] // *Lecture Notes in Computer Science (including subseries Lecture Notes in Artificial Intelligence and Lecture Notes in Bioinformatics)*. – 2017. – Vol. 10553 LNCS.

281. Upadhyay, M. Biomechanics of clear aligners: hidden truths & first principles. Vol. 11 / M. Upadhyay, S. A. Arqub. – 2022.

282. Vaid, N. R. Artificial Intelligence (AI) driven orthodontic care: A quest toward utopia? / N. R. Vaid // *Seminars in Orthodontics*. – 2021. – Vol. 27. – № 2. – P. 57-61.

283. Vaswani, A. Attention is all you need / A. Vaswani, N. Shazeer, N. Parmar [et al.] // *Advances in Neural Information Processing Systems*. – 2017. – Vols. 2017-Decem.

284. Venezia, P. Accuracy of orthodontic models prototyped for clear aligners therapy: A 3D imaging analysis comparing different market segments 3D printing protocols / P. Venezia, V. Ronsivalle, L. Rustico [et al.] // *Journal of Dentistry*. – 2022. – Vol. 124. – P. 104212.

285. Vesal, S. A multi-stage fully convolutional network for cardiac MRI segmentation / S. Vesal, A. Maier, N. Ravikumar. – 2019. – № May. – P. 1-11.

286. Vesal, S. Fully Automated 3D Cardiac MRI Localisation and Segmentation Using Deep Neural Networks / S. Vesal, A. Maier, N. Ravikumar // *Journal of Imaging*. – 2020. – Vol. 6. – № 7.

287. Vesal, S. Fully Automated 3D Cardiac MRI Localisation and Segmentation Using Deep Neural Networks / S. Vesal, A. Maier, N. Ravikumar // *Journal of Imaging*. – 2020. – Vol. 6. – № 7. – P. 0-19.

288. Vigneault, D. M.  $\Omega$ -Net (Omega-Net): Fully automatic, multi-view cardiac MR detection, orientation, and segmentation with deep neural networks / D. M. Vigneault, W. Xie, C. Y. Ho [et al.] // *Medical Image Analysis*. – 2018. – Vol. 48.

289. Vlachodimou, E. Is there an association between the gingival phenotype and the width of keratinized gingiva? A systematic review. Vol. 9 / E. Vlachodimou, I. Fragkioudakis, I. Vouros. – *Dent J (Basel)*, 2021.

290. Waard, O. de. The Prediction Accuracy of Digital Orthodontic Setups for the Orthodontic Phase before Orthognathic Surgery / O. de Waard, F. Baan, R. Bruggink [et al.] // *Journal of Clinical Medicine* 2022, Vol. 11, Page 6141. – 2022. – Vol. 11. – № 20. – P. 6141.

291. Wang, C. Automatic whole heart segmentation using deep learning and shape context / C. Wang, Ö. Smedby // *Lecture Notes in Computer Science (including subseries Lecture Notes in Artificial Intelligence and Lecture Notes in Bioinformatics)*. – 2018. – Vol. 10663 LNCS.

292. Wang, X. Supervised learning in spiking neural networks: A review of algorithms and evaluations / X. Wang, X. Lin, X. Dang // *Neural Networks*. – 2020. – Vol. 125. – Supervised learning in spiking neural networks. – P. 258-280.

293. Wang, Y. Organ at Risk Segmentation in Head and Neck CT Images Using a Two-Stage Segmentation Framework Based on 3D U-Net / Y. Wang, L. Zhao, M. Wang, Z. Song // *IEEE Access*. – 2019. – Vol. 7. – P. 144591-144602.

294. Weckmann, J. Influence of attachment bonding protocol on precision of the attachment in aligner treatments / J. Weckmann, S. Scharf, I. Graf [et al.] // *Journal of Orofacial Orthopedics*. – 2020. – Vol. 81. – № 1.

295. Weir, T. Clear aligners in orthodontic treatment / T. Weir // Australian Dental Journal. – 2017. – Vol. 62. – P. 58-62.

296. Weisinger, E. Microscopic and microrespirometer evaluation of the efficacy of the PMA index / E. Weisinger, J. H. Manhold, J. L. Doyle, K. Rustogi // Journal of periodontology. – 1970. – Vol. 41. – № 11. – P. 650-653.

297. Wilmes, B. Esthetic Class II treatment with the Beneslider and aligners. / B. Wilmes, M. Nienkemper, B. Ludwig [et al.] // Journal of clinical orthodontics : JCO. – 2012. – Vol. 46. – № 7. – P. 390-398.

298. Wolterink, J. M. Automatic segmentation and disease classification using cardiac cine MR images / J. M. Wolterink, T. Leiner, M. A. Viergever, I. Išgum // Lecture Notes in Computer Science (including subseries Lecture Notes in Artificial Intelligence and Lecture Notes in Bioinformatics). – 2018. – Vol. 10663 LNCS.

299. Wu, H. Automated left ventricular segmentation from cardiac magnetic resonance images via adversarial learning with multi-stage pose estimation network and co-discriminator / H. Wu, X. Lu, B. Lei, Z. Wen // Medical image analysis. – 2021. – Vol. 68.

300. Xia, Q. Automatic 3D Atrial Segmentation from GE-MRIs Using Volumetric Fully Convolutional Networks / Q. Xia, Y. Yao, Z. Hu, A. Hao // Lecture Notes in Computer Science (including subseries Lecture Notes in Artificial Intelligence and Lecture Notes in Bioinformatics). – 2019. – Vol. 11395 LNCS.

301. Xiong, Z. Fully Automatic Left Atrium Segmentation From Late Gadolinium Enhanced Magnetic Resonance Imaging Using a Dual Fully Convolutional Neural Network / Z. Xiong, V. V. Fedorov, X. Fu [et al.] // IEEE Transactions on Medical Imaging. – 2019. – Vol. 38. – № 2.

302. Xu, A. Threshold-based level set method of image segmentation / A. Xu, L. Wang, S. Feng, Y. Qu // Proceedings - 3rd International Conference on Intelligent Networks and Intelligent Systems, ICINIS 2010. – 2010.

303. Xu, C. Direct delineation of myocardial infarction without contrast agents using a joint motion feature learning architecture / C. Xu, L. Xu, Z. Gao [et al.] // Medical Image Analysis. – 2018. – Vol. 50.

304. Xu, X. 3D Tooth Segmentation and Labeling Using Deep Convolutional Neural Networks / X. Xu, C. Liu, Y. Zheng // IEEE Transactions on Visualization and Computer Graphics. – 2019. – Vol. 25. – № 7. – P. 2336-2348.

305. Xue, Y. A multi-path 2.5 dimensional convolutional neural network system for segmenting stroke lesions in brain MRI images / Y. Xue, F. G. Farhat, O. Boukrina [et al.] // NeuroImage: Clinical. – 2020. – Vol. 25.

306. Yan, W. Left Ventricle Segmentation via Optical-Flow-Net from Short-Axis Cine MRI: Preserving the Temporal Coherence of Cardiac Motion / W. Yan, Y. Wang, Z. Li [et al.] // Lecture Notes in Computer Science (including subseries Lecture Notes in Artificial Intelligence and Lecture Notes in Bioinformatics). – 2018. – Vol. 11073 LNCS.

307. Yang, H. Research on a segmentation and evaluation method combining tooth morphology features / H. Yang, S. Wang // International Journal of Morphology. – 2020. – Vol. 38. – № 5. – P. 1325-1329.

308. Yang, J. Autosegmentation for thoracic radiation treatment planning: A grand challenge at AAPM 2017 / J. Yang, H. Veeraraghavan, S. G. Armato [et al.] // Medical Physics. – 2018. – Vol. 45. – № 10.

309. Yang, X. Class-balanced deep neural network for automatic ventricular structure segmentation / X. Yang, C. Bian, L. Yu [et al.] // Lecture Notes in Computer Science (including subseries Lecture Notes in Artificial Intelligence and Lecture Notes in Bioinformatics). – 2018. – Vol. 10663 LNCS.

310. Yang, X. Hybrid loss guided convolutional networks for whole heart parsing / X. Yang, C. Bian, L. Yu [et al.] // Lecture Notes in Computer Science (including subseries Lecture Notes in Artificial Intelligence and Lecture Notes in Bioinformatics). – 2018. – Vol. 10663 LNCS.
311. Ye, C. Multi-depth fusion network for whole-heart CT image segmentation / C. Ye, W. Wang, S. Zhang, K. Wang // IEEE Access. – 2019. – Vol. 7.
312. Yu, F. Multi-scale context aggregation by dilated convolutions / F. Yu, V. Koltun // 4th International Conference on Learning Representations, ICLR 2016 - Conference Track Proceedings. – 2016.
313. Yu, L. Volumetric convnets with mixed residual connections for automated prostate segmentation from 3d MR images / L. Yu, X. Yang, H. Chen [et al.] // 31st AAAI Conference on Artificial Intelligence, AAAI 2017. – 2017.
314. Yue, Q. Cardiac Segmentation from LGE MRI Using Deep Neural Network Incorporating Shape and Spatial Priors / Q. Yue, X. Luo, Q. Ye [et al.] // Lecture Notes in Computer Science (including subseries Lecture Notes in Artificial Intelligence and Lecture Notes in Bioinformatics). – 2019. – Vol. 11765 LNCS.
315. Zabihollahy, F. Myocardial scar segmentation from magnetic resonance images using convolutional neural network / F. Zabihollahy, J. A. White, E. Ukwatta. – 2018.
316. Zhang, J. LU-NET: An improved U-net for ventricular segmentation / J. Zhang, J. Du, H. Liu [et al.] // IEEE Access. – 2019. – Vol. 7.
317. Zhang, L. When Unseen Domain Generalization is Unnecessary? Rethinking Data Augmentation / L. Zhang, X. Wang, D. Yang [et al.]. – 2019.
318. Zhang, N. Preparation and characterization of thermoplastic materials for invisible orthodontics / N. Zhang, Y. Bai, X. Ding, Y. Zhang // Dental Materials Journal. – 2011. – Vol. 30. – № 6.

319. Zheng, Q. Deep Learning for Robust Segmentation and Explainable Analysis of 3D and Dynamic Cardiac Images To cite this version : HAL Id : tel-02083415 PhD of Science Deep Learning for Robust Segmentation and Explainable Analysis of 3D and Dynamic Cardiac Images / Q. Zheng. – 2019.

320. Zheng, Q. 3-D Consistent and Robust Segmentation of Cardiac Images by Deep Learning With Spatial Propagation / Q. Zheng, H. Delingette, N. Duchateau, N. Ayache // IEEE Transactions on Medical Imaging. – 2018. – Vol. 37. – № 9.

321. Zhou, X. Three-dimensional CT image segmentation by combining 2D fully convolutional network with 3D majority voting / X. Zhou, T. Ito, R. Takayama [et al.] // Lecture Notes in Computer Science (including subseries Lecture Notes in Artificial Intelligence and Lecture Notes in Bioinformatics). – 2016. – Vol. 10008 LNCS. – P. 111-120.

322. Zhou, X. Deep learning of the sectional appearances of 3D CT images for anatomical structure segmentation based on an FCN voting method / X. Zhou, R. Takayama, S. Wang [et al.] // Medical Physics. – 2017. – Vol. 44. – № 10.

323. Zhou, X. Y. Normalization in training U-Net for 2-D biomedical semantic segmentation / X. Y. Zhou, G. Z. Yang // IEEE Robotics and Automation Letters. – 2019. – Vol. 4. – № 2.

324. Zhu, Y. Force changes associated with differential activation of en-masse retraction and/or intrusion with clear aligners / Y. Zhu, W. Hu, S. Li // Korean Journal of Orthodontics. – 2021. – Vol. 51. – № 1.

325. Zon, M. van. Automatic cardiac landmark localization by a recurrent neural network / M. van Zon, M. Veta, S. Li. – 2019.

326. Zotti, C. GridNet with automatic shape prior registration for automatic MRI cardiac segmentation / C. Zotti, Z. Luo, O. Humbert [et al.] // Lecture Notes in Computer



Science (including subseries Lecture Notes in Artificial Intelligence and Lecture Notes in Bioinformatics). – 2018. – Vol. 10663 LNCS.

327. Zotti, C. Convolutional Neural Network with Shape Prior Applied to Cardiac MRI Segmentation / C. Zotti, Z. Luo, A. Lalande, P. M. Jodoin // IEEE Journal of Biomedical and Health Informatics. – 2019. – Vol. 23. – № 3.

328. Zweers, J. Characteristics of periodontal biotype, its dimensions, associations and prevalence -a systematic review- / J. Zweers, R. Z. Thomas, D. E. Slot, A. S. Weisgold. – 2014.